

Novel insights into the regulation of nucleolar function and longevity by *ncl-1*

Inaugural-Dissertation

zur

Erlangung des Doktorgrades

der Mathematisch-Naturwissenschaftlichen Fakultät

der Universität zu Köln

vorgelegt von

Till Popkes-van Oepen

Aus Bottrop

Köln, Juli 2020

Berichtersteller:
(Gutachter)

Prof. Dr. Adam Antebi

Prof. Dr. Thorsten Hoppe

Tag der mündlichen Prüfung:

11.09.2020

Abstract

The nucleolus is primarily described as the control center for ribonuclear protein assembly and rRNA synthesis. However, there is increasing evidence that the nucleolus also plays a role in protein quality, genome stability and cell cycle progression. Previous studies demonstrated that the B-box type zinc finger protein *ncl-1* is tightly linked to nucleolar function, and that its loss leads to increased levels of the nucleolar marker fibrillarin (*fib-1*) and to an increased nucleolar area. These nucleolar phenotypes are accompanied by the abolishment of lifespan extension in the major longevity pathways. However, the molecular connection between *ncl-1*, nucleolar function and longevity remains elusive.

To identify molecular players and pathways that mediate the function of *ncl-1* on longevity, I performed transcriptomic and proteomic analysis, comparing wild-type worms to *ncl-1* worms in normal as well as the long-lived *glp-1* background. This analysis revealed some shared and some background-specific regulation of distinct biological pathways upon loss of *ncl-1*: While nuclear outputs such as ribosome biogenesis and rRNA production are increased in multiple tested genotypes, proteasomal components are decreased in *ncl-1* single mutants, while lysosomal components show lower abundance in *glp-1;ncl-1*. Interestingly, NCL-1 seems to affect at least a portion of regulated genes through direct binding of respective mRNAs. Based on transcriptomic and proteomic data, I conducted a follow-up RNA interference screen of potential mediators and uncovered nucleolar downstream processes of *ncl-1* including the RNase P/MRP complex and mitochondrial translation. Knockdown of the shared RNase P/MRP component POPL-1 as well as other RNase P/MRP factors extended lifespan in *glp-1;ncl-1* mutants. The same was observed for other rRNA processing and ribosome assembly factors as well as proteins involved in mitochondrial translation such as MRPS-16. Reduction of *popl-1* and *mrps-16* extended lifespan independent of nucleolar size, *fib-1* mRNA levels or steady state rRNA levels, thereby uncoupling nucleolar size from lifespan for the first time. Also, overall translation rate seems unaffected. Thus, the effect of NCL-1 on lifespan may

be mediated through altered ribosome assembly in *glp-1* worms, while being unaffected in the N2 background.

To further investigate the molecular mechanism of NCL-1 action, I conducted a Yeast-2-Hybrid assay and pulldown experiments to identify NCL-1 protein interactors. In a mini RNAi screen, I found that a reduction of the potential NCL-1 interactor and proteasomal factor RPN-11 affects nucleolar size in *glp-1* mutants, indicating a direct connection of NCL-1 to the proteasome. In line with this, *ncl-1* affects cellular proteostasis with the proteasome as a presumable key player, as *ncl-1* mutants are short-lived under modest thermal stress and are less motile. In addition, I observed that overall ubiquitylation levels are increased, and that proteasome substrates accumulate in *ncl-1* mutants.

In the pulldown experiments with NCL-1, I identified several mitochondrial factors in the co-enriched fraction of NCL-1. I also found that NCL-1 forms round network-like structures and strong foci resembling mitochondria within the hypodermis and muscle, further supporting a mitochondrial connection.

Further on I established a connection between the RNAi machinery, nucleolar size and lifespan with a central focus on the argonaut protein NRDE-3 being required for longevity and affecting nucleolar size.

Using a range of genetic and biochemical approaches, I found that *ncl-1* is a multifaceted gene that connects multiple important cellular pathways with a focus on nucleolar outputs, but also proteolytic processes. I identified the RNase P/MRP complex and mitochondrial translation as potential key processes for mediating the function of *ncl-1* in longevity.

Zusammenfassung

Der Nukleolus wird primär als Kontrollzentrum für die Assemblierung von ribonukleären Proteinen und rRNA-Synthese beschrieben. Es gibt jedoch immer mehr Hinweise darauf, dass der Nukleolus auch eine Rolle in der Protein-Qualitätskontrolle, der Genomstabilität und dem Zellzyklus spielt. Frühere Studien haben gezeigt, dass das B-Box Zinkfingerprotein NCL-1 eng mit der nukleolären Funktion verknüpft ist und dass sein Verlust zu erhöhten Leveln des nukleolären Markers Fibrillarin (*fib-1*) und zu einer Vergrößerung der nukleolären Fläche führt. Diese nukleolären Phänotypen gehen einher mit einer verkürzten Lebensdauer in den wichtigsten Langlebigkeitsmodellen. Der molekulare Zusammenhang zwischen *ncl-1*, der nukleolären Funktion und Langlebigkeit ist jedoch nach wie vor unklar.

Um die molekularen Akteure und Signalwege zu identifizieren, welche die Funktion von *ncl-1* auf Langlebigkeit vermitteln, führte ich eine Transkriptom- und Proteom-Analyse durch und verglich Wildtyp-Würmer mit *ncl-1*-Würmern - sowohl im normalen als auch im langlebigen *glp-1*-Hintergrund. Diese Analyse ergab einige gemeinsame und einige hintergrundspezifische Regulierungen verschiedener biologischer Signalwege und Faktoren in *ncl-1*-Mutanten: Während nukleoläre Outputs, wie die Ribosombiogenese und die rRNA-Produktion bei mehreren getesteten Genotypen erhöht waren sind die proteasomalen Komponenten bei einzelnen *ncl-1*-Mutanten vermindert, während die lysosomalen Komponenten in *glp-1;ncl-1* Würmern geringere Mengen aufweisen. Interessanterweise scheint NCL-1 zumindest einen Teil der regulierten Gene durch direkte Bindung der entsprechenden mRNAs zu beeinflussen. Basierend auf Transkriptom- und Proteom-Daten führte ich einen RNAi-Screen mit potenziellen Mediatoren durch und entdeckte nukleoläre Downstream-Prozesse von *ncl-1*, unter anderem den RNase P/MRP-Komplex und die mitochondriale Translation. Der Knockdown der gemeinsamen RNase P/MRP-Komponente POPL-1 sowie anderer RNase P/MRP-Faktoren verlängerte die Lebensspanne in *glp-1;ncl-1*-Mutanten. Dasselbe wurde bei anderen Faktoren der rRNA-Prozessierung und Ribosomen-Assemblierung sowie bei Proteinen beobachtet, die an der mitochondrialen Translation beteiligt sind, wie MRPS-16. Die Reduktion von *popl-1* und *mrps-16* verlängerte die Lebensdauer unabhängig von der nukleolären Größe, der

mRNA-Menge von *fib-1* oder den rRNA-Leveln und entkoppelte somit zum ersten Mal die nukleoläre Größe von der Lebensdauer. Auch die Translationsrate scheint unbeeinflusst zu bleiben. Daher könnte die Wirkung von NCL-1 auf die Lebensdauer durch eine veränderte Ribosomenanordnung in *glp-1*-Würmern vermittelt werden, während sie im N2-Hintergrund unbeeinflusst bleibt.

Um den molekularen Mechanismus von NCL-1 weiter zu untersuchen, führte ich einen Hefe-2-Hybrid-Assay und Pulldown-Experimente zur Identifizierung von NCL-1-Protein-Interaktoren durch. In einem Mini-RNAi-Screening stellte ich fest, dass eine Reduktion des proteasomalen Faktors und potenziellen NCL-1-Interaktors RPN-11 die nukleoläre Größe in *glp-1*-Mutanten beeinflusst, was auf eine direkte Verbindung von NCL-1 zum Proteasom hinweist. In Übereinstimmung damit beeinflusst *ncl-1* die zelluläre Proteostase mit dem Proteasom als mutmaßlichem Hauptakteur, da *ncl-1*-Mutanten unter mäßigem thermischem Stress kurzlebig und weniger beweglich sind. Darüber hinaus beobachtete ich, dass die Ubiquitylierung insgesamt erhöht ist und dass das genutzte *in vivo* Proteasom-Modell-Substrat in *ncl-1*-Mutanten akkumulierte. In den Pulldown-Experimenten mit NCL-1 identifizierte ich mehrere mitochondriale Faktoren in der ko-angereicherten Fraktion von NCL-1. Ich fand auch heraus, dass NCL-1 runde, netzwerkartige Strukturen mit starken punktuellen Fokuspunkten bildet, die den Mitochondrien in der Hypodermis und im Muskel ähneln, was eine mitochondriale Verbindung weiter unterstützt.

Weiterhin stellte ich eine Verbindung zwischen der RNAi-Maschinerie, der nukleolären Größe und der Lebensdauer fest, wobei der Schwerpunkt auf dem Argonaut-Protein NRDE-3 lag, welches für die Langlebigkeit in *glp-1*-Mutanten erforderlich ist und die nukleoläre Größe beeinflusst.

Mit Hilfe einer Reihe von genetischen und biochemischen Ansätzen fand ich heraus, dass *ncl-1* ein facettenreiches Gen ist, welches mehrere wichtige zelluläre Signalwege verbindet. Interessanterweise identifizierte ich den RNase P/MRP-Komplex und die mitochondriale Translation als potenzielle Schlüsselprozesse für die Vermittlung der Funktion von *ncl-1* auf Langlebigkeit.

Abbreviations

aa	Amino acid
ATP	Adenosine triphosphate
BCA	Bicinchoninic acid
BDR	Bacterial dietary restriction
bp	Base pairs
BSA	Bovine serum albumin
C	Celsius
<i>C. elegans</i>	<i>Caenorhabditis elegans</i>
CC	Cellular compartment
cDNA	Complementary DNA
CHX	Cycloheximide
CRISPR	Clustered Regularly Interspaced Short Palindromic Repeats
<i>D. melanogaster</i>	<i>Drosophila melanogaster</i>
DAPI	4',6-Diamidin-2-phenylindol
DFC	Dense fibrillar center
DIC	Differential interference contrast
DNA	Deoxyribonucleic acid
DR	Dietary restriction
dsRNA	Double-stranded RNA
DTT	Dithiothreitol
EM	Electron microscopy
EMS	Ethyl methane sulfonate
ER	Endoplasmic reticulum
EtOH	Ethanol
FC	Fibrillar center
FC	Fold change
GC	Granular component
GFP	Green fluorescent protein
GO	Gene ontology
h	Hours
IGF	Insulin growth factor
IP	Immunoprecipitation
IPTG	Isopropyl β -D-1-thiogalactopyranoside
ISR	Integrated stress response
ITS	Internal transcribed spacer
KEGG	Kyoto Encyclopedia of Genes and Genomes
LCS	Low complexity sequences
M	Molar
MF	Molecular function
min	Minutes

ml	Milliliter
mRNA	Massanger RNA
MS	Mass spectrometric
mtUPR	Mitochondrial unfolded protein respone
n	Nano
N2a	Neuro-2a
NGM	Nematode growth medium
NOR	Nucleolar organizer regions
ns	Not significant
OE	Overexpression
OP 50	E. coli strain OP50
PBS	Phosphate buffered saline
PCA	Principle component analysis
PCR	Polymerase chain reaction
Pol	Polymerase
PVDF	Polyvinylidenfluorid
Q1,2,3,4	Quadrant 1,2,3,4
qPCR	Quantitative polymerase chain reaction
rDNA	Ribosomal DNA
RISC	RNA-induced silencing complex
risiRNA	Ribosomal silencing RNA
RNA	Ribonucleic acid
RNAi	RNA interference
RNP	Ribonuclear protein
ROS	Reactive oxygen species
RPL	Large subunit ribosomal protein
rpm	Rounds per minute
RPS	Small subunit ribosomal protein
RQC	Ribosome quality control
rRNA	Ribosomal RNA
RT	Room temperature
SDS	Sodium dodecyl sulfate
sec	Seconds
Seq	Sequencing
siRNA	Silencing RNA
SNARE	N-ethylmaleimide-sensitive-factor attachment Receptor
snoRNA	Small nucleolar RNA
SRP	Signal recognition particle
TBST	Tris-buffered saline with Tween20
TOF	Time of flight
TOR	Target of rapamycin
tRF	TRNA-derived fragments

tRNA

U

UTR

UV

V

WT

Y2H

μ

°

Transfer RNA

Units

Untranslated region

Ultra violet

Volt

Wildtype

Yeast-2-Hybrid

Micro

Degree

Table of content

Introduction	1
1. <i>Aging research and its relevance for our society</i>	1
2. <i>C. elegans as a model organism</i>	2
3. <i>The genetics of aging</i>	4
3.1 Insulin signaling	4
3.2 Dietary restriction-mediated longevity	5
3.3 TOR longevity	5
3.4 Mitochondrial longevity	6
3.5 Gonadal longevity	7
4. <i>Convergent mechanisms of aging</i>	11
5. <i>The NCL-1 protein</i>	13
6. <i>The plurifunctional nucleolus</i>	16
6.1 The nucleolus – ribosomes and rRNA processing	17
6.2 The nucleolus – growth regulation and nutrient sensing in the context of aging	23
6.3 The nucleolus – protein folding in the context of aging	25
7. <i>Proteostasis during aging</i>	26
7.1 Protein biosynthesis during aging	26
7.2 tRNAs during aging	28
7.3 Ribosome quality control during aging	28
7.4 Protein folding during aging	29
7.5 Protein degradation during aging	29
8. <i>Stress Responses during aging</i>	31
<i>Aim of this study</i>	32
Results	34
<i>Chapter 1: NCL-1-dependent regulation of the RNase P/MRP complex and the mitochondrial ribosome link the nucleolus to lifespan control</i>	34
1. <i>NCL-1 alters transcriptomic and proteomic profile of nucleolar and mitochondrial gene products</i>	34
2. <i>Reduced RNase P/MRP activity and mitochondrial translation act downstream of ncl-1 to extend lifespan</i>	45
3. <i>popl-1 and mrps-16 act downstream of the nucleolus, uncoupling nucleolar size from lifespan</i>	51
4. <i>ncl-1 affects the translation machinery</i>	56
<i>Chapter 2: The molecular mechanism of NCL-1 action</i>	59
1. <i>NCL-1 is differentially expressed in different tissues and localizes to the outer mitochondrial membrane</i> ..	59
.....	63
2. <i>NCL-1 regulates nucleolar size cell non-autonomously</i>	64
3. <i>The RNA-binding activity of NCL-1 regulates nucleolar size</i>	66
4. <i>Protein-protein interactors of NCL-1</i>	68
4.1 A novel connection between the RNAi machinery, nucleolar size and lifespan	68
4.2 Unbiased identification of NCL-1 interacting proteins	71
5. <i>NCL-1 plays a role in cellular proteostasis</i>	74
6. <i>NCL-1 as check point for nucleolar size early in life</i>	77
Discussion	80

1. <i>ncl-1</i> affects the transcriptome and proteome dependent on the genetic background	82
2. <i>ncl-1</i> affects longevity via distinct nucleolar downstream processes	83
3. The RNase P/MRP complex and mitochondrial translation uncouple nucleolar size from longevity.....	88
4. The RNAi machinery as novel effector of the nucleolus and longevity	90
5. NCL-1 affects nucleolar size through direct binding to specific mRNAs.....	91
6. NCL-1 affects proteostasis through the proteasome	93
7. Summary.....	95
Future perspective	96
1. Further explore the link between the RNase P/MRP complex, nucleolar function and longevity.	96
2. Investigate how nucleolar size and <i>ncl-1</i> affect the ribosome.....	97
3. Explore the effect of <i>ncl-1</i> on mitochondrial biology	98
4. Deepen our understanding of the connection between <i>ncl-1</i> and proteostasis with special focus on the proteasome.....	99
5. Uncover and verify NCL-1 interactions on RNA and protein level.....	100
6. Further study the non-autonomous and tissue-specific effects of NCL-1.....	101
7. Transfer our knowledge about <i>ncl-1</i> -dependent regulation of nucleolar function and lifespan to higher organisms	101
8. Investigate nucleolar composition and size with aging	101
Material and Methods.....	103
1. <i>C. elegans</i> genetics and handling.....	103
1.1 Worm growth, maintenance.....	103
1.2 Worm synchronization.....	103
1.3 RNAi treatment	104
1.4 Genotyping	104
1.5 Lifespan analysis	104
1.6 Worm microscopy.....	105
1.7 Confocal imaging.....	105
1.8 Worm size measurements	106
1.9 GFP intensity quantification via copas biosorter	106
1.10 Motility assays	106
2. Molecular biology	107
2.1 RNA extraction	107
2.2 qPCR analysis	108
2.3 RNA-Sequencing	108
2.4 NCL-1-binding motif analysis	109
2.5 Molecular cloning	109
3. Biochemistry	110
3.1 Western Blot analysis.....	110
3.2 Puromycin incorporation assays	111
3.3 rRNA measurements	111
3.4 Immunoprecipitation (IP).....	112
3.5 Whole worm proteomics and IP candidate identification	113
3.6 Ribosome profiling.....	115
4. Cell culture	116
4.1 Transfection	116
4.2 Immunostaining	117
5. Statistical analysis	118

6. Software	118
Supplementary tables	119
References	123
Appendix	139
Acknowledgements	171
Work contributions	172
Erklärung	173
Curriculum vitae	174

Introduction

1. Aging research and its relevance for our society

Aging is defined as a time-dependent progressive decline of physiological and cellular functions. This implies an increasing susceptibility to infections, a decline in bone structure, a decline in sight, lowered regenerative capacity and an increase in cancer rate, among others (J. P. Liu 2014; López-Otín et al. 2013a). A main task for our future society and in particular science lies in understanding and defeating age-associated diseases such as Alzheimer's disease and Parkinson's disease, posing an increasing burden for all of us. Understanding the molecular basis of aging becomes a matter of increasing public interest – especially in the context of the current SARS Covid-19 pandemic, where the virus is primarily affecting individuals with higher age (Nikolich-Zugich et al. 2020). As our society is living longer and longer due to better medical care, safe supply of nutrients and better hygiene, aging phenotypes become more relevant in our daily life (United Nations Department of Economic and Social Affairs Population Division 2017).

For a long time, aging has been thought of as a general but random and therefore unstoppable process that accompanies us throughout our life. However, recent scientific discoveries clearly state that aging is not only a fine-tuned, regulated process but can also be slowed down and manipulated by either genetic or non-genetic interventions.

Over the last three decades, more and more resources were invested in understanding the underlying molecular processes of how we age. This resulted in a massive growth of knowledge, and the discovery of distinct hallmarks for aging and genetic regimes (López-Otín et al. 2013b). By definition, those hallmarks meet following criteria: Manifestation throughout aging, an increased aging rate through disturbance of the hallmark and healthier aging by triggering the hallmark processes. López-Otín *et al.* defined nine major hallmarks of aging, namely genomic instability, telomere attrition, epigenetic alterations, altered intracellular communication, stem cell exhaustion, cellular senescence, mitochondrial dysfunction, deregulated nutrient sensing and loss of protein homeostasis. Extensive research is carried out in all nine disciplines, slowly

completing our understanding of the underlying molecular mechanisms of aging. A better understanding of the involved pathways and signaling cascades will enable us to treat and potentially at some point to heal age-related diseases.

2. *C. elegans* as a model organism

Considering the relatively short existence of aging research, *C. elegans* has a long-lasting history in the field. Groundbreaking discoveries have been made and key pathways have been found or characterized using *C. elegans* as a model organism. The primary habitat of the nematode is soil and one can find it in all temperate climate zones. Sidney Brenner was the first to establish *C. elegans* as a laboratory model organism in the 70th (Brenner 1974). In particular for aging research, *C. elegans* is a very valuable model organism due to its very short lifespan of ~15 days combined with powerful genetic tools.

In adult state, *C. elegans* is roughly 1 mm long. Under lab conditions, hundreds of worms are living on an agarose layer inside a petri dish, with a lawn of bacteria serving as food. This makes *C. elegans* a very cost-effective model, enabling researchers to work with huge population sizes. In addition, the 3-day life cycle of *C. elegans* allows for growing and expanding populations in a time-efficient manner. *C. elegans* is a self-fertilizing hermaphrodite - therefore crossing different strains is fairly easy and epistasis experiments can be performed very fast and efficiently. *C. elegans* consists of 959 somatic cells, which enabled scientists to trace and document the development of each single cell over the worm's development (Sulston et al. 1983; Sulston and Horvitz 1977). The transparent nature of *C. elegans* makes it possible to easily take images also of internal structures, and makes it suitable for easy use of fluorescent tags. *C. elegans* was the first model organism with a completely sequenced genome, encoding for > 20.000 genes (Consortium, 1998).

Over the years it became clear that probably the greatest strength of the nematode is the possibility to use it for genetic screens. In 2006, Andrew Fire and Craig C. Mello were awarded the Nobel prize for the discovery of RNA interference (RNAi), which was first discovered in *C. elegans* (Fire et al. 1998). RNAi is a mechanism in which

organisms reduce the expression of certain genes upon stimulation with double-stranded RNA directed against these particular genes. Conducting RNAi experiments in *C. elegans* is strikingly easy, as it is possible to simply feed the worms with bacteria producing double-stranded DNA coding for the gene of interest - leading to a significant and fast reduction of its expression. RNAi can be used to perform high-throughput genetic screens (Boutros and Ahringer 2008; Murphy et al. 2003; Rual et al. 2004), where a whole library of genes is screened for phenotypes.

In addition, it is possible to perform EMS-based whole genome mutagenesis screens. EMS is a mutagenic compound that randomly mutates amino acids over the whole genome (Flibotte et al. 2010). Mutants with a distinct phenotype can then be picked and latest technology of whole genome sequencing and analysis software allow for clear identification of causative genes.

In the last years, *C. elegans* has also been used as a model for tissue-specific studies. Easily distinguishable tissues are however limited to gut, neurons, muscle, oocytes and hypodermis (Burkewitz et al. 2015; Y. Zhang et al. 2019).

3. The genetics of aging

For many years, scientists believed that aging is simply a passive decline of cellular and macroscopic features over time. However, intensive research throughout the last 40 years clearly demonstrated a fine-tuned molecular regulation of several aging-associated processes via specific pathways. We are now aware of not only one, but several genes, pathways and processes that can specifically affect lifespan and health span in a positive or negative manner.

Most groundbreaking discoveries on that field have been made in small model organisms such as yeast, *C. elegans* or *D. melanogaster*. However, it turned out that many findings are transferable also to higher organisms such as fish, rodents and even humans.

3.1 Insulin signaling

The first gene that has been described being linked to an extraordinary long life was the *daf-2* gene in *C. elegans*. Worms harboring a hypomorphic mutation, resulting in a partial loss of function in this particular gene, live up to impressive 100% longer than wildtype worms (Kenyon et al. 1993; Kimura et al. 1997). The *daf-2* gene codes for the insulin receptor in *C. elegans* but is conserved up to humans. Up to now, it has been shown that the insulin receptor can affect lifespan in several other organisms than *C. elegans* – including flies and rodents. There is also evidence for a human connection, in form of distinct DNA variants accumulating in exceptionally long-lived individuals (Pawlikowska et al. 2009; Suh et al. 2008). Another interesting finding has been made in dogs, where the inverse correlation of body weight and lifespan has been linked to specific mutations in the insulin receptor (Greer, Hughes, and Masternak 2011).

A few years after the discovery of the insulin signaling-longevity connection, *daf-16* was discovered as the downstream effector of *daf-2* by showing that *daf-2* longevity completely depends on this transcription factor. Under normal conditions, *daf-16* is phosphorylated and localizes to the cytosol. Upon mutation of the *daf-2* receptor, this phosphorylation is removed, which enables *daf-16* to shuttle into the nucleus where it activates certain genes triggering pro-longevity signaling pathways, among others (Lin et al. 1997; Ogg et al. 1997).

Over the years, researchers were able to identify additional key components of the pathway, where modulation results in an extended health- and/or lifespan (Hsu, Murphy, and Kenyon 2003; Murphy et al. 2003; Tepper et al. 2013; Tullet et al. 2008).

3.2 Dietary restriction-mediated longevity

Some *C. elegans* mutants such as *eat-2* confer their lifespan-extending effect through the mechanism of dietary restriction (DR). The connection between DR and longevity has already been described over 80 years ago, when McCay *et al.* showed that caloric restriction reduced body weight of rats and extended lifespan, while keeping growth potential for a much longer time than control animals (McCay et al., 1935). Next to a direct effect on lifespan, DR can delay the onset of age-associated diseases such as cardiovascular diseases, cancer and brain atrophy. A unique selling point of DR is the fact that it is highly reproducible up to primates, which show reduced incidence of diabetes, cancer, cardiovascular disease, and brain atrophy as well as slower aging upon 10-30% caloric restriction (Colman et al. 2009). Intriguingly, in a cohort of human volunteers undergoing caloric restriction, DR reduced the risk of suffering from cardiovascular diseases and cancer (Fontana et al. 2011). At the current state of knowledge, DR is one of the most interesting and intensively studied anti-aging interventions, as it is easily applicable and appears to be conserved up to humans. The downside of DR is a strong limitation of life quality. It is therefore important to uncover the underlying molecular mechanisms in the context of DR-mimicking drugs, which could be used as an anti-aging treatment in the future (Chiba et al. 2010; S. H. Lee and Min 2013).

3.3 TOR longevity

mTOR longevity is one of the most studied lifespan-extending regimes. mTOR is central to several aging-associated processes such as mitochondrial function, autophagy, immunity, cellular senescence, stem cell regulation and protein homeostasis (proteostasis) (Kapahi et al. 2010; Kolesnichenko et al. 2012; Morita et

al. 2015; Murakami et al. 2004; Vlahakis, Lopez Muniozguren, and Powers 2017; X. Wang et al. 2001; Weichhart et al. 2008).

mTOR functions as an intracellular amino acid and nutrient sensor, modulating the metabolism of the cell. Reduced mTOR signaling and knockdown of its components extend lifespan in worms, flies and mice (Harrison et al. 2009; Kaeberlein et al. 2005; Kapahi et al. 2004; Sheaffer, Updike, and Mango 2008; Vellai et al. 2003). This beneficial effect on lifespan is partially independent of the insulin signaling pathway in *C. elegans*, but depends on the availability of the transcription factors *pha-4* and *hif-1* as well as the heat shock factor *hsf-1*. The effect on longevity is however also mediated through regulation of *daf-16* and the proteostasis regulator *skn-1* (Robida-Stubbs et al. 2012). The lifespan-extending effect of reduced mTOR signaling is mainly conferred through the activation of S6 kinase and the following inhibition of 4E-BP (Syntichaki, Troulinaki, and Tavernarakis 2007). Loss of S6 kinase itself is sufficient to extend lifespan in worms, and interestingly results in a similar transcriptional profile as DR animals, suggesting a connection between both regimes (Selman et al. 2009). In line with this, DR longevity is TOR-dependent (Hansen et al. 2007).

The downstream effect of mTOR on lifespan is most likely mediated through changes in the cellular degradation and recycling processes, such as autophagy and the regulation of overall translation on the one hand, and the modulation of specific mRNA translation on the other hand (Papadopoli et al. 2019).

The drug rapamycin directly targets TOR and extends life- and health span in several model organisms from yeast to mammals. It is therefore proposed as one of the most promising anti-aging drugs (Bjedov et al. 2010; Harrison et al. 2009; Powers et al. 2006; Robida-Stubbs et al. 2012).

3.4 Mitochondrial longevity

TOR is closely linked to cellular metabolism - like the mitochondria, the powerhouse of the cell. Contrary to the original expectations, a mild reduction of mitochondria respiration results in an extended lifespan in worms, flies and mice (Copeland et al.

2009; Dell’Agnello et al. 2007; Pospisilik et al. 2007). It has also been demonstrated that a mutation in the mtDNA and electron transport chain components can extend replicative lifespan in yeast (B. Hwang, Jeong, and Lee 2012). One of the first discovered long-lived mutants was *clk-1*. *clk-1* worms harbor a mutation in the ubiquinone biosynthesis protein COQ9, which is important for mitochondrial respiration (Ewbank et al. 1997; Felkai 1999; Kayser et al. 2004; Lakowski and Hekimi 1996). Also mutations in a component of complex III of the respiratory chain, *isp-1*, and in the mitochondrial NADH dehydrogenase *nuo-6* can extend lifespan in *C. elegans* (Feng, Bussi re, and Hekimi 2001; W. Yang and Hekimi 2010).

The connection between mitochondrial function and longevity is conserved over species. For example, a reduced expression of genes encoding components of the electron transport chain complexes I, III, IV and V extends lifespan in flies (Copeland et al. 2009). Furthermore, the heterozygous knockout of the *clk-1* mouse ortholog MCLK1 is sufficient to extend lifespan in mice (X. Liu et al. 2005). Moreover, interfering with the cytochrome c production by depleting SURF1, which is important for the biogenesis of cytochrome c oxidase, results in longevity in mice (Dell’Agnello et al. 2007). Although there is a clear connection between reduced mitochondrial function and longevity, there are examples in which interfering with players of mitochondrial respiration in turn results in a shortened lifespan. For instance, a mutation in the succinate dehydrogenase cytochrome b560 subunit of the mitochondrial respiratory chain complex II reduces lifespan in worms (Ishii et al. 1998).

Collectively, mitochondrial longevity depends on a fine-tuned regulation of mitochondrial and mitochondria-associated processes such as respiration rate, mitochondrial morphology, translation and mitochondrial stress pathways (Brand 2014; Bratic and Larsson 2013).

3.5 Gonadal longevity

Gonadal longevity is a central aspect of this thesis, as most experiments on longevity were conducted in a germline-less background.

Genetic or physical removal of the proliferating germline extends lifespan in *C. elegans*. This effect however is specific to the elimination of the germ cells and is reversed once also the somatic gonad gets removed (Hsin and Kenyon 1999).

A widely used genetic model for germline removal is the *glp-1* system, which extends worm lifespan to about 60%. Throughout development, the distal tip cells of the somatic gonad release a gonad proliferation signal that is received by a germline receptor coded by the *glp-1* gene. A knockout of the *glp-1* gene therefore interrupts this soma-germ cell signaling cascade, resulting in long-lived worms lacking a germline. Accordingly, over-proliferation achieved by a *gdl-1* knockout leads to a lifespan shortening, tying the regulation of lifespan closely to the germline (Arantes-Oliveira et al. 2002).

The germline does not only affect lifespan in worms but its loss also extends lifespan in *D. melanogaster* via the insulin signaling pathway, by increasing FOXO and 4E-BP, indicating an underlying conserved signaling cascade (Flatt et al. 2008).

Interestingly, gonadal longevity has also in *C. elegans* been linked to insulin signaling as *glp-1* longevity is, among others, *daf-16*-dependent (Arantes-Oliveira et al. 2002).

Besides *daf-16*, also the transcription factors *daf-12* as well as its ligands *hsf-1*, *pha-4*, *nhr-80*, *tcer-1* and *skn-1* are required for the extended lifespan of *glp-1* mutants (Gerisch et al. 2001; Ghazi, Henis-Korenblit, and Kenyon 2009; Hansen et al. 2005; Lapierre et al. 2011; Steinbaugh et al. 2015; Yamawaki et al. 2010). All those factors are involved in the insulin signaling pathway, closely linking insulin signaling and gonadal longevity.

Although *daf-12* mediates its effect on gonadal longevity partially through *daf-16* target regulation, it has been shown to regulate also a *daf-16*-independent subset of genes - suggesting an additional, insulin-independent mechanism (Yamawaki et al., 2010).

Growing evidence supports a close connection between germline signals and fat metabolism, for example represented in the dependency of gonadal longevity on *lipl-4*, the ortholog of human LIPN, and *fat-5* (Goudeau et al. 2011; M. C. Wang, O'Rourke, and Ruvkun 2008). *lipl-4* codes for a triglyceride lipase, a key enzyme of lipid hydrolysis in *C. elegans*, and is increased in germline-less animals. Different genetic interventions such as loss of *glp-1*, *glp-4* and *lag-2* lead to a decreased fat storage whereas the

overexpression of GLP-1 increased fat by a factor of 1.7. *glp-1* worms treated with *lipl-4* RNAi exhibit increased fat content and the longevity is abolished, indicating a direct connection between fat metabolism and gonadal longevity (Wang, O'Rourke and Ruvkun, 2008). The fatty acid desaturase FAT-5 exhibits a similar pattern, being increased in germline less animals and required for their longevity. Its effect on lifespan is however completely independent from *daf-16* and depends on *daf-12*, presenting a second independent mechanism linking fat metabolism, the gonad and aging (Goudeau *et al.*, 2011).

More recent studies show a connection of gonadal signals and the immune regulator *irg-7* in *C. elegans*. Upon RNAi knockdown of *irg-7*, the longevity of *glp-1*, but not of DR worms or *daf-2* mutants, is completely abolished, indicating a specific implication of immunity downstream of germline signaling (Yunger *et al.* 2017).

An additional link has been established with the mitochondrial unfolded protein stress response (mtUPR) with special implication of ROS production. In worms, loss of germline leads to a *kri-1*-dependent increase of ROS and H₂S levels. The increase on ROS activates the mtUPR, whereas H₂S triggers the expression of a *skn-1*-dependent gene set resulting in an extended lifespan and a balance of redox species. *glp-1* longevity is abolished upon loss of *ubl-5* or *dve-1*, important factors regulating the mtUPR, as well as supplementation with the antioxidant Vitamin C, suggesting a causal connection between gonadal longevity and the *kir-1*-dependent signaling cascade (Wei and Kenyon 2016).

A recent *C. elegans* study from 2020 shows a dependency of gonadal longevity on the endogenous RNAi machinery. *glp-1* longevity requires not only the activity of the RNAi key enzyme *dcr-1*, but also several other components of the RNAi machinery. The effect on lifespan is dependent on an endo-siRNA-regulated tyrosine kinase which in turn affects *hsf-1* activity, closely linking gonadal longevity to *hsf-1* proteostasis with the endo-siRNA machinery as a key mediator (Cohen-Berkman *et al.*, 2020).

Gonadal longevity does not only depend on endo-siRNAs but apparently also on specific miRNAs. *glp-1* longevity is at least partially dependent on members of the miR-58 family, although the mechanism is probably insulin pathway-dependent (Z. Zhang *et al.* 2018).

Most studies on gonadal longevity have been conducted in simple model organisms such as *C. elegans* and *D. melanogaster*. However, also the removal of flower in plants extends lifespan (Leopold, Niedergang-Kamien, and Janick 1959). The connection between the germline and lifespan is probably conserved also in higher organisms, as transplantation of young ovaries extends the lifespan of female mice (Mason et al. 2011) and aging may be controlled by specific growth hormones from the germline (G. Zhang et al. 2013). The conservation of this link is further supported by the fact that several long-lived mouse models exhibit a reduced fertility or less progeny (Bartke and Brown-Borg 2004; Holzenberger et al. 2003).

4. Convergent mechanisms of aging

Lifespan can be extended by genetic changes, drug treatments, microbiota modulations or changes of environmental influences. Many of those interventions are known to work through a handful of pathways and mechanisms, such as insulin or TOR signaling or also the modulation of protein homeostasis or the immune system. However, the overarching network of lifespan regulation is still not completely understood. Interestingly, over the last years several processes and factors have been linked to not only one or two, but several of those lifespan-extending regimes. This led to the hypothesis that there must be common convergence points for longevity in form of master regulator factors or processes. A characterization of those nodal points could not only deepen our understanding of the aging process, but also constitute important targets for drug treatments against age-related diseases.

One of those branch points is autophagy, the recycling and degradation of dysfunctional or unnecessary proteins with help of membrane-wrapped autophagosomes. Autophagy is required for DR longevity, insulin longevity and also TOR longevity in different model organisms (Bjedov et al. 2010; Lapierre et al. 2011; Meléndez et al. 2003; Panowski et al. 2007). Furthermore, TOR longevity is closely linked to not only autophagy but also to lipid metabolism. For example, *lip1-4* is a downstream effector of TOR and is required for autophagy induction. Autophagy at the same time is required for lipolysis, tightly linking those two processes (Lapierre et al. 2011). Also in mammals there is an existing link between autophagy and lipid metabolism (Sardiello et al. 2009; Settembre et al. 2011, 2013; Singh et al. 2009).

Autophagy however by itself is not extending lifespan (Hansen et al. 2008). Two important transcription factors required for autophagy are *pha-4*/FOXO and *hlh-30*/TFEB. *pha-4* is the ortholog of the fork head transcription factor FOXO2 and exhibits sequence-specific DNA-binding activity. The autophagic response upon DR is *pha-4*-dependent and the factor is required not only for DR longevity, but also for TOR and germline longevity in worms (Hansen et al. 2008; Lapierre et al. 2011; Sheaffer, Updike, and Mango 2008). The link between TOR longevity, autophagy and *pha-4* has

been deeply investigated and it has been suggested that TOR and *pha-4* antagonize each other to regulate adult lifespan (Sheaffer, Updike, and Mango 2008).

The *C. elegans* TFEB ortholog HLH-30 is required for longevity in not only one, but several longevity regimes. The long-lived *eat-2*, *glp-1*, *daf-2*, *ckl-1* and *rsks-1* mutants show increased nuclear localization of HLH-30 and longevity is either completely or partially abolished in *hlh-30* double mutants. As DR mice also possess increased nuclear localization of TFEB, the mechanism of regulation may even be conserved in higher organisms (Lapierre et al. 2013).

Moreover, a decreased translation rate is sufficient to extend lifespan in worms. This is not only true for cytosolic translation, but also reduction of mitochondrial translation via knockdown of the mitochondrial ribosome subunit MRPS-5 extends lifespan (Houtkooper et al. 2013). Although loss of *mrps-5* induces the mtUPR, the lifespan effect is solely dependent on HLH-30 (Y. J. Liu et al. 2020).

In addition, our lab discovered the MML-1/MXL-2 transcription factor network as an important convergence point for longevity. Both transcription factors are required for lifespan extension induced by germline removal and reduced TOR signaling, insulin signaling and mitochondrial activity. In germline less worms, MML-1 accumulates in the nucleus and mediates its effect on lifespan through a downregulation of TOR via the leucyl-transfer RNA *lars-1* and modulation of HLH-30 activity. Interestingly, both transcription factors, HLH-30 and MML-1, work interdependent and regulate each other (Nakamura et al. 2016). Chip-Seq data shows that factors of the *mml-1/mxl-2* transcription factor network share common DNA targets with HLH-30 and PHA-4, which could explain the functional interconnections of many longevity regimes and the apparently encompassing effect on longevity (Johnson et al. 2014; O'Rourke and Ruvkun 2013).

Up to that point, most convergence points for longevity were dependent on specific transcription factors. However, our lab recently discovered the cytosolic zinc finger protein NCL-1 as additional master regulator for longevity. Loss of *ncl-1* either partially or completely abolishes *daf-2*, *eat-2*, *glp-1*, *ifg-1*, *mTOR* and *isp-1* longevity. *ncl-1* is a known regulator of nucleolar size. In line with this, small nucleolar size is a common

feature of various longevity regimes in worms, flies and mice. Furthermore, nucleolar size at day 1 of adulthood is predictive for individual lifespan in the worms, presenting the nucleolus as a potential biomarker for aging and a potential target for anti-aging treatments (Tiku et al. 2017).

5. The NCL-1 protein

The *ncl-1* gene has primarily been described in the context of an EMS screen, where its loss was found to increase nucleolar size in neurons, muscle cells and the hypodermis. No effect though was observed in the intestine and germline, where nucleoli are naturally large (Hedgecock and Herman 1995). The effect of NCL-1 on the nucleolus goes hand in hand with the regulation of known nucleolar downstream processes such as rRNA biogenesis. *ncl-1* mutants possess up to 2 times the levels of rRNA compared to wildtype worms and show enlarged body and cell size as well as higher protein content. In wildtype embryos, where nucleoli are largest, the *ncl-1* levels are low, suggesting NCL-1 as a repressor of nucleolar size and nucleolar functions such as ribosome and rRNA biogenesis (Frank and Roth 1998).

Structurally, NCL-1 belongs to the NHL-family, harboring 6 NHL repeats at its N-terminus. A common feature of this family of proteins is the existence of a RING domain as well as one or two B-Box domains. NCL-1 contains a B-box 1 and a B-box 2 domain within its C-terminal region. The B-boxes and the NHL repeats are linked by a coiled coil region (Figure 1). NHL domains resemble WD-repeat domains which are mainly known for the capability of protein-protein interactions - which is why also the NHL domain of *ncl-1* was for a long time solely considered as a protein-protein interaction domain (Slack and Ruvkun 1998). However, recent discoveries suggest an RNA-binding activity of the NHL domain and a close connection between the regulation of NCL-1 and its RNA-binding activity (Yi et al. 2015).

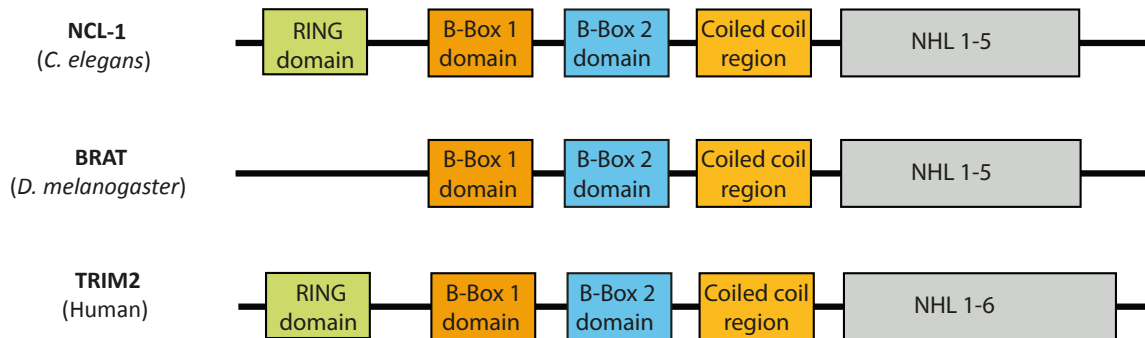


Figure 1. Domain structure of NCL-1 and the *D. melanogaster* and human orthologs BRAT and TRIM2. All three proteins include a B-Box 1 and B-Box 2 domain, followed by a coiled coil region. While NCL-1 and BRAT include 5 C-terminal NHL repeats, TRIM2 exhibits 6 NHL repeats. NCL-1 and TRIM2 show a RING domain at the N-terminus which has not been found in BRAT.

Little is known about the exact molecular mechanism of NCL-1 action. However, it has been shown that the extensively studied *D. melanogaster* brain tumor (*brat*) gene is a functional ortholog of NCL-1, as its expression in *C. elegans* rescues the nucleolar phenotype of *ncl-1* mutant worms. In addition, depletion of BRAT in cells results in increased nucleolar size and rRNA transcription, whereas the overexpression of BRAT shows the opposite phenotype (Frank, Edgar, and Roth 2002).

BRAT is known as a key regulator of proliferation and cell growth. It has been found to interact with the RNA-binding proteins NANOS and PUMILIO to specifically regulate hunchback (*hb*) mRNA in the fly (Sonoda and Wharton 2001). However, in addition to this combinatorial regulatory function, BRAT can also bind *hb* mRNA directly in a PUMILIO-independent manner. The interaction between BRAT and RNA is mediated through the six β -propeller shaped NHL repeat domains, exposing a positively charged top surface to the RNA (Loedige et al. 2014, 2015). Furthermore, several other BRAT mRNAs have been identified, suggesting that NHL family members affect several layers of regulation and pathways. The NHL domains of BRAT are conserved to ~80% and in vitro RNA-binding assays suggest the same RNA target motif for BRAT and NCL-1, suggesting a similar conserved function (Loedige et al. 2015).

Throughout development and cell divisions, the nucleolus undergoes a constant cycle of formation and collapsing (Hernandez-Verdun 2011). Investigation of transcript regulation during oogenesis has shown that ribosomal subunit mRNAs as well as rRNA-processing factor mRNAs and tRNA-processing factor mRNAs are strongly decreased in oocytes while NCL-1 levels are high. All of those mRNAs contain multiple copies of the NCL-1/BRAT RNA-binding motif TTGTT. Those transcripts are increased upon loss of *ncl-1*, suggesting that *ncl-1* destabilizes or deadenylates those transcripts during oogenesis (West et al. 2018).

The *ncl-1*-dependent regulation of nucleolar size is closely linked to the regulation of the nucleolar methyltransferase fibrillarin (FIB-1). Upon loss of *ncl-1*, *fib-1* transcript and protein levels are increased. Interestingly, the regulation of *fib-1* mRNA is 3'UTR-dependent and the *ncl-1* RNA-binding motif can be found several times within the *fib-1* 3'UTR, suggesting a direct regulation of *fib-1* mRNA. NCL-1 itself seems to be at least partially under the control of members of the *let-7* miRNA family, as mutation of the *let-7* binding site in the *ncl-1* 3'UTR results in mildly increased NCL-1 levels (Yi et al. 2015).

The functional axis of *ncl-1-fib-1*-nucleolar size has gained even more importance since *ncl-1* was discovered as a convergence point for longevity. Small nucleolar size is a hallmark of longevity and is observed in various longevity regimes, from worms up to mice. Upon loss of *ncl-1*, nucleolar size in long-lived *C. elegans* mutants increases and longevity is either partially or completely abolished (Tiku et al. 2017).

Whether the mechanism of *ncl-1* action is conserved also in higher organisms (other than worms and flies) still remains an open question. TRIM2 and TRIM3, both mammalian members of the NHL protein family, have been handled as the most promising orthologs of *ncl-1*/BRAT (Figure 1). However, the sequence conservation of the whole protein barely exceeds 30 % and several other TRIMs as well as other factors share similar motifs, suggesting that the (probably multiple) functions of *ncl-1* may have been distributed among a family of proteins throughout evolution.

6. The plurifunctional nucleolus

The nucleolus is a self-organizing system based on the localization of the transcription factor UBF which recruits RNA polymerase I. It forms around tandem repeats of rDNA loci and has been found in all eukaryotic species. Those repeated loci are called nucleolar organizer regions (NORs) of the chromosome. The single components of the nucleolus are held together by sol-gel phase transitions. Those are mediated by various weak binding interactions between intrinsically disordered low complexity sequences (LCSs), which are enriched in nucleolar RNA- and DNA-binding proteins (Frottin et al. 2019; Kato et al. 2012; Lam and Trinkle-Mulcahy 2015). The nucleolus as such is highly dynamic and undergoes complete breakdown followed by rapid reformation during cell division. Even during interphase, most nucleolar proteins do not permanently reside inside the nucleolus but shuttle between the nucleolus, the nucleus and the cytoplasm. This and the fact that a metabolically active cells needs to constantly produce thousands of ribosomes, makes the nucleolus one of the most transport activities-covering structure of the cell (D. Chen and Huang 2001; M. O.J. Olson and Dundr 2005; Phair and Misteli 2000).

The nucleolus is mostly known as a central hub for RNA polymerase I-dependent rRNA transcription and ribosome biogenesis. Based on EM pictures, the nucleolus can be divided into three sub-regions with different sub-processes. Several small, lightly stained regions represent the so-called fibrillar center (FC), where the rDNA is located. It is surrounded by the densely packed dense fibrillar components (DFC), and both are embedded in the granular component (GC) (Figure 2) (Shaw and Jordan 1995). For years, people believed that those visually distinguishable substructures are formed by pre-ribosomal particles in different stages. However, data from the last two decades suggests a much more differentiated composition and several additional nucleolar functions apart from ribosome biogenesis (Boisvert et al. 2007; M. O.J. Olson and Dundr 2005; Pederson 1998; Raška, Shaw, and Cmarko 2006; Rubbi and Milner 2003). Most of those comprise the maturation and processing of different RNA species and the assembly of ribonuclear complexes such as the signal recognition particle (SRP), the telomerase RNP as well as the processing of tRNAs and U6 small nuclear RNA. The nucleolus is involved in the regulation of cellular metabolism, telomere

length and cell cycle regulation, and has moreover been established as a central hub for the coordination of cellular stress responses and as a protein quality center with a particular role in aging (Boisvert et al. 2007; Boulon et al. 2010; Frottin et al. 2019; Mark O.J. Olson 2004; Pederson 1998; Raška, Shaw, and Cmarko 2006; Rubbi and Milner 2003; Tiku et al. 2017; Tsai and McKay 2002).

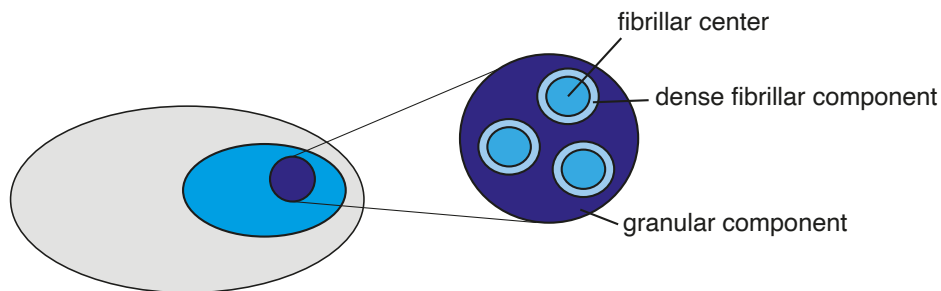


Figure 2. Nucleolar architecture. The nucleolus can be divided into three components. The fibrillar center is surrounded by the dense fibrillar component. Both are embedded in the granular component. Different steps of rRNA maturation take place at different locations within the nucleolus.

6.1 The nucleolus – ribosomes and rRNA processing

Ribosomes are one of the vital machineries in every living organism. Without ribosomes, the translation from mRNAs to proteins and therefore every step of cellular metabolism would be impossible. The ribosome consists of two different types of molecules - ribosomal proteins on the one hand and ribosomal RNAs on the other hand - which in combination form the functional ribonuclear protein complex, the ribosome. Every ribosome consists of about ~80 ribosomal proteins, of which most are highly conserved across organisms (Ben-Shem et al. 2010; Fox 2010). Ribosomal proteins are transcribed by RNA polymerase II and translated in the cytosol. From there, they are either relocated to the nucleolus, the nucleus or reside in the cytosol where they are added to the pre-mature ribosomes step by step (Figure 3).

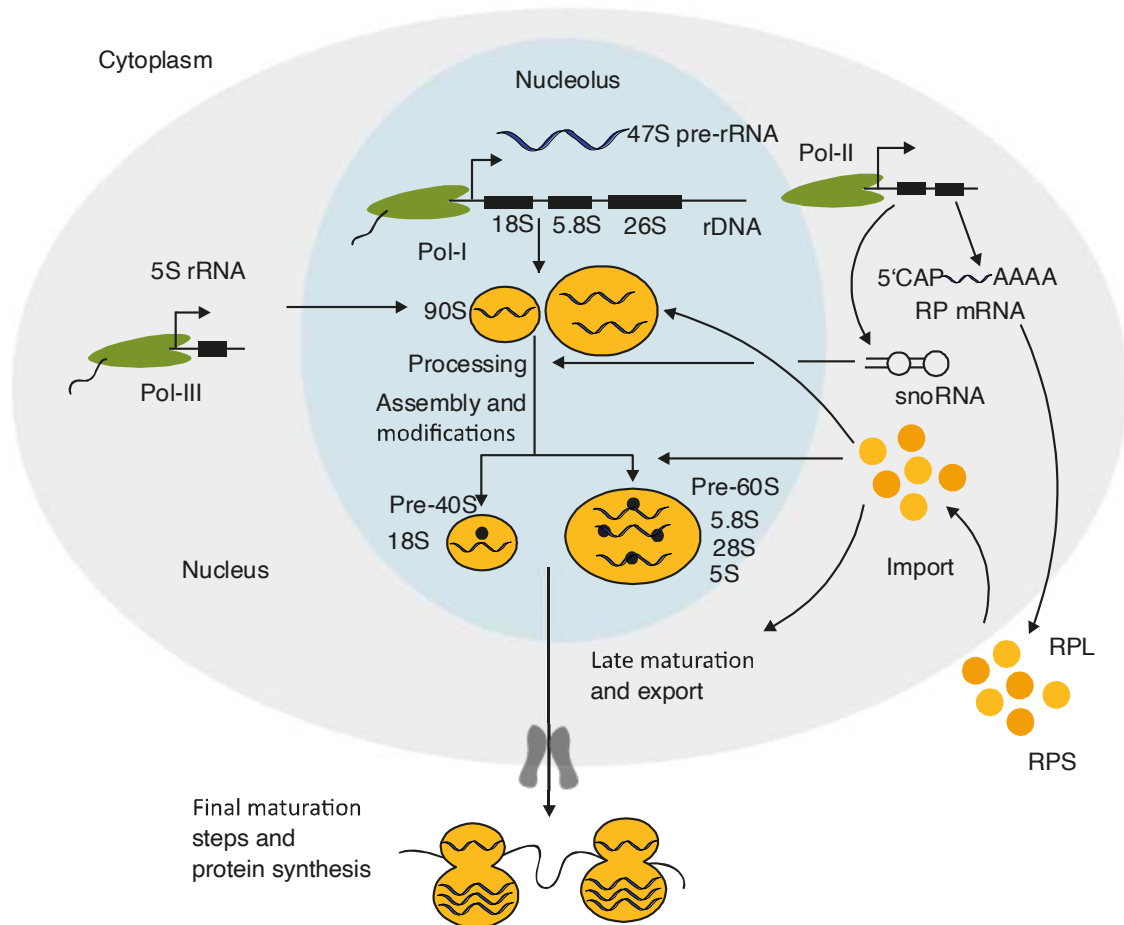


Figure 3. Schematic representation of ribosome biogenesis. The 47S rRNA precursor is produced inside the nucleolus by RNA polymerase I (Pol-I). The 47S rRNA precursor gets cleaved into 18S, 5.8S and 26S rRNA with several intermediates. The 5S rRNA is coded in the regular genome and gets transcribed by RNA polymerase III (Pol-III) and is subsequently imported into the nucleolus. Ribosomal protein (RP) genes are transcribed via RNA polymerase II (Pol-II) and are produced in the cytosol before they are reimported into the nucleus and the nucleolus. snoRNAs are also transcribed by RNA polymerase II in the nucleus and play an important role during various maturation steps. Several components are assembled within the nucleolus until the ribosomal pre-40S and pre-60S subunits are exported from the nucleolus for late maturation in the nucleus. Those next-stage pre-ribosomes are then exported to the cytosol, where final maturation takes place until the ribosome is functional and protein synthesis gets initiated. Adapted from Pelletier 2017, Nature reviews. (RPL = ribosomal proteins of large subunit, RPS = ribosomal proteins of small subunit, snoRNAs = small nucleolar RNAs)

The second component of the ribosome, the rRNA and its four forms, can be assigned into two different groups. 18S, 5.8S and 26/28S rRNA all arise from a long rRNA precursor that is transcribed in the nucleolus by RNA polymerase I. The 5S rRNA

though is coded outside the nucleolus in the normal genome under the transcriptional control of RNA polymerase III, which also transcribes tRNAs.

As mentioned above, the nucleolar coded rRNAs arise from the 45S precursor which consists of an external transcribed spacer region at the 5' and 3' end and the actual coding regions for 18S, 5.8S and 26S rRNA, separated by two internal transcribed spacer regions (Figure 4).

This precursor is then, with the help of numerous factors, cleaved into different precursor forms and finally the mature rRNAs in several steps. Although yeast has been the gold standard for examining rRNA processing, we also gained an increasing understanding of rRNA processing in higher organisms up to mammals. Unfortunately there is only little known about rRNA processing particularly in *C. elegans*, and besides a few experimentally confirmed snoRNAs and factors, all our knowledge is based on orthologs from other organisms (Hokii et al. 2010; Saijou et al. 2004).

However, studies conducted in yeast, frogs and mammals have shown that although there are differences, also broad similarities between those species exist, suggesting that we can utilize them for learning about rRNA processing in *C. elegans* (Borovjagin and Gerbi 1999; Dabeva et al. 1976; Loening, Jones, and Birnstiel 1969; Saijou et al. 2004; Udem and Warner 1973).

In mammals, the processing pathway branches after the endonucleolytic cleavage within ITS1 into the processing of the 18S rRNA and the 26S rRNA along with the 5.8S rRNA. The premature 40S particle containing the 18S rRNA is faster exported to the cytoplasm, while the pre-60S particle remains a bit longer in the granular component of the nucleolus (Hernandez-Verdun 2011). The composition of both premature particles is highly variable throughout maturation, and although large parts of the processing take place inside the nucleolus, it is continued in the nucleoplasm. Several exo- and endonucleases are involved in the processing procedure. One of those is the ribonuclear complex RNase P/MRP, which facilitates a certain step in 18S rRNA maturation in yeast and plays a role in human 18S rRNA processing (Goldfarb and Cech 2017; Mattijssen et al. 2011).

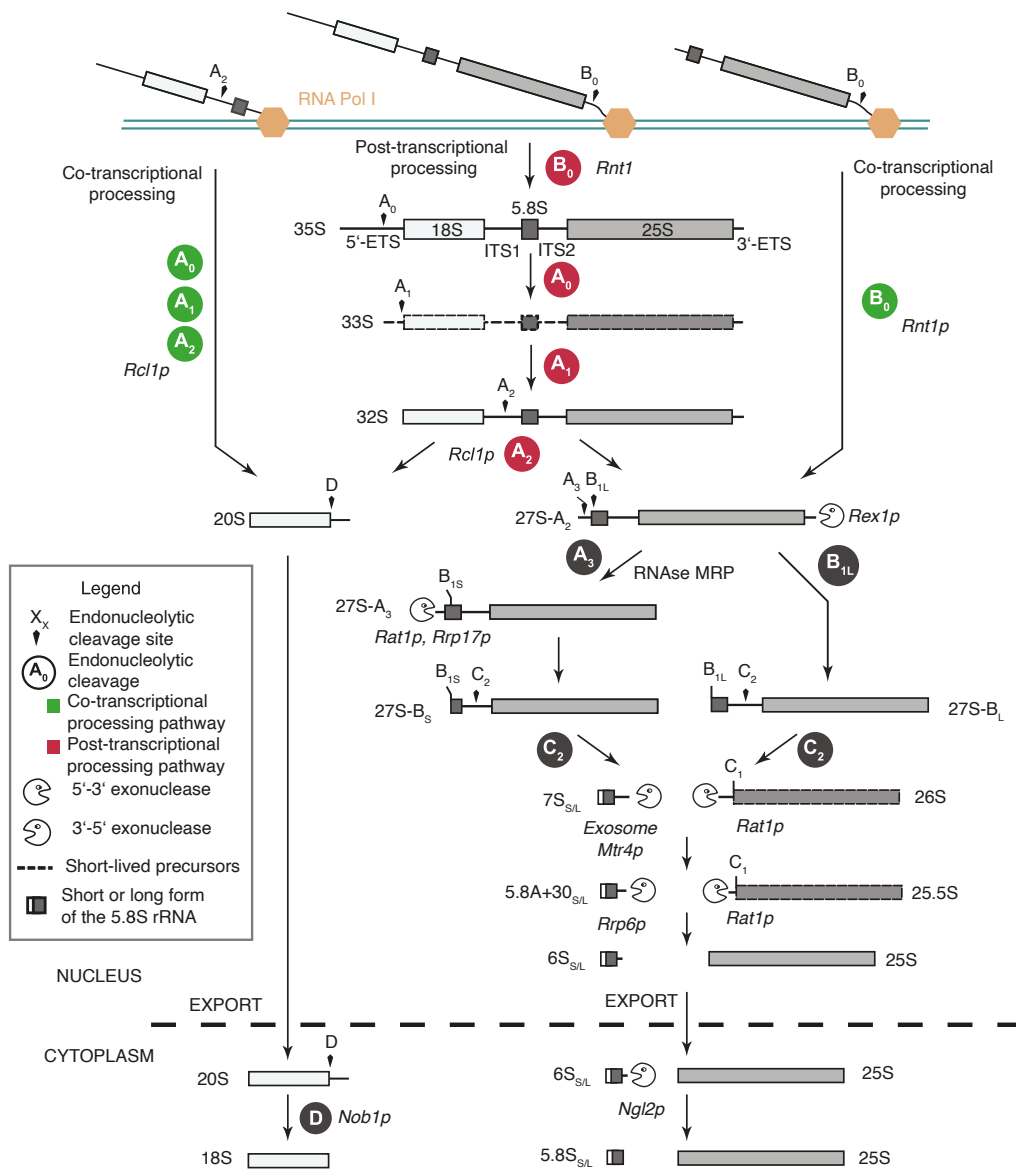


Figure 4. Pre-rRNA processing in yeast. Most rRNA transcripts are already processed co-transcriptionally by cleavage at sites A_0 , A_1 , A_2 and B_0 . Direct products are the 20S and 27S-A₂ pre-rRNAs (green, left and right side). A minority of transcripts, coming from the 35S pre-rRNA, is processed post-transcriptionally (red, middle). The last maturation step of the 20S precursor takes place in the cytosol after export of the pre-40S particle. Via an endonucleolytic cleavage by *Nob1p*, the 3' end gets removed yielding in the mature 18S rRNA. The maturation of the ribosomal large subunit components is split into two processing pathways which result in 25S and a long and a short version of 5.8S rRNA. The most abundant form is the short form which results from endonucleolytic cleavage of the 27S-A₂ pre-rRNA at site A_3 via *RNase MRP*, followed by exonucleolytic processing via *Rat1p* and *Rrp17p*. The final maturation of the 5.8S rRNA is executed in the cytosol by the exonuclease *Ngl2p*. The 25S and 5.8S precursor forms are cleaved at site C_2 before 25S rRNA maturation is finalized by cleavage at site C_1 and exonucleolytic removal of the 5' end in the nucleus. Adapted from Henras et al., 2015.

6.1.1 The RNase P/MRP complex

The RNase P/MRP complex is a key player in RNA processing, including the maturation of different rRNA species and in particular tRNAs. RNase P is a ribonuclear complex of ~410 kDa that was originally discovered processing the 5' leader of precursor tRNAs via its endonuclease activity (Altman and Smith 1971; Guerrier-Takada et al. 1983). The protein components of the RNase P complex assemble around a conserved RNA component essential for cleavage function. Interestingly, the RNA component duplicated throughout evolution, giving rise to the closely related RNase MRP (RNase for mitochondrial RNA processing) which shares a broad variety of protein components with the RNase P complex. The name MRP is misleading as the complex mainly localizes to the nucleolus, but it has firstly been discovered processing RNA primers for mitochondrial DNA replication. Indeed, both complexes do not only process one but several different species of RNAs, such as long non-coding RNAs, nucleolar and non-nucleolar coded rRNA, as well as specific mRNAs (Chamberlain et al. 1998; Fagerlund et al. 2015; Goldfarb and Cech 2017; Lygerou et al. 1996; Mattijssen et al. 2011; Noh et al. 2016; Saito et al. 2014). Probably based on the different RNA cores, both ribonuclear complexes possess different affinities towards pre-rRNA targets (Esakova and Krasilnikov 2010).

Processing such a broad variety of substrates, both complexes are implicated in several key processes of the cell such as chromatin remodeling, regulation of rRNA processing and ribosome biogenesis, as well as telomere length regulation. Besides others, the POP-1 component constitutes an obligatory but shared key component of the RNase P, the RNase MRP and the telomerase complex (Figure 5) (Jarrous 2002).

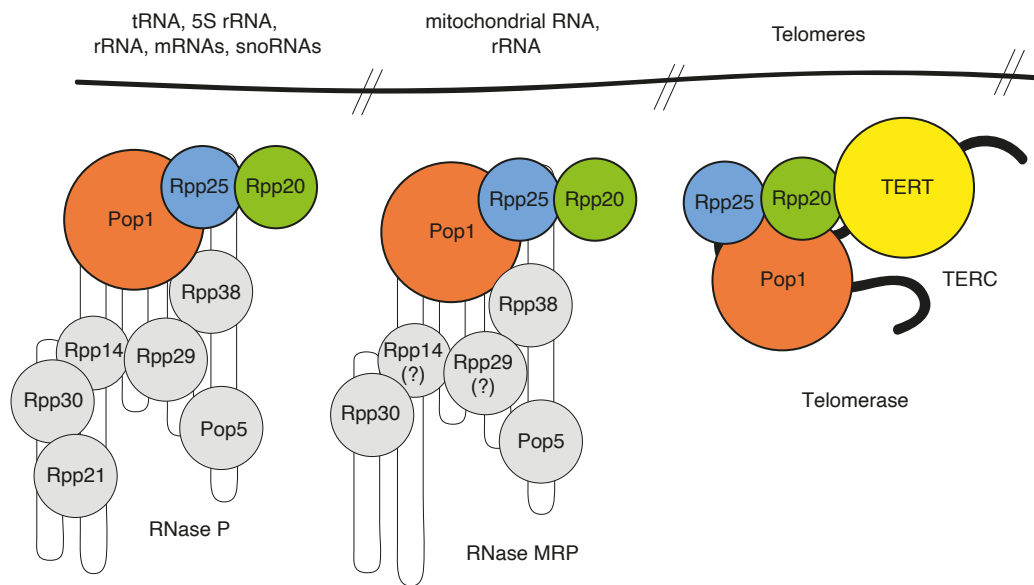


Figure 5. Shared components of the RNase P, RNase MRP and telomerase complex. Several protein components are shared between the RNase P, RNase MRP complex and the telomerase complex. The exact composition of all three complexes is still not completely explored. Distinct components such as Rpp21 have only been found in the RNase P complex. The RNase P and the RNase MRP complex bind different substrates and can be distinguished by their RNA component. Adapted from Esakova and Krasilnikov 2010; Jarrous 2017.

6.1.2 Protein synthesis at the ribosome

Protein synthesis is carried out by the ribosome and relies on a fine-tuned regulation on several levels. The translation process is divided into three stages: Initiation, elongation and termination. During the initiation phase, the 43S preinitiation complex assembles. It is consisting of the initiator Met-tRNA, members of the initiation factor families eIF2, eIF2B and eIF3, as well as the small 40S ribosomal subunit (Eliseev et al. 2018). The complex formation and stability are assisted by several additional factors. Mediated by members of the eIF4 family, the 43S complex then binds to the 5' cap structure of a mRNA. The scanning model then implies that the complex scans the mRNA until the Met-tRNA matches with a start-codon (Kozak 1989). This scanning process is poorly examined until now, but fits the existing data. Once the 43S complex found a start codon, it recruits the large 60S ribosomal subunit with help of members of the eIF-5 initiation factor family. All initiation factors then need to be released by

different mechanisms to result in a competent ribosome for translation elongation (Dever and Green 2012; Merrick and Pavitt 2018; Unbehaun et al. 2004).

A mature ribosome has 3 distinct sites - A=aminoacyl, P=peptidyl, E=exit. After the initiation, the Met-tRNA bound to the start codon is localized at the ribosomal P site. For the elongation start, an amino acid-loaded tRNA - the aminoacyl-tRNA - is delivered to the A site, assisted by the elongation factor eEF1A. eEF1A and its mitochondrial pendant EF-TU are active in a GTP-bound state and form the so-called ternary complex consisting of eIF2, GTP and the aminoacyl-tRNA. Binding of the aminoacyl-tRNA to its corresponding codon then induces the hydrolysis of GTP and the release of eEF1A. A key process during elongation is the formation of a peptide bond between the peptidyl-tRNA and the aminoacyl-tRNA. The peptide bond formation process takes place in a very specific and conserved niche within the ribosome, shaped by the rRNA component (Dever, Dinman, and Green 2018). At the same time, the tRNA from the A site is transferred to the P site and forms the new extended peptidyl-tRNA. Both the A/P and the P/E translocation are dependent on the elongation factor eEF2. After the translocation, an uncharged tRNA is positioned in the E site and then released to the cytosol - there are some suggestions for the exact release process, but those are still under debate. The whole elongation process depends indirectly or directly on various additional elongation factors.

6.2 The nucleolus – growth regulation and nutrient sensing in the context of aging

Growth of a cell and ultimately an organism is a conglomerate of several biochemical processes and its rate is determined by available nutrients and energy. Growth is closely linked to the production of all cellular components, and the balance between growth and biosynthetic processes is tightly regulated.

The nucleolus is a key player in the regulation of cellular growth and metabolism (Tiku and Antebi 2018; Tsai and McKay 2002). Such measures are important in particular in cancer research, which is why the connection has intensively been studied in this context.

Focusing on the link between aging and growth, especially the nutrient sensing pathways of insulin signaling and TOR signaling are of particular importance. Both

pathways are closely linked and insulin growth factor (IGF) signaling affects RNA polymerase I-dependent rRNA transcription in a PI3K- and TOR-dependent manner (James and Zomerdijk 2004). Furthermore, this translocation of IRS1 to the nucleus correlates with high rRNA transcription levels (Tu et al. 2002).

A lot of studies linking nucleolar function, growth and longevity have a special focus on mTOR. mTOR in its function as nutrient sensor acts as a gatekeeper for the cellular energy balance and therefore also regulates protein biosynthesis. Both TOR itself and the TOR pathway component *ruvb-1* do not only affect lifespan, but modulate nucleolar size as well as protein biosynthesis (Sheaffer, Updike, and Mango 2008).

Another important player in cell growth regulation is the protein kinase AKT, which directly inhibits the mTOR complex. Interestingly, RNA polymerase I-dependent rRNA transcription is AKT-dependent not only through TOR, but also in an independent manner, demonstrating the multi-level interconnection between nucleolar function, cell growth and lifespan regulation (J. C. Chan et al. 2011).

TOR is a key interface between aging and metabolism and its genetic or drug-mediated inhibition extends lifespan (Evans et al. 2011). This effect is probably at least partially dependent on a reduced protein biosynthesis, which is affected on several levels. As described earlier, TOR does not only affect the phosphorylation of the ribosomal protein S6 through S6K, but also translation initiation through 4E-BP (Hansen et al. 2007; Pan et al. 2007; Selman et al. 2009; Syntichaki, Troulinaki, and Tavernarakis 2007). A modest downregulation of protein biosynthesis in general is linked to extended lifespan.

TOR does not only directly bind to the rDNA locus in yeast, but also controls rDNA and tRNA promoters in mammalian cells (Kantidakis et al. 2010; H. Li et al. 2006; Tsang, Liu, and Zheng 2010).

In an additional layer of regulation, TOR modulates RNA polymerase I transcription through the regulation of the transcription factor TIF-IA, which directly affects UBF activity. As described earlier, UBF is a key component in nucleolar formation and the induction of RNA polymerase I-dependent rRNA transcription (Grewal, Evans, and Edgar 2007; Mayer et al. 2004). This finding is supported by the observation that rapamycin directly affects the phosphorylation of the C-terminus of UBF and thereby reducing rRNA transcription (Hannan et al. 2003; Tuan, Zhai, and Comai 1999).

Also other growth regulating pathways such as EGF, ERK and TGF- β signaling have been linked to rRNA transcription and lifespan regulation (Augustin et al. 2017; Demontis et al. 2014; Iwasa et al. 2010; Okuyama et al. 2010; Stefanovsky et al. 2001). ERK1/2 for example directly affect rRNA transcription via phosphorylation of UBF (Stefanovsky et al. 2001). In the same line, an RNAi-mediated knockdown of *lip-1*, which is the MAPK phosphatase *C. elegans* ortholog, increases lifespan in a *skn-1* and *daf-16*-independent manner (Okuyama et al. 2010).

6.3 The nucleolus – protein folding in the context of aging

As mentioned above, loss of proper protein homeostasis is a hallmark of aging (López-Otín et al. 2013a). A myriad of factors are involved in the maintenance of proteostasis, acting in protein production, folding, modification, degradation and sorting. One complex with significant implication in protein folding is the signal recognition particle (SRP) complex - a ribonucleoprotein composed of several protein components and an RNA component. It is an important player in the co-translational targeting of proteins to the endoplasmic reticulum for folding. Interestingly, there is growing evidence that the SRP complex is assembled inside the nucleolus, as protein and its RNA components were transiently detected inside the nucleolus (Jacobson and Pederson 1998; Politz et al. 2000). Furthermore, protein sorting can directly affect lifespan as a reduction of the nascent polypeptide chain complex in *C. elegans* leads to mis-sorting of proteins and a short lifespan (Gamerding et al. 2015).

Moreover, recent discoveries suggest the nucleolus itself as a phase-separated protein quality compartment. The study shows that misfolded proteins are targeted to the nucleolus in a stress-dependent manner to be stored for subsequent degradation. Furthermore, irreversible aggregation is prevented by transient interactions with nucleolar proteins in the granular component. With a decline in stress, proteins are released and refolded in a HSP70-dependent manner (Frottin et al. 2019).

7. Proteostasis during aging

Properly folded proteins are crucial for a majority of cellular processes and the homeostasis of those proteins is key to our survival. Our body installed a fine-tuned system to ensure that proteins are properly folded, produced and degraded at the correct timepoints and localize where they are needed. This network is termed proteostasis network and comprises more than a thousand components. Misfunctions in this network are mostly detrimental and can lead to severe disorders and diseases. Decline of proteostasis is a major hallmark of aging and closely linked with the onset of several age-associated diseases such as Alzheimer's disease, cancer and Parkinson's disease (López-Otín et al. 2013a).

The proteostasis network can be divided into three major sections - protein synthesis and folding, conformational maintenance and protein degradation.

7.1 Protein biosynthesis during aging

As elaborated earlier, the biogenesis of proteins underlies a regulatory network of different layers. On the one hand, the decision whether and to which extent a protein is synthesized is regulated on transcriptional levels by transcription factors, chromatin state, DNA modifications and mRNA metabolism. On the other hand, the actual process of mRNA translation is affected by several initiation, elongation and termination factors as well as the ribosome, its biogenesis and its components. Several factors of this machinery are affected by progressing age. The underlying molecular mechanisms have not yet been studied in great detail.

However, in several model organisms from invertebrates to mice, rats and humans, it has been shown that the overall levels of protein biosynthesis get reduced during aging. While there is evidence that ribosomal components aggregate (Reis-Rodrigues et al. 2012), the overall translation rate seems to decrease (Connors, Poppi, and Cant 2008; Motizuki and Tsurugi 1992), suggesting a mis-regulation of both parameter throughout aging. In humans, the copy number of rRNA coding genes is decreased in older individuals (Malinovskaya et al. 2018). A change in translation or specific modifications of proteins with aging is not the same for all tissues, as translation in the

aging mouse brain is decreased by 15 % while translation rate in the liver was decreased by only 2 % (Mobley et al. 2017; Ori et al. 2015).

A modest downregulation of translation extends lifespan in *C. elegans* and knockdown of the 60S ribosomal subunit biogenesis extends replicative lifespan in yeast (Hansen et al. 2007; Pan et al. 2007; Steffen et al. 2008; Syntichaki, Troulinaki, and Tavernarakis 2007). Interestingly, also the knockdown of the nucleolar GTPase NOG-1 in *C. elegans*, being involved in 60S ribosome subunit biogenesis, increases lifespan whereas its overexpression makes the worms short-lived (Y. Il Kim et al. 2014). The connection of a reduced translation and health benefits at older age seems to hold true not only for *C. elegans* and yeast, but also for *D. melanogaster*. Overexpression of the ribosome biogenesis-regulating gene *mnt* in skeletal muscle results in lower levels of nucleolar proteins and rRNA, extended lifespan and resulted in an improved climbing ability (Demontis et al. 2014).

As mitochondria have their own ribosomes with distinct ribosomal proteins, we can distinguish between mitochondrial and cytosolic translation. However, it seems as if mitochondrial translation behaves in a similar way during aging, as it also decreases (Rooyackers et al. 1996). Even more interesting is the fact that knockdown of the mitochondrial translation machinery is not only sufficient to extend lifespan, but also affects cytosolic translation through inter-organellar crosstalk in *C. elegans* (Houtkooper et al. 2013).

Not only the structural components of the ribosome and its regulating factors, but also factors directly involved in protein synthesis have been associated with aging and lifespan (Curran and Ruvkun 2007; Hansen et al. 2007; Kaeberlein et al. 2005; Kapahi et al. 2004; Pan et al. 2007; Steffen et al. 2008; Syntichaki, Troulinaki, and Tavernarakis 2007; Tohyama, Yamaguchi, and Yamashita 2008; Zid et al. 2009). The abundance of the translation elongation factor eEF2 was for example decreased in the pineal gland of old rats (Muñoz et al. 2017).

7.2 tRNAs during aging

A key resource of protein production is the cellular pool of tRNAs. For a proper translation, the cell requires efficient and accurate provision of amino acids to the ribosome. Although there are mathematically only 64 possible codons and only 20 amino acids, the human genome encodes for 506 tRNA genes, indicating a fine-tuned regulation. In addition, tRNAs are thought to be the most modified and most diversely modified nucleic acids of the cell (P. P. Chan and Lowe 2009). A common modification of tRNAs is the incorporation of 5-methylcytosin (m5C), resulting in the preferential expression of UUG rich transcripts (C. T. Y. Chan et al. 2010, 2012). Moreover, the proteome can be regulated by tRNA halves and tRNA-derived fragments (tRFs). Both derive from mature tRNAs by endonucleolytic cleavage at various sites. These species of non-coding RNA are involved in stress signaling as a signaling molecule, thereby shaping translation of distinct proteins (Fricker et al. 2019; Gebetsberger et al. 2012, 2017; Saikia and Hatzoglou 2015; Shen et al. 2018; Thompson and Parker 2009). Interestingly, not only the expression of tRFs changes with age, but also the loading and the abundance of distinct isoforms. Furthermore, a connection between tRFs and neurodegenerative diseases as well as brain aging has been established (Anderson and Ivanov 2014; Karaikos et al. 2015).

7.3 Ribosome quality control during aging

The ribosome itself has a specific protein quality check mechanism, called ribosomal quality control (RQC). Several steps can go wrong during active peptide chain elongation. Under stress conditions, the chaperone hsp-70 (usually ribosome-bound) localizes away from the ribosome to aid in protein folding, which then results in ribosome stalling (B. Liu, Han, and Qian 2013; Shalgi et al. 2013). Stalling can also be induced by non-optimal decoding of mRNAs and inhibitory mRNA stem loop structures. A connection between ribosome stalling and aging has recently been established by showing impaired ribosome recycling in the aging mouse brain (Sudmant et al. 2018). Stalled ribosomes are removed by the RQC machinery and the unfinished nascent chain is subjected to degradation (Brandman et al. 2012). Most studies dealing with

RQC have been conducted in yeast. Mechanistically, clearance happens through the formation of the RQC complex. Hel1 and other factors recognize and split the stalled ribosome and expose the tRNA which is still bound to the nascent peptide chain and the large ribosomal subunit. Rpc2 then binds to the tRNA and recruits the E3 ubiquitin ligase Ltn1. Subsequently, Rct2 elongates the nascent polypeptide chain in an mRNA-independent mechanism by adding the so-called CAT-tail consisting of randomly integrated alanine and threonine residues at the C-terminus, which is important for the degradation process. Ltn1 ubiquitinylates the peptide chain, which is then subjected in a Rpc1-dependent mechanism to proteasomal degradation by Cdc48 (Brandman et al. 2012; Joazeiro 2019; Kostova et al. 2017).

7.4 Protein folding during aging

To fulfill their function, most proteins have to fold into secondary structures. The accuracy and efficiency of this folding process is crucial for cellular and organismal survival, is regulated at several layers and underlies a tight control. From the birth of a protein at the ribosome, it is accompanied by folding helpers called chaperones, which biochemically force and hold the developing peptide chain into its three-dimensional structure. The activity of chaperones however decreases with age, leading to the accumulation of proteins and mis-folding events (Soti and Csermely 2003). A reason for this might be the availability of cellular ATP, as protein folding and degradation are both ATP-dependent processes and ATP availability decreases with age due to impaired fatty acid and glucose metabolism (Calderwood, Murshid, and Prince 2009). An overload of the chaperone system arises as a typical feature of aging (Walther et al. 2015).

7.5 Protein degradation during aging

A protein can not only get damaged or mis-folded during the actual biosynthesis process. Through its lifecycle, every protein is exposed to external and internal stimuli such as oxidation or irradiation which can affect its stability. Those damaged proteins, but also properly functional proteins need to be removed from the system on a regular

basis. The cell has two main machineries that can fulfill this task - autophagy and the proteasomal system. As discussed earlier, autophagy describes the engulfment of proteins or cellular structures by a lipid bilayer, forming the autophagosome. This round cellular structure then fuses with a lysosome to form the autolysosome, leading to the degradation of its content (Dikic and Elazar 2018; DE DUVE et al. 1955; Tsukada and Ohsumi 1993).

Proteins can also be degraded by the proteasome. The proteasome is a multi-subunit tunnel-shaped protein complex that cleaves the peptide bonds of proteins. A protein that needs to be degraded gets ubiquitinated by different E3 ligases and is subsequently translocated into the proteasome, where it gets degraded (Bedford et al. 2010; Coux, Tanaka, and Goldberg 1996).

Degradation products of both processes can afterwards be recycled by the cell. The regulation of both autophagy and the proteasome is highly interlinked and coordinated. With the progression of age, both mechanisms get deregulated - leading to the accumulation of damaged or aggregated proteins as well as a misbalance of several regulatory circles (Basisty, Meyer, and Schilling 2018; David et al. 2010; David 2012; Labbadia and Morimoto 2015; López-Otín et al. 2013a). In detail, the induction and fusion of autophagosomes is impaired in old individuals and the composition of the proteasome itself becomes imbalanced. An overall accumulation of ubiquitinated proteins is the consequence (Basisty, Meyer, and Schilling 2018; Vilchez, Saez, and Dillin 2014). Furthermore, communication between autophagy and proteasomal degradation gets lost with age, leading to a sensitization of the organism to protein folding stress stimuli (Bustamante et al. 2018; Gavilán et al. 2015). As discussed earlier, there is a clear connection between autophagy and the lifespan of an organism, although triggering autophagy itself does not extend lifespan. In contrast, the increase of proteasomal activity extends lifespan in worms (Vilchez et al. 2012).

8. Stress Responses during aging

Protein biosynthesis is closely linked to and a part of the cellular proteostasis network. The production of proteins is a very challenging task for the cell, as it comprises the exact interplay of hundreds of proteins. In case of failure, the cell installed several control mechanisms to ensure that proteins do not aggregate, are mis-localized or other harmful events take place.

Two ways through which the cell can modify its translation rate is by activating the integrated stress response (ISR) and/or activation of mTOR and its targets (Ryoo and Vasudevan 2017; Showkat, Beigh, and Andrabi 2014).

An essential branch point of the ISR is the translation initiation factor eIF2a, which can be inactivated by phosphorylation through one of four kinases. Phosphorylation of eIF2a leads to inhibition of the ternary complex formation. This results in lower translation of eIF2a-dependent transcripts. An essential point is that some mRNAs do not underly the control of eIF2a phosphorylation, such as *atf-5*. Upon phosphorylation of eIF2a, the transcription factor *atf-4* becomes de-repressed and can trigger further stress responses (Lu et al. 2004; Vattam and Wek 2004). Expression of *atf-4* also seems to be linked to the regulation of lifespan, as increased levels have been observed in long-lived dietary or methionine restricted mice as well as mice treated with the mTOR inhibitor rapamycin (W. Li, Li, and Miller 2014). Furthermore, *gcn-4*, the yeast ortholog of *atf-4*, affects replicative lifespan (Steffen et al. 2008).

Another interesting branch point between lifespan regulation and proteostasis is the eIF4E-binding protein (4E-BP), which is a direct substrate of TOR. Upon phosphorylation, 4E-BP binds to eIF4E and thereby inhibits cap-dependent translation. Again, specific mRNAs can escape the translational block as it has been reported in *D. melanogaster*, where mitochondria-specific transcripts are not affected (Zid et al. 2009).

Aim of this study

As discussed above, the scientific community makes considerable progress in understanding the underlying mechanisms of aging. Recently the nucleolus turned out to be a central hub for the regulation of lifespan in several longevity regimes in a *ncl-1*-dependent manner. The nucleolus is known for its role in ribosome biogenesis and the regulation of protein translation. Nevertheless, based on nucleolar composition, additional nucleolar functions such as the regulation of the cell cycle, metabolism, regulation of telomere length and implication in different stress pathways have been suggested over the years. We recently discovered that small nucleolar size is a hallmark of longevity and that not only nucleolar size, but also longevity is dependent on the gene *ncl-1*. The regulation of nucleolar size through *ncl-1* seems to work at least partially through direct binding to the 3'UTR of *fib-1* mRNA (Figure 6).

However, both the molecular connection between *ncl-1*, nucleolar function and longevity on the one hand as well as the mechanism of *ncl-1* action on the other hand remain elusive. Since the nucleolus emerged as a central player in lifespan regulation and is also known to be closely related to aging-associated diseases such as cancer, understanding the underlying molecular mechanisms of its regulation could pave the way for novel treatment of age-related diseases and aging itself. Therefore, it is highly important to understand nucleolar regulation in its encompassing complexity and to dissect nucleolar inputs mediated by NCL-1 and nucleolar outputs affecting lifespan, among others.

Therefore, the two main aims of my thesis are:

AIM 1: Uncovering the molecular links connecting nucleolar outputs and lifespan regulation.

AIM 2: Deciphering the molecular mechanisms of NCL-1 action.

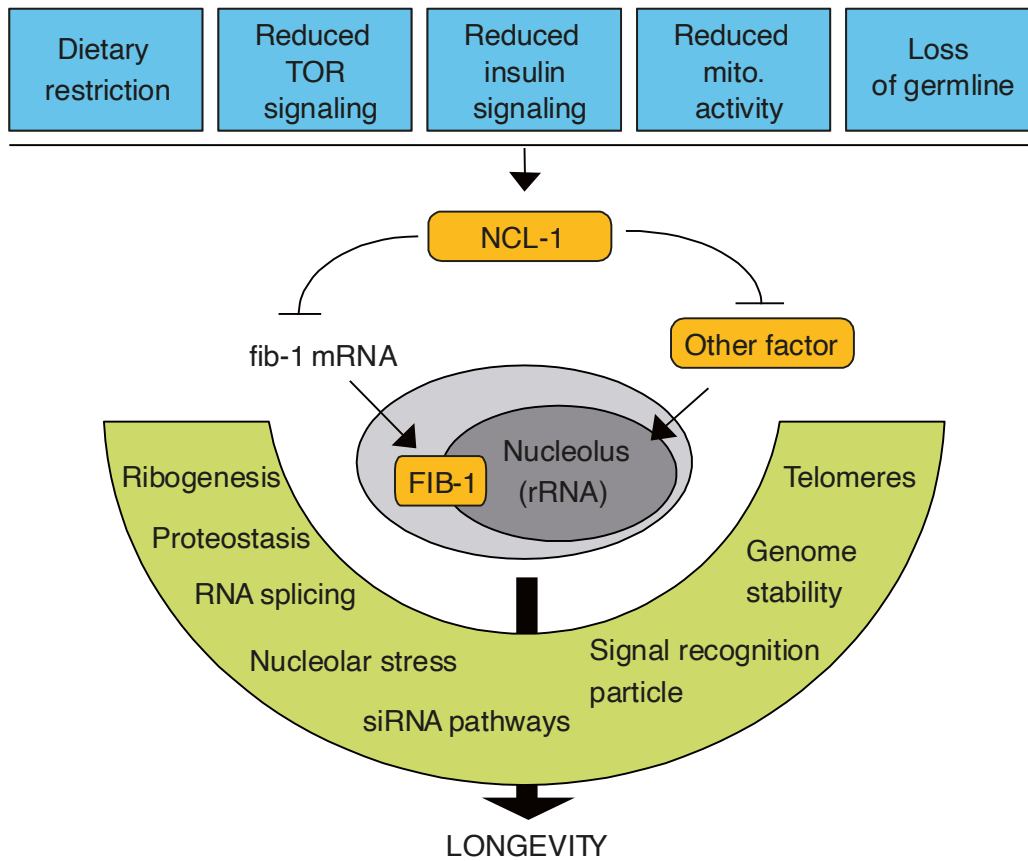


Figure 6. Working model on the connections between NCL-1, the nucleolus and longevity. Several longevity regimes converge on the cytosolic B-Box zinc finger protein NCL-1. NCL-1 is a known regulator of nucleolar size. The effect is partially mediated through direct binding of *fib-1* mRNA and additional unknown mechanisms. The connection between the nucleolus and longevity remains elusive, but several nucleolar outputs such as ribosome biogenesis, proteostasis, RNA splicing, nucleolar stress, siRNA pathways, the signal recognition particle, genome stability and telomere regulation are potential connections.

Results

Chapter 1: NCL-1-dependent regulation of the RNase P/MRP complex and the mitochondrial ribosome link the nucleolus to lifespan control

1. NCL-1 alters transcriptomic and proteomic profile of nucleolar and mitochondrial gene products

Our prior work demonstrated that nucleolar size and lifespan are inversely correlated. Notably, various long-lived worms, flies and mice representing canonical longevity pathways, as well as long-lived WT individuals within a worm population possess small nucleoli. NCL-1/BRAT is a crucial regulator of nucleolar function, whose mutation leads to enlarged nucleoli and a corresponding increase in rRNA production and the rRNA processing enzyme FIB-1/fibrillarin. In line with enhanced ribosome biogenesis, *ncl-1* mutants exhibit elevated levels of the ribosomal proteins RPS-6 and RPS-15 and increased rates of protein synthesis. Loss of *ncl-1* suppresses the small nucleolar phenotype and partially or completely abolishes the extended lifespan of various canonical *C. elegans* longevity mutants, acting downstream of these pathways. Similarly, *ncl-1* mutations lead to elevated levels of rRNA, FIB-1, RPS-6 and RPS-15 in the longevity backgrounds. On its own, *ncl-1* single mutants though show only minor or no effects on lifespan. Thus, *ncl-1* acts as a key convergent factor regulating nucleolar function and longevity in multiple aging pathways, but the global effects of *ncl-1* on gene expression remain unknown.

In order to gain further insight into the molecular events regulated by *ncl-1*, I first examined global transcriptomic and proteomic profiles of a *ncl-1(e1942)* mutation in WT as well as long-lived germline-less *glp-1(e2141)* backgrounds. (Figure 7A). I chose *glp-1(e2141)* because this strain allowed me to observe somatic changes without the confounding effects of germ cells and embryos. Furthermore, *ncl-1* is a strong suppressor of *glp-1* longevity.

The number of detected proteins can be limiting for proteomic analysis and influence sample comparability. Approximately 3000 proteins were quantified in all analyzed

samples (Figure 7B). To assess the quality of the samples, I conducted principal component (PCA) analysis on the raw counts of all replicates. Biological replicates from both RNA-seq and proteomic datasets showed clear clustering of the four tested genotypes, indicating a unique transcript and protein expression pattern for each genotype and good reproducibility (Figure 7C,D).

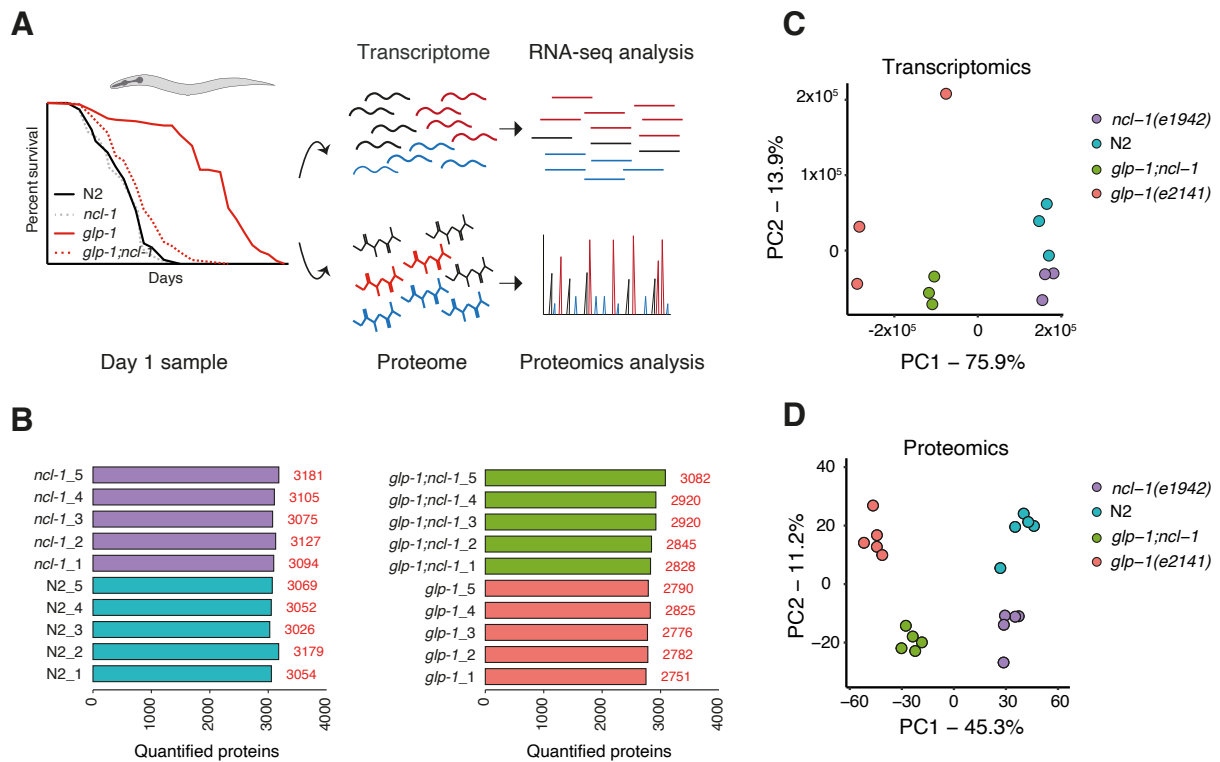


Figure 7. PCA analysis shows clustering of replicates of respective genotypes. (A) Setup of RNA-Seq and proteomic sample preparation. (B) Number of quantified proteins in proteomics in all four tested genotypes. (C,D) PCA plot shows a clear clustering of biological replicates from (C) RNA-seq and (D) proteomics of respective genotypes. (3 biological replicates for RNA-Seq, 5 biological replicates for proteomics, day 1 adults)

I then compared the RNA-Seq and proteomics data and visualized the degree of correlation. Plotting the raw counts of each candidate on transcript and protein level showed that both measurements largely correlate, with Pearson coefficients of 0.36 for N2 worms, 0.38 for *ncl-1(e1942)* worms, 0.48 for *glp-1(e2141)* worms and 0.49 for *glp-1;ncl-1* worms (Figure 8A-D). Coefficients within this range are in line with other published results, and therefore suitable for combined analysis (Molenaars et al. 2020).

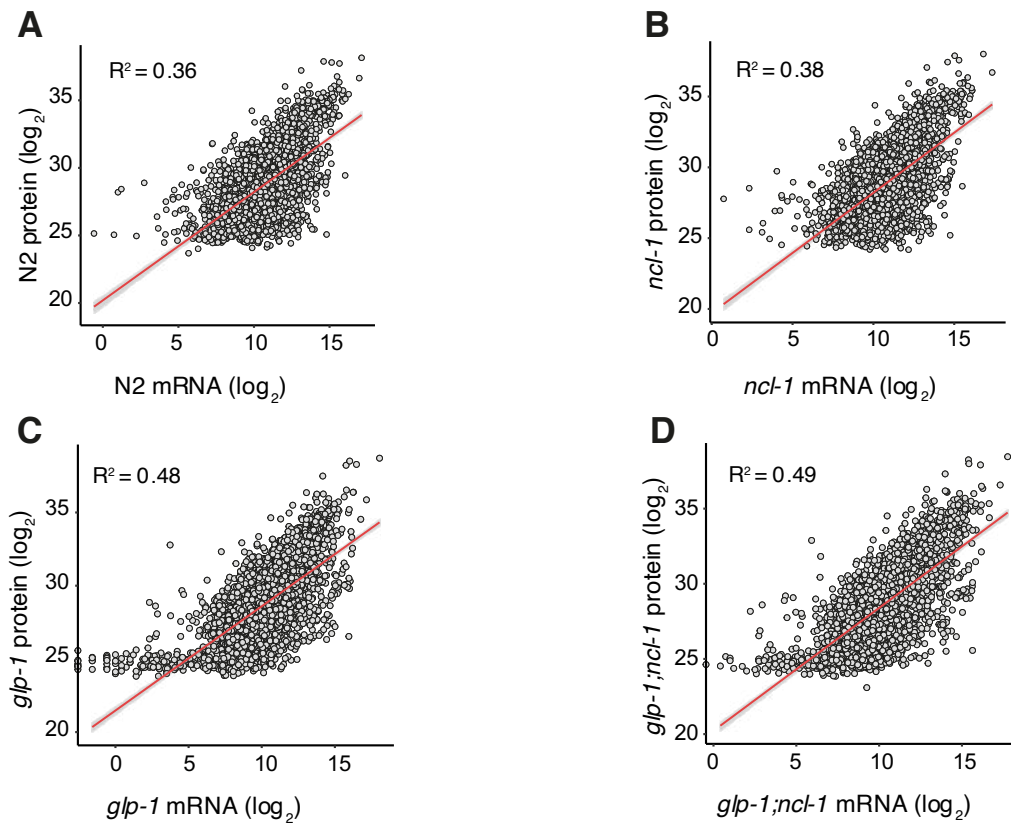


Figure 8. Omics analysis reveals a correlation between mRNA and protein levels. (A,B,C,D) Correlation plots of mRNA and protein abundance show a correlation for all tested genotypes. R^2 was calculated using R. Log₂ transformed raw counts of mRNA and proteins were plotted against each other. R^2 (N2) = 0.36, R^2 (*ncl-1*) = 0.38, R^2 (*glp-1*) = 0.48, R^2 (*glp-1;ncl-1*) = 0.49.

Differential gene expression analysis indicated robust changes in the transcriptome and proteome of the various genotypes. From the RNA-seq data comparing N2 and *ncl-1(e1942)* worms, I observed 2702 significantly upregulated and 3389 downregulated transcripts in *ncl-1(e1942)* versus WT (adj. $p < 0.05$), while from the proteomics data, I observed 243 upregulated and 165 downregulated proteins (Figure 9A). From the RNA-seq data comparing *glp-1(e2141)* and *glp-1;ncl-1* worms, I observed 1633 significantly upregulated and 960 downregulated transcripts in *glp-1;ncl-1* versus *glp-1(e2141)* (adj. $p < 0.05$), while from the proteomics data, I observed 331 upregulated and 320 downregulated proteins (Figure 9A).

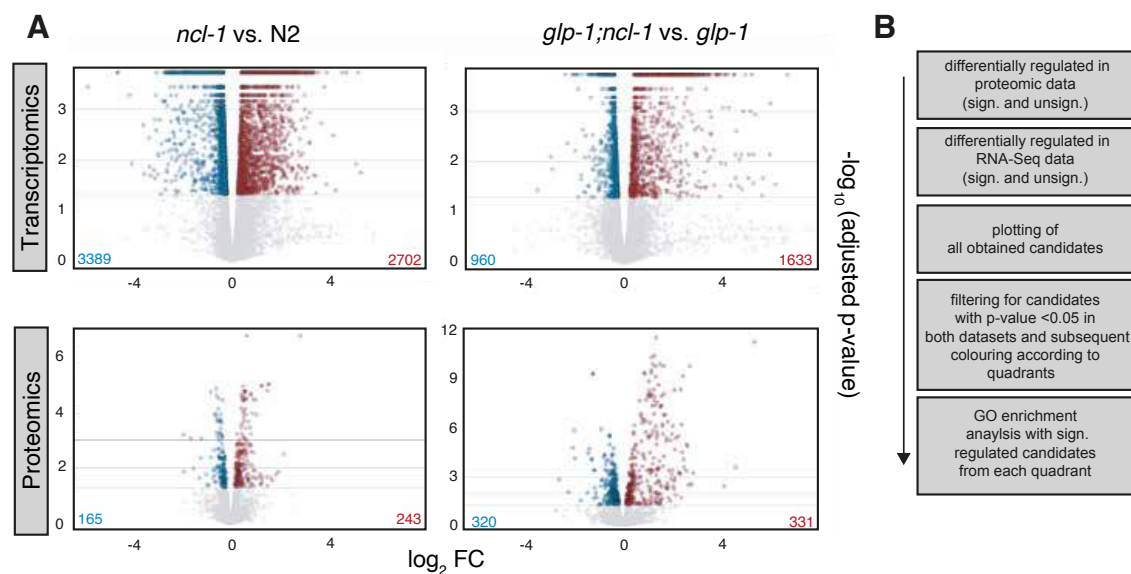


Figure 9. Differential transcript and protein regulation in *ncl-1(e1942)* mutants. (A) Volcano plots showing differential gene and protein regulation in *ncl-1(e1942)* and *glp-1;ncl-1* mutants. \log_2 fold change (FC) values are plotted against the adjusted p-values. Each dot represents a gene/protein while upregulated candidates with a p-value <0.05 are labelled red and downregulated are labelled blue. Total number of significantly up- or downregulated candidates is depicted in the bottom corners of each graph. (B) Analysis pipeline for overlapping analysis of proteomic and transcriptomic data.

I next focused on *ncl-1(e1942)* versus WT comparisons. Overlap of the RNA-Seq and proteomic datasets resulted in 232 commonly shared significant differentially regulated candidates (p<0.05). This analysis excluded 176 of the 408 differentially regulated proteins and 5859 of the 6091 differentially regulated mRNAs. The analysis pipeline for comparative transcriptomic and proteomic analysis is depicted in Figure 9B. A greater proportion of both transcripts and proteins were upregulated (61.3 %), rather than downregulated (38.7 %) in *ncl-1(e1942)* mutant worms, indicating a broad remodeling of gene expression (Figure 10A).

As an important internal control, nucleolar *fib-1* mRNA and protein levels were increased in *ncl-1(e1942)* mutants (Figure 10C), confirming our previously published *in vivo* data (Tiku et al. 2017).

To clarify which processes and cellular functions were differentially enriched in an unbiased manner, I conducted gene ontology analysis (cellular compartment analysis

– “KEGG pathways”, “biological pathways” and “molecular function” in appendix) for the genes within the indicated quadrants (Figure 10A,B). Analysis of quadrant 2 (Q2 - commonly upregulated) revealed a significant enrichment of candidates physically or functionally associated with both subunits of the pre-ribosome, the basement membrane and the nucleolus. The small subunit processome (which is involved in rRNA processing), striated muscle dense body and the mitochondrion were also among the top 7 compartments. Intriguingly, analysis of quadrant 3 (Q3 - commonly downregulated) showed that of the top 7 differentially regulated GO-terms, 4 were related to the proteasome, suggesting a connection between *ncl-1*, the nucleolus and the proteasome (Figure 10B).

Among the most upregulated differentially expressed gene products I observed were distinct chaperones, including the cytosolic heat shock protein *hsp-16.1* as well as the mitochondrial chaperone *hsp-60*, suggesting that loss of *ncl-1* results in cytosolic and mitochondrial stress. Relatedly, a strong increase in *tbb-6*, a tubulin involved in PERK-signaling, also suggests an impact on ER unfolded protein response. I also saw a modest increase of mitochondrial ribosome subunits such as *mrpl-38* on protein and mRNA levels (Figure 10C).

Among the commonly downregulated candidates, I observed that several proteasomal subunits such as *rpt-2*, *rpn-9* and *rpn-2* (in total 9 out of 40 described factors) were decreased in *ncl-1(e1942)* mutants, suggesting reduced proteasome activity. The expression of the nucleosome components *his-40* and *his-64* were also reduced, potentially indicating changes of the chromatin state (Figure 10C).

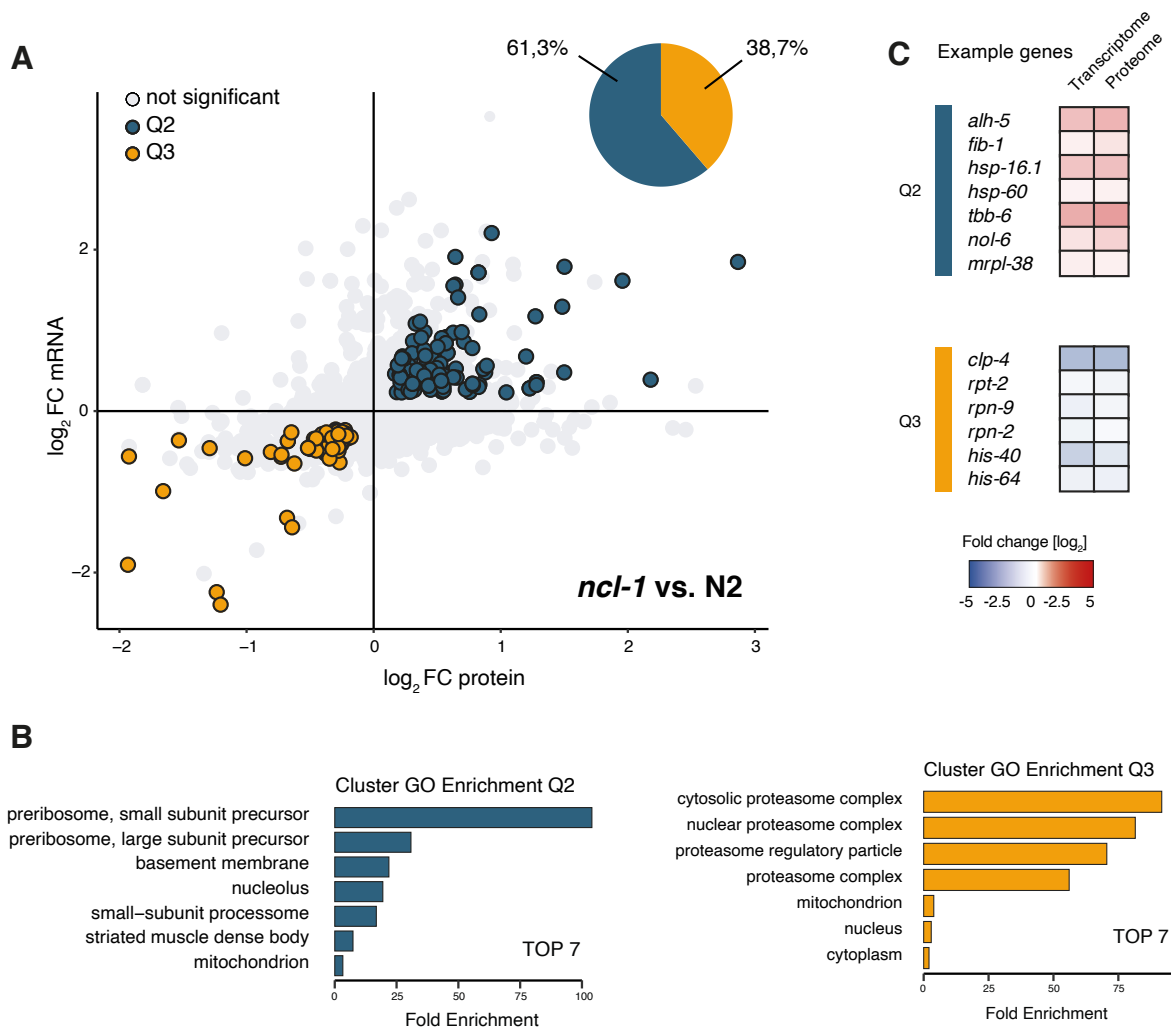


Figure 10. Differential transcript and protein regulation in *ncl-1(e1942)* mutants. (A) Co-regulation plot of transcript and protein fold changes of *ncl-1(e1942)* versus N2 samples. Quadrants are defined as Q1 posttranscriptionally repressed, Q2 co-upregulated, Q3 posttranscriptionally increased and Q4 co-downregulated. Pie charts shows percentage of candidate distribution in each quadrant, revealing most changes as co-regulated and a trend toward the upregulation of candidates. Colored candidates were significantly changing in both datasets with a p-value<0.05. Grey dots represent candidates with a p-value>0.05 in either transcriptomics or proteomics. (B) Top seven cellular compartments enriched in quadrant Q2 and Q3, derived from significant hits from (A). (C) Examples of co-upregulated and co-downregulated genes, derived from significant hits from (A).

To unravel the link between *ncl-1* and longevity, I next repeated a similar analysis as above comparing long-lived *glp-1(e2141)* to normal-lived *glp-1;ncl-1*.

An overlap of RNA-Seq and proteomic datasets resulted in 481 significantly regulated candidates. This analysis excluded 170 of the 651 differentially regulated proteins and 2112 of the 2593 differentially regulated mRNAs. Again, the data showed a bias towards upregulated transcripts and proteins (60.7%), while 38.1% of the candidates were downregulated in both datasets. As expected, nucleolar *fib-1* was upregulated at both transcript and protein levels (Figure 11A).

Gene ontology enrichment analysis of Q2 proteins showed an enrichment for ribosomes and their biogenesis, as well as the nucleolus. Furthermore, the mitochondrial small ribosomal subunit and mitochondria in general were among the top hits (Figure 11B).

The downregulated candidates in Q3 show a strong GO enrichment for lysosome related components, in particular the V-type ATPase complex. Among others, candidates localized in the peroxisomes, collagen trimers, the extracellular space, the mitochondrion and the extracellular region were enriched in the analyzed group (Figure 11B). I found a significant enrichment for immunity related factors, which is not presented in the figure due to lower fold enrichment score, recapitulating our previous finding of impaired pathogen resistance of *ncl-1* mutants (Tiku et al. 2018).

The number of differentially expressed genes in Q1 was not sufficient for GO enrichment analysis.

However, in contrast to the N2 vs. *ncl-1(e1942)* comparison, 2 % of the candidates were upregulated as transcripts but downregulated as proteins in quadrant 1 (Figure 5A). Such gene products included *gop-3/SAMM50*, which functions in mitochondrial cristae structure maintenance (Tang et al. 2020), *pcn-1/PCNAF* involved in the DNA damage repair machinery, *imb-3* implicated in the nuclear import of distinct ribosomal proteins, *rpl-11.1* large subunit ribosomal protein and *his-64* (Figure 11C) (Branzei and Foiani 2005; Zhao et al. 2019). These findings may indicate regulation at the level of protein translation or stability of these candidates.

Among the most strongly upregulated candidates in quadrant 2 (Q2- commonly upregulated) was the RNase P/MRP component *popl-1*, which catalyzes the processing and maturation of several RNA species, including rRNA and tRNA. I also observed upregulation of several cytosolic and mitochondrial heat shock response factors, such as *hsp-16.1* and *hsp-60*, as seen with the N2 vs. *ncl-1* comparison. Mitochondrial ribosomal subunits, such as *mrpl-45* and *mrps-5*, and the cytosolic ribosomal subunit *rpl-24.2* were also increased in *glp-1;ncl-1* double mutants. Moreover, I observed an increase in the RNA polymerase I subunit *rpoa-2* (Figure 11C), which is involved in the transcription of rRNA.

Among the gene products from quadrant 3 (Q3 - commonly downregulated), I observed reduced levels of the ER heat shock factor *hsp-4* and reduced levels of the innate immune genes *gstk-1*, *grd-3* and *lys-2*. Several vacuolar ATPase subunits and other lysosomal components were also reduced in *glp-1;ncl-1* double mutants, suggesting an impaired lysosomal activity. In contrast to the pattern seen in N2 versus *ncl-1(e1942)* comparisons, however, I did not see obvious changes in proteasome subunits.

NCL-1 is an RNA-binding protein that reportedly binds to UUGUU motifs, much like the fly ortholog BRAT (West et al. 2018). Furthermore, *ncl-1* has been suggested to bind to the *fib-1* mRNA 3'UTR (Yi et al. 2015), based on the prevalence of the UUGUU motif and the negative regulation of *fib-1* expression by *ncl-1*. I therefore analyzed the transcriptome data examining the abundance of this motif within the differentially regulated transcripts derived from the comparison *glp-1(e2141)* vs. *glp-1;ncl-1*. The number of UUGUU motifs was significantly enriched in the fraction of significantly regulated genes (Figure 11D).

Among the genes with a high fold change and high motif number I found several factors involved in rRNA transcription, rRNA processing and ribosome biogenesis, including *fib-1*, *utp-20*, *rpoa-2* and *ngp-1* suggesting NCL-1 as a gatekeeper for ribosome biogenesis on mRNA level (Figure 11E).

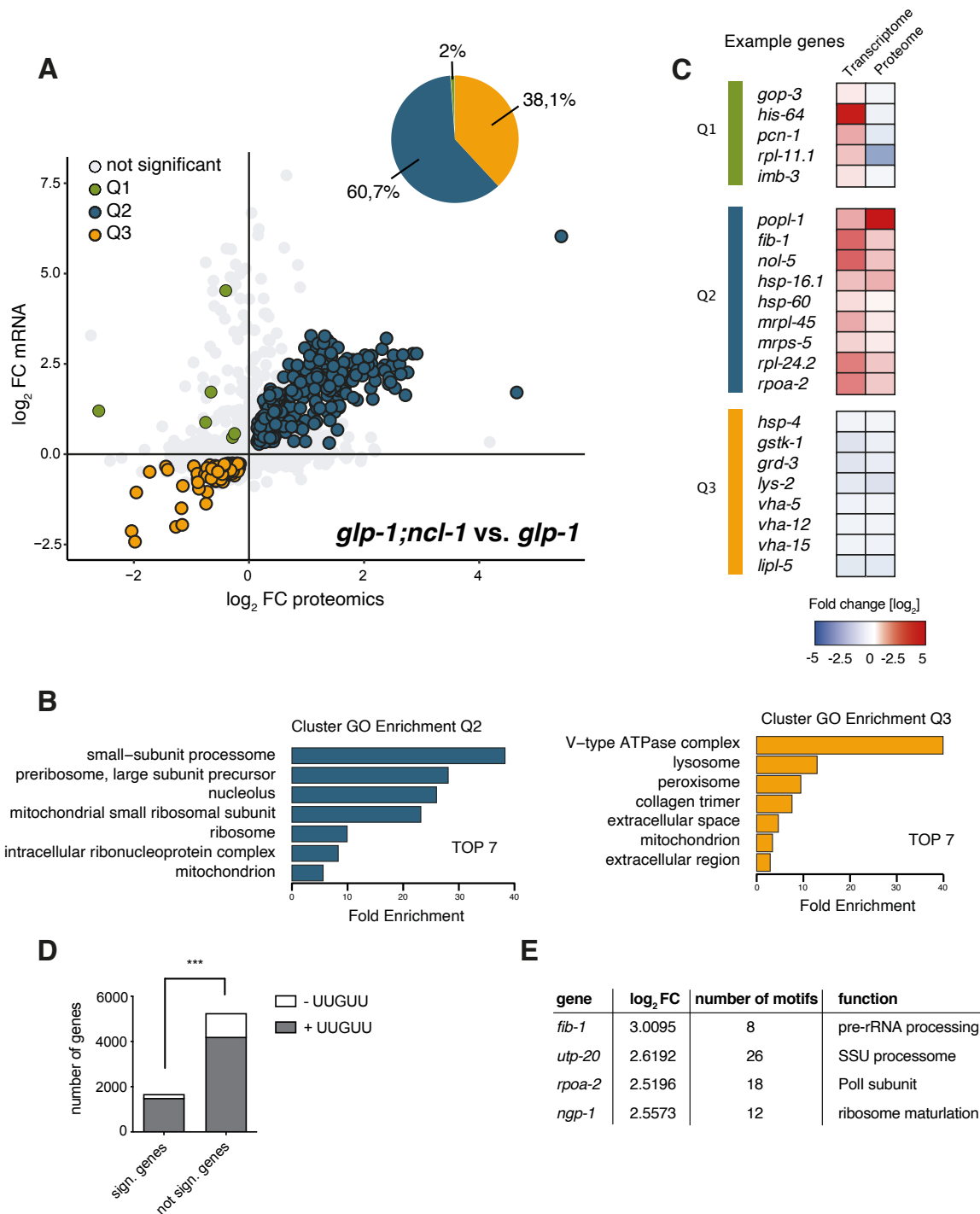


Figure 11. Differential transcript and protein regulation in *glp-1;ncl-1* mutants. (A) Co-regulation plot of transcript and protein fold changes of *glp-1;ncl-1* versus control samples. Quadrants are defined as Q1 posttranscriptionally repressed, Q2 co-upregulated, Q3 posttranscriptionally increased and Q4 co-downregulated. Pie charts shows percentage of candidate distribution in each quadrant, revealing most changes as co-regulated and a trend toward the up-regulation of candidates. Colored candidates are significantly changed in both datasets with a p -value < 0.05 . (B) Top seven cellular compartments enriched in quadrant Q2 and Q3, derived from significant hits from (A). (C) Examples of posttranscriptionally repressed, co-upregulated and co-downregulated genes, derived from significant hits from (A). (D) The NCL-1 mRNA-binding motif (UUGUU) is significantly enriched in the fraction of significantly regulated genes in *glp-1;ncl-1* mutants. Fisher's exact test, *** $p < 0.001$. (E) Example genes with high fold change on mRNA level and high motif number.

Although loss of *ncl-1* leads to a visible increase in nucleolar size in worms independent of their genetic background, it only reduces lifespan in long-lived worms. This suggests that the loss of *ncl-1* triggers a different response in different backgrounds. Accordingly, I observed different GO-terms enriched in the comparison of *ncl-1(e1942)* vs. N2 and *glp-1;ncl-1* vs. *glp-1(e1942)*.

To better understand this difference, I compared the differentially regulated genes independent of their up- or downregulation, and determined whether they were shared between *ncl-1* mutants (in both N2 and *glp-1* background), or unique (Figure 12A). 76 genes were shared, including the nucleolar methyl transferase *fib-1*, the heat shock factors *hsp-16.1* and *hsp-60* as well as mitochondrial and cytosolic ribosomal subunits and nucleolar proteins such as *nol-6*. 392 genes were specifically regulated in *glp-1;ncl-1* worms and 144 genes in *ncl-1(e1942)* single mutants (Figure 12A). Gene ontology enrichment analysis showed an enrichment for mitochondria-associated candidates in all three groups, indicating a link between *ncl-1* the nucleolus and mitochondria. Genes associated with the nucleolus and ribosome biogenesis were enriched in the common and the *glp-1;ncl-1*-specific fraction. In addition, mitochondrial small ribosomal subunits, pol-I and pol-III rRNA transcribing RNA polymerase subunits, as well as tRNA metabolism and snoRNP gene products were specifically enriched among the regulated genes in *glp-1;ncl-1* worms. Furthermore, key lysosomal genes were enriched only in the *glp-1;ncl-1*-specific candidates, while key proteasomal genes were enriched only in the *ncl-1* versus WT comparison (Figure 12B), suggesting distinct effects on the proteolytic machinery dependent on genetic background.

Next, I picked representative example candidates of each GO-term and visualized the direction and magnitude of regulation in each genotype in the form of heatmaps. Among the commonly regulated candidates, I observed an upregulation of nucleolus related transcripts and proteins in both genetic backgrounds. Fold changes were higher in *glp-1;ncl-1* mutants compared to *ncl-1(e1942)* worms. All proteasome components were solely downregulated in *ncl-1(e1942)* mutants. I occasionally observed a significant regulation of individual lysosome and peroxisome-associated candidates in *ncl-1(e1942)* mutants, but the regulation of the whole class was mainly a *glp-1;ncl-1*-specific feature (Figure 12C). Collectively, loss of *ncl-1* results in a

background unspecific upregulation of nucleolar processes. At the same time, different proteolytic processes were decreased in a background-specific manner.

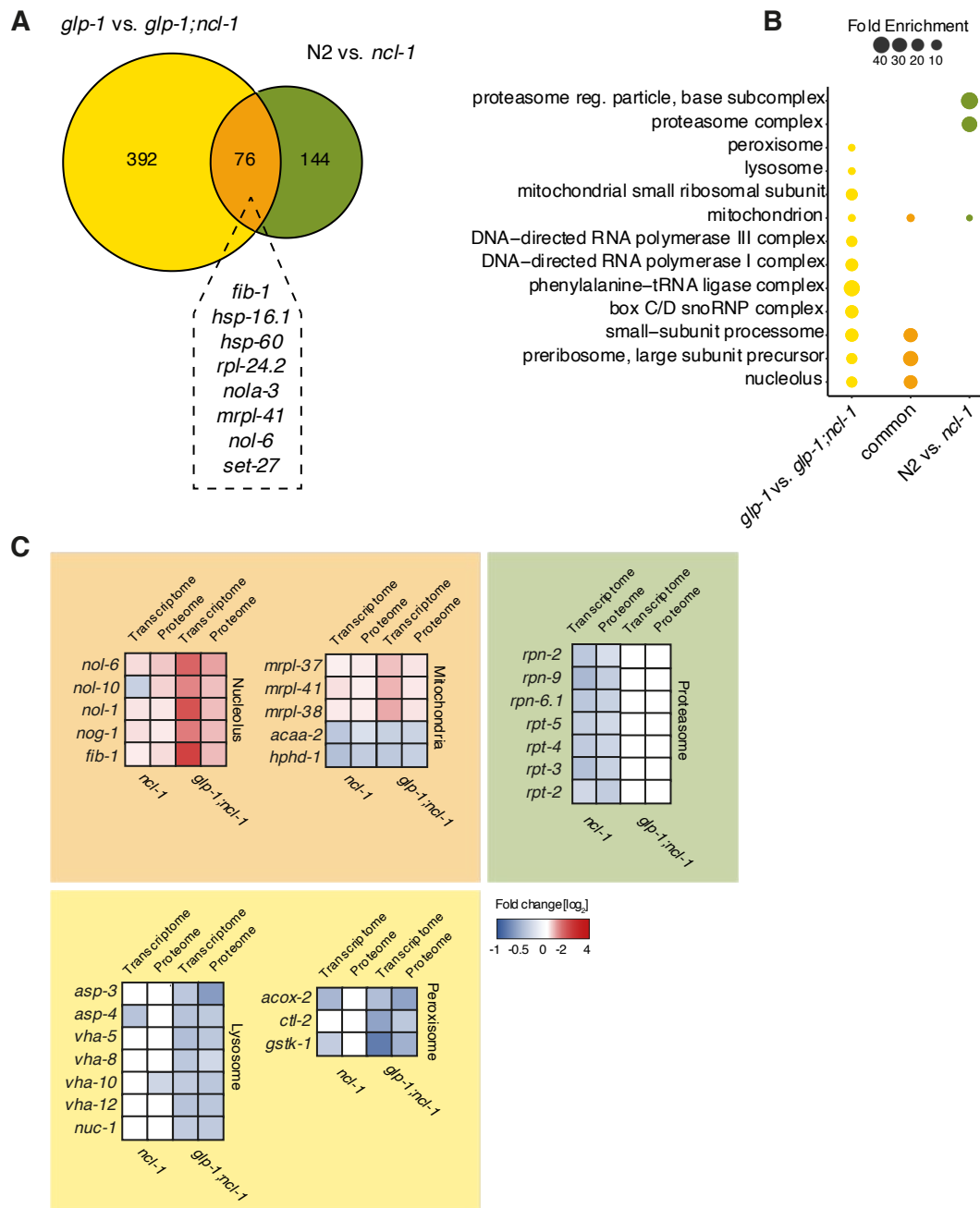


Figure 12. *ncl-1* affects different proteolytic processes in a background-specific manner. (A) Venn diagram depicts unique and shared regulated genes in *ncl-1(e1942)* and *glp-1;ncl-1* mutants. Commonly regulated example genes are highlighted. (B) GO-term enrichment analysis of different fractions from (A). Regulation of the proteasome is *ncl-1(e1942)*-specific whereas regulation of the lysosome and peroxisome are *glp-1;ncl-1*-specific. Dot size represents fold enrichment of GO-term. (C) Concrete regulation of example genes from GO-term analysis with fold change regulation in different backgrounds. Nucleolus and mitochondria associated candidates are commonly regulated in both backgrounds. All proteasome components and factors are solely regulated in *ncl-1(e1942)* mutants. The majority of changes regarding the lysosome and peroxisome are *glp-1;ncl-1*-specific.

2. Reduced RNase P/MRP activity and mitochondrial translation act downstream of *ncl-1* to extend lifespan

To decipher the link between nucleolar size and longevity, I performed a functional genomic RNAi lifespan rescue screen on genes regulated by *ncl-1*. I reasoned that genes strongly upregulated in the *glp-1;ncl-1* background could be responsible for eclipsing *glp-1* longevity. If so, then longevity might be restored upon knockdown of such lifespan affecting genes (Figure 13B). To filter suitable RNAi targets from my omics data, I used the following criteria: genes were upregulated in the *glp-1;ncl-1* mutants by at least a \log_2 FC of 1 in the proteomics data and significantly increased in the RNA-Seq data; they were conserved in mouse or human; and RNAi clones were available from existent Ahringer or Vidal RNAi libraries. I also supplemented the list with conserved candidates representing highly enriched GO-term clusters with some of the less strongly regulated candidates as well (mitochondria, tRNA metabolism, translation, germ cell development etc.). This filtering yielded 119 candidates to test on lifespan (Figure 13A).

Remarkably, out of 40 tested, 30 candidates prolonged *glp-1;ncl-1* lifespan upon knockdown (Figure 14), with 6 extending lifespan by more than 20%. Notably, *mrps-16*, whose expression was mildly increased upon loss of *ncl-1*, gave the strongest effect on lifespan upon knockdown, suggesting that even small changes in transcriptome and proteome can reveal molecules having a significant biological impact. Knockdown of *fib-1*, a key regulator of nucleolar function and longevity, showed a weak lifespan extension in this context. However, more recent results from our lab show that *fib-1* knockdown can further extend *glp-1;ncl-1* lifespan when using optimized conditions of RNAi (Torsten Buecher, personal communication).

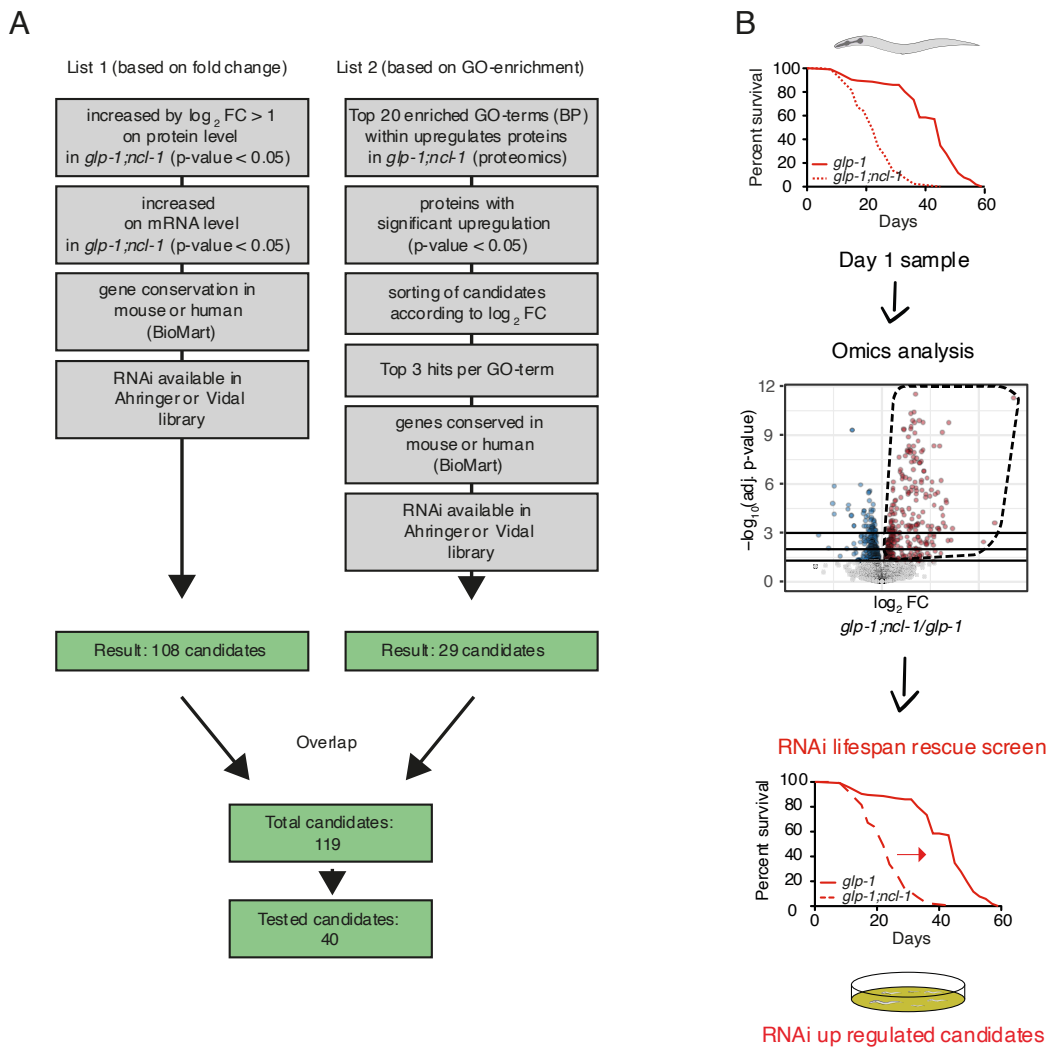


Figure 13. Candidate selection and RNAi screen setup. (A) Two lists based on fold change (List 1) and GO-term enrichment (List 2) were generated applying the presented parameters. Filtering resulted in 108 candidates from List 1 and 29 candidates on List 2. A combination of both lists lead to a total number of 119 candidates for the screen. 40 candidates were screened for lifespan in *glp-1; ncl-1* mutants. (B) RNAi lifespan rescue screen setup.

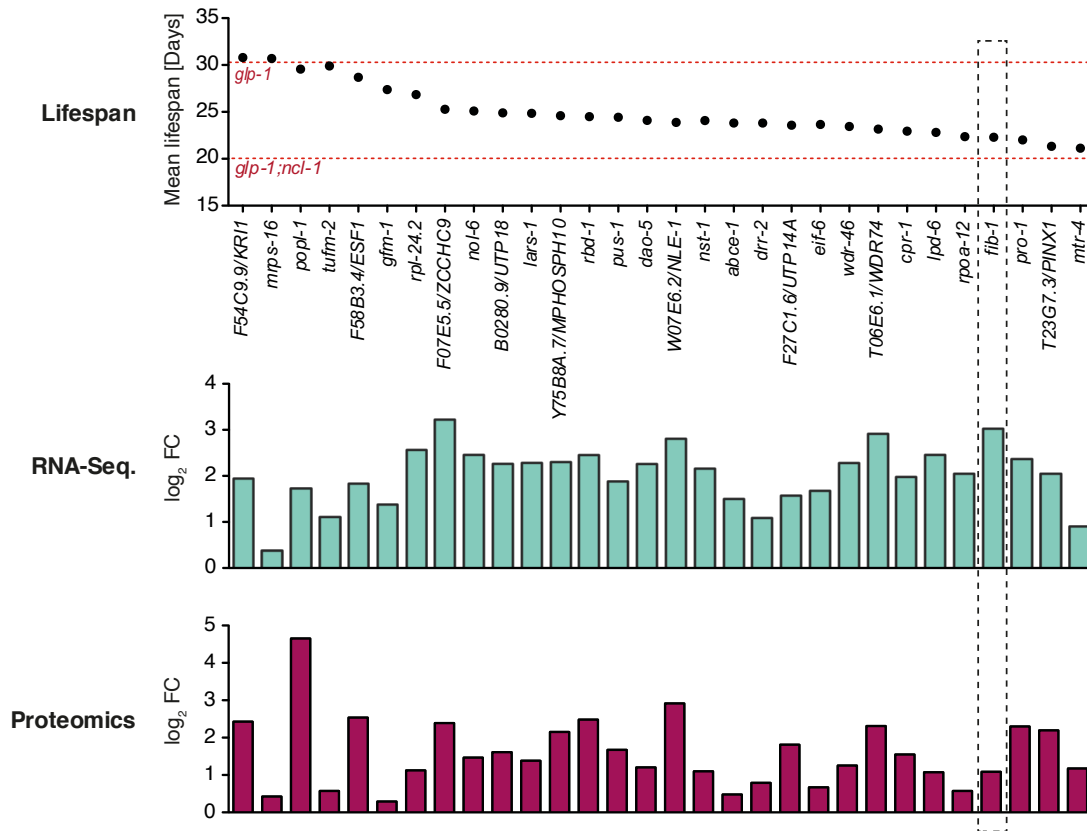


Figure 14. Candidates from RNAi lifespan rescue screen extend *glp-1;ncl-1* lifespan. Mean lifespan of *glp-1;ncl-1* worms upon RNAi-mediated candidate knockdown. Only candidates with positive effects are displayed. Candidate regulation on mRNA level shown in blue and on protein level shown in purple. The lower dashed red line depicts mean lifespan of *glp-1;ncl-1*, the upper dashed red line the mean lifespan of *glp-1(e2141)*. Lifespan experiments were performed once. Dashed black box highlights the effect of *fib-1* RNAi and its regulation. (1 replicate per lifespan, >100 worms per lifespan)

Manual visualization of the processes linked to the longevity conferring RNAi clones revealed multiple activities related to the regulation of protein biosynthesis: from rRNA transcription and maturation, tRNA processing, transport and loading to ribosome biogenesis and the ribosome itself (Figure 15), though some candidates affected longevity more strongly than others.

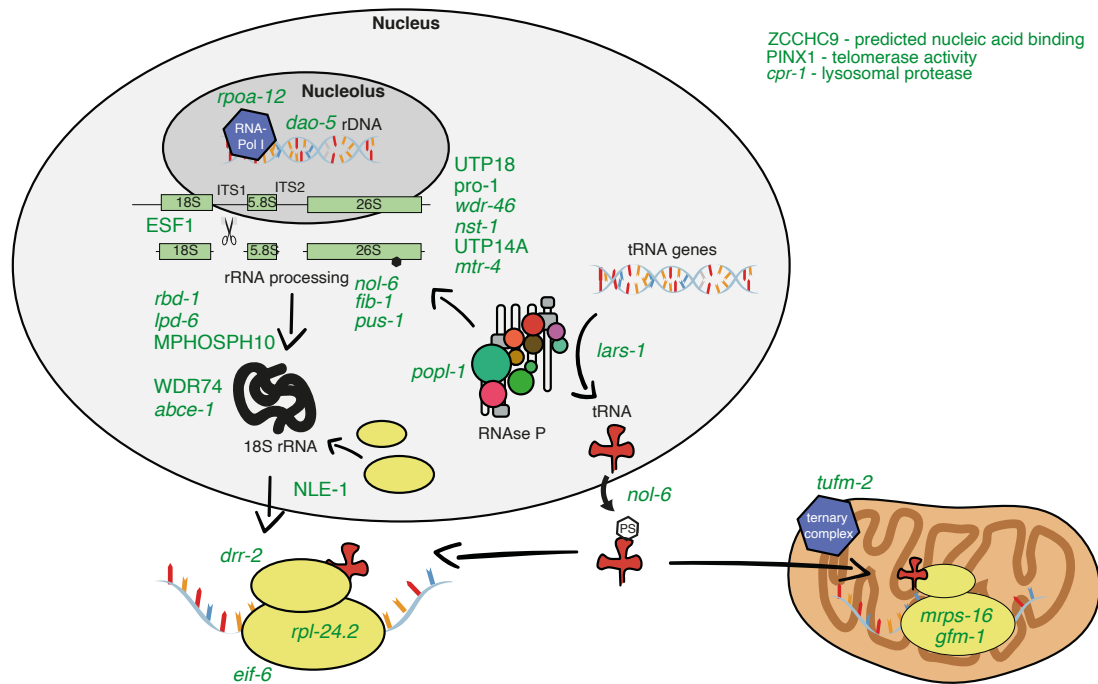


Figure 15. Mapping of positive screen candidates onto involved processes. Most positive screen candidates are involved in different layers of either rRNA transcription, rRNA processing, ribosome biogenesis or mitochondrial translation. Also tRNA metabolism is among the involved processes. Capitalized genes are mammalian orthologs of *C. elegans* genes without assigned names.

Top candidates from the longevity screen could generally be associated with a nucleolar or a mitochondrial function, and so I focused on the strongest candidates from both categories for further analysis. I observed highly reproducible lifespan extensions of *glp-1;ncl-1* double mutants upon *popl-1* and *mrps-16* RNAi (Figure 16A,C). *popl-1* is the *C. elegans* ortholog of POP1, which is an integral component of the RNase P and the RNase MRP complex. The RNase P/MRP complex is involved in the processing of diverse RNA species such as tRNAs, rRNAs, snoRNAs and also specific mRNAs (Esakova et al. 2011; Esakova and Krasilnikov 2010). Besides that, the RNase MRP complex is involved in the initiation of mitochondrial DNA replication (D. Y. Lee and Clayton 1998; Topper, Bennett, and Clayton 1992). *mrps-16* is the *C. elegans* ortholog of the mammalian MRPS16 which is a structural constituent of the mitochondrial ribosome.

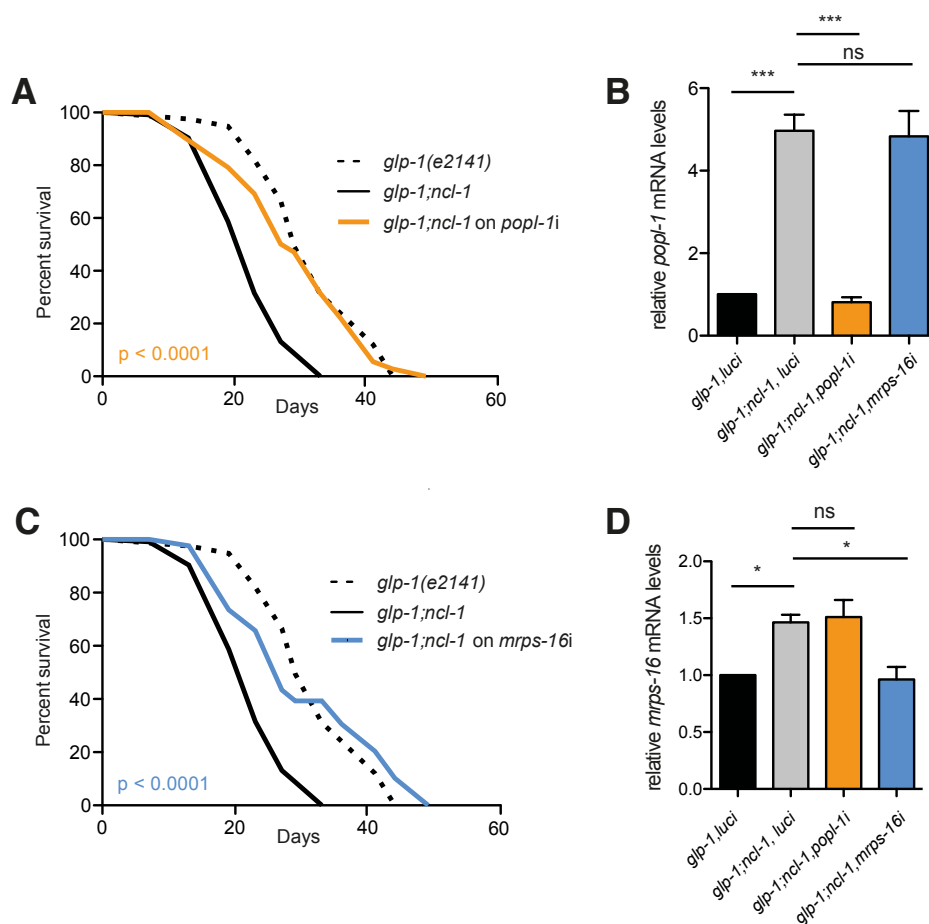


Figure 16. Reduction of the RNase P/MRP component POPL-1 and the mitochondrial ribosomal protein MRPS-16 independently extend *glp-1;ncl-1* lifespan. (A) Lifespan analysis of *glp-1;ncl-1* worms on *popl-1* and control (*luci*) RNAi. *glp-1;ncl-1* lifespan is extended upon *popl-1* reduction. *glp-1(e2141)* worms on luciferase RNAi as positive control. (>100 worms per lifespan, RNAi egg on, 3 biological replicates, Mantel-Cox Log rank test) (B) qPCR showing increased *popl-1* mRNA levels in *glp-1;ncl-1* mutants. *popl-1* levels are completely rescued upon RNAi treatment. *popl-1* RNAi does not affect *mrps-16* mRNA levels. (3 biological replicates, day 1 adults, error bars indicate SEM, One-way ANOVA with Dunnett's multiple comparison test, *** $p < 0.001$) (C) Lifespan analysis of *glp-1;ncl-1* worms on *mrps-16* and control RNAi. *glp-1;ncl-1* lifespan is extended upon *mrps-16* reduction. *glp-1(e2141)* worms on luciferase RNAi as positive control. (>100 worms per lifespan, 3 biological replicates, Mantel-Cox Log rank test) (D) qPCR showing increased *mrps-16* mRNA levels in *glp-1;ncl-1* mutants. *mrps-16* levels are completely rescued upon RNAi treatment. *mrps-16* RNAi does not affect *popl-1* mRNA levels. (3 biological replicates, day 1 adults, error bars indicate SEM, One-way ANOVA with Dunnett's multiple comparison test, * $p < 0.05$)

qPCR analysis in *glp-1;ncl-1* mutants confirmed that transcript levels of both genes were increased in *glp-1;ncl-1* mutants compared to *glp-1(e2141)* worms, to a similar extent as seen in RNA-Seq analysis. RNAi knockdown of the respective genes restored transcripts back to the levels observed in *glp-1(e2141)* worms, indicating an efficient and specific reduction of the mRNA of both genes (Figure 16B,D). Knockdown

of *popl-1* did not affect the transcript levels of *mrps-16* and *vice versa*, suggesting two separate pathways or two pathways that converge further downstream.

popl-1 is a key component of the RNase P complex, the partially mitochondrial RNase MRP complex and also the telomerase complex (Jarrous 2017). Due to its multifunctionality and shared components, it is challenging to identify the *popl-1* function that influences longevity. Therefore, I decided to look at other components of the RNase P/MRP complex in order to pinpoint the connection on one complex.

First, I concentrated on the regulation of other RNase P/MRP components in my RNA-Seq and proteomics datasets. As described earlier, I found a strong increase in POPL-1 protein level in *glp-1;ncl-1* mutants, but was unable to detect other components of these complexes, or did not see any significant change in their protein expression. However, at the RNA level I observed a significant increase in the expression of the complex components *rpp-29*, *rpp-30*, *rpp-25* (Figure 17A). From other studies in mammals and yeast we know that most complex components are shared between the RNase P, the RNase MRP and some with the telomerase complex (Figure 17B) (Esakova and Krasilnikov 2010; Jarrous 2017). I next tested if these regulated complex genes also influence longevity and conducted lifespan analyses in the same manner as for the RNAi rescue screen. RNAi-mediated knockdown of the candidates *rpp-29*, *rpp-25* and *rpp-29*, which were regulated at the mRNA level, extended lifespan. Knockdown of the non-regulated component *Y66A7A.2*, the ortholog of POP5, did not affect lifespan (Figure 17C). These findings indicate that there is a functional connection between the RNase P/MRP complex and the regulation of lifespan.

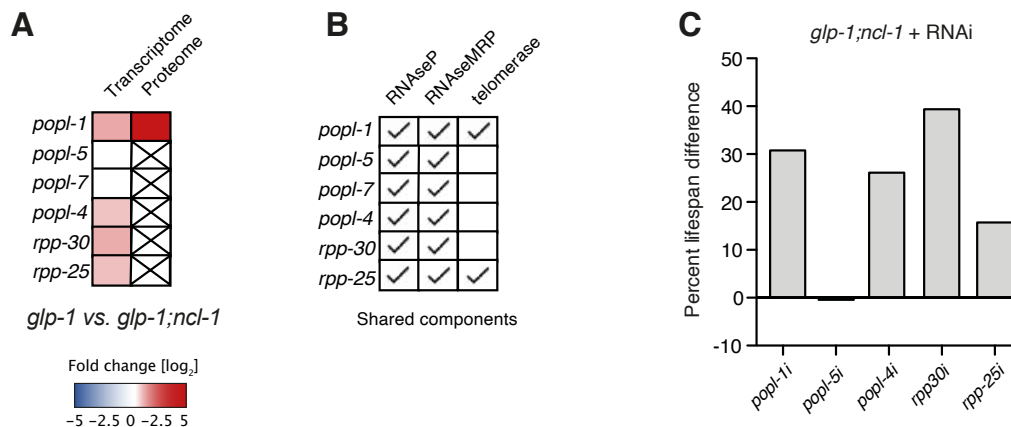


Figure 17. The RNase P/MRP complex is a linker between nucleolar size and lifespan. (A) Regulation of different RNase P/MRP components on mRNA and protein level in *glp-1;ncl-1*. POPL-1 is the only regulated component on protein level. More complex components and the RNA component are upregulated on mRNA level in *glp-1;ncl-1*. Boxes are crossed out for not detected proteins. (B) Shared components between the RNase P, the RNase MRP and the telomerase complex based on (Esakova and Krasilnikov 2010; Jarrous 2017). (C) Percentage of mean lifespan difference upon RNAi-mediated knockdown of different RNase P/MRP components compared to *glp-1;ncl-1*. Lifespan is extended upon reduction of RPP30, RPP29, RPP25 and POP1. POP5 does not affect *glp-1;ncl-1* lifespan. (>100 worms per lifespan, RNAi egg on, 1 biological replicate, Mantel-Cox Log rank test)

3. *popl-1* and *mrps-16* act downstream of the nucleolus, uncoupling nucleolar size from lifespan

The previous results demonstrate that the RNase P/MRP complex component *popl-1* and the mitochondrial ribosome component *mrps-16* regulate lifespan in *glp-1;ncl-1* mutants. However, it remains unclear whether one or both candidates affect lifespan through a rescue in nucleolar size or whether they can be functionally placed between the nucleolus and lifespan regulation. Therefore, I measured nucleolar size in the hypodermis of *glp-1;ncl-1* double mutants upon RNAi-mediated knockdown of *popl-1* and *mrps-16* at day 1 of adulthood. A reduction in both genes had no or minor effects on nucleolar size, indicating that both candidates affect lifespan either downstream of the nucleolus or in a parallel pathway (Figure 18A). I made a similar observation for neuronal nucleoli (data not shown). To exclude that the RNAi treatment affects nucleolar size only later in life, I repeated the measurements after several days of RNAi

treatment at day 6 of adulthood and again observed no change in nucleolar size (Figure 18B). Indeed, comparing hypodermal nucleolar size at day 1 of adulthood and day 6 of adulthood shows a trend towards an increase in nucleolar size in all conditions (Figure 18C).

To test whether *popl-1* and *mrps-16* RNAi treatments impact expression of nucleolar components, I conducted a qPCR analysis of the nucleolar marker *fib-1* in *glp-1;ncl-1* animals. *fib-1* mRNA levels remained unchanged at day 1 and day 6 upon RNAi treatment against *popl-1* and *mrps-16*, further supporting the idea that they act downstream of *ncl-1* (Figure 18D,E). It remains to be seen whether knockdown of these components affect nucleolar size in the WT background.

Loss of *ncl-1* is associated with increased cell size and body size in WT worms, as well as *glp-1* and *eat-2* worms (Tiku et al. 2017). Therefore, I also measured body size in *glp-1;ncl-1* double mutants upon RNAi-mediated knockdown of *popl-1* and *mrps-16*. Both treatments did not decrease body size of *glp-1;ncl-1* mutants (Figure 18F).

The nucleolus is the cellular site of rRNA synthesis, processing, and ribosome biogenesis. Our lab has previously demonstrated that nucleolar size correlates with steady state rRNA levels, and that rRNA levels are increased in *ncl-1* mutants (Tiku et al. 2017).

To test whether RNAi-mediated knockdown of either *popl-1* or *mrps-16* affects rRNA levels, I isolated RNA from day 1 worm samples and performed an RNA gel electrophoresis. Whether rRNA levels also remain unchanged later in life remains open though. Samples were normalized to worm number. As previously reported, rRNA levels were increased in *glp-1;ncl-1* compared to *glp-1* mutant (Figure 18G,H). Neither of the RNAi treatments decreased rRNA levels in the double mutant background, suggesting that the effect on lifespan is independent of steady state rRNA levels as well as nucleolar size.

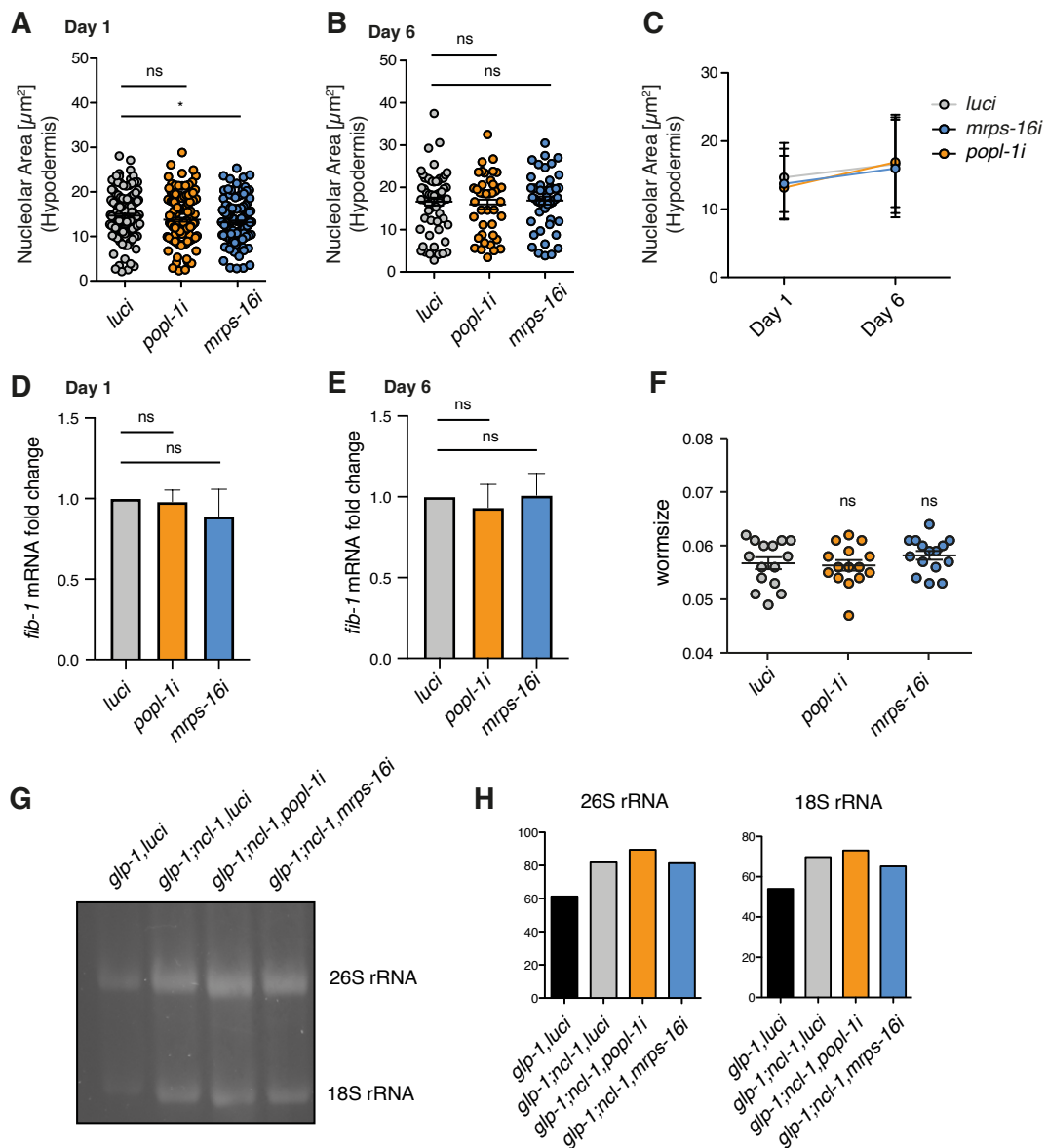


Figure 18. Nucleolar outputs are unaffected by a reduction in *popl-1* and *mrps-16*. (A) Nucleolar size in the hypodermis of *glp-1;ncl-1* mutants on *popl-1* and *mrps-16* RNAi at day 1 of adulthood. Nucleolar size is not changed upon *popl-1* RNAi and slightly reduced upon *mrps-16* RNAi compared to *luci* control. (3 biological replicates, One-way ANOVA with Dunnett's multiple comparison test) (B) Nucleolar size in the hypodermis of *glp-1;ncl-1* mutants on *popl-1* and *mrps-16* RNAi at day 6 of adulthood. Nucleolar size is not changed upon both RNAi treatments. (1 biological replicate, One-way ANOVA with Dunnett's multiple comparison test) (C) Hypodermal nucleolar size trends to increase from day 1 to day 6 independent of RNAi treatment. Changes are not significant. Plot based on data from (A) and (B). (D,E) qPCR analysis of *fib-1* mRNA levels. *fib-1* mRNA levels are neither effected on day 1 (D) nor on day 6 (E) of adulthood. (3 biological replicates, One-way ANOVA with Dunnett's multiple comparison test) (F) worm length is not affected by both RNAi treatments. (15 worms per genotype, 1 biological replicate, One-way ANOVA with Dunnett's multiple comparison test) (G,H) Stained RNA gel showing rRNA levels and quantification. 18S and 26S rRNA are increased in *glp-1;ncl-1* mutants and are not affected upon both RNAi treatments. (500 worms per sample, 2 biological replicates)

The processing of rRNA precursors and intermediates also takes place inside or in close proximity to the nucleolus. The RNase P/MRP complex is a crucial component of this processing machinery and is involved in the processing of 18S rRNA precursors as well as tRNAs. RNAi of *popl-1* or *mrps-16* did not affect the increased steady state rRNA levels in *glp-1;ncl-1* mutant animals. However, rRNA has a relatively long half-life (Stoykova et al. 1983) and steady state rRNA levels may not provide full insight into rRNA metabolism. Furthermore, changes in rRNA maturation can have drastic effects on cellular function and trigger ribosomal as well as nucleolar stress (Aubert et al. 2018; K. Yang, Yang, and Yi 2018).

I therefore sought to measure the expression level of rRNA precursors. Mature 18S, 5.8S and 26S rRNA derive from one long 45S precursor. This 45S precursor includes four non-coding regions that are gradually cleaved into several different processed forms. Two of them are located at both ends of the 45S rRNA precursor, called externally transcribed spacer (ETS), and two of them, named internally transcribed spacers (ITS), divide the coding regions of 18S rRNA and 26S from 5.8S rRNA (Figure 19A).

To quantify these different rRNA precursors, I used a recently published qPCR approach optimized for *C. elegans* (X. Zhou et al. 2017), in which different primers span different regions of the rRNA precursors and the combined readout of all qPCR measurements reveals the abundance of each specific precursor (Figure 19A).

I isolated total RNA from worms at day 1 of adulthood and prepared cDNA for qPCR. All probes showed an increase in rRNA precursor levels when comparing *glp-1;ncl-1* with *glp-1* mutants. In this comparison, all probes except for #7 showed a similar increase (2.5-3.0 fold in *glp-1;ncl-1*), suggesting a general upregulation of rRNA transcription upon loss of *ncl-1* in a *glp-1(e2141)* background. *popl-1* RNAi tended to further increase 18S rRNA precursors (primers #1, #2, #3), but not the precursor levels of 5.8S and 26S rRNA (primers #5, #6). In contrast to the changes comparing *glp-1(e2141)* worms and *glp-1;ncl-1* mutants, these changes did not reach significance. No changes were observed upon RNAi-mediated knockdown of *mrps-16* (Figure 19B). Additionally, the same trend was observed in worms harvested at day 6 upon *popl-1* RNAi but this time for primer pairs #2 and #5 (Figure 19C).

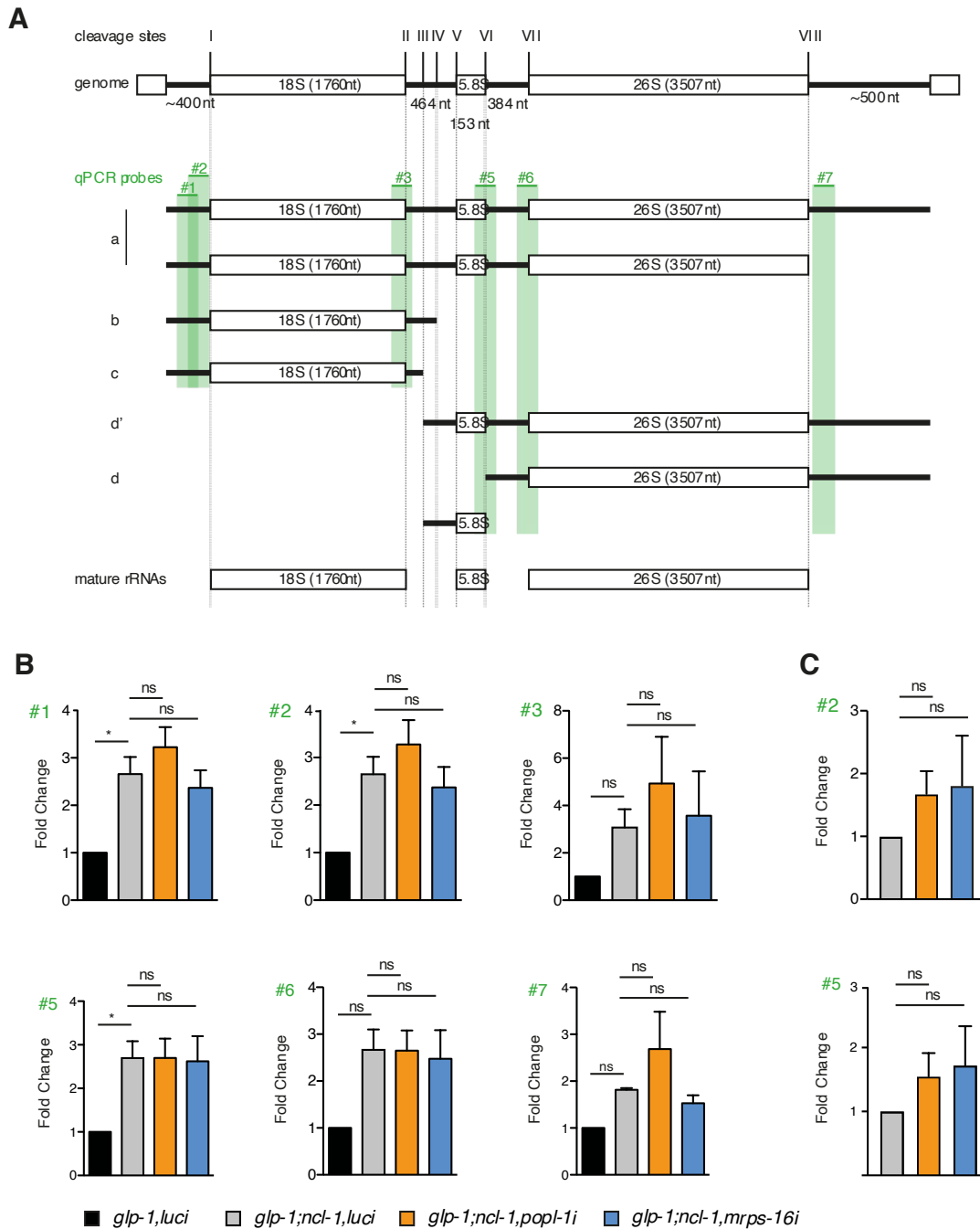


Figure 19. *popl-1* affects distinct rRNA maturation steps. (A) Schematic representation of rRNA processing steps and intermediates. qPCR probe binding sites to rRNA precursors are depicted in green. qPCR probes do not bind to mature rRNA. Figure adapted from Saijou et al., 2004. (B) qPCR results show a 2-3 fold increase of measured precursors in *glp-1; ncl-1*. Changes are not significant. 18S rRNA precursors are increased upon *popl-1* RNAi treatment. 26S rRNA precursors are not affected. *mrps-16* RNAi does not affect precursor levels. Measurements are normalized to *snb-1* mRNA. (3 biological replicates, day 1 adults, One-way ANOVA with Dunnett's multiple comparison test) (C) A similar trend was observed at day 6 of adulthood. This time also primer pair #5 shows an increasing trend. Changes are not significant. (3 biological replicates, day 6 adults, One-way ANOVA with Dunnett's multiple comparison test)

4. *ncl-1* affects the translation machinery

NCL-1 has been proposed to regulate protein translation rates in *C. elegans* (Frank and Roth 1998; Hedgecock and Herman 1995; Tiku et al. 2017). However, the question remains whether a knockdown of *popl-1* and *mrps-16* affects translation.

To address this question, I performed puromycin assays with *glp-1(e2141)* worms, *glp-1;ncl1* worms and both RNAi treatments in the double mutant background at day 1 of adulthood. For this experiment, worms were exposed to a defined concentration of puromycin for a certain amount of time. During peptide elongation, the compound gets incorporated into the newly produced polypeptide chains. A quantification of the incorporated puromycin can therefore give insight into the active translation rate of the worm. I observed a slight increase in overall translation upon loss of *ncl-1* in the *glp-1(e2141)* background (Figure 20A,B); however, the results were variable and need to be confirmed by a second method. In any case, I observed no reduction in puromycin incorporation upon *popl-1i* and *mrps-16i*, suggesting that their effect on lifespan is not mediated by a global decrease in translation.

In sum, *popl-1i* and *mrps-16i* apparently rescue longevity of *glp-1;ncl-1* independent of nucleolar size, fibrillarin expression, steady state rRNA production, and possibly protein synthesis.

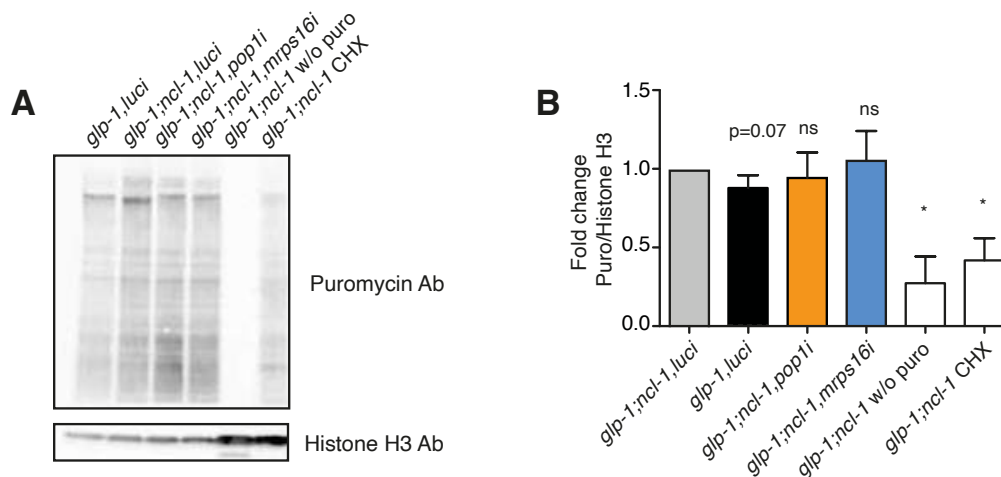


Figure 20. *pop1-1* and *mrps-16* do not affect overall translation. (A) Western blot shows puromycin incorporation to assess translation rate. (B) Quantification of signals from (A). *glp-1; ncl-1* mutants show a slight increase in translation compared to *glp-1(e2141)*. Both RNAi treatments do not affect puromycin incorporation rate. The negative control does not show a signal, the positive cycloheximide control shows decreased incorporation. Changes are not significant but consistent. (3 biological replicates, day 1 adults, One-way ANOVA with Dunnett's multiple comparison test, * $p < 0.05$, CHX = cycloheximide)

To gain further insight into mechanism, I next turned to ribosome profiling in order to quantify ribosome assembly and monosome to polysome ratios. These profiling experiments were performed under my supervision by Torsten Bücher, a master student in the lab. For the analysis we used *ncl-1(e1942)* mutants at day 1 of adulthood in a normal and long-lived *glp-1(e2141)* background. Profiling of *ncl-1(e1942)* single mutants and N2 worms did not reveal any differences in the ribosome profile (Figure 21A). Quantification of the different subunits, monosomes and polysomes also did not reveal any notable differences (Figure 21B).

In contrast, I found striking differences when I compared the profiles of *glp-1; ncl-1* double mutants to *glp-1(e2141)* mutants. Although the analysis input was normalized to RNA content, all peaks were higher in *glp-1; ncl-1* mutants, thus recapitulating the general upregulation of the ribosome biogenesis machinery observed with the omics analysis (Figure 21C). In particular, I found a strong increase in the ratio of 40S to 60S subunits as well as 40S to monosome ratio, suggesting an imbalance between the different ribosomal components and their assembly (Figure 21D). We further found an increased monosome to polysome ratio in *glp-1; ncl-1* mutants, suggesting an

accumulation of monosomes. This data indicates that the *ncl-1(e1942)* mutation remodels ribosome assembly in the long-lived *glp-1(e2141)* background.

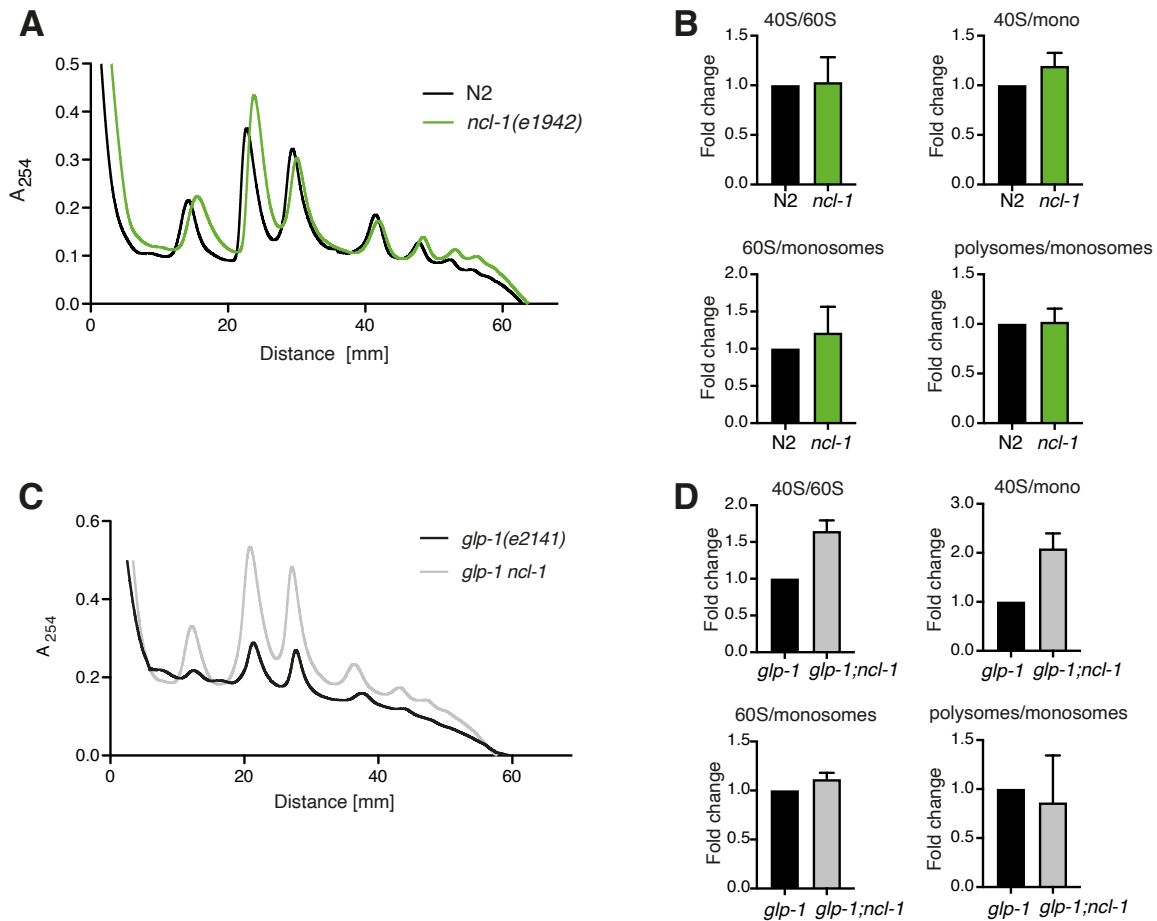


Figure 21. *ncl-1* affects ribosome profile only in long-lived background. (A) Ribosome profile of *ncl-1(e1942)* mutants in comparison to N2 worms is not changed. (B) Quantification and ratio of different subunits, monosomes and polysomes from profiles in (A). Ratios are not affected by *ncl-1(e1942)* mutation. Differences are not significant (3 biological replicates, day 1 adults, t-test) (C) Ribosome profile of *glp-1;ncl-1* mutants compared to *glp-1(e2141)* shows a different ribosome and subunit distribution. (D) Quantification and ratio of different subunits, monosomes and polysomes from profiles in (C). The 40S subunit is increased compared to the 60S subunit. The 40S subunit is increased compared to monosomes while 60S subunit is unchanged. The polysome to monosome ratio is unchanged. (2 biological replicates, day 1 adults)

Chapter 2: The molecular mechanism of NCL-1 action

The second chapter describes separate and important findings regarding the molecular mechanism of NCL-1 action. Despite its striking effect on nucleolar size, hardly anything is known about how NCL-1, a cytoplasmic protein, affects the nucleolus. In this chapter I examine possible mechanisms from the perspective of NCL-1 interaction partners, localization and regulation throughout aging.

1. NCL-1 is differentially expressed in different tissues and localizes to the outer mitochondrial membrane

All previous studies on NCL-1 levels or localization were conducted by using either worm strains overexpressing the protein or by using a NCL-1-specific antibody (Frank and Roth 1998; Tiku 2016). Both techniques have distinct limitations, including overexpression artifacts and the challenge of using *C. elegans* for antibody staining. Therefore, I generated two worm strains expressing endogenously FLAG and NEONGREEN tagged NCL-1 using CRISPR/Cas genome engineering (Figure 22A,B). FLAG-tagged NCL-1 allows for conducting biochemical assays such as immunoprecipitations of NCL-1, Western blotting and other biochemical assays. The fluorescent line allows the characterization of the subcellular and tissue localization of NCL-1 in more detail. I designed the constructs, and the strains were then generated by Sunybiotech, China. I confirmed the sequence of both strains via sequencing and validated the expression of both transgenes.

I found that NCL-1-FLAG is expressed in *ncl1::flag* worms and could detect bands with the corresponding size of all NCL-1 isoforms (Figure 22A). I examined the expression of NCL-1-NEONGREEN using fluorescent imaging and was also able to confirm expression in this strain. I verified that the obtained signal was specific to NCL-1, by treating the NCL-1-NEONGREEN worms with *ncl-1* RNAi. I observed decreased signal upon RNAi treatment, showing the specific expression of NCL-1-NEONGREEN (Figure 22B).

Using a *ncl-1* overexpressing worm strain, our lab previously showed that NCL-1 is not ubiquitously expressed but limited to certain tissues. I performed confocal imaging using the *ncl-1::neongreen* worms and was able to confirm our previous findings, with NCL-1-NEONGREEN being expressed in the vulva, neurons, pharynx and seam cells. Additionally, I observed expression in the hypodermis and the germline (Figure 22C).

To test whether the transgenes were functional, I measured nucleolar size in the hypodermis. I did not observe any significant changes in *ncl-1::flag* worms, indicating that the construct is functional and can be used for further analyses. However, I saw a significant increase in hypodermal nucleolar size in *ncl-1::neongreen* animals, indicating that the construct may not be fully functional (Figure 22D). Nevertheless, since the expression appears specific and the expression pattern resembles what we had observed before, I still used the strain for localization measurements, with appropriate caution.

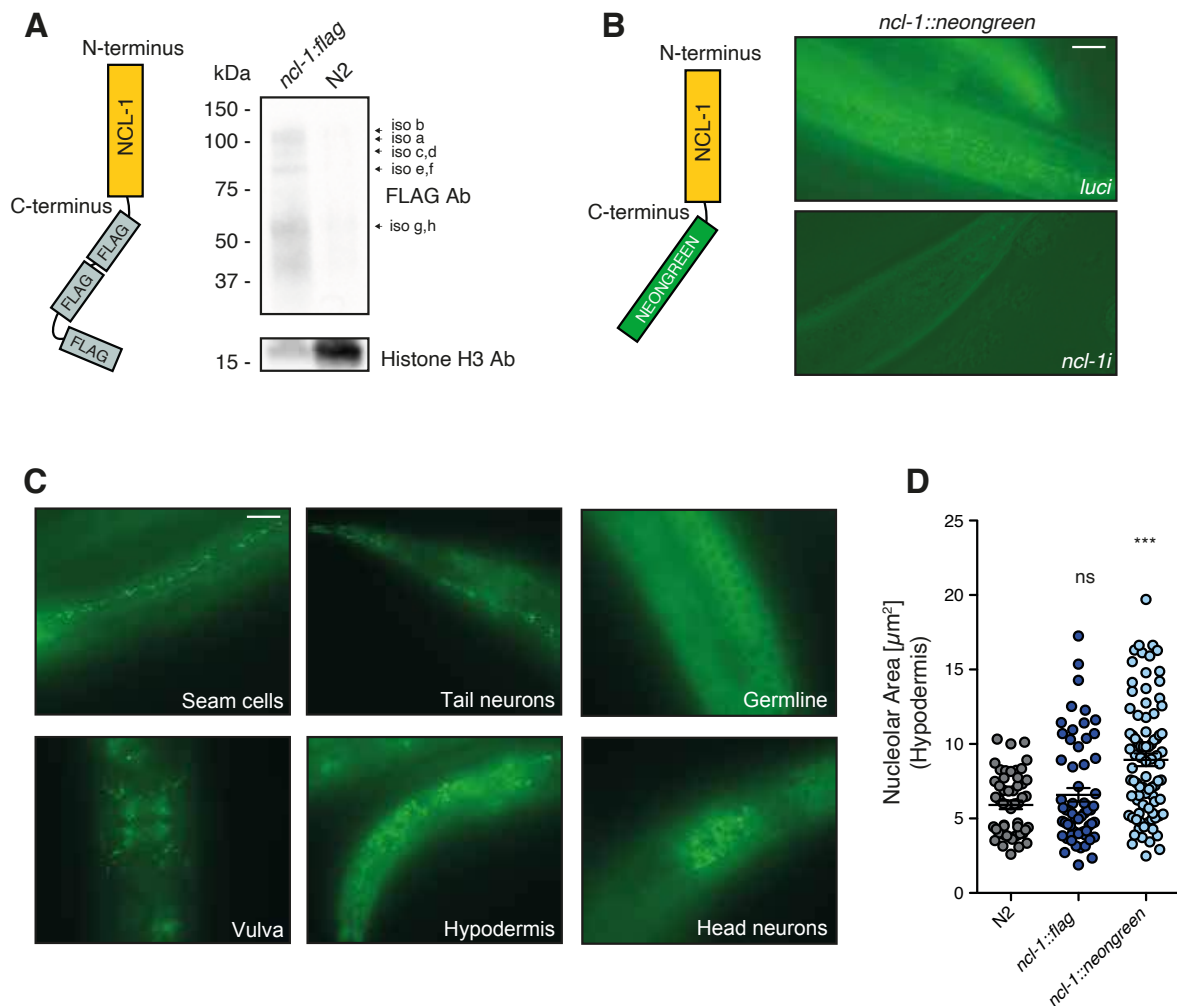


Figure 22. The expression pattern of NCL-1. (A) *ncl-1::flag* transgene structure and expression via Western Blot. All predicted isoforms were manually assigned and detected using FLAG antibody. Histone H3 serves as loading control. (1 biological replicate) (B) *ncl-1::neongreen* transgene structure and expression detected via fluorescent microscopy. *ncl-1* RNAi reduces the green signal, showing signal specificity. (1 biological replicate) (C) Expression of NCL-1-NEONGREEN in different tissues detected via confocal imaging. (1 biological replicate, 63x magnification, scale bar represents 20µm) (D) Nucleolar size is not changed in *ncl-1::flag* but increased in *ncl-1::neongreen* worms. (2 biological replicates, day 1 adults, One-way ANOVA with Dunnett's multiple comparison test, *** $p < 0.001$)

Though NCL-1 is known to be cytosolic, knowledge about its intracellular localization is limited. To address this question, I used confocal imaging and characterized the *ncl-1::neongreen* strain. Unexpectedly, I found NCL-1::NEONGREEN forming round network-like structures and strong foci resembling mitochondria within the hypodermis and muscle at day 1 of adulthood. To determine if these structures were mitochondria,

I stained *ncl-1::neongreen* worms with mitotracker. I observed an obvious overlap of both signals in large areas of hypodermis and muscle, with the NEONGREEN signal appearing to surround the mitotracker signal (Figure 23A). These findings suggest that NCL-1 protein is not simply dispersed in the cytosol, but that a significant fraction is associated with mitochondria in these tissues. I interpret these results with caution, given that the *ncl-1::neongreen* construct is not fully functional.

To examine subcellular localization of NCL-1 using a different system, I expressed NCL-1 under the CMV promoter in human cell culture. For these experiments, I cloned the longest cDNA isoform of *C. elegans* NCL-1 into a pcDNA3.1 vector fused to N-terminal FLAG-tag, to exclude that either the C-terminal tagging of NCL-1 or the NEONGREEN-tag itself affect NCL-1 localization. I subsequently transfected N2a cells with this construct and stained the cells with mitotracker and anti-FLAG antibodies. Confocal imaging here also showed that a fraction of NCL-1 surrounds the area of mitochondrial staining (Figure 23B). Collectively, these data suggest that NCL-1 may have a function associated with mitochondria.

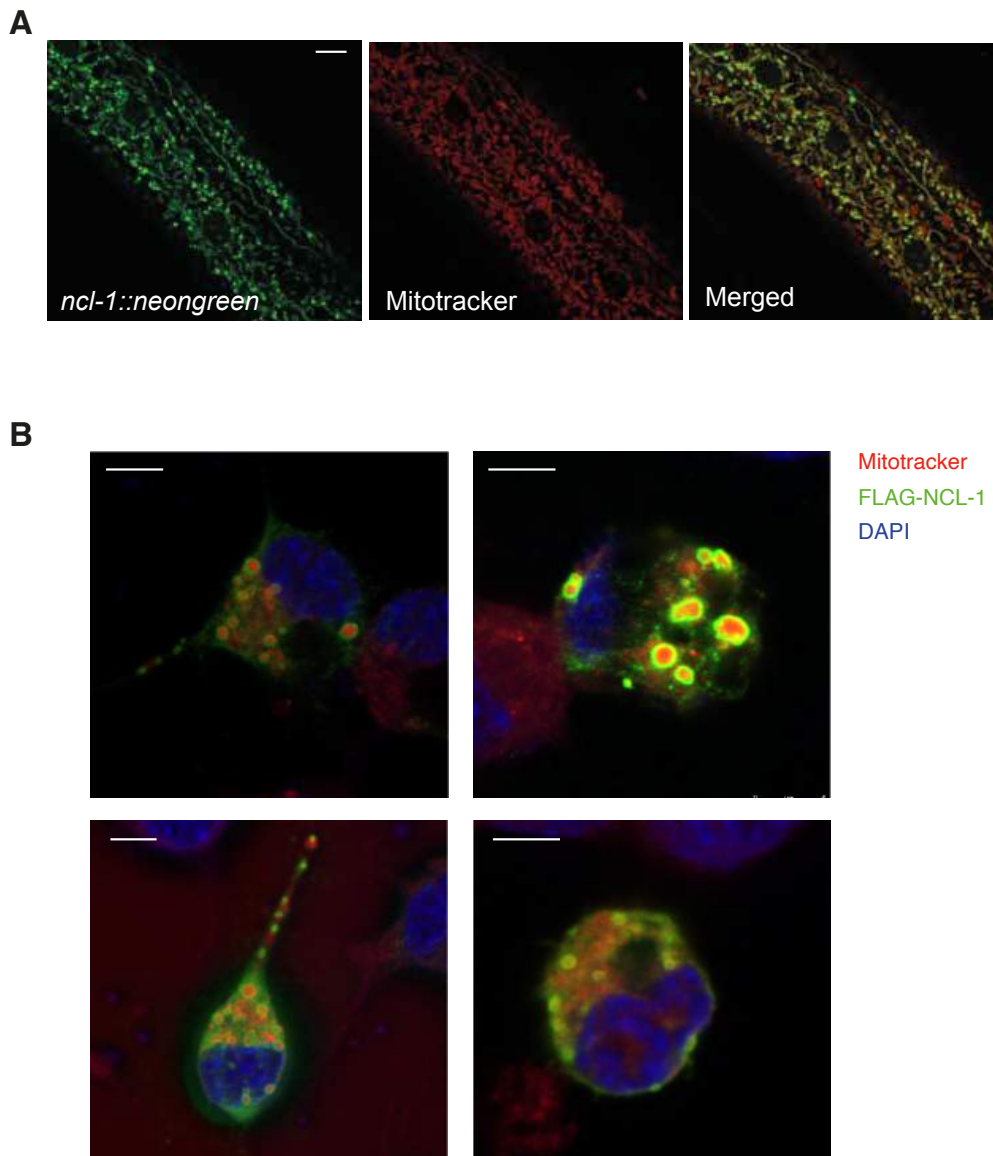


Figure 23. NCL-1 localizes to the outer mitochondrial membrane. (A) Confocal images of *ncl-1::neongreen* worms with mitotracker staining. The neongreen signal colocalizes or surrounds the mitochondrial staining. (>10 worms were imaged per sample, 3 biological replicates, day 1 adults, scale bar represents 20 μm) (B) Confocal images of N2a cells transfected with *flag::ncl-1* and stained with respective fluorescent antibody against the FLAG tag and mitotracker. The green NCL-1 signal localizes to the outer mitochondrial membrane. (>10 cells were imaged, 1 biological replicate, scale bars represent 5 μm)

2. NCL-1 regulates nucleolar size cell non-autonomously

NCL-1 is not expressed equally in all tissues, and generally tissue levels of expression inversely correlate with nucleolar size. This is also reflected in the diverse impact of *ncl-1* mutation on the change in nucleolar size in the various tissues. For example, the change of nucleolar size of gut cells is marginal (where expression is weak), while the increase in nucleolar size in neuronal and hypodermal cells is dramatic (where expression is strong). Because of these tissue-specific differences, I was curious to check whether the machinery that regulates nucleolar size is regulated intrinsically in different tissues, or if there is also communication between the tissues.

To study this question, I used a tissue-specific RNAi knockdown approach, using the SID-1 system. SID-1 is a dsRNA transporter and essential for the spreading of RNAi between tissues. Therefore, *sid-1* mutants are globally RNAi deficient. But by expressing *sid-1* in selected tissues, RNAi can be restored in a tissue-specific manner. For this study, I used *sid-1(qt9)* whole body deletion mutants and tissue-specific rescues in muscle, neurons and the intestine (*myo-2p*, *rab-3p*, *gly-19p*). I treated all strains with luciferase RNA control and *ncl-1* RNAi (Strains were kindly provided by the Hansen lab) (Figure 24A).

To begin with, I monitored nucleolar size in hypodermal cells of N2 worms, *sid-1* mutants, and the three tissue-specific rescue strains on day 1 of adulthood. As expected, *sid-1* mutants did not respond to the *ncl-1* RNAi treatment, while in N2 controls, hypodermal nucleolar size was strongly increased. Neither the knockdown of *ncl-1* in muscle or neurons affected hypodermal nucleolar size. Surprisingly, however, *ncl-1* RNAi in the gut caused a strong increase in nucleolar size in the hypodermis. This suggest that NCL-1 in the intestine may signal cell non-autonomously to other tissues (Figure 24B).

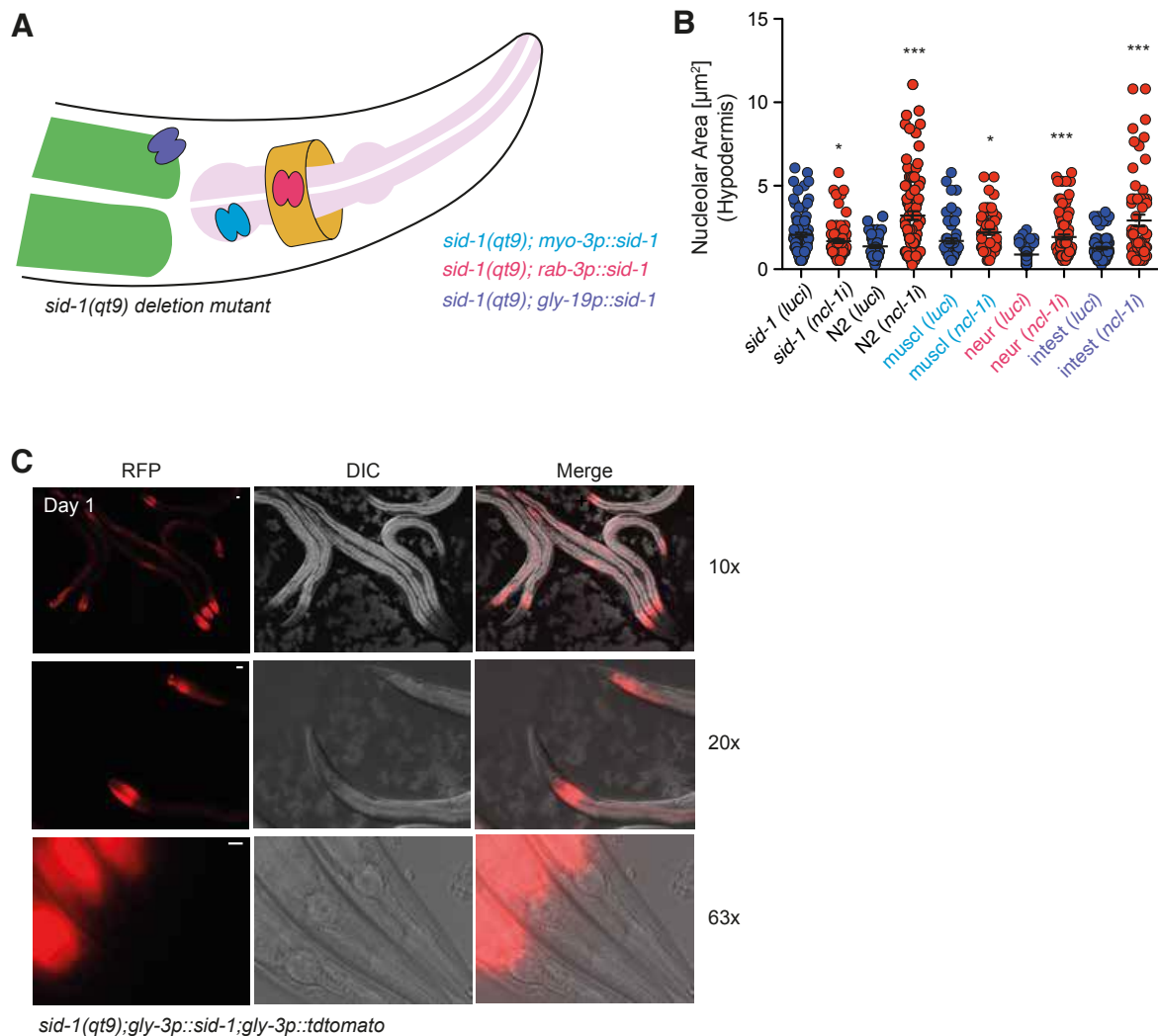


Figure 24. Tissue-specific reduction of *ncl-1* in the intestine increases hypodermal nucleolar size. (A) Schematic representation of tissue-specific *sid-1* rescue in whole body *sid-1(qt9)* deletion mutants. (B) Measurements of hypodermal nucleolar size upon *ncl-1* and control RNAi. A specific reduction of *ncl-1* in the intestine strongly increases nucleolar size in the hypodermis. (> 15 worms per genotype, day 1 adults, 2 biological replicates, t-test, * $p < 0.05$, *** $p < 0.001$) (C) Fluorescent imaging shows intestine-specific tomato expression. No signal was observed in the hypodermis. (>15 worms were imaged, 1 biological replicate, scale bars represent $20 \mu\text{m}$)

Because tissue-specific rescue of *sid-1* is depending on the tissue-specific tightness of the promoter, I investigated whether the gut promoter showed leakiness in the hypodermis. As an internal control, these strains express a fluorescent tomato construct under the same promoter as the SID-1 rescue construct, to monitor general leakiness. When I monitored the expression of this fluorescent marker at day 1 of

adulthood, I observed tissue-specific expression in the gut but no obvious fluorescent signal in the hypodermis or other tissues, indicating a tissue-specific expression of tomato and therefore SID-1 in gut cells at this stage (Figure 24C).

In summary, although NCL-1 has previously been described acting cell-autonomously, the presented data suggests a cell non-autonomous function and the intestine as an important regulatory tissue.

3. The RNA-binding activity of NCL-1 regulates nucleolar size

NCL-1 is a 982 amino acid long protein with 8 reported isoforms. NCL-1 contains several predicted structural domains, including an N-terminal RING domain, two N-terminal B-Box domains, followed by a coiled coil region and a C-terminal 6xNHL repeat domain (UniProt) (Figure 25A). The characterization of homologous proteins predicts functions for these domains. RING and B-Box domains often exhibit an E3 ubiquitin ligase function, making a possible connection to the ubiquitin proteasome system. These domains as well as coiled coil regions are also often found in other TRIM family members (Sardiello et al. 2008). Interestingly, it has recently been shown that the coiled coil domain of BRAT plays an important role in dimerization (C. Liu et al. 2019). In addition, this domain is known to mediate other protein-protein interactions. NHL repeat domains are known to possess an RNA-binding capacity and it has been shown the NHL domains of BRAT and of NCL-1 can bind specific RNA stretches. However, whether there is a specific domain that mediates the effect of NCL-1 on the nucleolus is unknown.

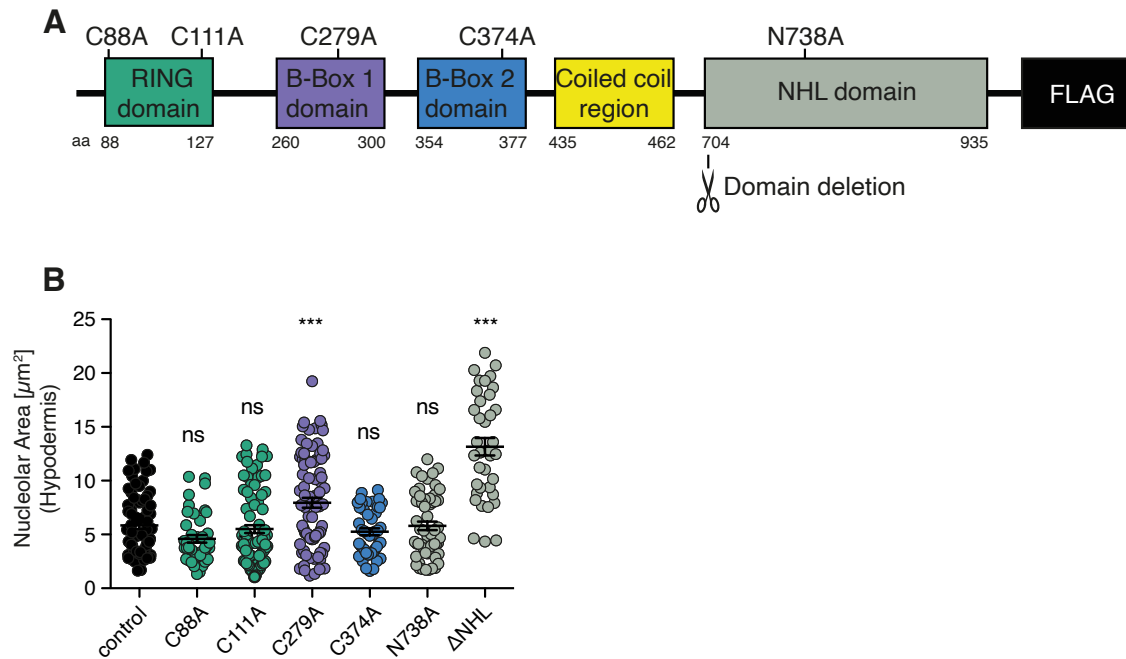


Figure 25. Deletion of NCL-1 NHL domain increase nucleolar size. (A) Schematic representation of predicted NCL-1 domains depicting mutations in active sites of each domain, a conserved residue within the NHL domain and start of the NHL deletion. (B) Hypodermal nucleolar size in the generated domain mutants. A deletion of the NHL domain leads to a strong increase in hypodermal nucleolar size. A weaker increase is observed for C279A mutants. (> 15 worms per genotype, day 1 adults, 2 biological replicates, One-way ANOVA with Dunnett's multiple comparison test, *** $p < 0.001$)

To perform a preliminary structure-function analysis of the NCL-1 protein, I made use of the *ncl-1::flag* worm strain. RING and B-Box domains exhibit their function through binding two zinc ions via certain cysteine and histidine residues. The coordination of those zinc ions is key for the functionality of the domains and a mutation is detrimental for the domains functionality (Anthony Massiah 2019; Laity, Lee, and Wright 2001). I exchanged one of those amino acids in each domain. In addition, I generated a mutant completely lacking the NHL domain and additionally mutated a highly conserved amino acid within the NHL domain. All mutated amino acids were changed to an alanine residue because of its chemical and physical properties. I performed the strain design myself; CRISPR gene editing as well as mutant selection was conducted by Sunybiotech, China. I confirmed the correct mutagenesis via sequencing.

To assess any impact on the nucleolus, I measured nucleolar size in the hypodermis of all generated mutants. Mutations in the RING domain and B-Box 1 as well as the conserved amino acid within the NHL domain did not result in any drastic changes. However, upon mutating the active site of B-Box 2, I detected a significant increase in nucleolar size. I saw a much larger increase upon deletion of the NHL domain, which was comparable to that seen in *ncl-1* null mutants (Figure 25B).

4. Protein-protein interactors of NCL-1

To better understand the mechanism of NCL-1 action I sought to identify protein interaction partners of NCL-1. I took three different approaches - a candidate approach based on publicly available data and two unbiased approaches using immunoprecipitation and a Yeast-2-Hybrid (Y2H) screen.

4.1 A novel connection between the RNAi machinery, nucleolar size and lifespan

The STRING database (string-db.org) offers a good overview of functional connections and protein-protein interactions of several proteins in different species, based on experimental data. One NCL-1 interactor is NRDE-3, which is the AGO1 ortholog in *C. elegans*. This interaction was observed from high throughput Y2H using NRDE-3 as bait (Simonis et al. 2009). *Nrde-3* is part of the endogenous RNAi machinery and plays an important role in nuclear RNAi pathways, binding silencing RNAs to transport them into the nucleus (Figure 26H) (Burkhart et al. 2011). NRDE-3 also binds ribosomal silencing RNAs which specifically silence rDNA loci (X. Zhou et al. 2017). Moreover, it has been shown that the argonaut protein AGO1 is an interaction partner of the NCL-1 drosophila ortholog BRAT (Neumüller et al. 2008) and there is evidence that the predicted human NCL-1 ortholog, TRIM32, interacts with Ago1 in a NHL-domain-dependent manner (Schwamborn, Berezikov, and Knoblich 2009).

Based on this intriguing connection to nucleolar function, I focused on NRDE-3 as a candidate interactor of NCL-1.

If NCL-1 and NRDE-3 act in the same pathway, then a reduction of NRDE-3 should similarly affect nucleolar size. To assess the effect of *nrde-3* on nucleolar size, I measured hypodermal nucleolar size in the *nrde-3(gg66)* mutant (Guang et al. 2008). Interestingly, I observed a weak but consistent 30% increase in nucleolar size compared to WT control. By comparison, loss of *ncl-1* leads to a vastly stronger increase of nucleolar size (>100 %) (Figure 26A). To generate a second line of evidence, I measured expression of a FIB-1::GFP reporter construct both by manual measurement via fluorescent microscopy and in an automated fashion using a copas biosorter. Both methods indicated that FIB-1::GFP reporter was increased in *nrde-3(gg66)* mutants, confirming a role for this gene in regulating nucleolar function similar to *ncl-1(e1942)* (Figure 26B,C,D).

Our previous studies demonstrated that the *ncl-1*-dependent increase of nucleolar size is accompanied by the partial or complete abolishment of longevity in several regimes. To test whether *nrde-3(gg66)* mutant also affect longevity, I crossed the *nrde-3* into the long-lived *glp-1(e2141)* and *daf-2(e1370)* mutant backgrounds. Lifespan analysis revealed that loss of *nrde-3* completely abolishes *glp-1(e2141)* longevity, but had only a minor or no effect on WT lifespan (Figure 26E). Hypodermal nucleolar size measurements in *glp-1;nrde-3* double mutants confirmed that the shorter lifespan was accompanied by an increase in nucleolar size, though to a lesser extent as in *glp-1;ncl-1* double mutants (Figure 26F). By contrast, I saw no effect of *nrde-3(gg66)* mutation on *daf-2(e1370)* lifespan (Figure 26G).

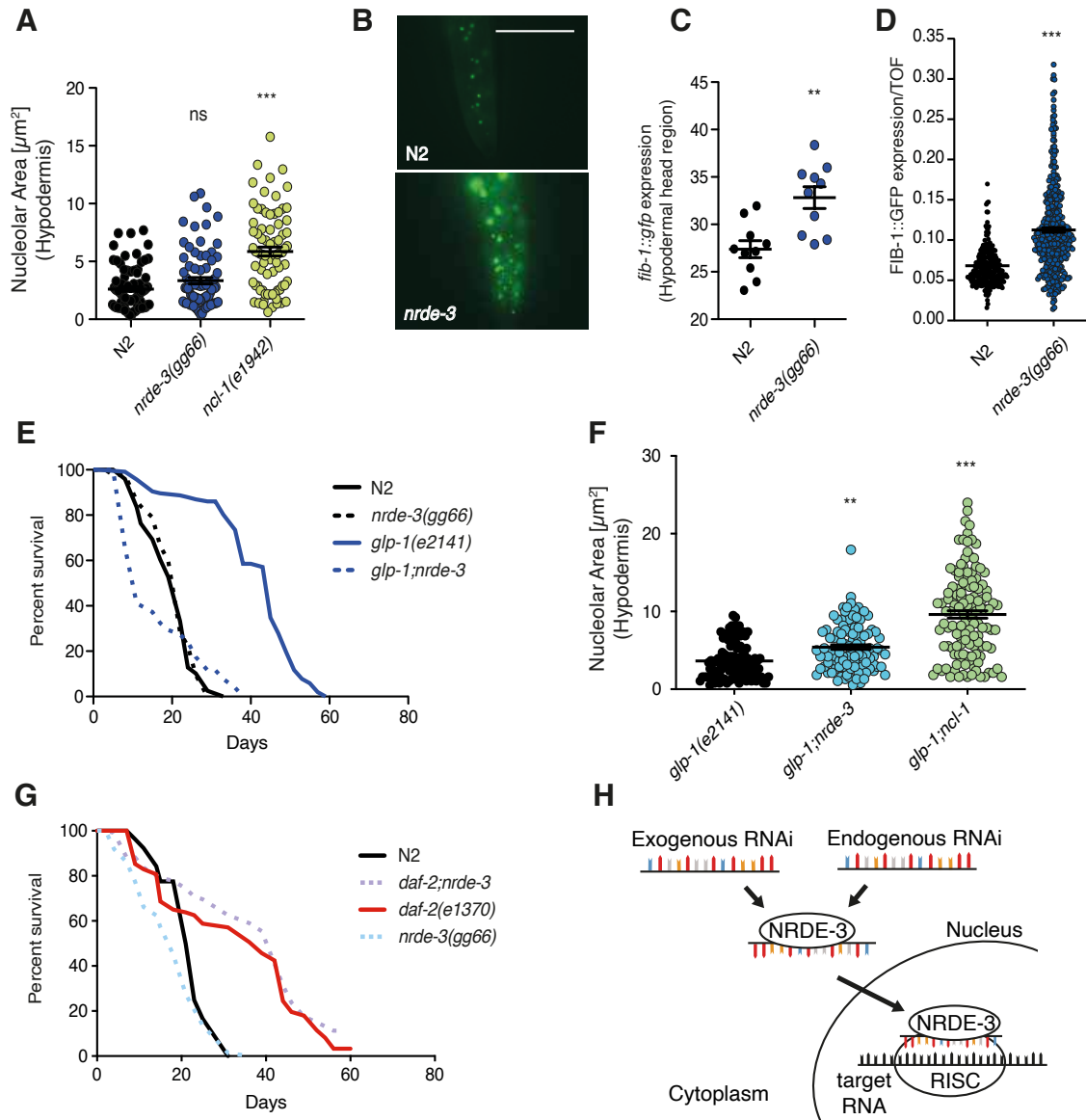


Figure 20. *nrde-3* affects nucleolar size and lifespan in a similar fashion as *ncl-1*. (A) Hypodermal nucleolar size measurements. Nucleolar size is significantly increased in *nrde-3(gg66)* and *ncl-1(e1942)* mutants. (3 biological replicates, day 1 adults, >20 worms per genotype, One-way ANOVA with Dunnett's multiple comparison test, *** $p < 0.001$) (B) Example images of FIB-1-GFP expression in the head region of *nrde-3(gg66)* mutants. (Scale bar represents 20 μm) (C) Quantification of (B). FIB-1-GFP expression is increased the head region of *nrde-3(gg66)* mutants. (10 worms per genotype, 2 biological replicates, day 1 adults, t-test, ** $p < 0.01$.) (D) Biosorter quantification of FIB-1-GFP signal in whole worms. The GFP signal is increased in *nrde-3(gg66)* mutants. (>500 worms per genotype, 1 biological replicate, day 1 adults, t-test, *** $p < 0.001$) (E) Lifespan analysis of *nrde-3(gg66)* mutants in WT and *glp-1(e2141)* background. *nrde-3* does not affect WT lifespan. *glp-1(e2141)* longevity is completely abolished upon loss of *nrde-3(gg66)*. (>100 worm per genotype, 3 biological replicates, Mantle Cox test) (F) Hypodermal nucleolar size measurements. Nucleolar size is significantly increased upon loss of *nrde-3* and *ncl-1* in a *glp-1(e2141)* background. (>20 worms per genotype, 2 biological replicates, day 1 adults, One-way ANOVA with Dunnett's multiple comparison test, ** $p < 0.01$, *** $p < 0.001$) (G) Lifespan analysis of *nrde-3(gg66)* mutants in WT and *daf-2(e1370)* background. Neither *daf-2* nor WT lifespan are affected by *nrde-3(gg66)*. (>100 worm per genotype, 2 biological replicates, Mantle Cox test)

4.2 Unbiased identification of NCL-1 interacting proteins

In addition to the candidate-based analysis of NCL-1 interactors, I also took two unbiased approaches. I first performed a Yeast-2-Hybrid screen in close collaboration with the company Hybrigenics Services, France. We started the screen with a full length NCL-1 protein construct, but due to strong auto-activation we were unable to use it as bait. Therefore, we tested 5 NCL-1 fragments of different sizes, covering different domains of the protein. We found a fragment covering the coiled coil region and the NHL domain as most suitable for the subsequent interaction screen, based on non-specific yeast growth on selective medium (Figure 27A). For the screen we used a library comprising proteins expressed in mixed stages of *C. elegans* development. Interaction analysis resulted in a list of 46 positive screen candidates. Based on their experience from previous Y2H screens, Hybrigenics Services assigned confidence scores for a real interaction to each candidate via bioinformatic big data analysis. The screen resulted in two very high confidence factors (REGE-1, PAR-5), three high confidence factors (SNAP-1, SPC-1 and EIF-3.B) as well as several medium

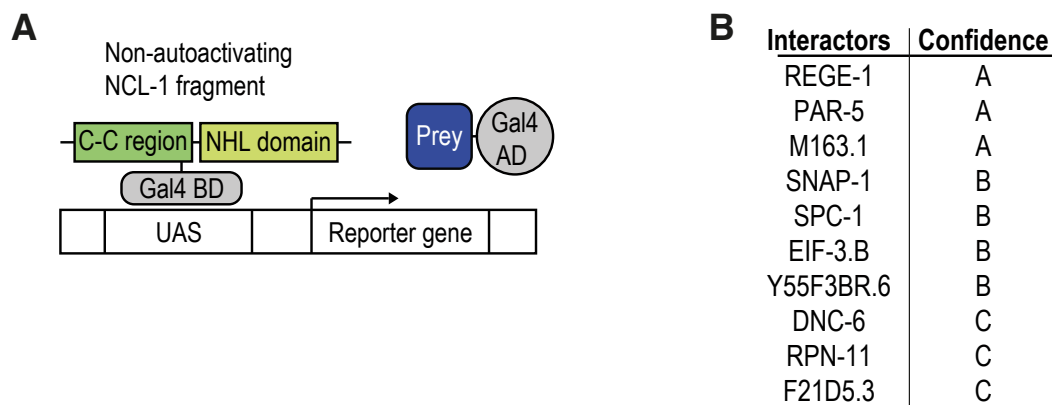


Figure 27. A Yeast-2-Hybrid screen identifies potential NCL-1 protein interaction partners. (A) Schematic representation of Yeast-2-Hybrid screen setup. A NCL-1 fragment covering the coiled coil and NHL domain of NCL-1 was used as bait. A mixed stage library of *C. elegans* proteins was used for prey screening. (B) Candidates based on bioinformatically determined confidence (very high (A) - good confidence (C)). Interactors with a „medium confidence“ and lower are not displayed.

confidence interactors. Out of those I considered DNC-6 and RPN-11 as biologically interesting and also worth further pursuit (Figure 27B).

In concert, I sought to identify NCL-1 interactors through pulldown and mass spectrometry analysis to find associated proteins (Figure 28A). For this, I made use of the *ncl-1::flag* strain and immunoprecipitated complexes from whole worm extracts derived from day 1 adults. I controlled for a specific enrichment of NCL-1-FLAG via Western blot analysis (Figure 28B), which was further on confirmed by mass spectrometric quantification (Figure 28C). Mass spectrometric identification of NCL-1-FLAG co-enriched proteins suggested several (>70) potential protein interactors (Figure 28C). Notably, two factors which were also found in the Y2H screen could also be confirmed in this approach. Both the SNARE protein SNAP-1 and the translation elongation factor EIF-3.B were found strongly co-enriched with the purified NCL-1-FLAG construct.

Manually going through the co-enriched fraction, I observed distinct compartments and complexes being represented more than others. Interestingly, three components of the nascent polypeptide-associated complex (ICD-1, ICD-2, HSP-110) and two components of the signal recognition particle complex (SRPA-68, SRPA-72), which both play an important role in assisting with protein translation and folding, were detected in the co-enriched fraction. Furthermore, several factors are resident to mitochondria, consistent with my microscopy data showing close proximity of NCL-1 to this organelle. Although RPN-11, which was identified in the Y2H screen, could not be confirmed via IP-MS, several components and factors related to the proteasome were found co-enriched with NCL-1-FLAG, namely RPN-13, RPT-5, RPN-5 and RPN-6.1 (Figure 28D).

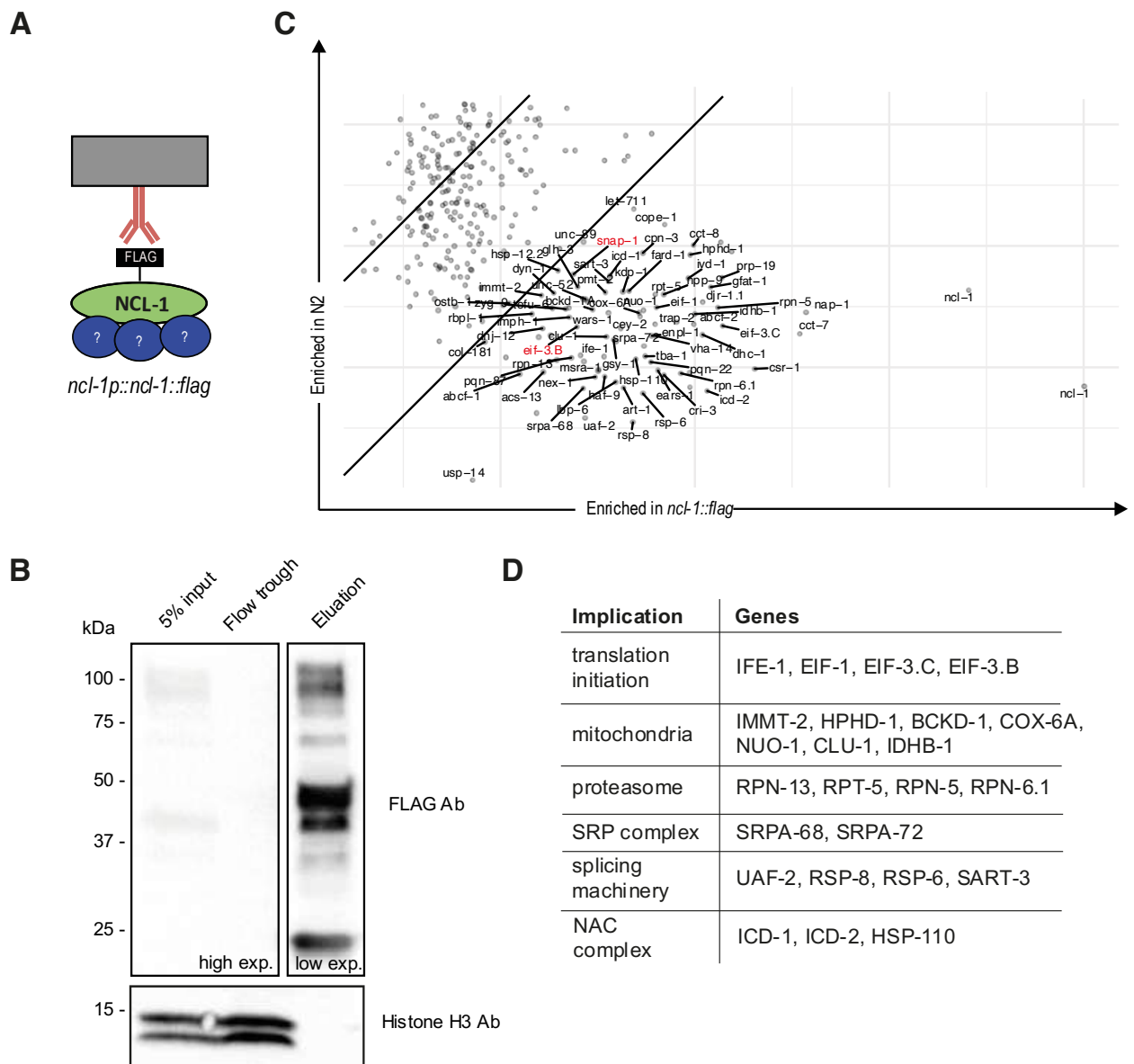


Figure 28. A combined immunoprecipitation - mass spectrometric approach suggests novel NCL-1 interactions partners in *C. elegans*. (A) Schematic representation of immunoprecipitation setup. (B) Western blot showing enrichment of NCL-1-FLAG isoforms after immunoprecipitation. (exp. = exposure time) (C) Co-enriched proteins with NCL-1-FLAG. NCL-1 is highly enriched and two candidates (SNAP-1, EIF-3B) from the Y2H screen are co-enriched (red). (1 biological replicate, day 1 adults) (D) Candidate groups with specific implications.

To follow up on the list of candidates, I tested their ability to affect nucleolar size. Therefore, I performed a mini screen of 7 candidates, and treated *glp-1(e2141)* worms with RNAi, measuring nucleolar size at day 1 of adulthood in the hypodermis. The only candidate with a notable increase of nucleolar size in two replicates was the

proteasomal subunit RPN-11, suggesting a possible direct link between NCL-1, nucleolar size regulation and the proteasome (Figure 29).

Furthermore, the enrichment for NCL-1-FLAG was high enough to enable us to identify a phosphorylation site within the coiled coil domain of NCL-1, providing a first hint of a possible mechanism regulating NCL-1 activity.

5. NCL-1 plays a role in cellular proteostasis

Aside from ribosomal function and protein synthesis, my omics data showed that several aspects of proteostasis were changed in response to *ncl-1* loss: the induction of cytosolic and mitochondrial stress responses indicated by the increased levels of *hsp-16.1* and *hsp-60* in *ncl-1(e1942)* mutants; induction of *hsp-70* on RNA level; a reduction of proteasomal subunits and factors specifically in *ncl-1(e1942)* mutants in a WT background; and a reduction of lysosomal subunits in the *glp-1(e2141)* background. To unravel the connection of *ncl-1* to these regulatory networks, I carried out preliminary experiments exploring the role in proteostasis.

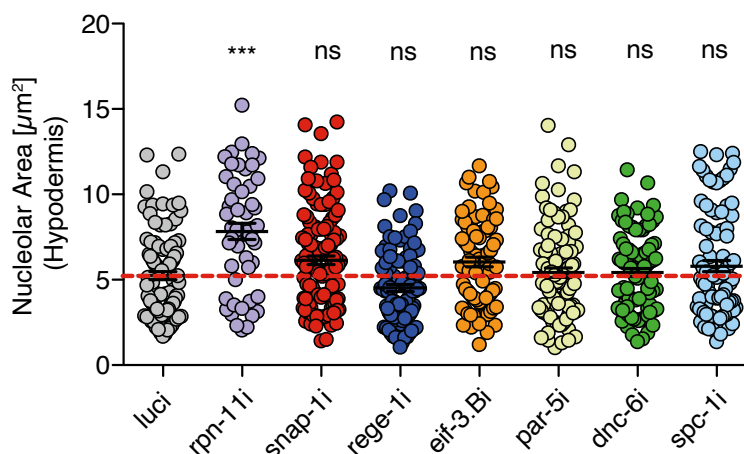


Figure 29. Reduction of the proteasomal factor *rpn-11* increases nucleolar size in *glp-1(e2141)*. (A) Hypodermal nucleolar size measurements in *glp-1(e2141)* mutants upon NCL-1 protein interactor knockdown. Nucleolar size is increased upon RNAi-mediated knockdown of *rpn-11*. (>20 worms per genotype, 2 biological replicates, day 1 adults, One-way ANOVA with Dunnett's multiple comparison test, *** $p < 0.001$)

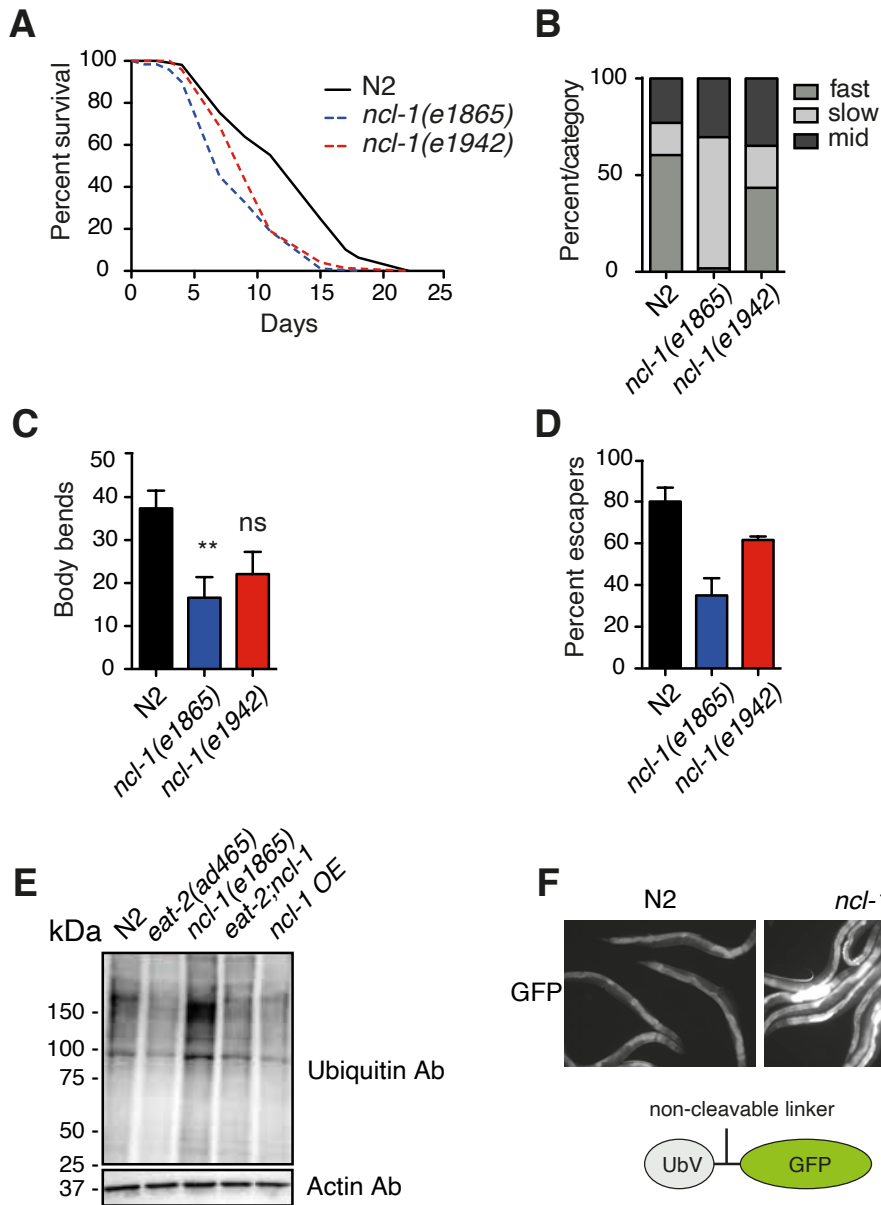


Figure 30. *ncl-1* affects the proteasomal protein degradation machinery. (A) Lifespan analysis of *ncl-1(e1942)* and *ncl-1(e1865)* worms under heatstress (25°C) applied from day 1 of adulthood. Worms with both *ncl-1* alleles live shorter than control. (> 100 worms per genotype, 3 biological replicates, Mantle Cox test) (B) Motility assessment of *ncl-1(e1942)* and *ncl-1(e1865)* worms at day 5 of adulthood under thermal stress (25°C). Worms with both *ncl-1* alleles move less. (>20 worms per genotype) (C) Body bend measurement shows a decreased motility for both *ncl-1* alleles at day 5 of adulthood. (10 worms per genotype, 1 biological replicate, One-way ANOVA with Dunnett's multiple comparison test, * p<0.05, ** p<0.01) (D) Motility measurement via circle assay show less motility for both *ncl-1* alleles compared to control. (>30 worms per genotype, 2 biological replicates) (E) Western blot showing *ncl-1*-dependent changes of overall ubiquitylation. (1 biological replicate, day 1 adults) (E) Proteasomal reporter strain shows substrate accumulation in *ncl-1(e1942)* mutants. (day 1 adults, 2 biological replicates)

As an initial test, I examined how *ncl-1* mutants react to thermal stress, which often induces protein misfolding. As normal *C. elegans* are maintained at 20°C under lab conditions, an increase of 5°C in temperature already evokes a slight protein folding stress (Zevian and Yanowitz 2014). To see how *ncl-1* mutants can cope with this stress, I let the worms develop at 20°C and shifted the plates to 25°C once the worms reached adulthood, and then followed their lifespan. I found that *ncl-1* mutants (both tested alleles) are ~20 % shorter-lived compared to N2 worms grown under the same conditions (Figure 30A), consistent with the idea that they may be more sensitive to thermal stress.

While conducting the lifespan experiments, I observed that *ncl-1* mutants move less under heat stress conditions from approximately day 5 on (Figure 30B). To quantify this observation, I aged worms under the same conditions and conducted motility assays at day 5 of adulthood. Motility was first measured by placing worms into a drop of M9 and counting body bends for 1 min. In a second assay, I drew a circle on the bottom of a seeded NGM plate and placed a fixed number of worms in the middle of the circle. The percentage of worms remaining in the circle was calculated after 3 min and used as a motility readout. In both measurements, *ncl-1* mutants showed decreased motility relative to WT at 25°C. (Figure 30C,D). This finding suggests that *ncl-1* mutants are somewhat heat sensitive. Whether this reflects changes in protein folding stress remains to be determined.

One way the cell removes aggregate-prone proteins ubiquitin-tagging, which serves as a signal for proteasomal degradation (Finley 2009). If proteasomal degradation is impaired, ubiquitinated proteins can accumulate. To measure the overall levels of ubiquitinated protein in *ncl-1(e1865)* mutants, I analyzed worm samples via Western blot using an anti-ubiquitin antibody. This analysis revealed an overall increase in ubiquitinated proteins in *ncl-1* mutants (Figure 30E). Based on this finding and the downregulation of proteasome-associated factors in *ncl-1(1942)* worms, I hypothesized that the proteasome might be less functional in these worms. To test this hypothesis, I used a well-established proteasome activity reporter strain expressing a UbV-fused GFP construct. *C. elegans* mutants with decreased proteasome activity show an accumulation of the GFP substrate (Segref, Torres, and Hoppe 2011).

Repeated measurements of *ncl-1(e1865)* mutants crossed into the reporter strain showed a clear increase in the GFP signal (Figure 30F).

6. NCL-1 as check point for nucleolar size early in life

The nucleolus has been described as a highly dynamic organelle throughout development. For example in yeast, nucleoli undergo an initial expansion phase, followed by fragmentation throughout aging (Lewinska et al. 2014; Sinclair, Mills, and Guarente 1997). However, available studies conducted in *C. elegans* only focus on nucleolar size during development or day one of adulthood. In particular, our published work looking at the connection between nucleolar size and longevity, which identified the nucleolus as a predictive marker for lifespan, was based on measurements at the beginning of adulthood. Knowledge about nucleolar size during *C. elegans* aging is lacking. I therefore wanted to better understand how nucleolar size changes with advancing age, and in particular whether these dynamics were altered in *ncl-1* mutants.

Therefore, I measured hypodermal nucleolar size and the nucleolar marker fibrillarin at day 1 of adulthood and compared it to worms at day 6 of adulthood (which can be considered as middle-aged adults). To monitor possible changes, I used Western blot analysis as well as DIC imaging of hypodermal nucleoli. Focusing on the obtained images of *glp-1(e2141)* worms, nucleoli at day 1 of adulthood were clearly defined and easy to identify. Nucleoli of *glp-1(e2141)* worms at day 6 seemingly possessed more unclear borders and are general less clearly visible in DIC images. A quantification and the comparison of both time points shows that nucleolar size tends to decrease in *glp-1(e2141)* animals until day 6 (Figure 31A,B). Similarly, FIB-1 decreases from day 1, over day 3 up to day 6 of adulthood in N2 animals (Figure 31C,D).

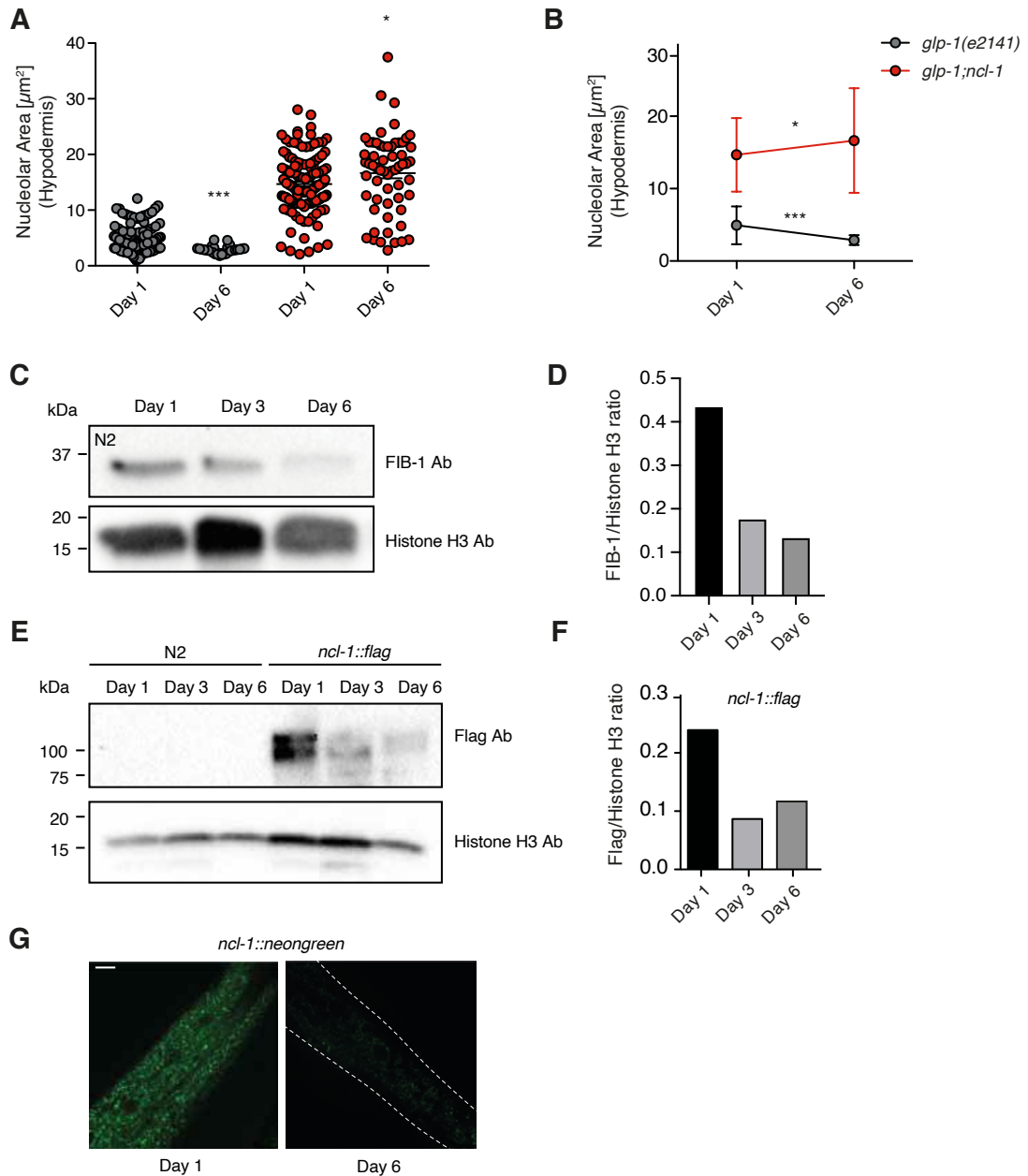


Figure 31. Nucleolar size and NCL-1 show dynamic changes with age. (A,B) Hypodermal nucleolar size measurements show a decreased nucleolar area in *glp-1(e2141)* mutants at day 6 of adulthood. Nucleolar size of *glp-1;nc1-1* mutants is increased. (> 20 worms per genotype, 1 biological replicate, day 1 adults, t-test, * $p < 0.05$, *** $p < 0.001$) (C,D) Western blot analysis and quantification show decrease of FIB-1 between day 1 and day 3 of adulthood. A weaker decrease is detected between day 3 and day 5. (1 biological replicate) (E,F) Western blot analysis and quantification show decreased levels of NCL-1 between day 1 and day 3 of adulthood. NCL-1 levels do not further decrease between day 3 and day 5. (1 biological replicate) (G) NCL-1-NEONGREEN is highly expressed at day 1 of adulthood. The signal intensity is strongly decreased at day 6 of adulthood. (>5 worms per timepoint, 2 biological replicates, scale bar represents 20 μm)

In contrast, nucleolar measurements of *glp-1;ncl-1* worms drew a completely different picture. Nucleolar size measurements at day 6 of adulthood revealed that nucleolar size did not decrease but rather tended to increase over time (Figure 31A,B). More clearly defined nucleoli were visible at day 6 of adulthood compared to *glp-1(e2141)* worms at the same age. These findings suggest that loss of *ncl-1* may not only affect nucleolar size at day 1 of adulthood, but that nucleolar expansion may continue throughout aging.

As NCL-1 itself has been described as a repressor of nucleolar size, I sought to explore if NCL-1 levels also change over time. To monitor NCL-1 levels, I made use of the previously described strains *ncl-1::flag* and *ncl-1::neongreen*. Western blot analysis of *ncl-1::flag* worms at day 1, day 3 and day 6 of adulthood revealed that NCL-1 levels decrease between day 1 and day 3. The levels did not further decrease up to day 6 (Figure 31E,F). Hypodermal images of *ncl-1::neongreen* at day 6 of adulthood compared to day 1 of adulthood support the decrease of NCL-1 over time (Figure 31G). This suggests that the WT decrease in nucleolar size with aging likely acts independently of *ncl-1*.

Discussion

I discovered that NCL-1 interacts with a whole network of different factors and processes by using different unbiased omics approaches, genetic screening and biochemical analysis, as well as candidate testing.

In particular, by an overlapping transcriptomic and proteomic analysis I identified *ncl-1*-dependent changes on mRNA and protein level in normal and long-lived background. While nucleolar outputs such as rRNA processing and ribosome biogenesis were commonly upregulated, others, such as a reduction of proteasomal factors (*ncl-1* vs. N2) and lysosomal components (*glp-1;ncl-1* vs. *glp-1*), were decreased depending on the genetic background. In that context, the RNA-binding function of NCL-1 seems important for the transcriptional response, as I found the RNA-binding motif of NCL-1 enriched in the fraction of significantly regulated mRNAs. This hypothesis was further supported by the finding that a deletion of only the NCL-1 NHL-domain leads to an increase in nucleolar size.

By conducting a genetic screen in *C. elegans*, I uncovered downstream processes of *ncl-1* mediating the effect on lifespan, including the RNase P/MRP complex and mitochondrial translation. In addition, my work further highlighted that NCL-1 has a multifaceted role, and its impact on longevity can be (at least partially) uncoupled from nucleolar size. Based on these findings I generated a model illustrating how NCL-1 is presumably linked to longevity (Figure 32).

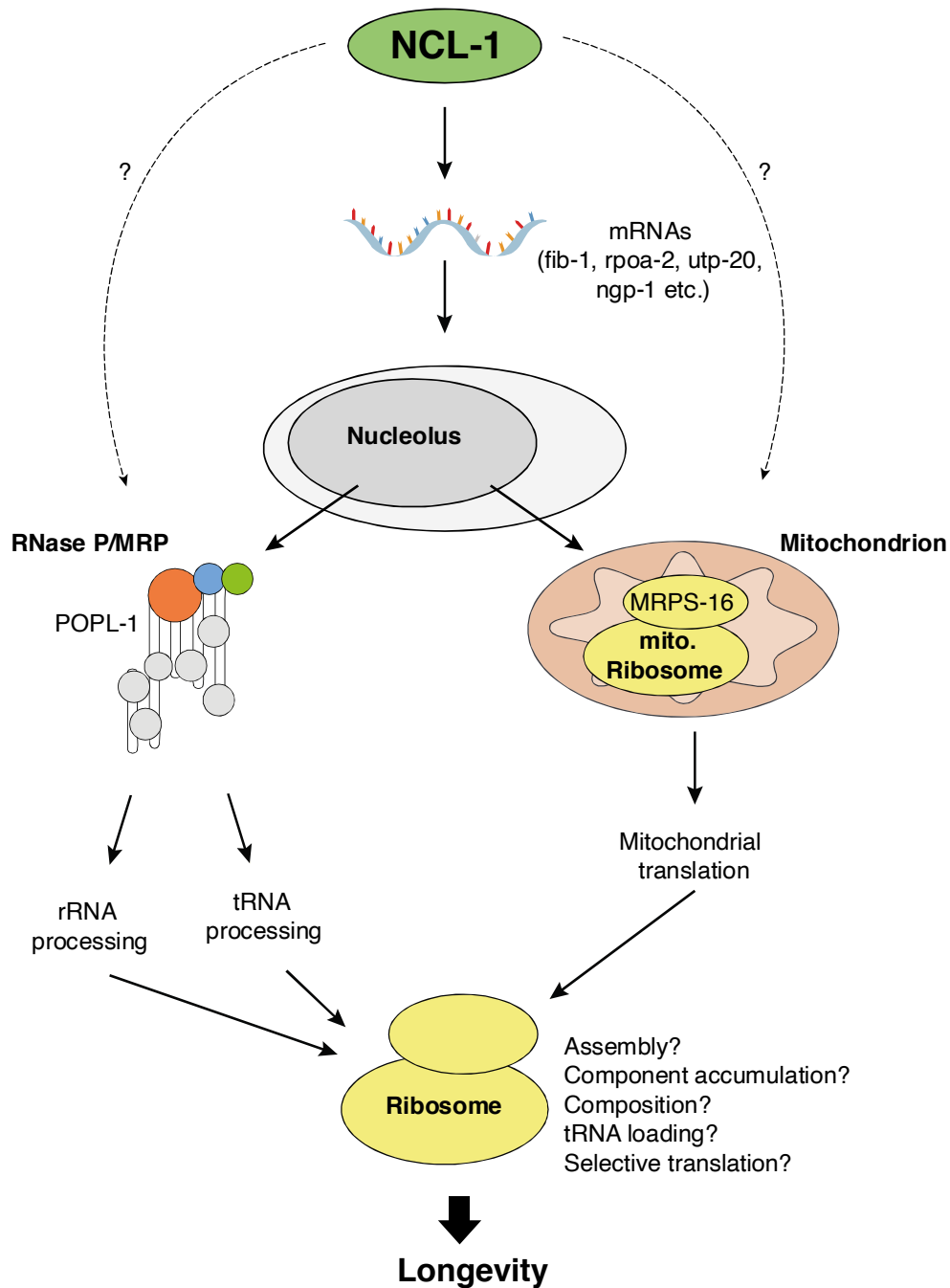


Figure 32. Working model of the connection between *ncl-1* and longevity. NCL-1 presumably binds and inhibits mRNAs affecting nucleolar size and function through a specific binding motif. Nucleolar increase caused by loss of *ncl-1* directly or indirectly affects the RNase P/MRP complex and mitochondrial translation besides other processes. A reduction of the RNase P/MRP component POPL-1 and the mitochondrial ribosome component MRPS-16 prolongs lifespan in *glp-1;ncl-1* mutants but does not affect nucleolar size. Through altered rRNA and/or tRNA processing the RNase P/MRP complex potentially affects the cytosolic ribosome. A similar effect is probably mediated through organellar crosstalk between the mitochondrial and cytosolic translation machinery. *glp-1;ncl-1* worms show an imbalance in ribosome assembly which may be the reason for the shortened lifespan. This effect is potentially reversed by a reduction of POPL-1 and MRPS-16.

1. *ncl-1* affects the transcriptome and proteome dependent on the genetic background

Nucleolar size is increased in *ncl-1* and *glp-1;ncl-1* mutants to a similar extent - lifespan, however, is only affected in long-lived but not in WT worms (Tiku et al. 2017). These findings suggest that the effect of *ncl-1* on downstream processes is dependent on the genetic background - a hypothesis that I found supported by my results from transcriptomic and proteomic analysis of different genotypes. The shared upregulation of rRNA processing, ribosome biogenesis factors and certain ribosomal proteins in all genotypes is in agreement with our previous findings of increased FIB-1 and rRNA levels as well as increased RPS-6 and RPS-15 (Tiku et al., 2017).

Most interesting, the observed decrease in proteasomal subunits is unique to *ncl-1* worms, while most lysosomal and peroxisomal components are decreased solely in *glp-1;ncl-1* worms. Clearly, NCL-1 has the potential to regulate many different cellular processes, such as proteostasis, translation, splicing and RNA metabolism. However, this potential seems only partially realized in any given genetic background.

Some of these differential responses to loss of *ncl-1* are likely due to pre-existing differences in gene regulation in the different backgrounds. For example, proteasomal activity is increased in *glp-1* mutants (Vilchez et al. 2012) and *glp-1* longevity depends on intestinal autophagy (Chang et al. 2017). It is therefore possible that the proteasome and lysosome biogenesis are already affected in a *glp-1* background, thereby masking or enhancing effects of *ncl-1* on both processes. To better understand the interplay between *ncl-1* and proteolytic processes, we should therefore also investigate those in other longevity regimes.

Separately, I found the expression of *hsp-16* and *hsp-6* increased in *ncl-1* mutants independent of the genetic background, suggesting that mitochondrial and cytosolic stress are induced upon loss of *ncl-1*. A possible explanation for the differential effect of *ncl-1* on lifespan in normal and long-lived backgrounds could therefore be a difference in their capacity for coping with *ncl-1*-induced stress.

Interestingly, a common feature of long-lived *C. elegans* worms is their resistance to different kinds of stress such as thermal, oxidative or pathogenic stress, mediated by the regulation of distinct stress responses, which is among others responsible for the extraordinary long lifespan (K. I. Zhou, Pincus, and Slack 2011). *daf-2* mutants, for example, possess hyperactivated *daf-16* and *hsf-1* leading to proteotoxic stress resistance (Volovik et al. 2014). Similarly, loss of germline in *C. elegans* increases pathogen resistance partially through activation of the transcription factor DAF-16 (Tekippe and Aballay 2010). Collectively, longevity depends on a tightly tuned balance between several cellular processes. This makes the organism on the one hand resistant to stress and therefore long-lived. On the other hand, it may be possible that it makes the organism more susceptible to a mis-balance in gene regulation. Loss of *ncl-1* induces a drastic remodeling of the transcriptome and proteome, affecting the regulation of various cellular processes. In long-lived animals with a potentially limited tolerance for mis-regulation, this shortens lifespan, while WT lifespan remains unaffected.

In this study I analyzed RNA-Seq and proteomic data, and shortlisted candidates for a genetic screen based on their differential regulation in both datasets. However, due to the technical limitations of proteomics, this approach yielded fewer candidates, which subsequently meant that I did not fully explore the information available from RNA-Seq data. As mentioned above, preliminary analysis of only RNA-Seq data showed additional background-specific regulation in *ncl-1* mutants, particularly of RNA metabolism, and should be considered in the future. Furthermore, it is important to keep in mind that *glp-1* worms lack a germline. As whole worm extracts were used for generating both transcriptomic and proteomic datasets, the absence of germline mRNAs and proteins may affect the comparative findings on mRNA and protein level.

2. *ncl-1* affects longevity via distinct nucleolar downstream processes

Over the years, the nucleolus has been established as a central hub for ribosome biogenesis and the production of other components of the protein biosynthesis

machinery such as tRNAs and the signal recognition particle. Furthermore, the nucleolus is closely connected to telomerase activity and production of the catalytic U6 RNA of the spliceosome (Boisvert et al. 2007; Didychuk, Butcher, and Brow 2018; Gonzalez et al. 2014), and has recently also been established as a protein quality control compartment (Frottin et al. 2019). Protein biosynthesis and protein quality are both closely linked to lifespan. A modest reduction of protein biosynthesis is sufficient to extend lifespan in several organisms and the longevity mediated by dietary restriction and TOR signaling is at least partially due to reduced mRNA translation (Bjedov et al. 2010; Kapahi et al. 2010; Stanfel et al. 2009; Zid et al. 2009). At the same time, the accumulation of un- or mis-folded proteins is a hallmark of aging (López-Otín et al. 2013a) and many lifespan extending interventions such as dietary restriction are dependent on cellular proteostasis (Matai et al. 2019; Steinkraus et al. 2008).

In an RNAi screen, I identified two of those nucleolar outputs, namely the RNase P/MRP complex with implication in RNA metabolism and furthermore mitochondrial translation as key downstream links between *ncl-1* and longevity. The RNase P/MRP complex affects several RNA species such as tRNAs, rRNA and specific mRNAs (Esakova and Krasilnikov 2010; Jarrous 2017). Mitochondrial translation in turn is closely linked to cytosolic translation and cellular proteostasis (Houtkooper et al. 2013; Molenaars et al. 2020).

Screen candidates were selected based on transcriptomic and proteomic measurements. Looking at the global outcome of the screen, a reduction of nucleolar outputs such as rRNA processing, ribosome biogenesis and tRNA metabolism as well as mitochondrial translation regulation extend lifespan in *glp-1;ncl-1* worms. However, it should be considered that not all initially listed candidates were screened and that the screen has certain limitations. RNAi was for example applied egg on, excluding candidates leading to developmental arrest. In general, RNAi efficiency is variable, leading to an inconsistent reduction of different genes. Dependent on the biological importance of a gene for the organismal survival, a strong or weak reduction may therefore make the difference between an extended or shortened lifespan. This problem could be bypassed by using different RNAi bacteria dilutions, which is hardly applicable in a screen though. This method could however be used for certain biologically interesting candidates.

Furthermore, downregulated genes in *glp-1;ncl-1* mutants were not considered at all due to the screen setup, but could constitute an important connection between *ncl-1* and longevity. We should therefore test whether for example an activation of lysosome biogenesis or proteasomal activity is sufficient to rescue *glp-1;ncl-1* longevity.

Due to the strong lifespan rescue upon RNAi-mediated knockdown of *popl-1* and *mrps-16*, I focused on those two candidates. In addition to *popl-1*, also a reduction of other RNase P/MRP complex components extended *glp-1;ncl-1* lifespan and among the top screen candidates were two more proteins involved in mitochondrial translation, namely *tufm-2* and *gfm-1*. These findings suggest that the RNase P/MRP complex and mitochondrial translation constitute vital connection between *ncl-1* and longevity.

To test whether RNase P/MRP or mitochondrial translation affect lifespan dependent or independent from nucleolar size, I measured nucleolar size upon knockdown of *popl-1* and *mrps-16*. In both cases the enlarged nucleolar size of *glp-1;ncl-1* double mutants was not affected and steady state rRNA levels remained increased, placing both candidates either downstream of the nucleolus or in direct connection to NCL-1 (Figure 26).

Knockdown of *popl-1* however resulted in the accumulation of specific rRNA precursors while *mrps-16* had no effect on rRNA levels at day 1 of adulthood, indicating that the effect of *popl-1* on lifespan may be mediated through alterations in rRNA processing while *mrps-16* acts through a different mechanism. Interestingly, only 18S precursors seem to accumulate upon *popl-1* RNAi, possibly suggesting a special role of the small ribosomal subunit. On the other hand, at day 6 of adulthood the two used probes (#2, #5) showed an increase upon reduction of both genes. To draw a final conclusion though, also the remaining probes need to be measured. Whether the observed changes in rRNA processing in the end have a functional implication for lifespan regulation remains open though.

Based on literature, the effect of *popl-1* reduction in rRNA processing could be expected as the vast majority of RNase P/MRP is found inside the nucleolus, the primary location for rRNA processing (Reimer et al. 1988). Furthermore, the RNase MRP complex directly binds to pre-ribosomal complexes and its composition is partially dependent on these binding events. A large fraction of RNase P and MRP associates to U3 snoRNAs, an important player in rRNA processing (Welting et al. 2006).

It remains an open question why *popl-1* knockdown does not affect steady-state rRNA levels and also why changes in pre-rRNA levels were mild and not significant. A possible explanation lies in the highly interconnected network, regulating rRNA processing and the biological relevance of the ribosomal machinery. For example, in yeast an inactivation of the RNase MRP complex does not completely block rRNA production, indicating that a parallel pathway exists that can bypass this production step. On the other hand, precursor measurements could also be influenced by the natural instability of pre-rRNA (Lindahl et al. 2009). It is also possible that the conducted rRNA measurements were not sensitive enough to detect consistent but small changes, and further experiments such as northern blot analysis should be considered in the future. As large parts of the cellular energy are allocated to ribosome biogenesis (Warner 1999), even small changes may have a great impact.

Alternatively, the RNase P/MRP complex facilitates several other functions: it shares components with the telomerase complex and is involved in the processing of several other RNA species, such as tRNAs, snoRNAs and specific mRNAs (Esakova et al. 2011; Esakova and Krasilnikov 2010; Jarrous 2002, 2017). It would be important to narrow down which function of the RNase P/MRP complex mediates the effect of *ncl-1* on longevity. Considering that tRNAs are crucial for mRNA translation and that lowered translation has been linked to longevity several times, tRNA metabolism comes into special focus (Hansen et al. 2007; Pan et al. 2007; Steffen et al. 2008b; Syntichaki, Troulinaki, and Tavernarakis 2007). In yeast, the available pool of tRNAs is altered upon stress and codon usage gets shifted towards the use of rare codons, resulting in a faster translation of stress factors (Torrent et al. 2018). Also in fission yeast, the transcriptional regulation of tRNAs has been linked to longevity (Shetty et al. 2020). It would therefore be interesting to analyze the tRNA landscape in a *ncl-1*-dependent manner and upon knockdown of *popl-1*.

rRNAs and tRNAs both come together at the ribosome and are important components of the translation machinery. Based on literature (Frank and Roth 1998) and findings in this thesis, the translation rate of *ncl-1* worms is increased. However, RNAi-mediated knockdown of neither *popl-1* nor *mrps-16* lead to a reduction of translation rate, suggesting that the positive effect on lifespan is not mediated through globally reduced

translation rates. On the other hand, it is too early to draw final conclusions due to assay limitations, and a second line of evidence such as radioactive methionine incorporation assays should be performed. It also might well be that changes in translation rate do not occur at day 1 of adulthood but become more important later in life.

Zooming in on the ribosome itself, *ncl-1* affects the ribosomal landscape in *glp-1* mutants but not in a WT background. I observed an accumulation of 40S ribosomal subunits in *glp-1;ncl-1* worms, indicating a disbalance of ribosome assembly and component production. Interestingly, aberrant ribosome biogenesis has been linked to compromised cellular fitness in yeast, suggesting that the shortened lifespan of *glp-1;ncl-1* worms may be caused by a disbalance in ribosome assembly (Tye et al. 2019). An imbalance of rRNA production, ribosomal protein expression and subsequent ribosome assembly stress has furthermore been shown to result in transcriptomic changes mediated via *hsp-70* and *hsf-1* (Albert et al. 2019). Interestingly, several HSF-1 targets are induced in *ncl-1* mutants (preliminary RNA-Seq analysis) and *hsp-70* is increased on transcript level.

Additional evidence for an imbalance of ribosome assembly can be found in the conducted genetic screen. Not only reduction of *popl-1*, which can lead to the accumulation of 18S rRNA (Gutmann, Gobert, and Giegé 2012), but also the *C. elegans* orthologs of KRI1 and ESF1 were positive candidates. KRI1 is implicated in 40S assembly while ESF1 is an important player in 18S rRNA processing (Peng et al. 2004; Sasaki, Toh-e, and Kikuchi 2000). Also considering the GO-term enrichment analysis it may be telling that the small subunit ribosome (*ncl-1* vs. N2) and the small subunit processome (*glp-1;ncl-1* vs. *glp-1*) are the most enriched terms. Interestingly, small ribosomal components are aggregation-prone in old *C. elegans* worms (Reis-Rodrigues et al. 2012), leading to the hypothesis that loss of *ncl-1* may induces a ribosomal subunit aggregation-associated premature aging phenotype. It would therefore be highly interesting to study the aggregation of ribosomal proteins in *ncl-1* mutants and to see whether this phenotype may be rescued by knockdown of *popl-1* or *mrps-16*. As a first indication we could compare the transcriptomic profiles of *ncl-1* mutants with the profiles of old worms to see whether similar stress pathways are activated.

Furthermore, changes in nucleolar size go hand in hand with altered levels of the methyltransferase fibrillarin, which is involved in the modification of rRNAs (Erales et al. 2017; Tiku et al. 2017). Interestingly, posttranslational modifications of ribosomal components result in an altered accuracy of the decoding machinery as well as changes in rRNA processing, which in turn affect protein folding and finally ribosomal function (Arragain et al. 2010; King et al. 2003). It would therefore be interesting to study how changes in nucleolar size affect rRNA and ribosomal protein modifications in the context of *ncl-1* mutants and the knockdown of *popl-1* and *mrps-16*. Nanopore rRNA sequencing and deeper proteomic analysis of *ncl-1* mutants could answer those two questions.

RNAi-mediated knockdown of *popl-1* does not affect mRNA levels of *mrps-16* and *vice versa*, suggesting two independent mechanisms. Nevertheless, we cannot exclude a common downstream convergence point as mitochondrial and cytosolic translation are closely interconnected. A reduction of *mrps-5* in *C. elegans*, human cells and mice for example reduces the polysome to monosome ratio not only in mitochondria but also affects cytosolic translation (Molenaars et al. 2020). Cellular compartments constantly communicate (Guaragnella et al. 2018; Hedtke et al. 1999; Malli and Graier 2019) and studying the link between *mrps-16* and *popl-1* could be an interesting starting point for novel insight into compartmental crosstalk between mitochondria and the nucleolus. On the other hand, POPL-1 and MRPS-16 might also be directly affected by NCL-1 either on protein or mRNA level independent of the nucleolus. I can also not exclude that POPL-1 and MRPS-16 both affect mitochondria, which then affect lifespan. This however appears rather unlikely as *mrps-16* transcript levels remain unchanged upon knockdown of *popl-1*.

3. The RNase P/MRP complex and mitochondrial translation uncouple nucleolar size from longevity

As discussed earlier, the correlation between small nucleoli and a long life seems an unbroken paradigm (Tiku et al. 2017). Here I demonstrate for the first time that lifespan

and nucleolar size can be uncoupled by interfering with the RNase P/MRP complex and mitochondrial translation. Although RNAi-mediated knockdown of *popl-1* and *mrps-16* rescue longevity in *glp-1;ncl-1* mutants, nucleolar size is not affected. This could be explained in two ways: (1) both processes could be affected directly by NCL-1, independent of the nucleolus or (2) they constitute a downstream connection between nucleolar size and lifespan (Figure 26). The first explanation appears rather unlikely as the RNase P/MRP localizes inside the nucleolus and is known to be involved in rRNA and tRNA processing (Esakova et al. 2011; Esakova and Krasilnikov 2010; Jarrous 2002, 2017). Similarly, mitochondrial ribosomes are assembled in the nucleolus and are therefore already connected to nucleolar function. The RNase P/MRP complex and mitochondrial translation therefore likely constitute a downstream connection between nucleolar size and lifespan (Figure 26), although for now we can only speculate which processes further downstream of RNase P/MRP and mitochondrial translation ultimately rescue longevity in *glp-1;ncl-1*.

Considering possible functional ribosomal changes, as discussed earlier, it is conceivable though that both processes indirectly or directly affect the ribosomal landscape, composition and thereby favor the translation of specific mRNAs. Aging individuals do not only show a general decline in translation but also a selective shift towards the translation of specific transcripts (Gonskikh and Polacek 2017). At the same time, nucleolar size changes with age as shown in this and other studies (Buchwalter and Hetzer 2017). It would therefore be interesting to study whether the translation of specific transcripts is favored in *ncl-1* mutants and whether this is reversed by knockdown of *popl-1* and *mrps-16*. Most interestingly those selectively translated mRNAs could subsequently be correlated with changes in ribosomal parameters such as composition, modification or tRNA loading. Ribosome sequencing in combination with the approaches mentioned above could shed light on this open question.

Alternatively, there is a different but very basic explanation for the effect of *ncl-1* on longevity and the rescue by a reduction of *popl-1* and *mrps-16*: *ncl-1* may induce the expression of pathogenic gene products which is simply reversed by a reduction of *popl-1* and *mrps-16* expression. However, RNA-Seq data from our lab shows that both

transcripts are also decreased in *daf-2* mutants and the knockdown of other mitochondrial ribosome components has already been demonstrated to extend lifespan (Houtkooper et al. 2013). Furthermore, preliminary lifespan data on at least *popl-1* RNAi in WT worms suggest a healthspan-extending effect. This suggests that there is a general link between RNase P/MRP, mitochondrial translation and longevity.

4. The RNAi machinery as novel effector of the nucleolus and longevity

In my thesis, I examined the argonaut protein NRDE-3 as a potential candidate interactor of NCL-1 based on publicly available Y2H data (Simonis et al. 2009). My own interaction studies of NCL-1 did not yield NRDE-3 as an interaction partner, but this could be due to technical limitations. First, the Y2H assay included in my work was done with only a fragment of NCL-1 covering the coiled coil and the NHL domain, and will have missed all proteins which interact with other domains of NCL-1. Second, protein-protein interactions are often transient and largely depend on purification conditions as well as the genetic background. To further confirm whether such an interaction takes place, I could therefore perform Co-IP experiments with altered buffer conditions focusing on NCL-1 and NRDE-3, or purify both proteins from bacteria or from insect cells and perform interaction studies *in vitro*.

Regardless of the direct binding, I found that *glp-1* longevity is fully dependent on *nrde-3* while *daf-2* longevity is not affected. Interestingly, loss of *nrde-3* also leads to a ~30 % increase of hypodermal nucleolar size and increased FIB-1-GFP levels. Preliminary data also shows that nucleolar size of *ncl-1* mutants is not further increased upon loss of *nrde-3*. In an unbiased EMS screen for modulators of nucleolar size, our lab additionally found that several other RNAi machinery factors increase the expression of FIB-1-GFP.

In sum these findings suggest a novel link between the RNAi machinery, nucleolar size and longevity similar to the one found for *ncl-1*. It should be noted, however, that the effect of *nrde-3* on nucleolar size is considerably weaker than the effect of *ncl-1*. If both

factors affect longevity through a shared pathway, the effect of *nrde-3* is probably only partially mediated through the nucleolus.

Loss of *ncl-1* significantly shortens *daf-2* longevity while it is not affected by *nrde-3*. This may indicate a *glp-1*-specific effect of *nrde-3*, although the effect on additional longevity regimes should be tested. Moreover, it would be important to also test other components of the RNAi machinery to state a general link to the nucleolus and lifespan.

Interestingly, the connection between the RNAi machinery and longevity has recently also been described by another group showing that *glp-1* longevity is dependent on several endo-siRNAi machinery factors including *nrde-3* (Cohen-Berkman et al. 2020).

To our knowledge, NCL-1 resides in the cytosol and how it affects nucleolar size is largely unknown. NRDE-3 however is known to bind silencing RNAs in the cytosol and shuttle into the nucleus to mediate gene silencing at the target loci. A new class of silencing RNAs has recently been identified in *C. elegans*, specifically targeting pre-rRNAs. These risiRNAs were identified being bound to NRDE-3 (X. Zhou et al. 2017). A direct interaction of NCL-1 and NRDE-3 could therefore constitute a possible explanation for how *ncl-1* affects rRNA expression on a molecular level. We should therefore measure the abundance of risiRNAs in *ncl-1* mutants. Furthermore, it would be interesting to perform *in situ* hybridizations of risiRNAs to examine a co-localization with NCL-1.

5. NCL-1 affects nucleolar size through direct binding to specific mRNAs

By performing a structure-function analysis I found that deleting the NHL domain of NCL-1 is sufficient to increase nucleolar size to a similar extent as observations in *ncl-1* mutants.

Interestingly, BRAT, the NCL-1 ortholog in *D. melanogaster*, also directly binds to and represses specific mRNAs through its NHL domain (Loedige et al. 2015). Sequence alignments of NCL-1 and BRAT show the highest conservation in the NHL-domain and

in vitro studies suggest a conserved RNA-binding motif for NCL-1 and BRAT (Loedige et al. 2015). A study in *C. elegans* focusing on embryonic development recently identified NCL-1 as a posttranscriptional regulator of ribosomal proteins, rRNA processing and tRNA synthetases. The effects were mediated through specific binding to UUGUU sequences within specific mRNAs and their subsequent downregulation (West et al. 2018). NCL-1 has furthermore been suggested to directly bind to *fib-1* mRNA, thereby affecting nucleolar size (Yi et al. 2015).

Analysis of the significantly regulated transcripts in *glp-1;ncl-1* worms revealed an enrichment of the UUGUU binding motif. Intriguingly, the binding motif occurs several times in the mRNA coding for *fib-1*, *rpoa-2* and *ngp-1*, which are all strongly upregulated in *glp-1;ncl-1* mutants and are directly linked to nucleolar function. This suggests that NCL-1 can at least partially mediate its effect on nucleolar size and potentially lifespan through direct binding and probably the suppression of nucleolar transcripts. We could probe such a mechanism by eCLIP experiments with NCL-1. This would not only provide information about bound RNAs, but would also reveal the exact binding motif of NCL-1. To test a functional implication of direct binding we would have to generate reporter strains with mutated binding sites and monitor mRNA levels and protein expression.

NCL-1 directly binding and regulating specific RNAs could also constitute a possible explanation for its localization to the outer mitochondrial membrane, as translation of mRNA to protein does not occur at random loci within the cell and localized translation can be seen as a regulative layer of protein production (Besse and Ephrussi 2008; Lécuyer et al. 2007; Poon et al. 2006). Several mitochondria-destined proteins for example are synthesized in close proximity to the outer mitochondrial membrane, suggesting that also regulatory factors may act in this location (Gehrke et al. 2015; Lesnik et al. 2014; Lesnik, Golani-Armon, and Arava 2015; Williams, Jan, and Weissman 2014). NCL-1 might be one of those factors, although the high number of binding motifs in nucleolar transcripts appears counterintuitive in this context. Nevertheless, it would be interesting to examine the RNA binding motif abundance also in mitochondrial transcripts more generally and further on examine an effect of NCL-1 on mitochondrial biology. Considering that *mrps-16* is one of the high confidence candidates from the conducted lifespan rescue screen in *glp-1;ncl-1* worms

and mitochondrial candidates are regulated in a *ncl-1*-dependent manner in both transcriptomics and proteomics, an effect on mitochondrial biology seems likely. It could be hypothesized that NCL-1 directly regulates mitochondrial transcripts which then affects mitochondrial biology. This may ultimately impact lifespan and could at the same time explain why knockdown of mitochondrial factors such as *mrps-16*, *gfm-1* and *tufm-2* extends lifespan in *glp-1;ncl-1*.

Technically seen, the structure-function analysis mentioned above exhibits certain limitations. Although the protein expression of all mutants including the Δ NHL deletion mutant was preliminary confirmed via western blotting, I cannot exclude that the deletion affects the NCL-1 structure, leading to a complete loss of function. Although a misfolded protein would probably be directly degraded, additional validation through the analysis of point mutants (which are typically less prone to misfolding) will be useful. In addition, we should therefore also generate deletion mutants of the other NCL-1 domains and control expression levels of the different mutated forms via western blotting.

6. NCL-1 affects proteostasis through the proteasome

ncl-1 mutants are short-lived and less mobile under thermal stress. Furthermore, overall ubiquitinylation is dependent on *ncl-1*, increased in *ncl-1* mutants and decreased in NCL-1 overexpressing worms, suggesting an accumulation of proteins destined for proteasomal degradation. In line with this, I saw substrate accumulation in a proteasome activity reporter strain in *ncl-1* mutants. The increased translation rate of *ncl-1* mutants may simply lead to an overload on the cellular proteolytic system. At the same time, transcriptomic and proteomic analysis revealed a reduction of proteasomal factors in *ncl-1* mutants, indicating a reduced proteasomal activity. Putting these findings into context, it is interesting to see that proteasomal activity declines with age and several neurodegenerative diseases are linked to a reduced proteasomal activity or failure in the ubiquitinylation system (Saez and Vilchez 2014). An aging organism is exposed to various types of stress, such as increased ROS levels. Those in turn affect protein folding and promote protein aggregation which can have

detrimental effects in combination with a decline of proteasomal function (Kamata and Hirata 1999; Santra, Dill, and De Graff 2019). The short lifespan of *ncl-1* mutants under thermal stress could therefore be explained by a similar mechanism, as protein folding stress seems induced while proteolytic processes such as proteasomal activity seem decreased. However, to verify the role of particular the proteasome, we would have to test proteasomal activity in *ncl-1* mutants *in vitro* by using model substrates and worm lysates and also test whether an overexpression of proteasomal factors may rescue the sensitivity to thermal stress.

The NCL-1 interaction studies that I performed also suggested a connection of NCL-1 to the proteasome. Several proteasomal components were co-enriched with NCL-1 in immunoprecipitation, and RPN-11 was a candidate NCL-1 protein interactor in the Y2H assay. Interestingly, knockdown of *rpn-11* leads to an increase in nucleolar size in *glp-1* animals, indicating a direct connection to the nucleolus. Although the direct interaction needs further biochemical evidence, these findings suggest that NCL-1 may not only affect the proteasome through transcriptional regulation, but also through direct physical interaction. Similar to NRDE-3, a direct interaction should be tested via Co-IP and biochemical interaction analyses with purified proteins. Also co-localization studies with fluorescently tagged proteins *in vivo* could give additional information about the connection between NCL-1 and the proteasome.

However, it remains an open question why NCL-1 may interact with the proteasome. A possible explanation is the potential E3 ligase function and ubiquitinating of proteins mediated by the RING and B-Box domains of NCL-1. On the other hand, it has been shown that the proteasome does not only degrade proteins but the 26S proteasome can also exhibit endoribonuclease activity and regulate cellular RNA metabolism (Kulichkova et al. 2010). This function of the proteasome is barely studied. Considering the potential binding of NCL-1 to the proteasome and mRNAs at the same time, it is possible that NCL-1 affects cellular processes through regulation of RNA via subjecting those to proteasomal degradation. In line with this hypothesis, a mutation in the catalytic site of the NCL-1 B-Box 1 domain results in notably increased nucleolar size, suggesting that the E3 ligase function of NCL-1 could play a role in this process.

7. Summary

In sum, I have identified a landscape of genetic and biochemical interactors of NCL-1. I found that *ncl-1* is a multifaceted gene that connects multiple important cellular pathways with a focus on nucleolar outputs but also proteolytic processes. Interestingly, I identified the RNase P/MRP complex and mitochondrial translation as potential key processes for mediating the function of *ncl-1* in longevity.

In my opinion, the most interesting future question deals with the mechanistic link between rRNA processing, mitochondrial translation and longevity. It would therefore be incredibly exciting to further focus on the effect of the RNase P/MRP complex on the tRNA and rRNA landscape and further downstream the ribosome and its components.

As our overall aim is to explore how the nucleolus is linked to lifespan though, it is highly important to further prove that both processes are not only linked to *ncl-1*, but generally correlate with nucleolar size. Understanding the mechanistic link between nucleolar size and lifespan will open the door for further studies on the nucleolus as a biomarker for ageing and disease, as well as potential therapeutic treatments targeting the nucleolus and nucleolar processes.

Future perspective

1. Further explore the link between the RNase P/MRP complex, nucleolar function and longevity.

A reduction of different RNase P/MRP components and in particular POPL-1 extends lifespan in *glp-1;ncl-1* worms independent from nucleolar size. My data suggests that the effect may be mediated through altered rRNA processing, but the underlying molecular connection remains vastly open.

The RNase P and MRP complex exhibit multiple functions and several components are shared with other ribonuclear protein complexes. Therefore, we will examine the different functions in *ncl-1* mutants with and without RNAi-mediated knockdown of *popl-1* and other complex components. By measuring overall changes in different tRNAs using micro arrays, we will get a first idea whether tRNA metabolisms is altered in a *ncl-1* dependent manner, presumably affecting different layer of protein biosynthesis. A potential effect may be reversed by a reduction of *popl-1* or other RNase P/MRP components. As the RNase P complex plays an important role in tRNA maturation by cleaving off the 5' tail of premature tRNAs, it would also be interesting to measure the levels of pre-tRNAs and whether those premature forms are incorrectly loaded onto the ribosome. In case we observe *ncl-1* dependent alterations of tRNA metabolism, we will deeper characterize and investigate the abundance of different tRNAs associated with ribosomal subunits, monosomes and polysomes using ribosome profiling and subsequent micro array analyses.

I found steady state rRNA levels and rRNA precursors uniformly increased in *glp-1;ncl-1* mutants. qPCR measurements of rRNA precursors provided first evidence that a reduction of RNase P/MRP complex activity may lead to the accumulation of specific pre-rRNAs. To further study the effects of the RNase P/MRP complex on rRNA maturation in *C. elegans*, we will perform northern blot analysis enabling us to specifically quantify changes in distinct precursor forms.

The fact that POPL-1 is a shared component between different complexes (RNase P, RNase MRP, telomerase complex) makes it challenging to identify the cause for its effect on lifespan. We will therefore not only measure the molecular outputs of the RNase P/MRP complex, but also measure its activity *in vitro* using model substrates.

Our data on RNase P/MRP regulation and its effect on lifespan is limited to germline longevity. However, as *ncl-1* is known as a master regulator of longevity and because the nucleolus has been established as a key player in the regulation of lifespan, we will test the observed effects also in other longevity regimes. Furthermore, we will explore the effect of the RNase P/MRP complex on nucleolar size and lifespan in a WT background to show a general connection between the RNase P/MRP complex and lifespan.

2. Investigate how nucleolar size and *ncl-1* affect the ribosome

Alterations in rRNA processing can have manifold effects such as changes in rRNA modifications, rRNA folding and a disbalance between mature rRNA and ribosomal proteins (Aubert et al. 2018).

In this thesis I show that the ratio of ribosomal subunits seems misbalanced in *glp-1;ncl-1* mutants, potentially facilitating the negative effect on *glp-1* longevity. In the future we will examine whether a reduction of either *popl-1* or *mrps-16* reverses this effect by making use of ribosome profiling.

It has been shown in old worms that particularly small ribosomal component tend to aggregate (Reis-Rodrigues et al. 2012). Therefore, it might well be that *ncl-1* induces an old-age-like phenotype and lifespan shortening could be caused by the aggregation of specific ribosomal subunits. We will therefore examine whether and which proteins aggregate in *ncl-1* mutants via mass spectrometry.

On the other hand, *ncl-1* and nucleolar size potentially affect ribosomal function through different mechanisms. We will therefore not only investigate *ncl-1*-dependent changes of rRNA modifications by nanopore sequencing, but also isolate ribosomes from *C. elegans* to investigate a potential incorporation of immature rRNAs and changes in protein composition. To do so, we will generate a worm strain with endogenously tagged ribosomes. Those will be immunoprecipitated followed by mass spectrometric measurements and northern blot analysis.

How exactly those potential changes may affect longevity remains elusive though and cannot be answered by these experiments. As one potentially important aspect, we will investigate translation fidelity by generating a reporter system in *C. elegans*

inspired by a system from *D. melanogaster* (Chen et al. 2020) and via mass spectrometry, where recent methodological developments made it possible to detect amino acid substitutions in a proteome-wide scale (Mordret et al. 2019).

As suggested before, alterations in tRNA abundance, but also changes within the ribosome potentially lead to a specific translation of gene sets. The transcriptomics and proteomics data generated in this study covers only one side of the coin and some observed changes could be *ncl-1*-specific without a causative link to nucleolar size. Therefore, we will conduct ribosome sequencing to identify mRNAs bound to different ribosomal fractions in *ncl-1* mutants and upon knockdown of *fib-1*. Contrary changes in both conditions will give us a direct overview about active mRNA translation for specific genes in close connection to nucleolar function.

3. Explore the effect of *ncl-1* on mitochondrial biology

Mitochondria are one of the most important players in cellular metabolism (Spinelli and Haigis 2018). The nucleolus is not only known as a central regulator of cellular metabolism, but in this thesis I furthermore observed NCL-1 localizing in close proximity to the outer mitochondrial membrane. Immunoprecipitation of NCL-1 and subsequent identification of co-enriched proteins also yielded several mitochondrial factors. Furthermore, a reduction of the mitochondrial ribosome component *mrps-16* rescues longevity in *glp-1;ncl-1* mutants and mitochondrial factors are regulated on mRNA and protein level in *ncl-1* and *glp-1;ncl-1* worms. Preliminary data on *ncl-1*-dependent changes of mitochondrial respiration and mitochondrial morphology support the theory of a connection between *ncl-1*, the nucleolus and mitochondrial function. We will therefore measure mitochondrial parameters such as oxygen consumption, ATP and mitochondrial DNA levels as well as mitochondrial morphology in *ncl-1* mutants in normal and long-lived backgrounds. Further on, we will investigate whether potential changes are reversed by a reduction of *popl-1* and *mrps-16*, as the positive effect on lifespan may be mediated through mitochondrial function.

The same parameters will be measured upon knockdown of *fib-1* to dissect whether effects are specifically connected to NCL-1 or to inter-organelle crosstalk between mitochondria and the nucleolus.

4. Deepen our understanding of the connection between *ncl-1* and proteostasis with special focus on the proteasome

In this study I am presenting evidence for a connection between *ncl-1*, the nucleolus and cellular proteostasis mediated by the proteasome. *ncl-1* mutants are short-lived upon protein folding stress induced by thermal stress, and less mobile. At the same time, several stress markers such as *hsp-16*, *hsp-6* and *hsp-70* are increased already under non-stressed conditions on mRNA and protein level, indicating proteotoxic stress. A possible explanation lies in a reduced proteasomal activity caused by reduced expression of ribosomal factors in *ncl-1* mutants. In line with this, I show that overall ubiquitinylation levels are altered in a *ncl-1*-dependent manner and that the accumulation of *in vivo* model substrates, using a transgenic strain containing a proteasomal substrate fused to GFP, is increased.

Furthermore, a Y2H screen as well as immunoprecipitations of NCL-1 suggest a direct interaction of NCL-1 with proteasomal factors. In particular RPN-11 is of high interest as its knockdown increases hypodermal nucleolar size in *glp-1* worms.

The regulation of proteasomal factors however appears as a unique feature of *ncl-1* single mutants and was not observed in *glp-1;ncl-1* mutants. We therefore do not know whether the drop in proteasomal activity is connected to lifespan regulation. On the other hand I found lysosomal components reduced in *glp-1;ncl-1*, suggesting that *ncl-1* affects different proteolytic processes in a background-specific manner.

Therefore, we will investigate the regulation of proteasomal and lysosomal factors in other longevity background upon loss of *ncl-1*. In addition, we will assess proteasome activity by crossing the proteasomal reporter strain into different longevity backgrounds and also via *in vitro* activity assays. We will furthermore examine lysosomal biology by lysosomal staining and making use of worm strains generated in our lab, expressing tagged versions of different lysosomal components.

The proteasome may be directly affected by NCL-1 or indirectly by changes in nucleolar function. By now we only have limited evidence for a direct connection between the proteasome and nucleolar size by showing that the proteasomal factor *rpn-11* affects nucleolar size. We will therefore also test whether a reduction of other proteasomal factors affects nucleolar size in different genetic backgrounds.

On the other hand, we will examine whether NCL-1 and the proteasome are linked on a molecular basis. We will therefore also test a direct biochemical interaction between

NCL-1 and proteasomal components via co-immunoprecipitation experiments. Granted that we observe a direct interaction, we will generate further domain deletion mutants of NCL-1 to pinpoint a particular interaction domain.

5. Uncover and verify NCL-1 interactions on RNA and protein level

By making use of a Y2H screen and mass spectrometric NCL-1 interactor identification, I was able to identify several potential NCL-1 protein interactors. Among the tested ones, only a reduction of *rpn-11* had a relatively strong effect on nucleolar size. However, the Y2H screen was only performed with a truncated version of NCL-1 and the protocol for immunoprecipitation needs further optimization. Especially the localization of NCL-1 in close proximity to mitochondria suggests an interaction with mitochondrial proteins, which the immunoprecipitations are not optimized for. We will therefore repeat the immunoprecipitations using different conditions. Furthermore, we will conduct interaction studies also in long-lived backgrounds as the interaction network of NCL-1 may be dependent on the genetic background.

Besides protein-protein interactors of NCL-1, also the interaction with RNAs moves into focus as the RNA binding capacity of NCL-1 appears crucial for the regulation of nucleolar size. We will therefore further dissect the correlation between the NCL-1 binding motif and gene regulation in the generated RNA-Seq data. At the same time, we will perform NCL-1 pulldowns and sequence the NCL-1-bound RNAs. The combination of both datasets will enable us to gain deep insight into the direct regulation of RNAs bound by NCL-1.

By now, the structure-function analysis was limited to a deletion mutant of the NHL domain and point mutants of the other domains. To validate that the NHL deletion does not cause dramatic folding effects, leading to a complete loss of function, we will express the truncated form in *ncl-1* mutants and monitor rescue of the nucleolar phenotype. We will furthermore generate additional deletion mutants of the other domains to ensure complete suppression of the respective domain activity.

6. Further study the non-autonomous and tissue-specific effects of NCL-1

NCL-1 is specifically expressed in distinct tissues and levels correlate with nucleolar size, indicating that NCL-1 might be more or less important for cellular homeostasis in different tissues. Moreover, a reduction of NCL-1 in the intestine of *C. elegans* affects nucleolar size in the hypodermis, indicating a cell non-autonomous effect. We will address both questions by generating tissue-specific over-expressor strains of tagged NCL-1. Lifespan analyses will be conducted using those strains to examine the importance of NCL-1 in different tissues for longevity, as well as nucleolar size measurements in different tissues to study the cell non-autonomous function of NCL-1.

7. Transfer our knowledge about *ncl-1*-dependent regulation of nucleolar function and lifespan to higher organisms

BRAT is a known functional and structural ortholog of NCL-1 in *D. melanogaster*. However, knowledge about NCL-1 orthologs in higher organism is largely absent. The closest relatives are several members of the TRIM protein family showing a similar domain structure often including RING, B-box and NHL domains. However, the sequence homology barely exceed 30 % for TRIM2 and TRIM3, which are mentioned in the literature as potential orthologs. In the future, we will examine the effect of reduced or increased expression of several TRIM proteins including TRIM2 and TRIM3 on nucleolar size in cells by using FIB1 levels as a proxy. Positive candidates will be expressed in *C. elegans ncl-1* mutants to test for a rescue of nucleolar size. The identification of mammalian NCL-1 orthologs would provide us with a valuable tool and enable us to transfer our knowledge about the connection between *ncl-1*, the nucleolus and lifespan to a higher organismal level.

8. Investigate nucleolar composition and size with aging

The nucleolus has recently been established as a center for protein quality control and a temporal storage location for misfolded proteins (Frottin et al. 2019). The connection

with aging however remains elusive and also a link to NCL-1 and nucleolar size is completely unexplored. In this thesis, I generated first evidence that nucleolar size as well as NCL-1 levels decrease with age. In how far these changes affect gene regulation though remains open. It would therefore be highly interesting to investigate transcriptomic and proteomic changes in *ncl-1* mutants not only early, but also late in life. It might well be that the effect of the nucleolus on lifespan is rather mediated by a change of nucleolar size over time than nucleolar size just early in life.

In this and our previous work we are concentrating on nucleolar size and nucleolar functions and its connection to lifespan regulation. It however remains unclear what a change of nucleolar size means on a molecular level. We therefore would like to investigate the nucleolar composition in worms with different nucleolar size - such as *ncl-1* mutants, WT worm and worms - upon *fib-1* RNAi treatment early and late in life.

Material and Methods

1. *C. elegans* genetics and handling

1.1 Worm growth, maintenance

C. elegans worms were grown and maintained on nematode growth medium (NGM) in petri dishes seeded with *E. coli* (OP50 strain) as food source, following the standard procedure (Brenner 1974). All strains were grown at 20°C from egg to death unless notes otherwise. *glp-1(e2141)* mutants were maintained at 15°C, because they do not develop a germ line at higher temperatures. To induce sterility *glp-1(e2141)* mutant eggs were transferred to 25°C for 52 hours and then used for experiments or moved back to 20°C for lifespan analysis.

Contaminated worm plates were cleaned by bleaching. Worms were washed off with M9 and collected in a 15 ml falcon tube. After a short centrifugation step to settle the worms, M9 buffer was replaced by 2 ml bleaching solution (1ml 5M KOH, 2ml NaClO, 7ml ddH₂O). The falcon was shaken for 6-10 min dependent in the amount of worms and checked for complete worm lysis under the microscope. The tubes were centrifuged for 2 min at 3000 rpm to settle the eggs and washed twice with fresh M9 buffer. Finally, eggs were plated on NGM growth plates beside the bacterial loan. Used worm strains are listed in Table 2.

1.2 Worm synchronization

Most experiments required synchronized worm populations. Worms were either synchronized by bleaching, if high worm numbers were required, or by egg laying. Hereby, gravid adult worms were placed on a NGM growth plate and let to lay eggs for 3-4 hours at 20°C or 15°C. Plates were then kept at 20°C or shifted to 25°C.

1.3 RNAi treatment

Knockdown of certain *C. elegans* genes was achieved by RNAi treatment. Worms were either grown on RNAi plates egg on or were transferred L4 on. RNAi plates were seeded with *E. coli* HT115 (DE3), transformed with a plasmid coding for the target gene to produce siRNA under control of a IPTG-inducible promoter. NGM media for RNAi plate preparation was supplemented by 1 mM Isopropyl β -D-1-thiogalactopyranoside (IPTG) and ampicillin (100 μ g/ml). Bacterial RNAi clones used for this thesis were provided by the Ahringer or the Vidal library (Kamath and Ahringer 2003; Rual et al. 2004). Bacterial plasmid sequence was confirmed by sequencing for each clone.

1.4 Genotyping

C. elegans genotyping was either achieved by phenotypical observations or via PCR and subsequent agarose gel analysis or in case of point mutations, sequencing. For PCR, single worms were collected in 10 μ l Single lysis buffer (10 mM Tris pH 8.3, 50 mM KCl, 2.5 mM MgCl₂, 0.45 % Tween 20, 0.45 % Triton X-100 (all v/v), 1 mg/ml proteinase K (NEB)) and frozen for 10 min at -80°C. Lysis was performed in a Thermocycler for 60 min at 65°C followed by 15 min at 95°C. 5 μ l of lysate were used for subsequent PCR reactions using DreamTaq Green DNA Polymerase (ThermoFisher Scientific) according to the manufacturer's instructions. Annealing temperature and elongation time were adapted according to target length and primer composition. PCR products were analyzed via agarose-gel electrophoresis or cleaned using QIAquick PCR Purification Kit (Qiagen) and submitted for sequencing at Eurofins.

1.5 Lifespan analysis

Worms used for lifespan analysis were synchronized by egg lay as described earlier. Assays were performed at 20°C or at 25°C to induce mild thermal stress. At least 100 worms per strain were transferred every one to three days to fresh plates until no eggs

were visible on the plates anymore. *glp-1(e2141)* animals were transferred once at day 15 to fresh plates. Worms were scored every second or third day for their survival. Exploded worms or worms showing internal hatching were censored from the analysis. Mean, median and maximum lifespan were calculated and survival curves were plotted using Prism Graphpad software.

1.6 Worm microscopy

Nucleolar size measurements were performed in images acquired via differential interference contrast (DIC) microscopy. Pictures were taken from synchronized worms at day 1 or day 6 of adulthood with a 100X magnification using an Axio Imager Z1 (Zeiss). For nucleolar size imaging, worms were anesthetized using 0.01 % sodium azide. Worms were imaged, once they stopped moving. Nucleolar size was manually quantified using the freehand tool of Fiji®.

FIB-1-GFP was visualized by fluorescent microscopy using an Axio Imager Z1 (Zeiss) with a magnification of 63x. The FIB-1-GFP signal was quantified in the head region of worms using Fiji®.

1.7 Confocal imaging

For imaging of *ncl-1::neongreen* and mitochondrial straining, confocal imaging with a magnification of 100x or 63x was conducted. For mitochondrial staining 150 μ l of 500 nM MitoTracker (MitoTracker™ Deep Red FM, M22426) were spread on top of the lawn of each plate (6 cm) 24 h before imaging. Plates were stored in an aluminum wrapped box from then on. Age matched worms at day 1 of adulthood were mounted on 5% agarose pads using 20 mM levamisol as anaesthetic and imaged with a Leica TCS SP8-X confocal microscope equipped with a white light laser.

1.8 Worm size measurements

Worm size was measured at day 1 of adulthood in an age-matched population. Pictures were taken at a 8x magnification under a binocular connected to a camera and worm length was manually assessed using Fiji®.

1.9 GFP intensity quantification via copas biosorter

Biometric Copas Biosorter and the program Flowjo were used for unbiased quantification of FIB-1-GFP in *nrde-3(gg66)* mutants. Day 1 adults from 2x10 cm NGM plates per genotype were washed off with M9 buffer and individual samples were analyzed. The mean GFP intensity (Median fluorescent intensity – MFI) was measured using Flowjo.

Only detection events with a fluorescent signal >50 were considered. The GFP signal was normalized to TOF in the final analysis before plotting.

1.10 Motility assays

1.10.1 Manual motility assessment

Worms were synchronized via egg lay and plates were shifted from 20°C to 25°C to induce heat stress from day 1 on. Motility was manually assessed after 5 days at 25°C. “High motility” was assigned to worms that moved without stimulus. “Medium motility” was assigned to worms that showed whole body movements upon gentle stimulation with a worm pick. “Low motility” was assigned to worms that only showed movement of the head upon stimulation. >45 worms were used per genotype.

1.10.2 Circle assay

Worms were synchronized via egg lay and plates were shifted from 20°C to 25°C to induce heat stress from day 1 on. A circle with a diameter of 2 cm was drawn at the

backside of a seeded 10 cm NGM plate. 30 life worms were transferred onto that plate after 5 days at 25°C. After 3 min the number of worms remaining inside the circle and the number of worms outside the circle was quantified.

1.10.3 Swimming assay

Worms were synchronized via egg lay and plates were shifted from 20°C to 25°C to induce heat stress from day 1 on. After 5 days at 25°C, 10 life worms were individually transferred to a drop of M9 on top of an unseeded NGM plate. Worms were allowed to adjust for 30 sec before motility was assessed. Body bends of each worm within a time window of 1 min was manually quantified.

2. Molecular biology

2.1 RNA extraction

Before RNA extraction, pipets, bench space, centrifuges and all used materials were decontaminated with RNazap solution. Age matched worms from 1-25 NGM growth plates were harvested in M9 buffer on ice in a 15 ml falcon tube. After a brief centrifugation step to settle the worms, the supernatant was discarded and worms were transferred with a glass pipet to a 1.5 ml eppendorf tube. Pellets were then flash frozen in liquid nitrogen and the worm cuticle was cracked by 4 freeze-thaw cycles using a water bath at 37°C and liquid nitrogen. Complete worm lysis was achieved by adding ~150 μ l of 1.0 mm Zirconia/Silica beads (FisherScientific) and shaking for 15 min at full speed in a TissueLyser LT (Qiagen). After lysis, the supernatant was transferred to a new 2 ml eppendorf tube and mixed with 700 μ l QIAzol solution. 120 μ l chloroform were added and the tube vortexed before being centrifuged for 15 min at 12000 rpm and 4°C to achieve phase separation. The upper liquid phase was carefully transferred to a new 1.5 ml eppendorf tube and mixed with 1/2 volume of 70% ethanol by pipetting. Subsequent RNA purification was performed using a RNeasy Mini Kit

(Qiagen) according to manufacturer's instructions. Quantity and quality were assessed using a NanoDrop 2000c (peqLab).

2.2 qPCR analysis

cDNA was prepared from total RNA samples using the iScript cDNA Synthesis Kit (BioRad) according to manufacturer's instructions. Power SYBR Green Master Mix (Applied Biosystems) was mixed with respective primer pairs and transferred to a 384-well plate using a JANUS automated workstation (PerkinElmer). cDNA was then quantified in a ViiA 7 Real-Time PCR system machine (Applied Biosystems). *snb-1* or *etf-1* served as endogenous controls. qPCR primer sequences are provided in Supplementary Table 3.

2.3 RNA-Sequencing

For RNA Seq analysis age matched worms from 5 full 10 cm NGM plates were harvested in ice cold M9. Worms were washed 3 times with M9 before the pellet was resuspended in 700 μ l QIAzol reagent (Qiagen). RNA was extracted as previously described. Libraries were prepared and sequenced by the CCG (ccg.uni-koeln.de) using paired end sequencing and a read length of 75 bp on a HiSeq2500 platform. Reads were mapped to reference genome (WBcel235, release 89) using hisat2 v2.1.0 (1). Guided transcript assembly was performed with StringTie v1.3.4d (1) and respective assemblies merged with cuffmerge v.2.2.1 (2). After feature quantification with cuffquant v.2.2.1 (2) differential gene expression was assessed using Cuffdiff v.2.2.1(2). Enrichment analysis was performed using DAVID (3) (Huang, Sherman, and Lempicki 2009b, 2009a; Jiao et al. 2012; Pertea et al. 2016; Trapnell et al. 2012).

2.4 NCL-1-binding motif analysis

Enrichment analysis of the NCL-1 RNA-binding motif within the regulated genes in *glp-1;ncl-1* was performed using custom python scripts. All transcript models were obtained (bed12 format) as well as sequence using transcript models and bedtools to get fasta sequence. Python package re was used to find all occurrences of the UUGUU motif within transcript sequences. The same package was used to identify stop codon sequences within the transcript sequences. The results were saved in table format (occurrence.TTGTT,genewise_summary.tsv) and occurrence.TTGTT.one_motif_per_line.tsv). The table of differentially expressed genes from RNA-Seq analysis in the comparison *glp-1(e2141)* vs. *glp-1;ncl-1* was merged with occurrence.TTGTT,genewise_summary.tsv. The total number of UUGUU motifs within the fraction of significantly and not significantly regulated genes was calculated regardless of up or downregulation. Fisher's exact test was used to assess the enrichment within each fraction.

2.5 Molecular cloning

New plasmids were constructed using restriction enzymes provided by NEB according to manufacturer's instructions and custom primers from Sigma. Digested plasmids and inserts were ligated using the Rapid DNA Ligation Kit (Merck) according to manufacturer's instructions. DH5a E. coli (Life Technologie) were transformed with ligation products and spread on LB-plates with 100 µg/ml ampicillin for selection. Plasmids were purified using the QIAprep Miniprep Kit (Qiagen) according to manufacturer's instructions. Plasmid sequences were determined by Sanger sequencing at Eurofins Genomics (Germany). Used plasmids and primers are provided in Supplementary Table 3,4.

3. Biochemistry

3.1 Western Blot analysis

For western blot analysis either a full grown plate with a mixed population or age matched worms were harvested in lysis buffer (50 mM Tris/HCL, 150 mM NaCl, 0.5% NP-40, protease and phosphatase inhibitors, pH 7.4) by washing or picking. Worms were lysed by sonification with 30s sonication followed by 30s break for 30 cycles or more in a Bioruptor (Diagenode). Protein concentration was determined via BCA assay using the Pierce BCA protein assay kit (Thermo Fisher Scientific) according to manufacturer's instructions. An equal protein amount was taken for Western Blot analysis, volumes equalized with lysis buffer and the sample was mixed with 6x Laemmli Buffer containing 50 mM DTT. After boiling at 95°C an equal sample volume was loaded onto a SDS-PAGE (BioRad) and proteins subsequently transferred to a PVDF or nitrocellulose membrane (BioRad) using the Trans-Blot Turbo Transfer System (BioRad). Membranes were blocked for 1 h (RT) or over night (4°C) with 5 % milk in Tris-buffered Saline + Tween20 (TBST) and decorated with primary antibodies, for 1-18 h depended on the antibody at 4°C. Primary antibodies were either suspended in 5 % mild or 1 % Bovine Serum Albumin (BSA). Subsequently membranes were washed with TBST three times with TBST at RT. Primary antibodies were coated with specific secondary antibodies at a concentration of 1:10000 in 5 % milk in TBST at RT for 1 h. Before signal detection, membranes were washed 5 times for 5 min with TBST at RT. Specific protein signals were detected using Western Lightening Plus-Enhanced Chemiluminescence Substrate (PerkinElmer) with 1 min incubation time and a ChemiDoc MP Imaging System (BioRad).

Table 1. List of antibodies used for Western blot analysis.

Antibody	Company	Cat. Number	Dilution
Flag M2	Sigma-Aldrich	A8592	1:1000
Histone H3	Abcam	ab1791	1:2000
Fibrillarin	Novus Biologicals	NB300-269	1:1000
Ubiquitin	Novus Biologicals	NB300-130SS	1:1000
Actin	Abcam	ab8224	1:5000
Puromycin	Millipore	MABE343	1:10000

3.2 Puromycin incorporation assays

A synchronized worm population was grown on NGM plates until day 1 of adulthood. The incubation mix for the assay was freshly prepared and pipetted into separate wells of a 12-well cell culture dish. Worms were washed off the NGM plates with M9 and washed with BDR medium once. After settling by gravity, worms were transferred to the incubation mix by using a glass pipette. Worms were incubated for 3 hours at 20°C on a shaker before harvesting and two washing steps with BDR. Finally, worms were resuspended in lysis buffer and lysed with BioRuptor lysis. Protein concentration was determined via BCA assay and samples were analyzed by western blotting (anti-puromycin, Millipore MABE343, 1:10000).

Incubation mix for each condition:

0.75 ml BDR medium

50 μ l puromycin (10 mg/ml, for control add water instead)

100 μ l water (for cycloheximide control add 100 μ l cycloheximide (20 mg/ml))

0.2 ml OP 50 bacteria (concentrated 10x and resuspended in BDR medium)

3.3 rRNA measurements

For rRNA measurements a 25 cm long 1.2 % agarose gel was prepared using 1x BPTE buffer (100 mM PIPES, 100 mM bis-tris, 10 mM EDTA). 1 sample volume was mixed with 0.5 volume of Northern max-glysample loading dye (Ambion AM8551) as

recommended by the manufacturer. The mix was vortexed thoroughly and heated in a thermo block at 50°C for 30 min without shaking. Samples were cooled on ice and briefly spun in a refrigerated centrifuge. Then samples were immediately loaded onto the gel. The gel was run for 17 h at 50V (~1.5V/cm) at 4°C and in the next morning voltage was increased to 80V (~2.23V/cm). The run was stopped when the bromphenol blue reached the bottom of the gel. rRNA was detected under UV light.

3.4 Immunoprecipitation (IP)

For immunoprecipitation *ncl-1::flag* worms and WT worms were synchronized via bleaching and grown until day 1 of adulthood. Worms from 25 full 10 cm NGM plates were harvested by washing with M9 and collected in a 15 ml falcon tube. The worm pellets were washed 3 times with cold M9 and once with cold lysis buffer. After settling worms were resuspended in cold lysis buffer (50 mM Tris/HCL, 150 mM NaCl, 0.5% NP-40, pH 7.4) with protease and phosphatase inhibitor and flash frozen in liquid nitrogen. Worm were lysed using the BioRuptor (Diagenode) with 30 s sonication followed by 30 s break for 30 cycles or more dependent on the amount of worms. The samples were transferred to a 1.5 ml eppendorf tube and centrifuged for 15 min, 13000 rpm at 4°C to remove debris. The supernatant was transferred to a new tube and protein concentration was determined by BCA assay.

For immunoprecipitation dynabeads (ThermoFisher Scientific 10004D) were vortexed for > 30 sec in the original tube. 50 μ l (1.5 mg beads) per sample were transferred to a new tube and equilibrated by washing with TBST buffer in a magnetic tube rack. 2 μ l per 50 μ l beads of primary FLAG antibody (Flag M2, Sigma-Aldrich A8592, 1 mg/ml) were diluted in 200 μ l TBST. The mixture was incubated for 2 h with rotation to allow optimal binding. The coated beads were then washed once with TBST buffer. After this step 5 % of the input were taken for Western blot analysis. The sample solution containing 10 mg of total protein was added to the coated beads and incubated over night at 4°C with rotation. The next morning the solution was put in a magnetic rack and the supernatant was removed by pipetting. 25 μ l of the supernatant were taken for later western blot analysis. Beads were washed once gently washed with TBST buffer and 25 μ l of the wash step were taken for later Western blot analysis. Finally, samples

were washed once with lysis buffer and for mass spectrometric measurements once with lysis buffer without detergent. After the last washing step 400 μ l were used for following mass spectrometric measurements and 100 μ l for western blot analysis. The supernatant was removed from the tube assigned for western blotting and 20 μ l lysis buffer and 5 μ l sample buffer were added to the tube. The samples were boiled for 5 min and used for western blot analysis.

Samples assigned for mass spectrometric measurements were washed once more with lysis buffer without NP-40 and the supernatant was removed. 100 μ l of elution buffer was added and samples were incubated for 30 min at 37°C. The supernatant was transferred to a 0.5 eppendorf tube and incubated over night to ensure complete tryptic digest. The digest was stopped the next morning by adding formic acid to a final concentration of 1%. Samples were cleaned using custom StageTips as described later.

3.5 Whole worm proteomics and IP candidate identification

For whole worm proteomics worms were synchronized by bleaching and grown until day 1 of adulthood on seeded NGM plates. Worms from 6 fully grown plates were harvested for each genotype by washing off the plates with M9. Worms were washed 3 times with M9 and once with water before the pellet was resuspended in 35 μ l lysis buffer. Samples were slowly defrosted on ice and incubated at 95°C for 10 min in a thermo block with 500 rpm shaking. Worms were lysed with the BioRuptor with 30 s sonication followed by 30 s break for 30 cycles, high performance. Tubes were centrifuged at 20000 rpm for 20 min before the supernatant was transferred to a fresh tube. Protein concentration was measured by nanodrop and 300 μ g were taken for trypsin digest. The samples were diluted 10 times and incubated with a ratio of 1:200 with trypsin over night at 37°C. The next morning, the digest was stopped by adding 50% formic acid to a final concentration of 1 %. Peptides were cleaned using custom made StageTips from the proteomics facility (Empore™, C18-SD for desalting 3M). C18-SD tips were washed with 200 μ l methanol by centrifugation. After a washing step with 200 μ l of 60% ACN in 0.1% formic acid and a washing step with 0.1% formic acid, the digests were loaded onto the tip. Digests were completely ran through the tip by

centrifugation for > 2 min. Tips were washed twice with 200 μ l 0.1% formic acid. Peptides were then eluted with 100 μ l 60% ACN in 0.1% formic acid by centrifugation at 1500 g for at least 4 min and collected in a tube. Peptides were completely dried in a Speed-Vac at 45°C for 45 min before being resuspended in 20 μ l of 0.1% formic acid. Peptide concentration was assessed by nanodrop and again dried in a Speed-Vac at 45°C for 45 min. Mass spectrometric measurements were carried out by the MS facility of the Max-Planck-Institute for biology of ageing.

For the total protein analysis, peptides were separated on a 25 cm, 75 μ m internal diameter PicoFrit analytical column (New Objective) packed with 1.9 μ m ReproSil-Pur 120 C18-AQ media (Dr. Maisch) using an EASY-nLC 1200 (Thermo Fisher Scientific). The column was maintained at 50 ÅC. Buffer A and B were 0.1 % formic acid in water and 0.1 % formic acid in 80 % acetonitrile. Peptides were separated on a segmented gradient from 6 % to 31% buffer B for 120 min and from 31 % to 50 % buffer B for 10 min at 200 nl/min. Eluting peptides were analyzed on a QExactive HF mass spectrometer (Thermo Fisher Scientific). Peptide precursor m/z measurements were carried out at 60000 resolutions in the 300 to 1800 m/z range. The top ten most intense precursors with charge state from 2 to 7 only were selected for HCD fragmentation using 25 % normalized collision energy. The m/z values of the peptide fragments were measured at a resolution of 30000 using a minimum AGC target of 8e3 and 55 ms maximum injection time. Upon fragmentation, precursors were put on a dynamic exclusion list for 45 sec.

For the identification of interacting partners, peptides were separated the same column and buffer composition as described above. Peptides were separated on a segmented gradient from 6 % to 31 % buffer B for 57 min and from 31 % to 44 % buffer B for 5 min at 200 nl/min. Eluting peptides were analyzed on a Orbitrap Fusion Tribrid mass spectrometer (Thermo Fisher Scientific). Peptide precursor m/z measurements were carried out at 60000 resolutions in the 350 to 1500 m/z range. The top ten most intense precursors with charge state from 2 to 7 only were selected for HCD fragmentation using 27 % normalized collision energy. The m/z values of the peptide fragments were measured at a resolution of 30000 using a minimum AGC target of 2e5 and 80 ms maximum injection time. Upon fragmentation, precursors were put on a dynamic exclusion list for 45 sec. Alternatively, peptides were analyzed on a QExactive HF

mass spectrometer (Thermo Fisher Scientific) using the same parameters except that the NCE was set to 27 %

For protein identification and quantification, the raw data were analyzed with MaxQuant version 1.5.2.8 or version 1.6.1.0 (Cox and Mann 2008) using the integrated Andromeda search engine (Cox et al. 2011). Peptide fragmentation spectra were searched against the canonical and isoform sequences of the *C. elegans* reference proteome (proteome ID UP000001940, downloaded May 2017 from UniProt). Methionine oxidation and protein N-terminal acetylation were set as variable modifications; cysteine carbamidomethylation was set as fixed modification. The digestion parameters were set to “specific” and “Trypsin/P,” The minimum number of peptides and razor peptides for protein identification was 1; the minimum number of unique peptides was 0. Protein identification was performed at a peptide spectrum matches and protein false discovery rate of 0.01. The “second peptide” option was on. Successful identifications were transferred between the different raw files using the “Match between runs” option. Label-free quantification (LFQ) (Cox et al. 2014) was performed using an LFQ minimum ratio count of 2. LFQ intensities were filtered for at least four valid values in at least one group and imputed from a normal distribution with a width of 0.3 and down shift of 1.8. Differential expression analysis was performed using limma (Ritchie et al. 2015).

3.6 Ribosome profiling

For ribosome profiling > 12 fully grown 10 cm NGM plates with age matched *C. elegans* were used per genotype. Worms were washed twice with ice cold M9 and once with M9 containing 1 mM cycloheximide. After a washing step with washing buffer (29 mM Tris (pH8,5), 140 mM KCl, 1.5 mM MgCl₂, 0.5 % NP40, 1 mM DTT, and 1 mM cycloheximide), worms were pelleted and resuspended in 350 μ l polysome lysis buffer (20 mM Tris (pH8,5), 140 mM KCl, 1,5 mM MgCl₂, 0,5 % NP40, 2 % PTE (polyoxyethylene-10-tridecylether), 1 % DOC (sodium deoxycholate), 1mM DTT, 1mM cycloheximide, 0,4U/uL RNasin). Worms were vortexed and incubated for 30 min on ice for lysis. After a 10 min centrifugation at 12000 rpm at 4°C. for clearing, the RNA

concentration was measured using a nanophotometer. Samples with a concentration of $> 1000 \text{ ng}/\mu\text{l}$ were used for further analysis.

A 15 % and 60 % sucrose solution was freshly prepared at the day of the experiment by adding 1 mM DTT and 1 mM cycloheximide to the stock buffer (20mM Tris (pH8,5), 140mM KCl, 1,5mM MgCl_2) followed by sterile filtering. For gradient preparation, 5.5 ml 15 % sucrose solution was pipetted into ultracentrifugation tubes. The 60 % sucrose solution was layered underneath 5.5 ml of 15 % sucrose solution by using a syringe and a blunt ended needle. Tubes were placed into the gradient master adjusted to a linear gradient 15 % to 60 % sucrose. 400 μg of RNA was pipetted on top of the gradient. The tubes were balanced with a precision scale.

Balanced tubes were placed into SW41Ti rotor and proceeded to ultracentrifugation at 39000 rpm for 3 hours at 4°C. Acceleration was set to maximum and deceleration was set to 2. The fraction collector was blanked with sucrose buffer. The piston speed was set to 0.1 mm/s, the distance to 2 mm and the number to 40, summing up to 80 fractions. Absorbance was measured at 254 nm. The area under each peak was quantified using Fiji and ratios were manually calculated.

4. Cell culture

4.1 Transfection

HEK cells were seeded one day before transfection (200.000 cells per 6 cm well) in normal cell growth medium. The next day, 2 μg of DNA were added per well. Two tubes were prepared per transfection the first containing 100 μl OptiMEM + 5 μl lipofectamine 2000 and the second 100 μl OptiMEM + DNA. The solution from tube 2 was then pipetted to tube 1 and incubated for 10-15 min at room temperature. 200 μl of transfection solution were then added to each well. Cells were incubated for 24 h at 37°C before preparation for confocal microscopy.

4.2 Immunostaining

For immunostaining of cells, coverslips were washed with 99 % EtOH and allowed to dry for 1 h. Coverslips were placed in a 6-well plate and rinsed with sterile water three times. Slips were dried for at least 45 min. Cell were grown until desired cell concentration was reached. Media and excess cell suspension were removed and cells were rinsed with PBS. For mitochondrial training, cells were treated with MitoTracker probe (MitoTracker™ Deep Red FM, ThermoFisher Scientific, M22426) according to manufacturer's instructions. From here on all incubation steps were performed in the dark. Cells were fixed by adding 4% paraformaldehyde in PBS (pH 7.4) a RT for 10 min. After fixation cells were washed three times with cold PBS. For permeabilization, cells were incubated with PBS + 0.1 % Triton X-100 for 10 min. Cells were then washed three times with cold PBS for 5 min each. For blocking, cells were incubated with 1 % BSA, 22.52 mg/ml (0.3 M) glycine in PBST (PBS + 0.1 % Tween20) for 30 min. Flag antibody (FLAG M2, Sigma-Aldrich A8592) in a 1:200 dilution in 1 % BSA in PBST was used for immunostaining. 100 μ l antibody solution was added onto the coverslip and incubated over night at 4°C. After staining cells were washed three times with PBS for 5 min. The secondary antibody (Alexa Fluor 488, Invitrogen A-21202) was diluted 1:500 in 1 % BSA and 100 μ l were pipetted onto coverslips. Cells were incubated for 1 h at RT in the dark. Cells were then washed three times with PBS for 5 min. For counter staining a small drop of Life Science ProLong Gold Antifade Mountant (ThermoFisher Scientific) including DAPI was added to the coverslip. The coverslip was inverted using tweezers and gently placed on a microscope slide. Excess mounting solution was removed and the slide was dried for 15 min in the dark before imaging. Cells were imaged with a imaged with a Leica TCS SP8-X confocal microscope equipped with a white light laser and DAPI diode.

5. Statistical analysis

Results are presented as mean + SD or SEM. Statistical analyses were performed using unpaired t-test or One-way ANOVA with following Dunnett's multiple comparisons test using GraphPad Prism (GraphPad software). Enrichment analysis was analyzed using Fisher's test. Significance levels are * $p < 0.05$, ** $p < 0.01$ and *** $p < 0.001$ versus respective control.

6. Software

Graphs were generated using GraphPad PRISM 6 or custom R scripts. The figure layout was designed by using Adobe Illustrator. NCL-1-binding motif enrichment analysis was performed using custom python scripts.

Western blot signals, worm length and nucleolar size as well as GFP intensity were quantified using the open source Fiji software based on ImageJ.

Supplementary tables

Table 2. List of used *C. elegans* strains.

Strain names	Genotypes
N2	Bristol (wild type)
AA3121	<i>ncl-1(e1865) III</i>
AA3122	<i>ncl-1(e1942) III</i>
AA4679	<i>nrde-3(gg66) X</i>
AA4668	<i>nrde-3(gg66); glp-1(2141ts)</i>
AA4669	<i>nrde-3(gg66); daf-2(e1370)</i>
PHX637	<i>ncl-1::flag(syb637)</i>
PHX702	<i>ncl-1::neongreen</i>
PHX1044	<i>ncl-1(syb1044 syb637)N738A</i>
PHX1037	<i>ncl-1(syb1037 syb637)</i>
PHX1035	<i>ncl-1(syb1035 syb637)</i>
PHX1094	<i>ncl-1(syb1094 syb637)</i>
PHX1065	<i>ncl-1(syb1065 syb637)</i>
PHX1056	<i>ncl-1(syb1056 syb637)</i>
AA2735	<i>glp-1(e2141ts)</i>
HC196	<i>sid-1(qt9) V.</i>
AA4651	<i>sid-1(qt9) V; uth1s236[gly-19p::tdtomato + gly-19p::sid-1]</i>
AA4652	<i>sid-1(qt9) V; uth1s237[s?(myo-3p::tomato::unc-54-3'UTR); s459(myo-3p::sid-1::unc-54-3'UTR)]</i>
AA4653	<i>sid-1(qt9) V; uth1s206[s401(rab-3p::tomato::unc-54-3'UTR); s461(rab-3p::sid-1::unc-54-3'UTR)]</i>

CB1370	<i>daf-2(e1370) III</i>
AA4331	<i>ncl-1(e1865) III; unc-119(ed4); Is[sur-5p::UbV-GFP]</i>
AA4335	<i>glp-1(e2141) III; ncl-1(e1942) III</i>
AA2684	<i>eat-2(ad465) II</i>
AA3123	<i>ncl-1(e1942) III; eat(ad465) II</i>
AA3325	<i>ncl-1(e1865); dhEx972(ncl-1::gfp; myo-2::mCherry)</i>
AA4105	<i>unc-119(ed4); Is[sur-5p::UbV-GFP]</i>
AA4331	<i>ncl-1(e1865) III; unc-119(ed4); Is[sur-5p::UbV-GFP]</i>

Table 3. List of used primers with their sequence.

Name	Target	Usage	Sequence (5'-3')
Fib-1 fw	<i>fib-1</i>	qPCR	CAAACGTTGTCCCAATTGTCTG
Fib-1 rv	<i>fib-1</i>	qPCR	GGAAGTTTTGGGCATTGAGAG
Popl-1 fw	<i>popl-1</i>	qPCR	AGCTTTCAACGTGGATTTCTG
Popl-1 rv	<i>popl-1</i>	qPCR	AGAGTTGGTGACATTCCTCT
Mrps-16 fw	<i>mrps-16</i>	qPCR	TAGGTCTGAAGATACGAGGGT
Mrps-16 rv	<i>mrps-16</i>	qPCR	GACAGGCCGAGAAGTTCAAG
pre-rRNA #1 fw	Pre-rRNA	qPCR	CTGTGTTTACACCCGAATGATTCTAG
pre-rRNA #1 rv	Pre-rRNA	qPCR	CTAATCGTGAGATGGGACACTCATACA
pre-rRNA #2 fw	Pre-rRNA	qPCR	CGCAGACATATAGTCTAGCGAG
pre-rRNA #2 rv	Pre-rRNA	qPCR	GATCCATAGATATTGCTGATGATTC
pre-rRNA #3 fw	Pre-rRNA	qPCR	AAAGTCGTAACAAGGTAG
pre-rRNA #3 rv	Pre-rRNA	qPCR	ATCTTAAGGTTTGTGGAT
pre-rRNA #5 fw	Pre-rRNA	qPCR	AACGCATAGCACCAACTG

pre-rRNA #5 rv	Pre-rRNA	qPCR	TCCGAAGAGAAGCCTAAG
pre-rRNA #6 fw	Pre-rRNA	qPCR	AATACTGGGATTCGTCTA
pre-rRNA #6 rv	Pre-rRNA	qPCR	GAGTTCAGGTTGAGATTAG
pre-rRNA #7 fw	Pre-rRNA	qPCR	CCTTTTCCTACACTCATGTCTTTGCAG
pre-rRNA #7 rv	Pre-rRNA	qPCR	GTTCTAAGTTTTTCTAAAGCAAGCACATTG
etf-3 fw	<i>etf-3</i>	qPCR	ACTTGATCTACAAGTGCGGAGGA
etf-3 rv	<i>etf-3</i>	qPCR	AAAGATCCCTTACCCATCTCCTG
snb-1 fw	<i>snb-1</i>	qPCR	GAATCATGAAGGTGAACGTGG
snb-1 rv	<i>snb-1</i>	qPCR	CCAATACTTGCGCTTCAGGG
Ncl-1 fw_I	<i>ncl-1</i>	PCR/Seq.	CTCTCGACGTTCCGGTACA
Ncl-1 fw_II	<i>ncl-1</i>	PCR/Seq.	GTTCCAAATGCCCATCTTC
Ncl-1 fw_III	<i>ncl-1</i>	PCR/Seq.	CGATATGCTCGATATGTTC
Ncl-1 fw_VI	<i>ncl-1</i>	PCR/Seq.	CTTTGGTGGATCCTCGCAATC
Ncl-1 fw_V	<i>ncl-1</i>	PCR/Seq.	GGAGAAGTAGTTGTCGCTG
ncl1(e1865)rv	<i>ncl-1</i>	PCR/Seq.	GATGTGGCCGGAAGGAAGC
ncl1(e1885)fw	<i>ncl-1</i>	PCR/Seq.	GGCTGTCAACCGTACCACC
ncl1(e1942)rv	<i>ncl-1</i>	PCR/Seq.	GACGAGTTCTGAAGCACGATG
ncl1(e1942)fw	<i>ncl-1</i>	PCR/Seq.	CATACCGTGATCCGAAGGTTC
Ncl1Neon_fw	<i>ncl-1::neongreen</i>	PCR/Seq.	GAAGTAGTTGTCGCTGATAACCA
Ncl1Neon_rv	<i>ncl-1::neongreen</i>	PCR/Seq.	GGAACGGAGCACTGCTCCA
Ncl1Neon_fw_In	<i>ncl-1::neongreen</i>	PCR/Seq.	GTTACACCTACGAGGGATCC
nrde-3_fw	<i>nrde-3</i>	PCR/Seq.	TGGGTGAGATGGGCTCTAAG

nrde-3_rv	<i>nrde-3</i>	PCR/Seq.	GTTCAAAGCGACGTCCATCC
Ncl1fl_fw	<i>ncl-1::flag</i>	PCR/Seq.	GGTCATGCGTGTAATCATTTCG
Ncl1fl_rv	<i>ncl-1::flag</i>	PCR/Seq.	CTTAGATGGGAGGGATAACATAAG
Ncl1fl_fw_In	<i>ncl-1::flag</i>	PCR/Seq.	GACGGTGACTATAAGGATCACG
SeqC88AC111A_fw	<i>ncl-1::flag</i>	PCR/Seq.	CACCCTCCCCTTTAGTACTG
SeqC88AC111A_rv	<i>ncl-1::flag</i>	PCR/Seq.	GAAGTCAGTGAGCAACGAGTC
SeqC279AC374_A_fw	<i>ncl-1::flag</i>	PCR/Seq.	GTTCGGATTTGGATCACC
SeqC279AC374_A_rv	<i>ncl-1::flag</i>	PCR/Seq.	CACTAAGCAAACCTTACGTCAG
CMV fw		PCR/Seq.	GTGGATAGCGGTTTGACTC
Ncl-1 NotI fw		Cloning	CGTAAGTGCGGCCGCTCATTCCGTATCTA GAAATTTGC
Ncl-1 KpnI rv		Cloning	CTGAGTAGGTACCCTAGATCTGGCTAGAA GCGGAAG

Table 4. List of used plasmids.

Plasmid name	Sequence information
pcDNA3.1_ncl-1_flag	<i>pCMV::flag::HA::ncl-1::polyA</i>

References

- Albert, Benjamin et al. 2019. "A Ribosome Assembly Stress Response Regulates Transcription to Maintain Proteome Homeostasis." *eLife* 8. <https://elifesciences.org/articles/45002> (March 6, 2020).
- Altman, S., and J. D. Smith. 1971. "Tyrosine tRNA Precursor Molecule Polynucleotide Sequence." *Nature New Biology* 233(36): 35–39.
- Anderson, Paul, and Pavel Ivanov. 2014. "tRNA Fragments in Human Health and Disease." *FEBS Letters*.
- Anthony Massiah, Michael. 2019. "Zinc-Binding B-Box Domains with RING Folds Serve Critical Roles in the Protein Ubiquitination Pathways in Plants and Animals." In *Ubiquitin Proteasome System - Current Insights into Mechanism Cellular Regulation and Disease*.
- Arantes-Oliveira, Nuno, Javier Apfeld, Andrew Dillin, and Cynthia Kenyon. 2002. "Regulation of Life-Span by Germ-Line Stem Cells in *Caenorhabditis Elegans*." *Science* 295(5554): 502–5.
- Arragain, Simon et al. 2010. "Post-Translational Modification of Ribosomal Proteins: Structural and Functional Characterization of RimO from *Thermotoga Maritima*, a Radical S-Adenosylmethionine Methyltransferase." *Journal of Biological Chemistry*.
- Aubert, Maxime, Marie Françoise O'donohue, Simon Lebaron, and Pierre Emmanuel Gleizes. 2018. "Pre-Ribosomal RNA Processing in Human Cells: From Mechanisms to Congenital Diseases." *Biomolecules*.
- Augustin, Hrvoje, Jennifer Adcott, Christopher J.H. Elliott, and Linda Partridge. 2017. "Complex Roles of Myoglianin in Regulating Adult Performance and Lifespan." *Fly*.
- B. Hwang, Ara, Dae-Eun Jeong, and Seung-Jae Lee. 2012. "Mitochondria and Organismal Longevity." *Current Genomics*.
- Bartke, Andrzej, and Holly Brown-Borg. 2004. "Life Extension in the Dwarf Mouse." *Current Topics in Developmental Biology* 63: 189–225.
- Basisty, Nathan, Jesse G. Meyer, and Birgit Schilling. 2018. "Protein Turnover in Aging and Longevity." *Proteomics*.
- Bedford, Lynn et al. 2010. "Assembly, Structure, and Function of the 26S Proteasome." *Trends in Cell Biology*.
- Ben-Shem, Adam, Lasse Jenner, Gulnara Yusupova, and Marat Yusupov. 2010. "Crystal Structure of the Eukaryotic Ribosome." *Science*.
- Besse, Florence, and Anne Ephrussi. 2008. "Translational Control of Localized MRNAs: Restricting Protein Synthesis in Space and Time." *Nature Reviews Molecular Cell Biology*.
- Bjedov, Ivana et al. 2010. "Mechanisms of Life Span Extension by Rapamycin in the Fruit Fly *Drosophila Melanogaster*." *Cell Metabolism* 11(1): 35–46.
- Boisvert, François Michel, Silvana Van Koningsbruggen, Joaquín Navascués, and Angus I. Lamond. 2007. "The Multifunctional Nucleolus." *Nature Reviews Molecular Cell Biology*.
- Borovjagin, Anton V., and Susan A. Gerbi. 1999. "U3 Small Nucleolar RNA Is Essential for Cleavage at Sites 1, 2 and 3 in Pre-rRNA and Determines Which rRNA Processing Pathway Is Taken in *Xenopus Oocytes*." *Journal of Molecular*

- Biology* 286(5): 1347–63. <http://www.ncbi.nlm.nih.gov/pubmed/10064702> (April 2, 2020).
- Boulon, Séverine et al. 2010. “The Nucleolus under Stress.” *Molecular Cell* 40(2): 216–27. <https://linkinghub.elsevier.com/retrieve/pii/S1097276510007525> (February 7, 2020).
- Boutros, Michael, and Julie Ahringer. 2008. “The Art and Design of Genetic Screens: RNA Interference.” *Nature Reviews Genetics*.
- Brand, Martin D. 2014. “The Role of Mitochondria in Longevity and Healthspan.” *Longevity & Healthspan*.
- Brandman, Onn et al. 2012. “A Ribosome-Bound Quality Control Complex Triggers Degradation of Nascent Peptides and Signals Translation Stress.” *Cell* 151(5): 1042–54. <https://linkinghub.elsevier.com/retrieve/pii/S0092867412013396> (February 19, 2020).
- Branzei, Dana, and Marco Foiani. 2005. “The DNA Damage Response during DNA Replication.” *Current Opinion in Cell Biology*.
- Bratic, Ana, and Nils Göran Larsson. 2013. “The Role of Mitochondria in Aging.” *Journal of Clinical Investigation*.
- Brenner, S. 1974. “The Genetics of *Caenorhabditis Elegans*.” *Genetics*.
- Buchwalter, Abigail, and Martin W. Hetzer. 2017. “Nucleolar Expansion and Elevated Protein Translation in Premature Aging.” *Nature Communications* 8(1).
- Burkewitz, Kristopher et al. 2015. “Neuronal CRTC-1 Governs Systemic Mitochondrial Metabolism and Lifespan via a Catecholamine Signal.” *Cell*.
- Burkhart, Kirk B. et al. 2011. “A Pre-mRNA-Associating Factor Links Endogenous Sirnas to Chromatin Regulation.” *PLoS Genetics*.
- Bustamante, Hianara A. et al. 2018. “Interplay between the Autophagy-Lysosomal Pathway and the Ubiquitin-Proteasome System: A Target for Therapeutic Development in Alzheimer’s Disease.” *Frontiers in Cellular Neuroscience*.
- Calderwood, Stuart K., Ayesha Murshid, and Thomas Prince. 2009. “The Shock of Aging: Molecular Chaperones and the Heat Shock Response in Longevity and Aging - A Mini-Review.” *Gerontology*.
- Chamberlain, Joel R., Yoon Lee, William S. Lane, and David R. Engelke. 1998. “Purification and Characterization of the Nuclear RNase P Holoenzyme Complex Reveals Extensive Subunit Overlap with RNase MRP.” *Genes and Development* 12(11): 1678–90. <http://www.ncbi.nlm.nih.gov/pubmed/9620854> (April 3, 2020).
- Chan, Clement T.Y. et al. 2010. “A Quantitative Systems Approach Reveals Dynamic Control of tRNA Modifications during Cellular Stress.” *PLoS Genetics*.
- — —. 2012. “Reprogramming of tRNA Modifications Controls the Oxidative Stress Response by Codon-Biased Translation of Proteins.” *Nature Communications*.
- Chan, Joanna C. et al. 2011. “AKT Promotes rRNA Synthesis and Cooperates with C-MYC to Stimulate Ribosome Biogenesis in Cancer.” *Science Signaling*.
- Chan, Patricia P., and Todd M. Lowe. 2009. “GtRNADB: A Database of Transfer RNA Genes Detected in Genomic Sequence.” *Nucleic Acids Research*.
- Chang, Jessica T. et al. 2017. “Spatiotemporal Regulation of Autophagy during *Caenorhabditis Elegans* Aging.” *eLife*.
- Chen, Danyang, and Sui Huang. 2001. “Nucleolar Components Involved in Ribosome Biogenesis Cycle between the Nucleolus and Nucleoplasm in Interphase Cells.” *Journal of Cell Biology*.
- Chiba, Takuya et al. 2010. “Development of Calorie Restriction Mimetics as Therapeutics for Obesity, Diabetes, Inflammatory and Neurodegenerative

- Diseases.” *Current Genomics*.
- Cohen-Berkman, Moran et al. 2020. “Endogenous SiRNAs Promote Proteostasis and Longevity in Germlineless *C. Elegans*.” *eLife*.
- — —. “Endogenous SiRNAs Promote Proteostasis and Longevity in Germline Less *C. Elegans*.” *eLife*.
https://elifesciences.org/articles/50896?utm_source=researcher_app&utm_medium=referral&utm_campaign=RESR_MRKT_Researcher_inbound (March 31, 2020).
- Colman, Ricki J. et al. 2009. “Caloric Restriction Delays Disease Onset and Mortality in Rhesus Monkeys.” *Science*.
- Connors, M. T., D. P. Poppi, and J. P. Cant. 2008. “Protein Elongation Rates in Tissues of Growing and Adult Sheep.” *Journal of Animal Science*.
- Copeland, Jeffrey M. et al. 2009. “Extension of *Drosophila* Life Span by RNAi of the Mitochondrial Respiratory Chain.” *Current Biology* 19(19): 1591–98.
- Coux, Olivier, Keiji Tanaka, and Alfred L. Goldberg. 1996. “Structure and Functions of the 20S and 26S Proteasomes.” *Annual Review of Biochemistry*.
- Cox, Jürgen et al. 2011. “Andromeda: A Peptide Search Engine Integrated into the MaxQuant Environment.” *Journal of Proteome Research*.
- — —. 2014. “Accurate Proteome-Wide Label-Free Quantification by Delayed Normalization and Maximal Peptide Ratio Extraction, Termed MaxLFQ.” *Molecular and Cellular Proteomics*.
- Cox, Jürgen, and Matthias Mann. 2008. “MaxQuant Enables High Peptide Identification Rates, Individualized p.p.b.-Range Mass Accuracies and Proteome-Wide Protein Quantification.” *Nature Biotechnology*.
- Curran, Sean P., and Gary Ruvkun. 2007. “Lifespan Regulation by Evolutionarily Conserved Genes Essential for Viability.” *PLoS Genetics*.
- Dabeva, M. D. et al. 1976. “Intranuclear Maturation Pathways of Rat Liver Ribosomal Ribonucleic Acids.” *Biochemical Journal* 160(3): 495–503.
- David, Della C. et al. 2010. “Widespread Protein Aggregation as an Inherent Part of Aging in *C. Elegans*” ed. Julie Ahringer. *PLoS Biology* 8(8): e1000450.
<https://dx.plos.org/10.1371/journal.pbio.1000450> (February 19, 2020).
- — —. 2012. “Aging and the Aggregating Proteome.” *Frontiers in Genetics*.
- Dell’Agnello, Carlotta et al. 2007. “Increased Longevity and Refractoriness to Ca²⁺-Dependent Neurodegeneration in Surf1 Knockout Mice.” *Human Molecular Genetics*.
- Demontis, Fabio, Vishal K. Patel, William R. Swindell, and Norbert Perrimon. 2014. “Intertissue Control of the Nucleolus via a Myokine-Dependent Longevity Pathway.” *Cell Reports* 7(5): 1481–94.
<https://www.sciencedirect.com/science/article/pii/S2211124714003763?via%3Dihub> (June 12, 2019).
- Dever, Thomas E., Jonathan D. Dinman, and Rachel Green. 2018. “Translation Elongation and Recoding in Eukaryotes.” *Cold Spring Harbor Perspectives in Biology*.
- Dever, Thomas E., and Rachel Green. 2012. “The Elongation, Termination, and Recycling Phases of Translation in Eukaryotes.” *Cold Spring Harbor Perspectives in Biology*.
- Didychuk, Allison L., Samuel E. Butcher, and David A. Brow. 2018. “The Life of U6 Small Nuclear RNA, from Cradle to Grave.” *RNA*.
- Dikic, Ivan, and Zvulun Elazar. 2018. “Mechanism and Medical Implications of

- Mammalian Autophagy." *Nature Reviews Molecular Cell Biology*.
- DE DUVE, C. et al. 1955. "Tissue Fractionation Studies. 6. Intracellular Distribution Patterns of Enzymes in Rat-Liver Tissue." *The Biochemical journal*.
- Eliseev, Boris et al. 2018. "Structure of a Human Cap-Dependent 48S Translation Pre-Initiation Complex." *Nucleic Acids Research*.
- Erales, Jenny et al. 2017. "Evidence for RRNA 2'-O-Methylation Plasticity: Control of Intrinsic Translational Capabilities of Human Ribosomes." *Proceedings of the National Academy of Sciences of the United States of America*.
- Esakova, Olga et al. 2011. "Substrate Recognition by Ribonucleoprotein Ribonuclease MRP." *RNA*.
- Esakova, Olga, and Andrey S Krasilnikov. 2010. "Of Proteins and RNA: The RNase P/MRP Family." *RNA (New York, N.Y.)* 16(9): 1725–47.
<http://www.ncbi.nlm.nih.gov/pubmed/20627997> (March 9, 2020).
- Evans, Daniel S., Pankaj Kapahi, Wen Chi Hsueh, and Lutz Kockel. 2011. "TOR Signaling Never Gets Old: Aging, Longevity and TORC1 Activity." *Ageing Research Reviews*.
- Ewbank, Jonathan J. et al. 1997. "Structural and Functional Conservation of the *Caenorhabditis Elegans* Timing Gene *Clk-1*." *Science*.
- Fagerlund, Robert D., Anna Perederina, Igor Berezin, and Andrey S. Krasilnikov. 2015. "Footprinting Analysis of Interactions between the Largest Eukaryotic RNase P/MRP Protein Pop1 and RNase P/MRP RNA Components." *RNA* 21(9): 1591–1605.
- Felkai, S. 1999. "CLK-1 Controls Respiration, Behavior and Aging in the Nematode *Caenorhabditis Elegans*." *The EMBO Journal*.
- Feng, Jinliu, Frédéric Bussi re, and Siegfried Hekimi. 2001. "Mitochondrial Electron Transport Is a Key Determinant of Life Span in *Caenorhabditis Elegans*." *Developmental Cell*.
- Finley, Daniel. 2009. "Recognition and Processing of Ubiquitin-Protein Conjugates by the Proteasome." *Annual Review of Biochemistry*.
- Fire, A. et al. 1998. "Potent and Specific Genetic Interference by Double-Stranded RNA in *Caenorhabditis Elegans*." *Nature* 391(6669): 806–11.
<https://www.nature.com/articles/35888> (July 1, 2020).
- Flatt, Thomas et al. 2008. "Drosophila Germ-Line Modulation of Insulin Signaling and Lifespan." *Proceedings of the National Academy of Sciences of the United States of America* 105(17): 6368–73.
<http://www.ncbi.nlm.nih.gov/pubmed/18434551> (March 30, 2020).
- Flibotte, Stephane et al. 2010. "Whole-Genome Profiling of Mutagenesis in *Caenorhabditis Elegans*." *Genetics*.
- Fontana, Luigi, Ricki J. Colman, John O. Holloszy, and Richard Weindruch. 2011. "Calorie Restriction in Nonhuman and Human Primates." In *Handbook of the Biology of Aging*, Elsevier Inc., 447–61.
- Fox, George E. 2010. "Origin and Evolution of the Ribosome." *Cold Spring Harbor perspectives in biology*.
- Frank, Deborah J., Bruce A. Edgar, and Mark B. Roth. 2002. "The *Drosophila Melanogaster* Gene Brain Tumor Negatively Regulates Cell Growth and Ribosomal RNA Synthesis." *Development* 129(2): 399–407.
- Frank, Deborah J., and Mark B. Roth. 1998. "Ncl-1 Is Required for the Regulation of Cell Size and Ribosomal RNA Synthesis in *Caenorhabditis Elegans*." *Journal of Cell Biology*.

- Fricker, Roger et al. 2019. "A TRNA Half Modulates Translation as Stress Response in *Trypanosoma Brucei*." *Nature Communications*.
- Frotin, F. et al. 2019. "The Nucleolus Functions as a Phase-Separated Protein Quality Control Compartment." *Science* 365(6451).
- Gamerding, Martin, Marie Anne Hanebuth, Tancred Frickey, and Elke Deuerling. 2015. "The Principle of Antagonism Ensures Protein Targeting Specificity at the Endoplasmic Reticulum." *Science*.
- Gavilán, Elena et al. 2015. "Age-Related Dysfunctions of the Autophagy Lysosomal Pathway in Hippocampal Pyramidal Neurons under Proteasome Stress." *Neurobiology of Aging*.
- Gebetsberger, Jennifer et al. 2017. "A TRNA-Derived Fragment Competes with mRNA for Ribosome Binding and Regulates Translation during Stress." *RNA Biology*.
- Gebetsberger, Jennifer, Marek Zywicki, Andrea Künzi, and Norbert Polacek. 2012. "TRNA-Derived Fragments Target the Ribosome and Function as Regulatory Non-Coding RNA in *Haloferax Volcanii*." *Archaea*.
- Gehrke, Stephan et al. 2015. "PINK1 and Parkin Control Localized Translation of Respiratory Chain Component MRNAs on Mitochondria Outer Membrane." *Cell Metabolism*.
- Gerisch, Birgit et al. 2001. "A Hormonal Signaling Pathway Influencing *C. Elegans* Metabolism, Reproductive Development, and Life Span." *Developmental Cell* 1(6): 841–51.
- Ghazi, Arjumand, Sivan Henis-Korenblit, and Cynthia Kenyon. 2009. "A Transcription Elongation Factor That Links Signals from the Reproductive System to Lifespan Extension in *Caenorhabditis Elegans*" ed. Stuart K. Kim. *PLoS Genetics* 5(9): e1000639. <https://dx.plos.org/10.1371/journal.pgen.1000639> (March 30, 2020).
- Goldfarb, Katherine C., and Thomas R. Cech. 2017. "Targeted CRISPR Disruption Reveals a Role for RNase MRP RNA in Human Preribosomal RNA Processing." *Genes and Development* 31(1): 59–71.
- Gonskikh, Yulia, and Norbert Polacek. 2017. "Alterations of the Translation Apparatus during Aging and Stress Response." *Mechanisms of Ageing and Development* 168: 30–36.
<https://www.sciencedirect.com/science/article/pii/S0047637416302214?via%3Di> hub (October 1, 2019).
- Gonzalez, Omar Garcia et al. 2014. "Telomerase Stimulates Ribosomal DNA Transcription under Hyperproliferative Conditions." *Nature Communications*.
- Goudeau, Jérôme et al. 2011. "Fatty Acid Desaturation Links Germ Cell Loss to Longevity Through NHR-80/HNF4 in *C. Elegans*" ed. Marc Tatar. *PLoS Biology* 9(3): e1000599. <https://dx.plos.org/10.1371/journal.pbio.1000599> (March 30, 2020).
- Greer, Kimberly A., Larry M. Hughes, and Michal M. Masternak. 2011. "Connecting Serum IGF-1, Body Size, and Age in the Domestic Dog." *Age*.
- Grewal, Savraj S., Justin R. Evans, and Bruce A. Edgar. 2007. "Drosophila TIF-IA Is Required for Ribosome Synthesis and Cell Growth and Is Regulated by the TOR Pathway." *Journal of Cell Biology*.
- Guang, Shouhong et al. 2008. "An Argonaute Transports SiRNAs from the Cytoplasm to the Nucleus." *Science*.
- Guaragnella, Nicoletta, Liam P. Coyne, Xin Jie Chen, and Sergio Giannattasio. 2018. "Mitochondria-Cytosol-Nucleus Crosstalk: Learning from *Saccharomyces*

- Cerevisiae.” *FEMS Yeast Research*.
- Guerrier-Takada, Cecilia et al. 1983. “The RNA Moiety of Ribonuclease P Is the Catalytic Subunit of the Enzyme.” *Cell* 35(3 PART 2): 849–57.
- Gutmann, Bernard, Anthony Gobert, and Philippe Giegé. 2012. “PRORP Proteins Support RNase P Activity in Both Organelles and the Nucleus in Arabidopsis.” *Genes and Development*.
- Hannan, Katherine M. et al. 2003. “MTOR-Dependent Regulation of Ribosomal Gene Transcription Requires S6K1 and Is Mediated by Phosphorylation of the Carboxy-Terminal Activation Domain of the Nucleolar Transcription Factor UBF†.” *Molecular and Cellular Biology*.
- Hansen, Malene et al. 2007. “Lifespan Extension by Conditions That Inhibit Translation in *Caenorhabditis Elegans*.” *Aging Cell* 6(1): 95–110.
<http://doi.wiley.com/10.1111/j.1474-9726.2006.00267.x> (October 1, 2019).
- — —. 2008. “A Role for Autophagy in the Extension of Lifespan by Dietary Restriction in *C. Elegans*.” *PLoS Genetics* 4(2): e24.
- Hansen, Malene, Ao-Lin Hsu, Andrew Dillin, and Cynthia Kenyon. 2005. “New Genes Tied to Endocrine, Metabolic, and Dietary Regulation of Lifespan from a *Caenorhabditis Elegans* Genomic RNAi Screen.” *PLoS Genetics* 1(1): e17.
<https://dx.plos.org/10.1371/journal.pgen.0010017> (March 30, 2020).
- Harrison, David E. et al. 2009. “Rapamycin Fed Late in Life Extends Lifespan in Genetically Heterogeneous Mice.” *Nature*.
- Hedgecock, E. M., and R. K. Herman. 1995. “The Ncl-1 Gene and Genetic Mosaics of *Caenorhabditis Elegans*.” *Genetics*.
- Hedtke, Boris, Ina Wagner, Thomas Börner, and Wolfgang R. Hess. 1999. “Inter-Organellar Crosstalk in Higher Plants: Impaired Chloroplast Development Affects Mitochondrial Gene and Transcript Levels.” *Plant Journal*.
- Henras, Anthony K et al. 2015. “An Overview of Pre-Ribosomal RNA Processing in Eukaryotes.” *Wiley interdisciplinary reviews. RNA* 6(2): 225–42.
<http://www.ncbi.nlm.nih.gov/pubmed/25346433> (June 25, 2019).
- Hernandez-Verdun, Danièle. 2011. “Assembly and Disassembly of the Nucleolus during the Cell Cycle.” *Nucleus*.
- Hokii, Yusuke et al. 2010. “A Small Nucleolar RNA Functions in RRNA Processing in *Caenorhabditis Elegans*.” *Nucleic Acids Research*.
- Holzenberger, Martin et al. 2003. “IGF-1 Receptor Regulates Lifespan and Resistance to Oxidative Stress in Mice.” *Nature* 421(6919): 182–87.
- Houtkooper, Riekelt H. et al. 2013. “Mitonuclear Protein Imbalance as a Conserved Longevity Mechanism.” *Nature*.
- Hsin, Honor, and Cynthia Kenyon. 1999. “Signals from the Reproductive System Regulate the Lifespan of *C. Elegans*.” *Nature* 399(6734): 362–66.
- Hsu, Ao Lin, Coleen T. Murphy, and Cynthia Kenyon. 2003. “Regulation of Aging and Age-Related Disease by DAF-16 and Heat-Shock Factor.” *Science*.
- Huang, Da Wei, Brad T. Sherman, and Richard A. Lempicki. 2009a. “Bioinformatics Enrichment Tools: Paths toward the Comprehensive Functional Analysis of Large Gene Lists.” *Nucleic Acids Research*.
- — —. 2009b. “Systematic and Integrative Analysis of Large Gene Lists Using DAVID Bioinformatics Resources.” *Nature Protocols*.
- Ishii, Naoaki et al. 1998. “A Mutation in Succinate Dehydrogenase Cytochrome b Causes Oxidative Stress and Ageing in Nematodes.” *Nature*.
- Iwasa, Hiroaki, Simon Yu, Jian Xue, and Monica Driscoll. 2010. “Novel EGF Pathway

- Regulators Modulate C. Elegans Healthspan and Lifespan via EGF Receptor, PLC- γ , and IP3R Activation." *Aging Cell*.
- Jacobson, Marty R., and Thoru Pederson. 1998. "Localization of Signal Recognition Particle RNA in the Nucleolus of Mammalian Cells." *Proceedings of the National Academy of Sciences of the United States of America*.
- James, Martyn J., and Joost C.B.M. Zomerdijk. 2004. "Phosphatidylinositol 3-Kinase and MTOR Signaling Pathways Regulate RNA Polymerase I Transcription in Response to IGF-1 and Nutrients." *Journal of Biological Chemistry*.
- Jarrous, Nayef. 2002. "Human Ribonuclease P: Subunits, Function, and Intranuclear Localization." *RNA (New York, N.Y.)* 8(1): 1–7.
<http://www.ncbi.nlm.nih.gov/pubmed/11871657> (August 23, 2019).
- — —. 2017. "Roles of RNase P and Its Subunits." *Trends in genetics: TIG* 33(9): 594–603. <http://www.ncbi.nlm.nih.gov/pubmed/28697848> (August 23, 2019).
- Jiao, Xiaoli et al. 2012. "Databases and Ontologies DAVID-WS: A Stateful Web Service to Facilitate Gene/Protein List Analysis." *BIOINFORMATICS APPLICATIONS NOTE* 28(13): 1805–6.
<http://david.abcc.ncifcrf.gov/content.jsp?file=WS.html>. (July 7, 2020).
- Joazeiro, Claudio A.P. 2019. "Mechanisms and Functions of Ribosome-Associated Protein Quality Control." *Nature Reviews Molecular Cell Biology*.
- Johnson, David W. et al. 2014. "The Caenorhabditis Elegans Myc-Mondo/Mad Complexes Integrate Diverse Longevity Signals" ed. Kaveh Ashrafi. *PLoS Genetics* 10(4): e1004278. <https://dx.plos.org/10.1371/journal.pgen.1004278> (March 27, 2020).
- Kaeberlein, Matt et al. 2005. "Cell Biology: Regulation of Yeast Replicative Life Span by TOR and Sch9 Response to Nutrients." *Science*.
- Kamata, Hideaki, and Hajime Hirata. 1999. "Redox Regulation of Cellular Signalling." *Cellular Signalling*.
- Kamath, Ravi S., and Julie Ahringer. 2003. "Genome-Wide RNAi Screening in Caenorhabditis Elegans." *Methods*.
- Kantidakis, Theodoros et al. 2010. "MTOR Associates with TFIIC, Is Found at TRNA and 5S RRNA Genes, and Targets Their Repressor Maf1." *Proceedings of the National Academy of Sciences of the United States of America*.
- Kapahi, Pankaj et al. 2004. "Regulation of Lifespan in Drosophila by Modulation of Genes in the TOR Signaling Pathway." *Current Biology*.
- — —. 2010. "With TOR, Less Is More: A Key Role for the Conserved Nutrient-Sensing TOR Pathway in Aging." *Cell Metabolism*.
- Karaiskos, Spyros, Ammar S. Naqvi, Karl E. Swanson, and Andrey Grigoriev. 2015. "Age-Driven Modulation of TRNA-Derived Fragments in Drosophila and Their Potential Targets." *Biology Direct*.
- Kato, Masato et al. 2012. "Cell-Free Formation of RNA Granules: Low Complexity Sequence Domains Form Dynamic Fibers within Hydrogels." *Cell*.
- Kayser, Ernst Bernhard, Margaret M. Sedensky, Phil G. Morgan, and Charles L. Hoppel. 2004. "Mitochondrial Oxidative Phosphorylation Is Defective in the Long-Lived Mutant Clk-1." *Journal of Biological Chemistry*.
- Kenyon, Cynthia et al. 1993. "A C. Elegans Mutant That Lives Twice as Long as Wild Type." *Nature* 366(6454): 461–64.
- Kim, Young Il et al. 2014. "Nucleolar GTPase NOG-1 Regulates Development, Fat Storage, and Longevity through Insulin/IGF Signaling in C. Elegans." *Molecules and Cells*.

- Kimura, Koutarou D., Heidi A. Tissenbaum, Yanxia Liu, and Gary Ruvkun. 1997. "Daf-2, an Insulin Receptor-like Gene That Regulates Longevity and Diapause in *Caenorhabditis Elegans*." *Science*.
- King, Thomas H., Ben Liu, Ryan R. McCully, and Maurille J. Fournier. 2003. "Ribosome Structure and Activity Are Altered in Cells Lacking SnoRNPs That Form Pseudouridines in the Peptidyl Transferase Center." *Molecular Cell*.
- Kolesnichenko, Marina et al. 2012. "Attenuation of TORC1 Signaling Delays Replicative and Oncogenic RAS-Induced Senescence." *Cell Cycle*.
- Kostova, Kamena K. et al. 2017. "CAT-Tailing as a Fail-Safe Mechanism for Efficient Degradation of Stalled Nascent Polypeptides." *Science*.
- Kozak, M. 1989. "The Scanning Model for Translation: An Update." *Journal of Cell Biology*.
- Kulichkova, Valentina A. et al. 2010. "26S Proteasome Exhibits Endoribonuclease Activity Controlled by Extra-Cellular Stimuli." *Cell Cycle*.
- Labbadia, Johnathan, and Richard I Morimoto. 2015. "The Biology of Proteostasis in Aging and Disease." *Annual Review of Biochemistry*.
- Laity, J. H., B. M. Lee, and P. E. Wright. 2001. "Zinc Finger Proteins: New Insights into Structural and Functional Diversity." *Current Opinion in Structural Biology*.
- Lakowski, Bernard, and Siegfried Hekimi. 1996. "Determination of Life-Span in *Caenorhabditis Elegans* by Four Clock Genes." *Science*.
- Lam, Yun Wah, and Laura Trinkle-Mulcahy. 2015. "New Insights into Nucleolar Structure and Function." *F1000Prime Reports* 7.
- Lapierre, Louis R. et al. 2013. "The TFEB Orthologue HLH-30 Regulates Autophagy and Modulates Longevity in *Caenorhabditis Elegans*." *Nature Communications* 4.
- Lapierre, Louis R., Sara Gelino, Alicia Meléndez, and Malene Hansen. 2011. "Autophagy and Lipid Metabolism Coordinately Modulate Life Span in Germline-Less *C. Elegans*." *Current Biology* 21(18): 1507–14.
- Lécuyer, Eric et al. 2007. "Global Analysis of mRNA Localization Reveals a Prominent Role in Organizing Cellular Architecture and Function." *Cell*.
- Lee, Daniel Y., and David A. Clayton. 1998. "Initiation of Mitochondrial DNA Replication by Transcription and R-Loop Processing." *Journal of Biological Chemistry*.
- Lee, Shin Hae, and Kyung Jin Min. 2013. "Caloric Restriction and Its Mimetics." *BMB Reports*.
- Leopold, A. C., Ethel Niedergang-Kamien, and Jules Janick. 1959. "Experimental Modification of Plant Senescence." *Plant Physiology* 34(5): 570–73.
- Lesnik, Chen et al. 2014. "OM14 Is a Mitochondrial Receptor for Cytosolic Ribosomes That Supports Co-Translational Import into Mitochondria." *Nature Communications*.
- Lesnik, Chen, Adi Golani-Armon, and Yoav Arava. 2015. "Localized Translation near the Mitochondrial Outer Membrane: An Update." *RNA Biology* 12(8): 801–9. <http://www.tandfonline.com/doi/full/10.1080/15476286.2015.1058686> (January 16, 2020).
- Lewinska, Anna et al. 2014. "Links between Nucleolar Activity, RDNA Stability, Aneuploidy and Chronological Aging in the Yeast *Saccharomyces Cerevisiae*." *Biogerontology*.
- Li, Hong et al. 2006. "Nutrient Regulates Tor1 Nuclear Localization and Association with RDNA Promoter." *Nature*.

- Li, Weiquan, Xinna Li, and Richard A. Miller. 2014. "ATF4 Activity: A Common Feature Shared by Many Kinds of Slow-Aging Mice." *Aging Cell*.
- Lin, Kui, Jennie B. Dorman, Aylin Rodan, and Cynthia Kenyon. 1997. "Daf-16: An HNF-3/Forkhead Family Member That Can Function to Double the Life-Span of *Caenorhabditis Elegans*." *Science* 278(5341): 1319–22. <https://science.sciencemag.org/content/278/5341/1319> (July 2, 2020).
- Lindahl, Lasse et al. 2009. "RNase MRP Is Required for Entry of 35S Precursor RRNA into the Canonical Processing Pathway." *RNA*.
- Liu, Botao, Yan Han, and Shu Bing Qian. 2013. "Cotranslational Response to Proteotoxic Stress by Elongation Pausing of Ribosomes." *Molecular Cell*.
- Liu, Chunhua et al. 2019. "Crystal Structure of the Coiled-Coil Domain of *Drosophila* TRIM Protein Brat." *Proteins: Structure, Function and Bioinformatics*.
- Liu, Jun Ping. 2014. "Molecular Mechanisms of Ageing and Related Diseases." *Clinical and Experimental Pharmacology and Physiology*.
- Liu, Xingxing et al. 2005. "Evolutionary Conservation of the Clk-1-Dependent Mechanism of Longevity: Loss of Mcl1 Increases Cellular Fitness and Lifespan in Mice." *Genes and Development*.
- Liu, Yasmine J. et al. 2020. "Mitochondrial Translation and Dynamics Synergistically Extend Lifespan in *C. Elegans* through HLH-30." *Journal of Cell Biology* 219(6). <https://rupress.org/jcb/article/doi/10.1083/jcb.201907067/151623/Mitochondrial-translation-and-dynamics> (April 8, 2020).
- Loedige, Inga et al. 2014. "The NHL Domain of BRAT Is an RNA-Binding Domain That Directly Contacts the Hunchback mRNA for Regulation." *Genes and Development*.
- — —. 2015. "The Crystal Structure of the NHL Domain in Complex with RNA Reveals the Molecular Basis of *Drosophila* Brain-Tumor-Mediated Gene Regulation Accession Numbers 4ZLR GSE71663 GSE73000 Loedige et Al." *Cell Reports* 13. <http://dx.doi.org/10.1016/j.celrep.2015.09.068> (July 11, 2019).
- Loening, U. E., K. W. Jones, and M. L. Birnstiel. 1969. "Properties of the Ribosomal RNA Precursor in *Xenopus Laevis*; Comparison to the Precursor in Mammals and in Plants." *Journal of Molecular Biology* 45(2): 353–66. <http://www.ncbi.nlm.nih.gov/pubmed/5367033> (April 2, 2020).
- López-Otín, Carlos et al. 2013a. "The Hallmarks of Aging." *Cell* 153(6): 1194.
- — —. 2013b. "The Hallmarks of Aging." *Cell*.
- Lu, Phoebe D. et al. 2004. "Cytoprotection by Pre-Emptive Conditional Phosphorylation of Translation Initiation Factor 2." *EMBO Journal*.
- Lygerou, Zoi, Christine Allmang, David Tollervey, and Bertrand Séraphin. 1996. "Accurate Processing of a Eukaryotic Precursor Ribosomal RNA by Ribonuclease MRP in Vitro." *Science*.
- Malinovskaya, Elena M. et al. 2018. "Copy Number of Human Ribosomal Genes with Aging: Unchanged Mean, but Narrowed Range and Decreased Variance in Elderly Group." *Frontiers in Genetics*.
- Malli, Roland, and Wolfgang F. Graier. 2019. "IRE1 α Modulates ER and Mitochondria Crosstalk." *Nature Cell Biology*.
- Mason, Jeffrey B et al. 2011. "Transplantation of Young Ovaries Restored Cardioprotective Influence in Postreproductive-Aged Mice." *Aging cell* 10(3): 448–56. <http://www.ncbi.nlm.nih.gov/pubmed/21385306> (April 1, 2020).
- Matai, Latika et al. 2019. "Dietary Restriction Improves Proteostasis and Increases Life Span through Endoplasmic Reticulum Hormesis." *Proceedings of the*

- National Academy of Sciences of the United States of America.*
- Mattijssen, Sandy et al. 2011. "Viperin mRNA Is a Novel Target for the Human RNase MRP/RNase P Endoribonuclease." *Cellular and Molecular Life Sciences* 68(14): 2469–80.
- Mayer, Christine, Jian Zhao, Xuejun Yuan, and Ingrid Grummt. 2004. "MTOR-Dependent Activation of the Transcription Factor TIF-IA Links rRNA Synthesis to Nutrient Availability." *Genes and Development*.
- McCay, C. M., M. F. Crowell, and L. A. Maynard. 1989. "The Effect of Retarded Growth upon the Length of Life Span and upon the Ultimate Body Size. 1935." *Nutrition (Burbank, Los Angeles County, Calif.)*.
- Meléndez, Alicia et al. 2003. "Autophagy Genes Are Essential for Dauer Development and Life-Span Extension in *C. Elegans*." *Science* 301(5638): 1387–91.
- Merrick, William C., and Graham D. Pavitt. 2018. "Protein Synthesis Initiation in Eukaryotic Cells." *Cold Spring Harbor Perspectives in Biology*.
- Mobley, Christopher B. et al. 2017. "Aging in Rats Differentially Affects Markers of Transcriptional and Translational Capacity in Soleus and Plantaris Muscle." *Frontiers in Physiology*.
- Molenaars, Marte et al. 2020. "A Conserved Mito-Cytosolic Translational Balance Links Two Longevity Pathways." *Cell Metabolism* 31(3): 549-563.e7.
- Morita, Masahiro et al. 2015. "MTOR Coordinates Protein Synthesis, Mitochondrial Activity." *Cell Cycle*.
- Motizuki, Mitsuyoshi, and Kunio Tsurugi. 1992. "The Effect of Aging on Protein Synthesis in the Yeast *Saccharomyces Cerevisiae*." *Mechanisms of Ageing and Development*.
- Muñoz, Mario F. et al. 2017. "Aging and Oxidative Stress Decrease Pineal Elongation Factor 2: In Vivo Protective Effect of Melatonin in Young Rats Treated With Cumene Hydroperoxide." *Journal of Cellular Biochemistry*.
- Murakami, Mirei et al. 2004. "MTOR Is Essential for Growth and Proliferation in Early Mouse Embryos and Embryonic Stem Cells." *Molecular and Cellular Biology*.
- Murphy, Coleen T. et al. 2003. "Genes That Act Downstream of DAF-16 to Influence the Lifespan of *Caenorhabditis Elegans*." *Nature*.
- Nakamura, Shuhei et al. 2016. "Mondo Complexes Regulate TFEB via TOR Inhibition to Promote Longevity in Response to Gonadal Signals." *Nature Communications* 7.
- Neumüller, Ralph A. et al. 2008. "Mei-P26 Regulates MicroRNAs and Cell Growth in the *Drosophila* Ovarian Stem Cell Lineage." *Nature*.
- Nikolich-Zugich, Janko et al. 2020. "SARS-CoV-2 and COVID-19 in Older Adults: What We May Expect Regarding Pathogenesis, Immune Responses, and Outcomes." *GeroScience*.
- Noh, Ji Heon et al. 2016. "HuR and GRSF1 Modulate the Nuclear Export and Mitochondrial Localization of the lncRNA RMRP." *Genes and Development*.
- O'Rourke, Eyleen J., and Gary Ruvkun. 2013. "MXL-3 and HLH-30 Transcriptionally Link Lipolysis and Autophagy to Nutrient Availability." *Nature Cell Biology*.
- Ogg, Scott et al. 1997. "The Fork Head Transcription Factor DAF-16 Transduces Insulin-like Metabolic and Longevity Signals in *C. Elegans*." *Nature*.
- Okuyama, Tetsuya et al. 2010. "The ERK-MAPK Pathway Regulates Longevity through SKN-1 and Insulin-like Signaling in *Caenorhabditis Elegans*." *Journal of Biological Chemistry*.

- Olson, M. O.J., and Miroslav Dundr. 2005. "The Moving Parts of the Nucleolus." *Histochemistry and Cell Biology*.
- Olson, Mark O.J. 2004. "Sensing Cellular Stress: Another New Function for the Nucleolus?" *Science's STKE: signal transduction knowledge environment*.
- Ori, Alessandro et al. 2015. "Integrated Transcriptome and Proteome Analyses Reveal Organ-Specific Proteome Deterioration in Old Rats." *Cell Systems*.
- Pan, Kally Z. et al. 2007. "Inhibition of mRNA Translation Extends Lifespan in *Caenorhabditis Elegans*." *Aging Cell* 6(1): 111–19.
- Panowski, Siler H. et al. 2007. "PHA-4/Foxa Mediates Diet-Restriction-Induced Longevity of *C. Elegans*." *Nature* 447(7144): 550–55.
- Papadopoli, David et al. 2019. "Open Peer Review MTOR as a Central Regulator of Lifespan and Aging [Version 1; Peer Review: 3 Approved]." <https://doi.org/10.12688/f1000research.17196.1> (April 7, 2020).
- Pawlikowska, Ludmila et al. 2009. "Association of Common Genetic Variation in the Insulin/IGF1 Signaling Pathway with Human Longevity." *Aging Cell* 8(4): 460–72. [/pmc/articles/PMC3652804/?report=abstract](https://pubmed.ncbi.nlm.nih.gov/19381204/) (July 2, 2020).
- Pederson, Thoru. 1998. "The Plurifunctional Nucleolus." *Nucleic Acids Research*.
- Peng, Wen Tao et al. 2004. "ESF1 Is Required for 18S RRNA Synthesis in *Sccharomyces Cerevisiae*." *Nucleic Acids Research*.
- Pertea, Mihaela et al. 2016. "Transcript-Level Expression Analysis of RNA-Seq Experiments with HISAT, StringTie and Ballgown." *Nature Protocols*.
- Phair, Robert D., and Tom Misteli. 2000. "High Mobility of Proteins in the Mammalian Cell Nucleus." *Nature*.
- Politz, Joan C. et al. 2000. "Signal Recognition Particle Components in the Nucleolus." *Proceedings of the National Academy of Sciences of the United States of America*.
- Poon, Michael M. et al. 2006. "Identification of Process-Localized MRNAs from Cultured Rodent Hippocampal Neurons." *Journal of Neuroscience*.
- Pospisilik, J. Andrew et al. 2007. "Targeted Deletion of AIF Decreases Mitochondrial Oxidative Phosphorylation and Protects from Obesity and Diabetes." *Cell*.
- Powers, R. Wilson et al. 2006. "Extension of Chronological Life Span in Yeast by Decreased TOR Pathway Signaling." *Genes and Development*.
- Raška, Ivan, Peter J. Shaw, and Dušan Cmarko. 2006. "New Insights into Nucleolar Architecture and Activity." *International Review of Cytology*.
- Reimer, Georg, Ivan Raška, Ulrich Scheer, and Eng M. Tan. 1988. "Immunolocalization of 7-2-Ribonucleoprotein in the Granular Component of the Nucleolus." *Experimental Cell Research*.
- Reis-Rodrigues, Pedro et al. 2012. "Proteomic Analysis of Age-Dependent Changes in Protein Solubility Identifies Genes That Modulate Lifespan." *Aging Cell*.
- Ritchie, Matthew E. et al. 2015. "Limma Powers Differential Expression Analyses for RNA-Sequencing and Microarray Studies." *Nucleic Acids Research*.
- Robida-Stubbs, Stacey et al. 2012. "TOR Signaling and Rapamycin Influence Longevity by Regulating SKN-1/Nrf and DAF-16/FoxO."
- Rooyackers, Olav E., Deborah B. Adey, Philip A. Ades, and K. Sreekumaran Nair. 1996. "Effect of Age on in Vivo Rates of Mitochondrial Protein Synthesis in Human Skeletal Muscle." *Proceedings of the National Academy of Sciences of the United States of America*.
- Rual, Jaen François et al. 2004. "Toward Improving *Caenorhabditis Elegans* Phenome Mapping with an ORFeome-Based RNAi Library." *Genome Research*.

- Rubbi, Carlos P., and Jo Milner. 2003. "Disruption of the Nucleolus Mediates Stabilization of P53 in Response to DNA Damage and Other Stresses." *EMBO Journal*.
- Ryoo, Hyung Don, and Deepika Vasudevan. 2017. "Two Distinct Nodes of Translational Inhibition in the Integrated Stress Response." *BMB Reports*.
- Saez, Isabel, and David Vilchez. 2014. "The Mechanistic Links Between Proteasome Activity, Aging and Age-related Diseases." *Current Genomics*.
- Saijou, Eiko et al. 2004. "RBD-1, a Nucleolar RNA-Binding Protein, Is Essential for Caenorhabditis Elegans Early Development through 18S Ribosomal RNA Processing." *Nucleic acids research* 32(3): 1028–36.
<http://www.ncbi.nlm.nih.gov/pubmed/14872060> (April 2, 2020).
- Saikia, Mridusmita, and Maria Hatzoglou. 2015. "The Many Virtues of tRNA-Derived Stress-Induced RNAs (tIRNAs): Discovering Novel Mechanisms of Stress Response and Effect on Human Health." *Journal of Biological Chemistry*.
- Saito, Yuichiro et al. 2014. "RNase MRP Cleaves Pre-tRNA^{Ser}-Met in the tRNA Maturation Pathway" ed. Thomas Preiss. *PLoS ONE* 9(11): e112488.
<http://dx.plos.org/10.1371/journal.pone.0112488> (April 3, 2020).
- Santra, Mantu, Ken A. Dill, and Adam M.R. De Graff. 2019. "Proteostasis Collapse Is a Driver of Cell Aging and Death." *Proceedings of the National Academy of Sciences of the United States of America*.
- Sardiello, Marco et al. 2008. "Genomic Analysis of the TRIM Family Reveals Two Groups of Genes with Distinct Evolutionary Properties." *BMC Evolutionary Biology*.
- . 2009. "A Gene Network Regulating Lysosomal Biogenesis and Function." *Science* 325(5939): 473–77.
- Sasaki, Takeshi, Akio Toh-e, and Yoshiko Kikuchi. 2000. "Yeast Krr1p Physically and Functionally Interacts with a Novel Essential Kri1p, and Both Proteins Are Required for 40S Ribosome Biogenesis in the Nucleolus." *Molecular and Cellular Biology*.
- Schwamborn, Jens C., Eugene Berezikov, and Juergen A. Knoblich. 2009. "The TRIM-NHL Protein TRIM32 Activates MicroRNAs and Prevents Self-Renewal in Mouse Neural Progenitors." *Cell*.
- Segref, Alexandra, Serena Torres, and Thorsten Hoppe. 2011. "A Screenable in Vivo Assay to Study Proteostasis Networks in Caenorhabditis Elegans." *Genetics*.
- Selman, Colin et al. 2009. "Ribosomal Protein S6 Kinase 1 Signaling Regulates Mammalian Life Span." *Science*.
- Settembre, Carmine et al. 2011. "TFEB Links Autophagy to Lysosomal Biogenesis Europe PMC Funders Group." *Science* 332(6036): 1429–33.
- Settembre, Carmine, Alessandro Fraldi, Diego L. Medina, and Andrea Ballabio. 2013. "Signals from the Lysosome: A Control Centre for Cellular Clearance and Energy Metabolism." *Nature Reviews Molecular Cell Biology*.
- Shalgi, Reut et al. 2013. "Widespread Regulation of Translation by Elongation Pausing in Heat Shock." *Molecular Cell*.
- Shaw, P J, and E G Jordan. 1995. 11 *Annual Rev. Cell Dev. Biol* *THE NUCLEOLUS*.
www.annualreviews.org (April 6, 2020).
- Sheaffer, Karyn L., Dustin L. Updike, and Susan E. Mango. 2008. "The Target of Rapamycin Pathway Antagonizes Pha-4/FoxA to Control Development and Aging." *Current Biology* 18(18): 1355–64.
- Shen, Yijing et al. 2018. "Transfer RNA-Derived Fragments and tRNA Halves:

- Biogenesis, Biological Functions and Their Roles in Diseases.” *Journal of Molecular Medicine*.
- Shetty, Mihir et al. 2020. “Maf1-Dependent Transcriptional Regulation of TRNAs Prevents Genomic Instability and Is Associated with Extended Lifespan.” *Aging Cell*.
- Showkat, Mehvish, Mushtaq A. Beigh, and Khurshid I. Andrabi. 2014. “mTOR Signaling in Protein Translation Regulation: Implications in Cancer Genesis and Therapeutic Interventions.” *Molecular Biology International*.
- Simonis, Nicolas et al. 2009. “Empirically Controlled Mapping of the *Caenorhabditis Elegans* Protein-Protein Interactome Network.” *Nature Methods*.
- Sinclair, David A., Kevin Mills, and Leonard Guarente. 1997. “Accelerated Aging and Nucleolar Fragmentation in Yeast SGS1 Mutants.” *Science*.
- Singh, Rajat et al. 2009. “Autophagy Regulates Lipid Metabolism.” *Nature*.
- Slack, Frank J., and Gary Ruvkun. 1998. “A Novel Repeat Domain That Is Often Associated with RING Finger and B-Box Motifs.” *Trends in Biochemical Sciences* 23(12): 474–75.
- Small Nucleoli and Reduced Ribosomal Biogenesis Are Hallmarks of Longevity*. 2016.
- Sonoda, Junichiro, and Robin P Wharton. 2001. “Drosophila Brain Tumor Is a Translational Repressor.” www.genesdev.org/cgi/doi/10.1101/ (October 8, 2019).
- Soti, Csaba, and Péter Csermely. 2003. “Aging and Molecular Chaperones.” *Experimental Gerontology*.
- Stanfel, Monique N., Lara S. Shamieh, Matt Kaerberlein, and Brian K. Kennedy. 2009. “The TOR Pathway Comes of Age.” *Biochimica et Biophysica Acta - General Subjects*.
- Stefanovsky, Victor Y. et al. 2001. “An Immediate Response of Ribosomal Transcription to Growth Factor Stimulation in Mammals Is Mediated by ERK Phosphorylation of UBF.” *Molecular Cell*.
- Steffen, Kristan K. et al. 2008a. “Yeast Life Span Extension by Depletion of 60S Ribosomal Subunits Is Mediated by Gcn4.” *Cell* 133(2): 292–302. <https://linkinghub.elsevier.com/retrieve/pii/S0092867408002882> (February 7, 2020).
- — —. 2008b. “Yeast Life Span Extension by Depletion of 60S Ribosomal Subunits Is Mediated by Gcn4.” *Cell*.
- Steinbaugh, Michael J. et al. 2015. “Lipid-Mediated Regulation of SKN-1/Nrf in Response to Germ Cell Absence.” *eLife* 4(JULY2015).
- Steinkraus, Katherine A. et al. 2008. “Dietary Restriction Suppresses Proteotoxicity and Enhances Longevity by an Hsf-1-Dependent Mechanism in *Caenorhabditis Elegans*.” *Aging Cell*.
- Stoykova, A. S., K. P. Dudov, M. D. Dabeva, and A. A. Hadjiolov. 1983. “Different Rates of Synthesis and Turnover of Ribosomal RNA in Rat Brain and Liver.” *Journal of Neurochemistry* 41(4): 942–49. <https://pubmed.ncbi.nlm.nih.gov/6555219/> (July 5, 2020).
- Sudmant, Peter H. et al. 2018. “Widespread Accumulation of Ribosome-Associated Isolated 3’ UTRs in Neuronal Cell Populations of the Aging Brain.” *Cell Reports*.
- Suh, Yousin et al. 2008. “Functionally Significant Insulin-like Growth Factor I Receptor Mutations in Centenarians.” *Proceedings of the National Academy of Sciences of the United States of America*.
- Sulston, J. E., and H. R. Horvitz. 1977. “Post-Embryonic Cell Lineages of the

- Nematode, *Caenorhabditis Elegans*.” *Developmental Biology*.
- Sulston, J. E., E. Schierenberg, J. G. White, and J. N. Thomson. 1983. “The Embryonic Cell Lineage of the Nematode *Caenorhabditis Elegans*.” *Developmental Biology*.
- Syntichaki, Popi, Kostoula Troulinaki, and Nektarios Tavernarakis. 2007. “EIF4E Function in Somatic Cells Modulates Ageing in *Caenorhabditis Elegans*.” *Nature* 445(7130): 922–26.
- Tang, Junhui et al. 2020. “Sam50–Mic19–Mic60 Axis Determines Mitochondrial Cristae Architecture by Mediating Mitochondrial Outer and Inner Membrane Contact.” *Cell Death and Differentiation*.
- Tekippe, Michael, and Alejandro Aballay. 2010. “*C. Elegans* Germline-Deficient Mutants Respond to Pathogen Infection Using Shared and Distinct Mechanisms.” *PLoS ONE*.
- Tepper, Ronald G. et al. 2013. “PQM-1 Complements DAF-16 as a Key Transcriptional Regulator of DAF-2-Mediated Development and Longevity.” *Cell*.
- Thompson, Debrah M., and Roy Parker. 2009. “Stressing Out over TRNA Cleavage.” *Cell*.
- Tiku, Varnesh et al. 2017. “Small Nucleoli Are a Cellular Hallmark of Longevity.” *Nature Communications* 8(1): 16083.
<http://www.nature.com/articles/ncomms16083> (June 27, 2019).
- — —. 2018. “Nucleolar Fibrillarin Is an Evolutionarily Conserved Regulator of Bacterial Pathogen Resistance.” *Nature Communications* 9(1): 3607.
<http://www.ncbi.nlm.nih.gov/pubmed/30190478> (April 8, 2020).
- Tiku, Varnesh, and Adam Antebi. 2018. “Nucleolar Function in Lifespan Regulation.” *Trends in cell biology* 28(8): 662–72.
<http://www.ncbi.nlm.nih.gov/pubmed/29779866> (June 27, 2019).
- Tohyama, Daisuke, Atsushi Yamaguchi, and Toshihide Yamashita. 2008. “Inhibition of a Eukaryotic Initiation Factor (EIF2Bδ ,/F11A3.2) during Adulthood Extends Lifespan in *Caenorhabditis Elegans* .” *The FASEB Journal*.
- Topper, James N., Jeffrey L. Bennett, and David A. Clayton. 1992. “A Role for RNase MRP in Mitochondrial RNA Processing.” *Cell*.
- Torrent, Marc et al. 2018. “Cells Alter Their TRNA Abundance to Selectively Regulate Protein Synthesis during Stress Conditions.” *Science signaling* 11(546).
<http://www.ncbi.nlm.nih.gov/pubmed/30181241> (March 12, 2020).
- Trapnell, Cole et al. 2012. “Differential Gene and Transcript Expression Analysis of RNA-Seq Experiments with TopHat and Cufflinks.” *Nature Protocols*.
- Tsai, Robert Y.L., and Ronald D.G. McKay. 2002. “A Nucleolar Mechanism Controlling Cell Proliferation in Stem Cells and Cancer Cells.” *Genes and Development*.
- Tsang, Chi Kwan, Hui Liu, and X. F. Steven Zheng. 2010. “MTOR Binds to the Promoters of RNA Polymerase I- And III-Transcribed Genes.” *Cell Cycle*.
- Tsukada, Miki, and Yoshinori Ohsumi. 1993. “Isolation and Characterization of Autophagy-Defective Mutants of *Saccharomyces Cerevisiae*.” *FEBS Letters*.
- Tu, Xiao et al. 2002. “Nuclear Translocation of Insulin Receptor Substrate-1 by Oncogenes and Igf-I: Effect on Ribosomal RNA Synthesis.” *Journal of Biological Chemistry*.
- Tuan, JoAnn C., Weiguo Zhai, and Lucio Comai. 1999. “Recruitment of TATA-Binding Protein–TAFI Complex SL1 to the Human Ribosomal DNA Promoter Is Mediated by the Carboxy-Terminal Activation Domain of Upstream Binding

- Factor (UBF) and Is Regulated by UBF Phosphorylation.” *Molecular and Cellular Biology*.
- Tullet, Jennifer M.A. et al. 2008. “Direct Inhibition of the Longevity-Promoting Factor SKN-1 by Insulin-like Signaling in *C. Elegans*.” *Cell* 132(6): 1025–38.
- Tye, Blake W et al. 2019. “Proteotoxicity from Aberrant Ribosome Biogenesis Compromises Cell Fitness.” *eLife* 8. <https://elifesciences.org/articles/43002>.
- Udem, S A, and J R Warner. 1973. “The Cytoplasmic Maturation of a Ribosomal Precursor Ribonucleic Acid in Yeast.” *The Journal of biological chemistry* 248(4): 1412–16. <http://www.ncbi.nlm.nih.gov/pubmed/4568815> (April 2, 2020).
- Unbehaun, Anett, Sergei I. Borukhov, Christopher U.T. Hellen, and Tatyana V. Pestova. 2004. “Release of Initiation Factors from 48S Complexes during Ribosomal Subunit Joining and the Link between Establishment of Codon-Anticodon Base-Pairing and Hydrolysis of EIF2-Bound GTP.” *Genes and Development*.
- United Nations Department of Economic and Social Affairs Population Division. 2017. “World Population Prospects The 2017 Revision.” *World Population Prospects The 2017*.
- Vattem, Krishna M., and Ronald C. Wek. 2004. “Reinitiation Involving Upstream ORFs Regulates ATF4 mRNA Translation in Mammalian Cells.” *Proceedings of the National Academy of Sciences of the United States of America*.
- Vellai, Tibor et al. 2003. “Influence of TOR Kinase on Lifespan in *C. Elegans*.” *Nature*.
- Vilchez, David et al. 2012. “RPN-6 Determines *C. Elegans* Longevity under Proteotoxic Stress Conditions.” *Nature*.
- Vilchez, David, Isabel Saez, and Andrew Dillin. 2014. “The Role of Protein Clearance Mechanisms in Organismal Ageing and Age-Related Diseases.” *Nature Communications*.
- Vlahakis, Ariadne, Nerea Lopez Muniozgueren, and Ted Powers. 2017. “Mitochondrial Respiration Links TOR Complex 2 Signaling to Calcium Regulation and Autophagy.” *Autophagy*.
- Volovik, Yuli et al. 2014. “Differential Regulation of the Heat Shock Factor 1 and DAF-16 by Neuronal Nhl-1 in the Nematode *C. Elegans*.” *Cell Reports*.
- Walther, Dirk M. et al. 2015. “Widespread Proteome Remodeling and Aggregation in Aging *C. Elegans*.” *Cell*.
- Wang, Meng C., Eyleen J. O’Rourke, and Gary Ruvkun. 2008. “Fat Metabolism Links Germline Stem Cells and Longevity in *C. Elegans*.” *Science* 322(5903): 957–60. <http://www.ncbi.nlm.nih.gov/pubmed/18988854> (March 30, 2020).
- Wang, Xuemin et al. 2001. “Regulation of Elongation Factor 2 Kinase by P90RSK1 and P70 S6 Kinase.” *EMBO Journal*.
- Warner, Jonathan R. 1999. “The Economics of Ribosome Biosynthesis in Yeast.” *Trends in Biochemical Sciences* 24(11): 437–40. <https://linkinghub.elsevier.com/retrieve/pii/S0968000499014607> (February 19, 2020).
- Wei, Yuehua, and Cynthia Kenyon. 2016. “Roles for ROS and Hydrogen Sulfide in the Longevity Response to Germline Loss in *Caenorhabditis Elegans*.” *Proceedings of the National Academy of Sciences of the United States of America* 113(20): E2832–41. <http://www.ncbi.nlm.nih.gov/pubmed/27140632> (March 31, 2020).
- Weichhart, Thomas et al. 2008. “The TSC-MTOR Signaling Pathway Regulates the

- Innate Inflammatory Response.” *Immunity*.
- Welting, Tim J.M., Bastiaan J. Kikkert, Walther J. Van Venrooij, and Ger J.M. Pruijn. 2006. “Differential Association of Protein Subunits with the Human RNase MRP and RNase P Complexes.” *RNA*.
- West, Sean M et al. 2018. “Developmental Dynamics of Gene Expression and Alternative Polyadenylation in the *Caenorhabditis Elegans* Germline.” *Genome biology* 19(1): 8. <http://www.ncbi.nlm.nih.gov/pubmed/29368663> (June 12, 2019).
- Williams, Christopher C., Calvin H. Jan, and Jonathan S. Weissman. 2014. “Targeting and Plasticity of Mitochondrial Proteins Revealed by Proximity-Specific Ribosome Profiling.” *Science*.
- Yamawaki, Tracy M. et al. 2010. “The Somatic Reproductive Tissues of *C. Elegans* Promote Longevity through Steroid Hormone Signaling” ed. Marc Tatar. *PLoS Biology* 8(8): e1000468. <https://dx.plos.org/10.1371/journal.pbio.1000468> (March 30, 2020).
- Yang, Kai, Jie Yang, and Jing Yi. 2018. “Nucleolar Stress: Hallmarks, Sensing Mechanism and Diseases.” *Cell Stress*.
- Yang, Wen, and Siegfried Hekimi. 2010. “Two Modes of Mitochondrial Dysfunction Lead Independently to Lifespan Extension in *Caenorhabditis Elegans*.” *Aging Cell*.
- Yi, Yung Hsiang et al. 2015. “A Genetic Cascade of Let-7-Ncl-1-Fib-1 Modulates Nucleolar Size and RRNA Pool in *Caenorhabditis Elegans*.” *PLoS Genetics* 11(10).
- Yunger, Elad et al. 2017. “Innate Immunity Mediated Longevity and Longevity Induced by Germ Cell Removal Converge on the C-Type Lectin Domain Protein IRG-7.” *PLoS Genetics* 13(2): e1006577. <http://www.ncbi.nlm.nih.gov/pubmed/28196094> (March 31, 2020).
- Zevian, Shannin C., and Judith L. Yanowitz. 2014. “Methodological Considerations for Heat Shock of the Nematode *Caenorhabditis Elegans*.” *Methods*.
- Zhang, Guo et al. 2013. “Hypothalamic Programming of Systemic Ageing Involving IKK- β , NF-KB and GnRH.” *Nature* 497(7448): 211–16. <http://www.ncbi.nlm.nih.gov/pubmed/23636330> (April 1, 2020).
- Zhang, Yue et al. 2019. “Neuronal TORC1 Modulates Longevity via Ampk and Cell Nonautonomous Regulation of Mitochondrial Dynamics in *C. Elegans*.” *eLife*.
- Zhang, Zhao et al. 2018. “Global Analysis of tRNA and Translation Factor Expression Reveals a Dynamic Landscape of Translational Regulation in Human Cancers.” *Communications Biology* 1(1): 234. <http://www.nature.com/articles/s42003-018-0239-8> (August 21, 2019).
- Zhao, Shuyi et al. 2019. “Sas10 Controls Ribosome Biogenesis by Stabilizing Mpp10 and Delivering the Mpp10–Imp3–Imp4 Complex to Nucleolus.” *Nucleic Acids Research*.
- Zhou, Katherine I., Zachary Pincus, and Frank J. Slack. 2011. “Longevity and Stress in *Caenorhabditis Elegans*.” *Aging*.
- Zhou, Xufei et al. 2017. “RdRP-Synthesized Antisense Ribosomal siRNAs Silence Pre-RRNA via the Nuclear RNAi Pathway.” *Nature Structural and Molecular Biology*.
- Zid, Brian M. et al. 2009. “4E-BP Extends Lifespan upon Dietary Restriction by Enhancing Mitochondrial Activity in *Drosophila*.” *Cell*.

Appendix

Table 5. Lifespan analyses of RNAi rescue screen. p-values for statistical analyses were calculated using Mantel-Cox Log Rank test. Worms that escaped the dishes, had internal hatching or had bursting of vulva were censored from the experiments.

RNAi treatment	Sequence	Median survival (days)	Censored	Deaths	p-value	Ref. Control
RNAi lifespan rescue screen						
<i>luci</i>	<i>glp-1(e2141)</i>	29	16	64		
<i>luci</i>	<i>glp-1;ncl-1</i>	23	27	93	<0.0001	<i>glp-1(e2141)</i>
<i>toe-1i</i>	ZK430.1	18	22	78	0.0108	<i>glp-1;ncl-1</i>
<i>nst-1i</i>	K01C8.9	23	20	100	0.0381	<i>glp-1;ncl-1</i>
<i>puf-12i</i>	ZK945.3	19	13	47	0.0278	<i>glp-1;ncl-1</i>
<i>eif-3.Gi</i>	F22B5.2	19	13	87	0.0001	<i>glp-1;ncl-1</i>
<i>Y75B8A.7i</i>	Y75B8A.7	23	10	90	0.0184	<i>glp-1;ncl-1</i>
<i>eef-1B.2i</i>	Y41E3.10	27	8	104	0.0033	<i>glp-1;ncl-1</i>
<i>lpd-7i</i>	R13A5.12	19	30	90	<0.0001	<i>glp-1;ncl-1</i>
<i>C04H5.1i</i>	C04H5.1	19	43	77	0.0183	<i>glp-1;ncl-1</i>
<i>F58B3.4i</i>	F58B3.4	29	36	84	<0.0001	<i>glp-1;ncl-1</i>
<i>wdr-46i</i>	F28D1.1	23	14	44	0.2694	<i>glp-1;ncl-1</i>
<i>rbd-1i</i>	T23F6.4	23	11	89	0.0201	<i>glp-1;ncl-1</i>
<i>drr-2i</i>	T12D8.2	23	28	92	0.1262	<i>glp-1;ncl-1</i>
<i>abce-1i</i>	Y39E4B.1	23	15	105	0.0604	<i>glp-1;ncl-1</i>
<i>popl-1i</i>	C05D11.9	29	38	82	<0.0001	<i>glp-1;ncl-1</i>
<i>T06E6.1i</i>	T06E6.1	23	11	69	0.3425	<i>glp-1;ncl-1</i>
<i>pus-1i</i>	W06H3.2	27	15	52	0.3141	<i>glp-1;ncl-1</i>
<i>cpr-1i</i>	C52E4.1	27	21	99	0.0104	<i>glp-1;ncl-1</i>
<i>ngp-1i</i>	T19A6.2	18	9	82	<0.0001	<i>glp-1;ncl-1</i>
<i>dao-5i</i>	C25A1.10	23	19	61	0.0972	<i>glp-1;ncl-1</i>
<i>nol-58i</i>	W01B11.3	19	53	67	<0.0001	<i>glp-1;ncl-1</i>
<i>rpl-24.2i</i>	C03D6.8	27	32	8	0.0624	<i>glp-1;ncl-1</i>

<i>F54C9.9i</i>	F54C9.9	33	50	70	<0.0001	<i>glp-1;ncl-1</i>
<i>F07E5.5i</i>	F07E5.5	27	37	23	0.0001	<i>glp-1;ncl-1</i>
<i>pro-1i</i>	R166.4	19	15	105	0.0003	<i>glp-1;ncl-1</i>
<i>T23G7.3i</i>	T23G7.3	19	35	45	0.2398	<i>glp-1;ncl-1</i>
<i>mrps-16i</i>	F56D1.3	27	37	23	<0.0001	<i>glp-1;ncl-1</i>
<i>gfm-1i</i>	F29C12.4	27	4	34	0.0002	<i>glp-1;ncl-1</i>
<i>W07E6.2i</i>	W07E6.2	23	108	12	0.0499	<i>glp-1;ncl-1</i>
<i>nars-1i</i>	F22D6.3	13	39	81	<0.0001	<i>glp-1;ncl-1</i>
<i>EIF-6i</i>	C47B2.5	23	20	100	0.0957	<i>glp-1;ncl-1</i>
<i>C43E11.4i</i>	C43E11.4	29	58	62	<0.0001	<i>glp-1;ncl-1</i>
<i>pfd-3i</i>	T06G6.9	19	28	92	<0.0001	<i>glp-1;ncl-1</i>
<i>B0511.6i</i>	B0511.6	19	45	75	<0.0001	<i>glp-1;ncl-1</i>
<i>fkf-5i</i>	C50F2.6	18	25	95	<0.0001	<i>glp-1;ncl-1</i>
<i>nath-10i</i>	F55A12.8	19	29	91	<0.0001	<i>glp-1;ncl-1</i>
<i>F27C1.6i</i>	F27C1.6	19	17	63		<i>glp-1;ncl-1</i>
<i>nol-6i</i>	Y51H7C.11	23	30	90	0.0070	<i>glp-1;ncl-1</i>

Table 6. Lifespan analyses upon knockdown of RNase P/MRP complex components. p-values for statistical analyses were calculated using Mantel-Cox Log Rank test. Worms that escaped the dishes, had internal hatching or had bursting of vulva were censored from the experiments.

RNAi treatment	Sequence	Median survival (days)	Censored	Deaths	p-value	Ref. Control
<i>luci</i>	<i>glp-1;ncl-1</i>	20	32	88		
<i>rpp-30i</i>	H35B03.2	30	49	101	<0.0001	<i>glp-1;ncl-1</i>
<i>pop-4i</i>	C15C6.4	25	50	100	<0.0001	<i>glp-1;ncl-1</i>
<i>pop-5i</i>	Y66A7A.2	20	82	38	0.8543	<i>glp-1;ncl-1</i>
<i>luci</i>	<i>glp-1;ncl-1</i>	19	26	94		
<i>rpp25i</i>	ZK632.14	23	45	75	<0.0001	<i>glp-1;ncl-1</i>

Table 7. Lifespan analyses. p-values for statistical analyses were calculated using Mantel-Cox Log Rank test. Worms that escaped the dishes, had internal hatching or had bursting of vulva were censored from the experiments.

Strain	Median survival (days)	Censored	Deaths	p-value	Ref. Control
<i>glp-1; luci</i>	28	55	70	0.0002	<i>glp-1;ncl-1;luci</i>
<i>glp-1;ncl-1; luci</i>	25	40	60		
<i>glp-1;ncl-1; popl-1i</i>	30	41	84	<0.0001	<i>glp-1;ncl-1;luci</i>
<i>glp-1;ncl-1; mrps-16i</i>	25	37	88	0.0271	<i>glp-1;ncl-1;luci</i>
<i>glp-1; luci</i>	26	20	130	<0.0001	<i>glp-1;ncl-1;luci</i>
<i>glp-1;ncl-1; luci</i>	23	41	109		
<i>glp-1;ncl-1; popl-1i</i>	26	56	94	0.0046	<i>glp-1;ncl-1;luci</i>
<i>glp-1;ncl-1; mrps-16i</i>	30	60	90	<0.0001	<i>glp-1;ncl-1;luci</i>
N2 (25°C)	12	41	79		
<i>ncl-1(e1942)</i> (25°C)	12	69	51	0.1090	N2
<i>ncl-1(e1865)</i> (25°C)	12	21	99	0.0003	N2
N2 (25°C)	11	38	87		
<i>ncl-1(e1942)</i> (25°C)	8	28	97	<0.0001	N2
<i>ncl-1(e1865)</i> (25°C)	8	16	109	<0.0001	N2
N2 (25°C)	15	33	92		
<i>ncl-1(e1942)</i> (25°C)	9	43	82	<0.0001	N2
<i>ncl-1(e1865)</i> (25°C)	7	16	109	<0.0001	N2
N2	22	77	43		
<i>glp-1(2141)</i>	43	36	84	<0.0001	N2
<i>glp-1;nrde-3</i>	11	5	115	<0.0001	<i>glp-1</i>
N2	22	70	50		
<i>nrde-3(gg66)</i>	22	84	35	0.4300	N2
<i>glp-1(2141)</i>	45	42	78	<0.0001	N2
<i>glp-1;nrde-3</i>	11	20	100	<0.0001	<i>glp-1</i>
N2	18	49	51		
<i>nrde-3(gg66)</i>	15	50	50	0.0019	N2
<i>glp-1(e2141)</i>	32	21	79	<0.0001	N2

<i>glp-1;nrde-3</i>	11	7	93	<0.0001	<i>glp-1</i>
N2	21	55	70		
<i>nrde-3(gg66)</i>	18	40	85	0.1444	N2
<i>daf-2(1370)</i>	36	48	77	<0.0001	N2
<i>daf-2;nrde-3</i>	42	47	78	0.0003	<i>daf-2</i>

Table 8. Hypodermal nucleolar size measurements.

Strain/Condition	Average nucleolar area (μm^2)	Standart deviation	% change relative to control	Relative control
N2	2.61	1.81		
<i>nrde-3(gg66)</i>	3.34	2.46	27.58	N2
<i>ncl-1(e1982)</i>	5.86	3.40	123.97	N2
N2	2.83	1.98		
<i>nrde-3(gg66)</i>	4.43	2.31	56.60	N2
<i>ncl-1(e1982)</i>	8.64	3.83	205.26	N2
N2	1.23	0.64		
<i>nrde-3(gg66)</i>	2.37	1.80	92.86	N2
<i>ncl-1(e1982)</i>	6.42	3.78	421.67	N2
<i>glp-1(e2141)</i>	3.63	2.28		
<i>glp-1;nrde-3</i>	5.42	3.05	49.25	<i>glp-1</i>
<i>glp-1;ncl-1</i>	9.60	5.41	164.38	<i>glp-1</i>
N2	7.57	3.41		
<i>ncl-1::neongreen</i>	9.29	4.79	22.72	N2
<i>ncl-1::flag</i>	6.69	3.42	-11.63	N2
N2	5.91	2.06		
<i>ncl-1::neongreen</i>	8.94	3.94	51.24	N2
<i>ncl-1::flag</i>	6.59	3.52	11.44	N2

<i>ncl-1::flag</i>	5.84	2.84		
AL42	4.59	2.31	-21.36	<i>ncl-1::flag</i>
AL43	5.50	3.47	-5.76	<i>ncl-1::flag</i>
AL44	7.95	4.33	36.28	<i>ncl-1::flag</i>
AL45	4.21	2.19	-27.88	<i>ncl-1::flag</i>
AL52	5.80	2.94	-0.57	<i>ncl-1::flag</i>
AL53	13.16	4.95	125.51	<i>ncl-1::flag</i>
<i>sid-1/luci</i>	1.68	1.08		
<i>sid-1/ncl-1i</i>	2.06	1.26	22.46	<i>sid-1/luci</i>
N2/ <i>luci</i>	1.37	0.70		
N2/ <i>ncl-1i</i>	3.22	2.40	135.24	N2/ <i>luci</i>
<i>sid-1; myo-3p::sid-1::unc-54-3'UTR/luci</i>	1.70	1.21		
<i>sid-1; myo-3p::sid-1::unc-54-3'UTR/ncl-1i</i>	2.22	1.24	30.97	<i>sid-1; myo-3p::sid-1::unc-54-3'UTR/luci</i>
<i>sid-1; rab-3p::sid-1::unc-54-3'UTR/luci</i>	0.89	0.49		
<i>sid-1; rab-3p::sid-1::unc-54-3'UTR/ncl-1i</i>	1.93	1.39	118.06	<i>sid-1; rab-3p::sid-1::unc-54-3'UTR/luci</i>
<i>sid-1; gly-19p::tdtomato + gly-19p::sid-1/luci</i>	1.26	0.75		
<i>sid-1; gly-19p::tdtomato + gly-19p::sid-1/ncl-1i</i>	2.92	2.70	131.44	<i>sid-1; gly-19p::tdtomato + gly-19p::sid-1/luci</i>
<i>glp-1;ncl-1/luci</i>	14.67	5.07		
<i>glp-1;ncl-1/pop1-1i</i>	13.75	5.14	-6.26	<i>glp-1;ncl-1/luci</i>
<i>glp-1;nc-11/mrps16i</i>	13.17	4.67	-10.23	<i>glp-1;ncl-1/luci</i>
<i>glp-1;ncl-1/luci</i>	23.90	10.74		
<i>glp-1;ncl-1/pop1-1i</i>	25.71	10.75	7.57	<i>glp-1;ncl-1/luci</i>
<i>glp-1;nc-11/mrps16i</i>	29.25	11.26	22.39	<i>glp-1;ncl-1/luci</i>
<i>glp-1;ncl-1/luci</i>	13.86	5.17		
<i>glp-1;ncl-1/pop1-1i</i>	12.46	5.04	-10.08	<i>glp-1;ncl-1/luci</i>
<i>glp-1;nc-11/mrps16i</i>	10.63	4.46	-23.32	<i>glp-1;ncl-1/luci</i>

<i>glp-1;ncl-1/luci/day6</i>	16.65	7.22		
<i>glp-1;ncl-1/pop1-1i/day6</i>	15.98	7.16	-4.02	<i>glp-1;ncl-1/luci/day6</i>
<i>glp-1;nc-11/mrps16i/day6</i>	16.91	6.58	1.57	<i>glp-1;ncl-1/luci/day6</i>
<i>glp-1/luci/day1</i>	4.94	2.62		
<i>glp-1/luci/day6</i>	2.89	0.68	-41.53	<i>glp-1/luci/day1</i>
<i>glp-1;ncl-1/luci/day1</i>	14.67	5.07		
<i>glp-1;ncl-1/luci/day6</i>	16.65	7.22	13.49	<i>glp-1;ncl-1/luci/day1</i>
<i>glp-1/luci</i>	4.94	2.62		
<i>glp-1/rpn-11i</i>	6.46	2.81	30.75	<i>glp-1/luci</i>
<i>glp-1/snap-1i</i>	6.52	2.88	31.94	<i>glp-1/luci</i>
<i>glp-1/rege-1i</i>	5.49	2.45	11.18	<i>glp-1/luci</i>
<i>glp-1/eif-3.Bi</i>	6.26	2.74	26.60	<i>glp-1/luci</i>
<i>glp-1/par-5i</i>	6.22	3.10	25.83	<i>glp-1/luci</i>
<i>glp-1/dnc-6i</i>	5.79	2.43	17.24	<i>glp-1/luci</i>
<i>glp-1/spc-1i</i>	5.56	2.78	12.44	<i>glp-1/luci</i>
<i>glp-1/luci</i>	5.23	2.40		
<i>glp-1/rpn-11i</i>	7.83	3.41	49.63	<i>glp-1/luci</i>
<i>glp-1/snap-1i</i>	6.14	2.91	17.33	<i>glp-1/luci</i>
<i>glp-1/rege-1i</i>	4.52	2.11	-13.70	<i>glp-1/luci</i>
<i>glp-1/eif-3.Bi</i>	6.05	2.60	15.49	<i>glp-1/luci</i>
<i>glp-1/par-5i</i>	5.42	2.74	3.48	<i>glp-1/luci</i>
<i>glp-1/dnc-6i</i>	5.42	2.34	3.61	<i>glp-1/luci</i>
<i>glp-1/spc-1i</i>	5.80	3.13	10.74	<i>glp-1/luci</i>

Table 9. Positive Yeast-2-hybrid candidates.

Wormbase ID	Global PBS	Gene
WBGene00010935	A	<i>M163.1</i>
WBGene00003920	A	<i>par-5</i>

WBGene00016845	N/A	<i>C50F7.5</i>
WBGene00008505	N/A	<i>F01G4.6</i>
WBGene00016260	A	<i>rege-1</i>
WBGene00014233	B	<i>alpha-B-crystallin</i>
WBGene00001225	B	<i>eif-3.B</i>
WBGene00017016	B	<i>snap-1</i>
WBGene00004951	B	<i>spc-1</i>
WBGene00009008	C	<i>F21D5.3</i>
WBGene00021827	C	<i>dnc-6</i>
WBGene00019882	N/A	<i>R05D3.9</i>
WBGene00004467	C	<i>rpn-11</i>
WBGene00012117	N/A	<i>T28B11.1</i>
WBGene00015658	D	<i>C09G12.9</i>
WBGene00016353	D	<i>C33F10.4</i>
WBGene00021756	N/A	<i>Y50D7A.8</i>
WBGene00303021	D	<i>F02A9.10</i>
WBGene00008645	D	<i>F10C2.4</i>
WBGene00000123	N/A	<i>ama-1</i>
WBGene00000186	N/A	<i>ark-1</i>
WBGene00018164	D	<i>F38A5.7</i>
WBGene00000779	N/A	<i>cpn-3</i>
WBGene00000785	N/A	<i>cpr-5</i>
WBGene00019084	D	<i>F59A6.2</i>
WBGene00010681	D	<i>Protein MAK-1</i>
WBGene00020498	D	<i>T14B4.1</i>
WBGene00013677	D	<i>Y105E8A.19</i>
WBGene00021531	D	<i>Y42G9A.1</i>
WBGene00021831	D	<i>Y54E10A.11</i>
WBGene00000608	D	<i>col-19</i>
WBGene00007184	D	<i>ctr-9</i>
WBGene00001973	N/A	<i>hmg-3</i>
WBGene00001086	D	<i>dpy-27</i>
WBGene00001131	D	<i>dys-1</i>
WBGene00003497	N/A	<i>mup-4</i>
WBGene00006465	D	<i>fntb-1</i>
WBGene00020230	N/A	<i>nep-2</i>

WBGene00001502	D	<i>ftt-2</i>
WBGene00016405	D	<i>hecd-1</i>
WBGene00003183	D	<i>mei-1</i>
WBGene00003210	D	<i>mel-28</i>
WBGene00003559	D	<i>ncl-1</i>
WBGene00003637	D	<i>nhr-47</i>
WBGene00003639	D	<i>nhr-49</i>
WBGene00010627	D	<i>nol-56</i>
WBGene00003794	D	<i>npp-8</i>
WBGene00003980	D	<i>pes-7</i>
WBGene00006444	N/A	<i>shn-1</i>
WBGene00004106	D	<i>pqn-15</i>
WBGene00004367	D	<i>ric-8</i>
WBGene00004855	D	<i>sma-1</i>
WBGene00011312	N/A	<i>trcs-2</i>
WBGene00009337	D	<i>uig-1</i>
WBGene00006801	D	<i>unc-68</i>
WBGene00006876	D	<i>vab-10</i>
WBGene00006926	N/A	<i>vit-2</i>
WBGene00006947	N/A	<i>wrt-1</i>
WBGene00022127	N/A	<i>yop-1</i>

Table 10. Candidates assigned to different quadrants in comparative omics analysis. Only candidates with a significant fold change in transcriptomic and proteomic analysis ($p < 0.05$) are listed.

Gene name	log ₂ FC RNA	log ₂ FC protein	Wormbase gene ID
Q2 – <i>ncl-1</i> vs. N2			
<i>C45B2.2</i>	2.20532	0.928412393	WBGene00016659
<i>fkf-4</i>	1.91021	0.643038236	WBGene00001429
<i>ZK970.7</i>	1.84793	2.866911388	WBGene00014173
<i>sodh-1</i>	1.78824	1.501457156	WBGene00010790
<i>fkf-5</i>	1.71687	0.825256745	WBGene00001430

<i>tbb-6</i>	1.61511	1.957524984	WBGene00006539
<i>Y57A10A.23</i>	1.56623	0.643663605	WBGene00013263
<i>F57H12.6</i>	1.55151	0.627619076	WBGene00019021
<i>T09B4.8</i>	1.40767	0.664453802	WBGene00020382
<i>alh-5</i>	1.29298	1.483708193	WBGene00000111
<i>ttr-26</i>	1.19846	0.831312902	WBGene00013079
<i>hsp-16.1</i>	1.17405	1.273126234	WBGene00002015
<i>dct-18</i>	1.10779	0.365220423	WBGene00010266
<i>iff-2</i>	1.08385	0.330942502	WBGene00002065
<i>cpr-5</i>	0.980239	0.399632792	WBGene00000785
<i>M02H5.8</i>	0.977772	0.692035889	WBGene00019744
<i>dhp-2</i>	0.971009	0.626237846	WBGene00000964
<i>col-92</i>	0.916814	0.57003384	WBGene00000667
<i>aagr-4</i>	0.910647	0.374310014	WBGene00018682
<i>lea-1</i>	0.903777	0.535980641	WBGene00002263
<i>lbp-5</i>	0.866116	0.309542493	WBGene00002257
<i>lys-7</i>	0.859061	0.710045429	WBGene00003096
<i>rpl-24.2</i>	0.840957	0.567082713	WBGene00004437
<i>T03D8.6</i>	0.795886	0.503145034	WBGene00011393
<i>spp-2</i>	0.780769	0.776131554	WBGene00004987
<i>Y37A1B.5</i>	0.755981	0.398827181	WBGene00012538
<i>ngp-1</i>	0.721185	0.581258483	WBGene00003596
<i>skr-4</i>	0.71682	0.302381988	WBGene00004810
<i>lys-4</i>	0.702997	0.5662068	WBGene00003093
<i>set-27</i>	0.685772	0.40641421	WBGene00022173
<i>tag-10</i>	0.683907	0.452112024	WBGene00006404
<i>alp-1</i>	0.677473	0.226884087	WBGene00001132
<i>F26G1.5</i>	0.676342	1.199372411	WBGene00017841
<i>phy-2</i>	0.66741	0.442714816	WBGene00004025
<i>ZK1055.7</i>	0.652887	0.221283172	WBGene00022848
<i>epi-1</i>	0.652392	0.222419837	WBGene00001328
<i>lam-2</i>	0.645632	0.236082854	WBGene00016913
<i>nas-37</i>	0.637844	0.28997177	WBGene00003553
<i>F08B12.4</i>	0.588056	0.5246629	WBGene00008572
<i>W10C8.5</i>	0.568289	0.190723103	WBGene00021128
<i>T14D7.1</i>	0.565535	0.276802492	WBGene00011767

<i>nol-6</i>	0.561437	0.889251491	WBGene00021789
<i>pxn-1</i>	0.555561	0.406940753	WBGene00004256
<i>gfm-1</i>	0.534759	0.495870624	WBGene00009246
<i>cpn-4</i>	0.528725	0.291495262	WBGene00000780
<i>gst-39</i>	0.526111	0.646639634	WBGene00001787
<i>T06E6.1</i>	0.521986	0.862802088	WBGene00011538
<i>ifa-1</i>	0.515141	0.207416655	WBGene00002050
<i>C43E11.9</i>	0.510888	0.445913962	WBGene00016607
<i>T07A9.8,nog-1</i>	0.506575	0.338972732	WBGene00020297
<i>mrpl-41</i>	0.498217	0.277460371	WBGene00015185
<i>icl-1</i>	0.497032	0.276340772	WBGene00001564
<i>C45B2.1</i>	0.491925	0.364466523	WBGene00016658
<i>maph-1.1</i>	0.480174	0.197042571	WBGene00009306
<i>C47E12.7</i>	0.479481	0.877656372	WBGene00008151
<i>C16A3.6</i>	0.478868	1.499363678	WBGene00015811
<i>dhs-9</i>	0.478661	0.61239199	WBGene00000973
<i>gst-28</i>	0.476194	0.396302644	WBGene00001776
<i>F49E2.5</i>	0.461059	0.168458432	WBGene00009888
<i>nap-1</i>	0.450194	0.516216489	WBGene00017075
<i>K03E5.2</i>	0.447471	0.20476837	WBGene00019361
<i>lys-1</i>	0.443854	0.449743926	WBGene00003090
<i>W01F3.2</i>	0.4416	0.553124823	WBGene00012185
<i>pes-8</i>	0.439638	0.348587655	WBGene00003981
<i>nol-1</i>	0.438871	0.398077617	WBGene00021073
<i>F52C9.3</i>	0.429392	0.373435697	WBGene00018674
<i>ife-2</i>	0.428259	0.348347966	WBGene00002060
<i>F53F4.11</i>	0.42587	0.345173293	WBGene00009993
<i>fkf-3</i>	0.425103	0.320572103	WBGene00001428
<i>B0511.6,arch-1</i>	0.419489	0.626401	WBGene00015232
<i>cri-2</i>	0.414758	0.211787686	WBGene00019478
<i>ost-1</i>	0.41468	0.538557411	WBGene00003893
<i>tag-151</i>	0.414286	0.652946563	WBGene00006497
<i>inx-13</i>	0.409258	0.449124687	WBGene00002135
<i>cyn-1</i>	0.396094	0.445000938	WBGene00000877
<i>gly-8</i>	0.394562	0.294838252	WBGene00001633
<i>tyr-4</i>	0.392786	0.323206537	WBGene00016419

<i>gyg-1</i>	0.392487	0.288965183	WBGene00006863
<i>aagr-1</i>	0.389012	2.179560833	WBGene00017071
<i>lpd-7</i>	0.387551	0.425830698	WBGene00003063
<i>T19B10.2</i>	0.381016	0.321399427	WBGene00011831
<i>Y54E10BR.4</i>	0.375185	0.531257706	WBGene00021843
<i>lec-4</i>	0.359695	0.484906782	WBGene00002267
<i>inx-12</i>	0.358711	1.281202986	WBGene00002134
<i>nex-1</i>	0.357585	0.338704478	WBGene00003588
<i>gcst-1</i>	0.352632	0.211869295	WBGene00017765
<i>ZC247.1</i>	0.340688	0.295543005	WBGene00013859
<i>Y92H12BL.1</i>	0.338959	0.777361004	WBGene00022363
<i>mrpl-38</i>	0.338017	0.305999705	WBGene00021327
<i>Y48B6A.1</i>	0.333626	0.785254103	WBGene00012978
<i>kgb-1</i>	0.331958	0.339999902	WBGene00002187
<i>F55F8.3</i>	0.327226	0.832038725	WBGene00018891
<i>F55H12.4</i>	0.326088	0.333108761	WBGene00010135
<i>pcca-1</i>	0.325989	0.291590221	WBGene00017864
<i>gsnl-1</i>	0.325121	0.292444515	WBGene00010593
<i>C01B10.3</i>	0.324167	0.319725535	WBGene00015278
<i>nath-10</i>	0.323555	1.28073698	WBGene00018866
<i>Y61A9LA.10</i>	0.320988	0.781351288	WBGene00022021
<i>aldo-1</i>	0.320589	0.284048259	WBGene00011474
<i>cyn-6</i>	0.320126	0.541217541	WBGene00000882
<i>Y48G8AL.5</i>	0.313255	0.431041933	WBGene00021686
<i>pck-1</i>	0.300528	0.54599895	WBGene00021043
<i>Y54H5A.2</i>	0.298687	0.825753585	WBGene00021900
<i>fib-1</i>	0.29867	0.549368971	WBGene00001423
<i>C25A1.16,nola-3</i>	0.284073	0.442969383	WBGene00007708
<i>inx-16</i>	0.282115	1.227374966	WBGene00002138
<i>inx-16</i>	0.282115	1.227374966	WBGene00002138
<i>arrd-25</i>	0.279797	0.257704918	WBGene00007296
<i>C49G7.3</i>	0.268812	0.724879772	WBGene00016781
<i>C24H12.4</i>	0.264193	0.447183031	WBGene00016073
<i>F37C4.5</i>	0.264006	0.273605915	WBGene00018145
<i>mthf-1</i>	0.262179	0.288187175	WBGene00015512
<i>mrpl-37</i>	0.261554	0.32023588	WBGene00013004

<i>Y48A6B.3</i>	0.25588	0.550308877	WBGene00012964
<i>pyp-1</i>	0.250438	0.221781587	WBGene00008149
<i>gta-1</i>	0.243641	0.20565944	WBGene00001794
<i>K10C3.5</i>	0.242695	0.537177368	WBGene00010732
<i>hsp-60</i>	0.240563	0.278406676	WBGene00002025
<i>calu-1</i>	0.240279	0.291230039	WBGene00019760
<i>K05C4.5</i>	0.238856	0.754545136	WBGene00010582
<i>mua-6</i>	0.234132	0.18237459	WBGene00003485
<i>Y45F10D.7</i>	0.231815	1.044359054	WBGene00012887
<i>idh-1</i>	0.231565	0.220101499	WBGene00010317
Q3 – <i>ncl-1</i> vs. N2			
<i>asb-1</i>	-0.344639	-0.47003362	WBGene00000206
<i>bag-1</i>	-0.413723	-0.25487655	WBGene00000236
<i>bca-1</i>	-0.339016	-0.20572184	WBGene00000245
<i>clp-4</i>	-1.90372	-1.9334887	WBGene00000545
<i>col-8</i>	-0.520793	-0.38311307	WBGene00000597
<i>dnj-19</i>	-0.33351	-0.30758413	WBGene00001037
<i>dpy-30</i>	-0.376488	-0.34708724	WBGene00001088
<i>ech-6</i>	-0.264771	-0.29321192	WBGene00001155
<i>emr-1</i>	-0.460086	-0.41525787	WBGene00001309
<i>fkf-6</i>	-0.424289	-0.28134744	WBGene00001431
<i>gst-1</i>	-0.411153	-0.27942193	WBGene00001749
<i>his-40</i>	-1.32177	-0.68157796	WBGene00001914
<i>his-64</i>	-0.407079	-0.42569976	WBGene00001938
<i>hrp-2</i>	-0.314041	-0.29151108	WBGene00002000
<i>hsr-9</i>	-0.371516	-0.67529524	WBGene00002027
<i>let-418</i>	-0.384713	-0.37720503	WBGene00002637
<i>nmy-2</i>	-0.386906	-0.3762895	WBGene00003777
<i>npp-7</i>	-0.311794	-0.2891249	WBGene00003793
<i>npp-9</i>	-0.289634	-0.28123802	WBGene00003795
<i>nsf-1</i>	-0.273544	-0.2501723	WBGene00003818
<i>ntl-3</i>	-0.352463	-0.41820076	WBGene00003826
<i>pas-2</i>	-0.270106	-0.28950471	WBGene00003923
<i>pbs-5</i>	-0.319681	-0.33964649	WBGene00003951
<i>pcn-1</i>	-0.566096	-0.72855218	WBGene00003955
<i>ran-2</i>	-0.280717	-0.30731928	WBGene00004303

<i>ran-5</i>	-0.373086	-0.41529291	WBGene00004306
<i>rnp-3</i>	-0.398338	-0.33980934	WBGene00004386
<i>rpn-2</i>	-0.318975	-0.19010801	WBGene00004459
<i>rpn-6.1</i>	-0.331462	-0.26237986	WBGene00004462
<i>rpn-7</i>	-0.2357	-0.22508659	WBGene00004463
<i>rpn-9</i>	-0.412441	-0.28518756	WBGene00004465
<i>rpt-2</i>	-0.228639	-0.29892434	WBGene00004502
<i>rpt-3</i>	-0.362115	-0.26300943	WBGene00004503
<i>rpt-4</i>	-0.305886	-0.24188543	WBGene00004504
<i>rpt-5</i>	-0.2777	-0.21914618	WBGene00004505
<i>rsp-1</i>	-0.428844	-0.29735044	WBGene00004698
<i>rsp-3</i>	-0.41984	-0.2899632	WBGene00004700
<i>sur-5</i>	-0.258167	-0.27643488	WBGene00006351
<i>F29B9.5,ubc-9</i>	-0.46861	-0.50120804	WBGene00006706
<i>ubc-18</i>	-0.424269	-0.323391	WBGene00006713
<i>usp-14</i>	-0.376335	-0.25313139	WBGene00006856
<i>zyg-9</i>	-0.407254	-0.35099732	WBGene00006994
<i>plin-1</i>	-0.413715	-0.31239011	WBGene00007024
<i>pfd-4</i>	-0.312412	-0.27285944	WBGene00007107
<i>B0285.4</i>	-0.289715	-0.39000885	WBGene00007137
<i>acly-2</i>	-0.50624	-0.8093029	WBGene00007150
<i>C05C10.3</i>	-0.424652	-0.28819114	WBGene00007330
<i>rmd-2</i>	-0.314439	-0.21740332	WBGene00007786
<i>D1086.6</i>	-0.243138	-0.30259886	WBGene00008393
<i>F21D5.1</i>	-0.540407	-0.72522364	WBGene00009006
<i>pyk-1</i>	-0.252607	-0.28425044	WBGene00009126
<i>aca-2</i>	-0.322634	-0.18094937	WBGene00009952
<i>tbcb-1</i>	-0.410344	-0.30172047	WBGene00009987
<i>F54D5.12</i>	-0.63569	-0.26859234	WBGene00010055
<i>ensa-1</i>	-0.337517	-0.28077807	WBGene00010730
<i>R05H5.3</i>	-0.649237	-0.62369221	WBGene00011038
<i>R09B3.3</i>	-0.28613	-0.40665502	WBGene00011156
<i>T11G6.8</i>	-0.421762	-0.47622444	WBGene00011722
<i>T13F2.2</i>	-0.257464	-0.24965565	WBGene00011743
<i>T24B8.5</i>	-0.584202	-1.01191538	WBGene00011979
<i>ebp-2</i>	-0.264208	-0.37216408	WBGene00012156

<i>Y37D8A.2</i>	-0.552153	-0.3582572	WBGene00012544
<i>Y38F1A.6</i>	-0.363803	-0.29556422	WBGene00012608
<i>Y59A8B.10</i>	-0.330912	-0.32723858	WBGene00013347
<i>Y62H9A.4</i>	-0.48885	-0.45107009	WBGene00013392
<i>ZK1320.9</i>	-0.493961	-0.32033624	WBGene00014258
<i>tsg-101</i>	-0.305713	-0.2156579	WBGene00015658
<i>tiar-1</i>	-0.491569	-0.27667714	WBGene00015943
<i>rpb-2</i>	-0.338783	-0.45268749	WBGene00016140
<i>acd-1</i>	-0.456707	-0.51630196	WBGene00016943
<i>F09F7.4</i>	-0.588887	-0.34731995	WBGene00017301
<i>pud-2.1</i>	-1.43941	-0.64173768	WBGene00017490
<i>pud-4</i>	-2.24308	-1.23506988	WBGene00017498
<i>pud-3</i>	-2.3976	-1.20433611	WBGene00017501
<i>rpa-1</i>	-0.458845	-1.29055213	WBGene00017546
<i>clcc-1</i>	-0.362594	-1.53254084	WBGene00017772
<i>F26B1.2</i>	-0.445951	-0.27856214	WBGene00017816
<i>cec-5</i>	-0.470507	-0.32416003	WBGene00017993
<i>F44B9.8</i>	-0.561684	-1.92556989	WBGene00018409
<i>H34C03.2</i>	-0.284628	-0.27756735	WBGene00019259
<i>dcap-1</i>	-0.263447	-0.64749719	WBGene00021929
<i>ZK105.1</i>	-0.991735	-1.65634083	WBGene00022653

Q1 – *glp-1;ncl-1* vs. *glp-1*

<i>air-1</i>	0.881788	-0.75397758	WBGene00000098
<i>gop-3</i>	0.464345	-0.28597341	WBGene00001662
<i>his-64</i>	4.52768	-0.40397066	WBGene00001938
<i>pcn-1</i>	1.72101	-0.66057575	WBGene00003955
<i>rpl-11.1</i>	1.19934	-2.60971429	WBGene00004422
<i>C53D5.5</i>	0.570444	-0.25111492	WBGene00016906

Q2 – *glp-1;ncl-1* vs. *glp-1*

<i>aars-2</i>	1.33984	0.455544061	WBGene00000197
<i>exos-4.2</i>	1.12567	1.127734559	WBGene00000202
<i>byn-1</i>	2.17674	1.970908545	WBGene00000276
<i>cct-4</i>	0.652713	0.220030622	WBGene00000379
<i>cct-5</i>	0.834692	0.21728459	WBGene00000380
<i>cct-6</i>	0.545334	0.218715019	WBGene00000381
<i>clu-1</i>	0.638997	0.20108616	WBGene00000550

<i>cpr-1</i>	1.97395	1.547149601	WBGene00000781
<i>ctl-1</i>	6.03084	5.426259274	WBGene00000830
<i>cts-1</i>	0.324644	0.164658365	WBGene00000833
<i>cyn-1</i>	1.29351	0.430072519	WBGene00000877
<i>dao-5</i>	2.25282	1.202187679	WBGene00000931
<i>dap-3</i>	1.08444	0.459378315	WBGene00000933
<i>dhp-2</i>	0.643618	0.384527044	WBGene00000964
<i>ech-2,tag-30</i>	0.558883	0.390138941	WBGene00001151
<i>egl-45</i>	0.599746	0.182613449	WBGene00001209
<i>EIF-3.C</i>	0.616351	0.25377145	WBGene00001226
<i>EIF-3.D</i>	0.763536	0.26187462	WBGene00001227
<i>EIF-3.E</i>	0.778728	0.202022558	WBGene00001228
<i>EIF-3.G</i>	0.907848	0.308098839	WBGene00001230
<i>EIF-3.H</i>	0.752947	0.200214628	WBGene00001231
<i>EIF-6</i>	1.65798	0.666938011	WBGene00001234
<i>epi-1</i>	0.34786	0.142646802	WBGene00001328
<i>qars-1</i>	0.821548	0.190240465	WBGene00001336
<i>ears-1</i>	0.851596	0.266921256	WBGene00001337
<i>fib-1</i>	3.0095	1.085580882	WBGene00001423
<i>fkB-4</i>	1.79776	0.37266927	WBGene00001429
<i>fkB-5</i>	1.43005	0.526370897	WBGene00001430
<i>fars-1</i>	0.867187	0.272503112	WBGene00001497
<i>fars-3</i>	1.14919	0.403936261	WBGene00001498
<i>hmg-12</i>	0.832334	0.464322584	WBGene00001977
<i>hoe-1</i>	1.69928	0.690120883	WBGene00001983
<i>hars-1</i>	1.033	0.242200478	WBGene00002001
<i>hsp-16.1</i>	1.28449	1.566967651	WBGene00002015
<i>hsp-16.2</i>	1.52731	2.150947368	WBGene00002016
<i>hsp-60</i>	0.687285	0.21972119	WBGene00002025
<i>C56C10.7,icd-1</i>	0.953922	0.296619592	WBGene00002045
<i>ife-2</i>	0.511567	0.188544977	WBGene00002060
<i>ima-3</i>	0.429165	0.372086242	WBGene00002074
<i>C53D5.5,imb-3</i>	0.570444	0.427339466	WBGene00002077
<i>inf-1</i>	0.768733	0.246616698	WBGene00002083
<i>kars-1</i>	0.918749	0.36375594	WBGene00002238
<i>let-716</i>	1.58512	0.9207344	WBGene00002850

<i>lpd-2</i>	2.18915	1.38185004	WBGene00003059
<i>lpd-6</i>	2.43572	1.071788223	WBGene00003062
<i>lpd-7</i>	2.23931	1.200863458	WBGene00003063
<i>lars-1</i>	2.28297	1.381828196	WBGene00003073
<i>mac-1</i>	2.46368	2.36127464	WBGene00003119
<i>map-2</i>	0.829119	0.422410904	WBGene00003130
<i>mbf-1</i>	0.595743	0.25038342	WBGene00003148
<i>mars-1</i>	0.950631	0.278063875	WBGene00003415
<i>ngp-1</i>	2.55731	1.655913483	WBGene00003596
<i>nars-1</i>	1.23281	0.430399767	WBGene00003815
<i>nst-1</i>	2.14964	1.099385066	WBGene00003821
<i>pro-1</i>	2.36031	2.297471057	WBGene00004185
<i>pars-1</i>	0.873933	0.157020501	WBGene00004189
<i>pus-1</i>	1.8758	1.66724152	WBGene00004248
<i>rbd-1</i>	2.44518	2.483107228	WBGene00004315
<i>rpc-1</i>	1.59264	1.553203737	WBGene00004411
<i>rpl-24.2</i>	2.54631	1.124882002	WBGene00004437
<i>spd-5</i>	0.310593	1.394322261	WBGene00004955
<i>sars-1</i>	0.968085	0.327862321	WBGene00005663
<i>tag-151</i>	2.32514	1.615406985	WBGene00006497
<i>abcf-1</i>	1.09135	0.369126	WBGene00006512
<i>tin-9.1</i>	1.17169	1.361517559	WBGene00006572
<i>tin-10</i>	0.896522	0.398889288	WBGene00006573
<i>tin-13</i>	0.459839	0.317780892	WBGene00006574
<i>trm-1</i>	2.02736	0.836245074	WBGene00006613
<i>tars-1</i>	0.773577	0.298666475	WBGene00006617
<i>unc-45</i>	0.519523	0.335804894	WBGene00006781
<i>vig-1</i>	1.70804	0.38509447	WBGene00006924
<i>wars-1</i>	1.44876	0.517818877	WBGene00006945
<i>tufm-1</i>	0.722203	0.144809941	WBGene00007000
<i>tufm-2</i>	1.09893	0.567484197	WBGene00007001
<i>B0024.11</i>	1.76231	1.554483583	WBGene00007101
<i>B0491.1,B0491.7</i>	1.83031	2.117318134	WBGene00007194
<i>C01F6.9</i>	0.352777	0.979741146	WBGene00007223
<i>C04H5.1</i>	1.63232	2.717615538	WBGene00007312
<i>dohh-1,rpb-6</i>	1.28916	0.618088765	WBGene00007555

<i>mrps-22</i>	1.25689	0.405197575	WBGene00007564
<i>rrbs-1</i>	2.61143	1.807298878	WBGene00007617
<i>C16C10.2</i>	1.63514	0.99560427	WBGene00007623
<i>C16C10.8</i>	2.33342	0.980021008	WBGene00007628
<i>C25A1.16,nola-3</i>	1.97481	1.300195143	WBGene00007708
<i>mrpl-34</i>	1.26229	0.39645434	WBGene00007712
<i>mrps-31</i>	0.852617	0.395601644	WBGene00007859
<i>pyp-1</i>	0.549557	0.24871318	WBGene00008149
<i>C47E12.7</i>	2.53938	1.697344332	WBGene00008151
<i>C56A3.5</i>	1.97572	1.140646985	WBGene00008344
<i>mrps-5</i>	0.892886	0.4316747	WBGene00008452
<i>E02H1.6</i>	2.13329	0.605123212	WBGene00008458
<i>F08B12.4</i>	0.418059	0.394704404	WBGene00008572
<i>F11A10.7</i>	2.17022	1.476518321	WBGene00008688
<i>rpoa-2</i>	2.51962	1.073362939	WBGene00008781
<i>F20B10.3</i>	1.5025	1.876575688	WBGene00008967
<i>mrps-33</i>	0.997737	0.279989204	WBGene00009013
<i>F23B12.7</i>	1.90688	1.146769479	WBGene00009084
<i>mrpl-54</i>	0.718815	0.333171446	WBGene00009128
<i>wdr-46</i>	2.26607	1.252930359	WBGene00009211
<i>gfm-1</i>	1.37323	0.287242801	WBGene00009246
<i>F40F8.1</i>	0.338865	0.268590721	WBGene00009575
<i>F53F4.11</i>	2.80277	1.298106707	WBGene00009993
<i>atad-3</i>	1.00152	0.217963798	WBGene00010015
<i>F54C9.9</i>	1.94142	2.427953198	WBGene00010044
<i>rpac-19</i>	2.47315	1.348029218	WBGene00010230
<i>F58B3.4</i>	1.82842	2.536977028	WBGene00010231
<i>ddx-17</i>	0.536801	0.44725612	WBGene00010260
<i>JC8.2</i>	2.49068	1.846423985	WBGene00010435
<i>K01G5.5</i>	2.8284	1.158973948	WBGene00010478
<i>K05C4.5</i>	2.71361	2.039083415	WBGene00010582
<i>mrps-15</i>	0.708443	0.276489055	WBGene00010624
<i>K07C5.4</i>	2.90907	1.17320194	WBGene00010627
<i>K07F5.14</i>	2.22559	0.796228245	WBGene00010638
<i>K09E4.3</i>	0.673628	1.536842234	WBGene00010721
<i>K10C3.5</i>	1.88926	0.835146828	WBGene00010732

<i>sodh-1</i>	1.81382	1.639361335	WBGene00010790
<i>M28.5</i>	2.93996	0.970775968	WBGene00010896
<i>mrps-34</i>	1.2006	0.457707217	WBGene00010905
<i>metr-1</i>	0.36111	0.779686638	WBGene00010988
<i>R05D11.4,paxt-1</i>	1.31836	1.494458964	WBGene00011032
<i>rbm-28</i>	2.26406	2.756660459	WBGene00011043
<i>pdcd-2</i>	0.925264	0.977942906	WBGene00011116
<i>mrpl-49</i>	1.13192	0.508406175	WBGene00011247
<i>T03D8.6</i>	0.694294	0.252323054	WBGene00011393
<i>T04A8.6</i>	3.16216	1.362509585	WBGene00011408
<i>cchl-1</i>	0.925212	0.276550471	WBGene00011527
<i>T06E6.1</i>	2.90818	2.311140381	WBGene00011538
<i>drr-2</i>	1.07182	0.788222268	WBGene00011730
<i>mrpl-51</i>	0.712838	0.470445897	WBGene00011740
<i>T13F2.2</i>	0.787009	0.259948045	WBGene00011743
<i>T23G7.3</i>	2.03417	2.192829072	WBGene00011966
<i>T25G3.3,chs-1</i>	2.03758	0.825864011	WBGene00012030
<i>abcf-2</i>	1.59474	0.353721114	WBGene00012097
<i>ctps-1</i>	1.37764	0.49128131	WBGene00012316
<i>mtr-4</i>	0.901836	1.172626348	WBGene00012342
<i>W09C5.1</i>	1.39911	1.16031542	WBGene00012351
<i>mrpl-12</i>	1.19764	0.403832237	WBGene00012361
<i>Y17G7B.12,glb-29</i>	2.22249	1.83292726	WBGene00012465
<i>Y39A1A.14</i>	2.73916	2.016769962	WBGene00012652
<i>pro-3</i>	1.64657	0.860512546	WBGene00012676
<i>Y39B6A.33</i>	2.27532	1.39683981	WBGene00012692
<i>mrps-35</i>	0.438674	0.248267888	WBGene00012697
<i>abce-1</i>	1.4871	0.476132613	WBGene00012714
<i>Y41E3.11,eef-1B.2</i>	0.553951	0.288141863	WBGene00012768
<i>mrps-28</i>	1.49221	0.254724806	WBGene00012830
<i>Y44F5A.1</i>	2.24607	1.517011634	WBGene00012858
<i>Y45F10D.7</i>	2.13377	1.611244265	WBGene00012887
<i>rsks-1</i>	0.353542	0.375158916	WBGene00012929
<i>Y48A6B.3</i>	3.04982	1.437307983	WBGene00012964
<i>Y48B6A.1</i>	2.72789	2.129878791	WBGene00012978
<i>Y48B6A.13</i>	1.56143	0.942977335	WBGene00012984

<i>Y48C3A.20</i>	1.76205	1.628984021	WBGene00012998
<i>rpoa-1</i>	1.16656	1.488848535	WBGene00012999
<i>mrpl-37</i>	0.997899	0.428937513	WBGene00013004
<i>ttr-26</i>	0.61206	0.637365546	WBGene00013079
<i>Y53C12B.1</i>	1.88361	1.497055355	WBGene00013143
<i>Y53C12B.2</i>	1.33887	1.573380932	WBGene00013144
<i>nsun-5</i>	2.49727	2.12852511	WBGene00013151
<i>Y54E5A.5</i>	1.6288	0.471217742	WBGene00013200
<i>Y54G9A.7</i>	1.08502	0.338656252	WBGene00013210
<i>Y57A10A.27</i>	2.64346	1.704763931	WBGene00013267
<i>mrps-7</i>	0.957709	0.370738182	WBGene00013324
<i>Y75B8A.7</i>	2.29271	2.151375566	WBGene00013544
<i>Y105C5B.5</i>	0.479054	0.447615281	WBGene00013647
<i>yars-1</i>	0.767058	0.270665932	WBGene00013677
<i>Y111B2A.12</i>	1.63252	1.358140857	WBGene00013735
<i>prmt-1</i>	1.27101	0.345476574	WBGene00013766
<i>ZC434.4</i>	2.33115	1.321304556	WBGene00013892
<i>ZK265.6</i>	2.78112	2.846227677	WBGene00013958
<i>ZK512.2</i>	2.70873	1.433169087	WBGene00013983
<i>ZK795.3</i>	2.52314	1.808446797	WBGene00014083
<i>ZK858.7</i>	2.03412	1.800881226	WBGene00014120
<i>puf-12</i>	2.54152	1.644990185	WBGene00014165
<i>ZK970.7</i>	0.84552	1.133405453	WBGene00014173
<i>mrpl-9</i>	1.65775	0.540583188	WBGene00015025
<i>B0238.11</i>	0.747059	0.872929186	WBGene00015075
<i>B0280.9</i>	2.25529	1.610698973	WBGene00015104
<i>mrpl-41</i>	1.18351	0.362029136	WBGene00015185
<i>B0511.6,arch-1</i>	1.67922	1.685934982	WBGene00015232
<i>C01B10.8</i>	2.05757	0.857797196	WBGene00015282
<i>hpo-32</i>	1.9668	1.077968278	WBGene00015313
<i>C02F5.3</i>	1.01877	0.392463302	WBGene00015346
<i>C03H5.3</i>	1.68135	1.08930509	WBGene00015405
<i>C05C8.2</i>	2.31035	2.363250716	WBGene00015461
<i>C05D11.9</i>	1.70837	4.651637472	WBGene00015486
<i>sams-3</i>	1.32881	0.713428173	WBGene00015538
<i>C17G10.2</i>	2.19152	1.319601474	WBGene00015916

<i>C18A3.3</i>	2.95034	1.544163522	WBGene00015941
<i>C24H12.4</i>	2.1997	1.214801748	WBGene00016073
<i>mrps-18C</i>	1.28201	0.333750355	WBGene00016142
<i>C26F1.3</i>	0.93888	1.406302789	WBGene00016148
<i>sdha-2</i>	0.495505	0.269610678	WBGene00016392
<i>C43E11.9</i>	3.27732	1.078596137	WBGene00016607
<i>acer-1</i>	0.469536	0.277497601	WBGene00016630
<i>C44E4.4</i>	2.14497	0.771763675	WBGene00016653
<i>C45B2.2</i>	1.03468	0.508363591	WBGene00016659
<i>C48B6.2</i>	2.42351	1.159954306	WBGene00016740
<i>sucg-1</i>	0.711985	0.264719171	WBGene00016844
<i>lam-2</i>	0.435571	0.162025598	WBGene00016913
<i>CD4.3</i>	0.495835	0.285011438	WBGene00016989
<i>nap-1</i>	1.90139	0.914031161	WBGene00017075
<i>F07E5.5</i>	3.2051	2.38799904	WBGene00017210
<i>rpc-2</i>	1.59996	0.715593044	WBGene00017300
<i>mrps-9</i>	0.919162	0.238282126	WBGene00017319
<i>F10E7.5</i>	2.47373	2.047250196	WBGene00017347
<i>F13H8.2</i>	2.61925	1.892869602	WBGene00017435
<i>rpoa-49</i>	2.22028	1.181148943	WBGene00017749
<i>F27C1.6</i>	1.56484	1.811346859	WBGene00017855
<i>pcca-1</i>	0.281019	0.173750381	WBGene00017864
<i>nol-10</i>	1.8988	1.023151434	WBGene00017989
<i>abcf-3</i>	1.03525	0.289800591	WBGene00018339
<i>F42A10.5</i>	0.520631	0.192895319	WBGene00018341
<i>F52C9.3</i>	1.51892	0.435866294	WBGene00018674
<i>F53E10.6</i>	2.49793	2.616803175	WBGene00018762
<i>mrpl-40</i>	0.394814	0.325526083	WBGene00018793
<i>nath-10</i>	2.73703	2.509725421	WBGene00018866
<i>F55F8.2</i>	2.47	2.069618138	WBGene00018890
<i>F55F8.3</i>	2.11004	1.366887412	WBGene00018891
<i>mff-2,wdr-12</i>	1.65037	1.114280116	WBGene00018893
<i>F56D1.2,mrps-16</i>	0.357536	0.423677969	WBGene00018961
<i>H06I04.3</i>	2.06241	1.255328785	WBGene00019168
<i>H24K24.4</i>	1.75055	0.956619401	WBGene00019241
<i>rpb-5</i>	1.1762	0.562617642	WBGene00019246

<i>rpac-40</i>	2.73791	1.25307262	WBGene00019275
<i>K04C2.2</i>	1.97048	1.418648516	WBGene00019380
<i>K07H8.10</i>	2.50866	1.057348791	WBGene00019510
<i>K12H4.3</i>	2.21599	2.637296786	WBGene00019678
<i>riok-1</i>	1.26999	1.184118896	WBGene00019698
<i>mtss-1</i>	1.78316	0.780378146	WBGene00019800
<i>R02F2.7</i>	2.11736	2.431825633	WBGene00019836
<i>larp-1</i>	0.330586	0.273374632	WBGene00020097
<i>R151.8,hsp-75</i>	1.05526	0.366550139	WBGene00020110
<i>T02H6.1</i>	1.87874	1.494625092	WBGene00020171
<i>T07A9.8,nog-1</i>	2.08263	1.087738365	WBGene00020297
<i>T09B4.8</i>	1.20457	0.449954985	WBGene00020382
<i>tin-44</i>	0.373358	0.193964703	WBGene00020383
<i>T10B5.3</i>	1.81079	1.141778498	WBGene00020389
<i>T20B12.3</i>	2.48464	0.694672733	WBGene00020601
<i>T22D1.3</i>	0.915224	0.706685694	WBGene00020682
<i>mmps-2</i>	0.68723	0.341991454	WBGene00020718
<i>T28A11.2</i>	0.63947	0.289793296	WBGene00020869
<i>nol-5</i>	3.06342	1.199426926	WBGene00020915
<i>W03F9.1</i>	1.9921	0.897022464	WBGene00020999
<i>W04C9.4</i>	2.80304	1.290305826	WBGene00021026
<i>W06E11.1</i>	1.27602	0.89144563	WBGene00021061
<i>nol-1</i>	2.7281	1.058290496	WBGene00021073
<i>W07E6.2</i>	2.78357	2.913598387	WBGene00021074
<i>tomm-22</i>	0.45246	0.41511877	WBGene00021133
<i>Y22D7AL.10</i>	0.549509	0.187747188	WBGene00021248
<i>Y23H5B.5</i>	2.80019	1.423535756	WBGene00021276
<i>Y23H5B.6</i>	1.7574	1.40854959	WBGene00021277
<i>mrpl-38</i>	1.35117	0.432322021	WBGene00021327
<i>Y37E11B.5</i>	1.54402	0.375274764	WBGene00021377
<i>prdx-6</i>	1.20588	0.471304081	WBGene00021401
<i>Y39G10AR.8</i>	0.669296	0.184565106	WBGene00021466
<i>Y41D4B.11</i>	2.18846	1.449437265	WBGene00021514
<i>Y46E12BL.2</i>	1.46656	1.159651346	WBGene00021595
<i>Y48G1A.4</i>	2.31745	1.873462875	WBGene00021660
<i>Y48G8AL.5</i>	1.61735	0.745833499	WBGene00021686

<i>gcn-1</i>	0.882087	0.255999548	WBGene00021697
<i>Y49F6B.2</i>	2.04289	1.565218765	WBGene00021715
<i>nol-6</i>	2.43627	1.466405178	WBGene00021789
<i>Y53G8AR.6</i>	0.483487	0.257446649	WBGene00021813
<i>Y54E10A.6</i>	1.664	0.824279136	WBGene00021828
<i>mrpl-17</i>	0.450733	0.366997271	WBGene00021829
<i>Y54E10A.10</i>	3.07512	1.295773868	WBGene00021830
<i>Y54E10BR.4</i>	1.81584	1.35443681	WBGene00021843
<i>Y54H5A.1</i>	2.60182	1.222933041	WBGene00021899
<i>Y54H5A.2</i>	1.88312	1.400376565	WBGene00021900
<i>mrps-25</i>	0.783161	0.336405907	WBGene00021920
<i>Y55F3AM.13</i>	0.782661	0.199690123	WBGene00021930
<i>Y61A9LA.10</i>	2.19299	1.858056132	WBGene00022021
<i>icd-2</i>	1.08206	0.26480735	WBGene00022042
<i>Y66H1A.4</i>	3.26667	1.315803584	WBGene00022046
<i>set-27</i>	0.768752	0.605711518	WBGene00022173
<i>sqd-1</i>	0.988862	0.273413804	WBGene00022235
<i>Y73E7A.2</i>	1.29682	1.426375855	WBGene00022269
<i>Y92H12BL.1</i>	1.76448	0.740781013	WBGene00022363
<i>mrpl-15</i>	1.05309	0.408938696	WBGene00022373
<i>Y94H6A.5</i>	2.38262	1.998579554	WBGene00022378
<i>Y102E9.2</i>	0.688467	0.930812834	WBGene00022420
<i>mrpl-45</i>	1.68875	0.485620632	WBGene00022493
<i>toe-1</i>	1.27157	1.231687035	WBGene00022739
<i>ZK430.7</i>	2.134	1.187296424	WBGene00022742
<i>ZK546.14</i>	2.46016	0.839782641	WBGene00022765
<i>ZK1127.4</i>	1.99661	2.460254853	WBGene00022851
<i>exos-4.1,tin-9.2</i>	1.17777	0.437119568	WBGene00044083
<i>tag-267</i>	2.69391	2.077415831	WBGene00044318
<i>mrps-30</i>	0.826816	0.460920898	WBGene00044321
<i>mrpl-39</i>	1.62854	0.356509726	WBGene00044344
<i>F49D11.10</i>	2.74667	2.673651444	WBGene00045433
<i>F52C12.6</i>	0.75897	0.740075978	WBGene00138717
Q3 – <i>glp-1;ncl-1</i> vs. <i>glp-1</i>			
<i>alh-12</i>	-0.415628	-0.37429566	WBGene00000118
<i>app-1</i>	-0.284235	-0.27472707	WBGene00000155

<i>asp-1</i>	-0.301527	-0.68057393	WBGene00000214
<i>asp-3</i>	-0.322631	-0.58524804	WBGene00000216
<i>asp-4</i>	-0.348927	-0.3151751	WBGene00000217
<i>pah-1</i>	-0.323438	-0.27014292	WBGene00000240
<i>col-8</i>	-0.632699	-0.43592862	WBGene00000597
<i>col-19</i>	-0.351828	-0.43655427	WBGene00000608
<i>col-20</i>	-0.453795	-0.70726236	WBGene00000609
<i>col-98</i>	-0.516935	-0.57911218	WBGene00000673
<i>col-103</i>	-0.485537	-0.39164263	WBGene00000677
<i>col-106</i>	-0.44853	-0.48312269	WBGene00000680
<i>col-124</i>	-0.50764	-0.77138046	WBGene00000698
<i>col-129</i>	-0.489177	-1.7250618	WBGene00000703
<i>col-178</i>	-0.333043	-0.95865995	WBGene00000751
<i>col-181</i>	-0.49588	-0.75604266	WBGene00000754
<i>col-184</i>	-0.426885	-0.43921661	WBGene00000757
<i>cpl-1</i>	-0.323404	-0.36980901	WBGene00000776
<i>cpr-6</i>	-0.464085	-0.50895708	WBGene00000786
<i>cpz-1</i>	-0.415742	-0.44491001	WBGene00000788
<i>ctl-2</i>	-0.540762	-0.32432958	WBGene00000831
<i>dnj-7</i>	-0.26738	-0.30237201	WBGene00001025
<i>dsc-4</i>	-0.497105	-0.37991205	WBGene00001099
<i>bcat-1</i>	-0.252484	-0.35773122	WBGene00001149
<i>ech-6</i>	-0.269546	-0.26745421	WBGene00001155
<i>ftn-2</i>	-0.328355	-0.32291074	WBGene00001501
<i>gfi-1</i>	-0.380689	-0.43452469	WBGene00001581
<i>gly-4</i>	-0.300584	-0.34665944	WBGene00001629
<i>grd-3</i>	-0.734199	-0.52923966	WBGene00001692
<i>gst-10</i>	-0.479756	-0.38237695	WBGene00001758
<i>gst-27</i>	-0.418285	-0.47179559	WBGene00001775
<i>gst-36</i>	-0.285355	-0.37347434	WBGene00001784
<i>hsp-4</i>	-0.324976	-0.31313577	WBGene00002008
<i>lbp-6</i>	-0.254691	-0.21621911	WBGene00002258
<i>C56G2.7,let-767</i>	-0.250218	-0.28761798	WBGene00002891
<i>lys-2</i>	-0.621125	-0.84101581	WBGene00003091
<i>nid-1</i>	-0.3928	-0.36204082	WBGene00003738
<i>nmy-1</i>	-0.300137	-0.32092537	WBGene00003776

<i>nuc-1</i>	-0.30207	-0.30882034	WBGene00003828
<i>osm-11</i>	-0.411537	-0.67255306	WBGene00003891
<i>pkc-2</i>	-0.356757	-0.40705745	WBGene00004033
<i>pod-2</i>	-0.482814	-0.30768349	WBGene00004076
<i>spl-1</i>	-0.43377	-0.37850287	WBGene00004981
<i>spp-3</i>	-0.350026	-0.4033205	WBGene00004988
<i>spp-5</i>	-0.43498	-0.51461228	WBGene00004990
<i>spp-14</i>	-0.536572	-0.4529828	WBGene00004999
<i>spp-17</i>	-0.549805	-0.71379221	WBGene00005002
<i>sur-5</i>	-0.437415	-0.30258735	WBGene00006351
<i>tag-18</i>	-0.440931	-0.26576381	WBGene00006408
<i>tag-147</i>	-0.399134	-0.30007865	WBGene00006493
<i>unc-52</i>	-0.388079	-0.17102283	WBGene00006787
<i>unc-87</i>	-0.265612	-0.15546832	WBGene00006819
<i>cal-5</i>	-0.69493	-0.43577064	WBGene00006861
<i>vha-5</i>	-0.374887	-0.32726894	WBGene00006914
<i>vha-8</i>	-0.320991	-0.22731277	WBGene00006917
<i>vha-10</i>	-0.300166	-0.31411649	WBGene00006919
<i>vha-12</i>	-0.350182	-0.33292696	WBGene00006921
<i>vit-3</i>	-0.595649	-0.61351497	WBGene00006927
<i>C08F11.11</i>	-0.310781	-0.4074864	WBGene00007458
<i>cbl-1</i>	-0.694256	-0.54711807	WBGene00007533
<i>rmd-2</i>	-0.273853	-0.2097483	WBGene00007786
<i>C32H11.4</i>	-1.49461	-1.17257077	WBGene00007867
<i>idh-2</i>	-0.270983	-0.27362445	WBGene00007942
<i>ttr-44</i>	-0.621375	-0.53021286	WBGene00008341
<i>D1054.10</i>	-0.400553	-0.41504277	WBGene00008377
<i>D1054.11</i>	-0.406808	-0.62704991	WBGene00008378
<i>D1086.3</i>	-1.04228	-0.72430454	WBGene00008390
<i>D1086.6</i>	-0.531262	-0.52737809	WBGene00008393
<i>D1086.7</i>	-0.336516	-0.47363126	WBGene00008394
<i>F07A11.5</i>	-0.591693	-0.2508642	WBGene00008548
<i>acox-2</i>	-0.374626	-0.53940732	WBGene00008565
<i>F13D12.6</i>	-0.681631	-0.89084642	WBGene00008741
<i>F15G9.1</i>	-0.36353	-0.26374784	WBGene00008865
<i>pyk-1</i>	-0.381123	-0.32251295	WBGene00009126

<i>hpo-34</i>	-0.357596	-0.23620988	WBGene00009259
<i>clcc-65</i>	-0.540943	-0.89732941	WBGene00009396
<i>F46G10.1</i>	-0.749538	-0.57870055	WBGene00009796
<i>acaa-2</i>	-0.267084	-0.25219129	WBGene00009952
<i>F54D5.12</i>	-0.531601	-0.28341472	WBGene00010055
<i>F54F7.3</i>	-0.425404	-0.56447819	WBGene00010065
<i>F55B11.2</i>	-0.436331	-0.60283975	WBGene00010084
<i>nkb-3</i>	-0.342314	-0.38347251	WBGene00010117
<i>F57C2.5</i>	-0.268136	-0.35244301	WBGene00010197
<i>K01C8.1</i>	-0.445556	-0.37596438	WBGene00010456
<i>K11H3.3</i>	-0.352203	-0.35763323	WBGene00010780
<i>LLC1.2</i>	-0.401719	-0.51161278	WBGene00010793
<i>ugt-62</i>	-0.519283	-0.44632526	WBGene00010904
<i>M106.3</i>	-0.340287	-0.36833434	WBGene00010911
<i>R07E5.13</i>	-0.493233	-0.35032703	WBGene00011119
<i>cpt-2</i>	-0.278508	-0.22917512	WBGene00011122
<i>R102.2</i>	-0.586544	-0.43773004	WBGene00011289
<i>R102.4</i>	-0.507915	-0.41331408	WBGene00011291
<i>ttr-46</i>	-0.39091	-0.56226293	WBGene00011571
<i>del-6</i>	-0.305834	-0.33361795	WBGene00011891
<i>T24B8.5</i>	-0.87502	-1.14975638	WBGene00011979
<i>T25B9.9</i>	-0.29134	-0.21285245	WBGene00012015
<i>T25C12.3</i>	-0.432338	-0.31372353	WBGene00012018
<i>T28D6.3</i>	-0.72648	-0.49431666	WBGene00012123
<i>clcc-50</i>	-0.619579	-0.60753612	WBGene00012253
<i>W04G3.5</i>	-0.263297	-0.29350392	WBGene00012258
<i>Y37D8A.2</i>	-0.453349	-0.43573742	WBGene00012544
<i>Y38F1A.6</i>	-0.317049	-0.27432918	WBGene00012608
<i>dct-16</i>	-0.411209	-0.28616197	WBGene00012615
<i>Y39E4A.3</i>	-0.297952	-0.17222758	WBGene00012713
<i>Y39G8B.1</i>	-0.263459	-0.23591546	WBGene00012722
<i>Y43F8C.13</i>	-0.426052	-0.36592024	WBGene00012834
<i>Y57G11B.5</i>	-0.536516	-0.68053768	WBGene00013297
<i>Y62H9A.3</i>	-0.647655	-0.57810518	WBGene00013391
<i>Y62H9A.4</i>	-0.610776	-0.48319175	WBGene00013392
<i>Y62H9A.5</i>	-0.427519	-0.56212145	WBGene00013393

<i>Y62H9A.6</i>	-0.476357	-0.5647118	WBGene00013394
<i>acs-5</i>	-0.288881	-0.2347108	WBGene00013575
<i>ZC373.2</i>	-0.390513	-0.48855083	WBGene00013867
<i>ZK512.7</i>	-0.343114	-0.54547448	WBGene00013986
<i>glb-1</i>	-0.955574	-0.86938048	WBGene00014030
<i>gdh-1</i>	-0.472213	-0.19151105	WBGene00014095
<i>ZK1058.9</i>	-0.253761	-0.19629187	WBGene00014207
<i>ZK1307.1</i>	-0.67403	-0.47182384	WBGene00014244
<i>gstk-1</i>	-0.765466	-0.45372229	WBGene00014251
<i>ZK1320.3</i>	-0.552579	-0.76401657	WBGene00014253
<i>ptps-1</i>	-0.58452	-0.44740268	WBGene00015010
<i>B0286.3</i>	-0.343404	-0.35627336	WBGene00015116
<i>ugt-46</i>	-0.729721	-0.57551377	WBGene00015141
<i>C06A6.4</i>	-0.462086	-0.36062175	WBGene00015509
<i>C06G3.5</i>	-0.363578	-0.27381215	WBGene00015551
<i>C07D8.6</i>	-0.34161	-0.3171956	WBGene00015565
<i>C12D12.1</i>	-0.474043	-0.30148415	WBGene00015713
<i>C14F11.4</i>	-0.350429	-0.30285777	WBGene00015780
<i>flu-2</i>	-0.57043	-0.40243721	WBGene00015802
<i>C16A3.10</i>	-0.412311	-0.34132236	WBGene00015814
<i>C17F4.7</i>	-0.586173	-0.44103561	WBGene00015913
<i>C26B9.5</i>	-0.391061	-0.36302993	WBGene00016134
<i>ampd-1</i>	-0.286929	-0.264941	WBGene00016415
<i>C39D10.8</i>	-0.349777	-0.26250073	WBGene00016535
<i>acbp-1</i>	-0.301375	-0.33046719	WBGene00016655
<i>acd-1</i>	-0.382656	-0.72651028	WBGene00016943
<i>atic-1</i>	-0.269686	-0.23513404	WBGene00016957
<i>pud-2.1</i>	-2.01112	-1.26904836	WBGene00017490
<i>pud-4</i>	-2.12821	-2.0388593	WBGene00017498
<i>pud-3</i>	-2.42224	-1.98023653	WBGene00017501
<i>F17E9.4</i>	-0.325908	-0.39403734	WBGene00017541
<i>F19C7.1</i>	-0.379804	-0.37474775	WBGene00017591
<i>F25B4.8</i>	-0.615471	-0.72776551	WBGene00017771
<i>clcc-1</i>	-0.341701	-1.44164832	WBGene00017772
<i>F25B5.3</i>	-0.444952	-0.38789112	WBGene00017775
<i>F28B4.3</i>	-0.332603	-0.26483189	WBGene00017892

<i>skpo-3</i>	-0.357856	-0.28870719	WBGene00017968
<i>F32A5.8</i>	-0.296146	-0.28362133	WBGene00017971
<i>F38B6.4</i>	-0.38081	-0.32871907	WBGene00018174
<i>drd-2</i>	-0.388492	-0.35301503	WBGene00018237
<i>acs-1</i>	-0.409645	-0.27109998	WBGene00018488
<i>F54E2.1</i>	-0.59787	-0.53131541	WBGene00018823
<i>F56A4.2</i>	-1.37081	-0.74583171	WBGene00018910
<i>H34I24.2</i>	-0.437515	-0.37156237	WBGene00019261
<i>K02F3.2</i>	-0.32447	-0.37372971	WBGene00019326
<i>Iron-7</i>	-0.327517	-0.41939613	WBGene00019351
<i>asp-14,fah-1</i>	-0.430552	-1.41206581	WBGene00019619
<i>K11G12.5</i>	-0.468467	-0.27886157	WBGene00019656
<i>K12H4.7</i>	-0.268014	-0.40027749	WBGene00019682
<i>aagr-2</i>	-0.263915	-0.2677652	WBGene00019895
<i>R08E3.1</i>	-0.415334	-0.39359135	WBGene00019957
<i>hpo-19</i>	-0.414125	-0.42968265	WBGene00020268
<i>T08H10.1</i>	-0.338394	-0.33141506	WBGene00020369
<i>vha-15</i>	-0.341473	-0.37069443	WBGene00020507
<i>T21H3.1</i>	-0.281484	-0.38174637	WBGene00020662
<i>T22B7.7</i>	-0.777324	-0.88723835	WBGene00020674
<i>T26C12.1</i>	-0.359436	-0.329828	WBGene00020831
<i>W01B11.6</i>	-0.522886	-0.51347112	WBGene00020917
<i>pud-1.2</i>	-1.95601	-1.16018522	WBGene00021236
<i>Y47G6A.22</i>	-0.311895	-0.3203276	WBGene00021647
<i>Y54F10AM.8</i>	-0.300895	-0.23941214	WBGene00021852
<i>Y71H2AM.13</i>	-0.396026	-0.39630586	WBGene00022178
<i>Y71H10B.1</i>	-0.264028	-0.18982012	WBGene00022201
<i>acp-6</i>	-0.694909	-0.48671696	WBGene00022245
<i>nlp-40</i>	-0.39635	-0.40628398	WBGene00022276
<i>ttr-48</i>	-0.442209	-0.31948135	WBGene00022515
<i>lipI-5</i>	-0.671986	-0.65354698	WBGene00022642
<i>ZK105.1</i>	-1.0584	-1.95775916	WBGene00022653
<i>cth-2</i>	-0.551225	-0.46199009	WBGene00022856
<i>mhc-7</i>	-0.319963	-0.43402223	WBGene00023451
<i>D1086.11</i>	-0.282786	-0.42874058	WBGene00044081
<i>F13G11.3</i>	-0.403609	-0.64319614	WBGene00045038

Table 11. Gene-ontology enrichment analysis of different quadrants in the comparisons *ncl-1* vs. N2 and *glp-1;ncl-1* vs. *glp-1*. Only terms with $p < 0.05$ and count > 7 are listed.

Quadrant/ comparison	Category	Term	Count	Fold- enrichment	p-value	
Q2/ <i>glp-1</i> vs. <i>glp-1;ncl-1</i>	KEGG	Ribosome biogenesis in eukaryotes	35	12.915	<0.0001	
		RNA polymerase	8	9.594	<0.0001	
		Pyrimidine metabolism	11	4.797	0.0001	
		RNA transport	12	3.198	0.0010	
		Ribosome	12	2.449	0.0082	
		Purine metabolism	10	2.767	0.0086	
		Cellular component	nucleolus	55	25.982	<0.0001
			small-subunit processome	25	38.293	<0.0001
			mitochondrion	47	5.603	<0.0001
			ribosome	31	9.917	<0.0001
	preribosome, large subunit precursor		15	28.081	<0.0001	
	intracellular ribonucleoprotein complex		24	8.309	<0.0001	
	mitochondrial small ribosomal subunit		11	23.167	<0.0001	
	nucleus		67	1.794	<0.0001	
	nucleoplasm		8	8.253	<0.0001	
	cytosol		18	2.964	0.0001	
	cytoplasm	47	1.565	0.0017		

	mitochondrial inner membrane	8	3.964	0.0040
	intracellular	16	2.063	0.0108
Biological pathway	nematode larval development	161	3.479	<0.0001
	reproduction	160	3.125	<0.0001
	receptor-mediated endocytosis	94	5.522	<0.0001
	rRNA processing	33	25.376	<0.0001
	embryo development ending in birth or egg hatching	165	2.299	<0.0001
	ribosome biogenesis	27	26.425	<0.0001
	translation	48	7.950	<0.0001
	hermaphrodite genitalia development	65	3.793	<0.0001
	ribosomal large subunit biogenesis	13	31.101	<0.0001
	gonad development	38	4.743	<0.0001
	maturation of SSU-rRNA from tricistronic rRNA transcript (SSU-rRNA, 5.8S rRNA, LSU-rRNA)	14	20.096	<0.0001
	tRNA aminoacylation for protein translation	12	17.225	<0.0001
	maturation of LSU-rRNA	8	21.531	<0.0001
	formation of translation preinitiation complex	8	21.531	<0.0001
	translational initiation	10	9.787	<0.0001
	gamete generation	14	5.688	<0.0001
	RNA secondary structure unwinding	9	10.766	<0.0001
	tRNA processing	9	10.199	<0.0001
	methylation	11	5.149	0.0001
	germ cell development	15	3.549	0.0001
	protein folding	9	4.355	0.0010

		inductive cell migration	11	3.290	0.0019
		body morphogenesis	27	1.888	0.0022
		striated muscle myosin	9	2.655	0.0201
		thick filament assembly			
		determination of adult	33	1.456	0.0279
		lifespan			
		protein transport	8	2.461	0.0440
Molecular		RNA binding	44	6.096	<0.0001
function					
		snoRNA binding	11	39.496	<0.0001
		aminoacyl-tRNA ligase	15	18.466	<0.0001
		activity			
		structural constituent of	25	6.018	<0.0001
		ribosome			
		nucleotide binding	60	2.552	<0.0001
		translation initiation factor	11	11.285	<0.0001
		activity			
		ATP binding	48	2.177	<0.0001
		DNA-directed RNA	9	12.509	<0.0001
		polymerase activity			
		ligase activity	15	5.212	<0.0001
		methyltransferase activity	12	5.560	<0.0001
		nucleic acid binding	27	2.644	<0.0001
		ATP-dependent RNA	9	8.079	<0.0001
		helicase activity			
		unfolded protein binding	8	7.834	0.0001
		helicase activity	10	4.841	0.0002
		GTPase activity	9	3.802	0.0024
		GTP binding	12	2.405	0.0111
Q3/<i>glp-1</i> vs.	KEGG	Metabolic pathways	35	3.059	<0.0001
<i>glp-1;ncl-1</i>					
		Biosynthesis of antibiotics	18	6.165	<0.0001
		Lysosome	9	6.837	<0.0001
		Biosynthesis of amino	8	7.075	0.0001
		acids			

Q2/N2 vs. <i>ncl-1</i>	Cellular component	collagen trimer	11	7.568	<0.0001
		lysosome	8	12.942	<0.0001
		extracellular space	10	4.640	0.0003
		mitochondrion	12	3.388	0.0007
		extracellular region	8	2.893	0.0196
	Biological pathway	oxidation-reduction process	24	4.144	<0.0001
		metabolic process	26	2.205	0.0002
		lipid metabolic process	10	4.272	0.0005
		innate immune response	11	3.128	0.0026
		proteolysis	11	2.680	0.0077
		molting cycle, collagen and cuticulin-based cuticle	8	2.404	0.0478
		Molecular function	catalytic activity	20	4.133
	oxidoreductase activity		19	3.414	<0.0001
	structural constituent of cuticle		11	4.965	0.0001
	hydrolase activity		19	1.817	0.0147
	peptidase activity		8	2.708	0.0275
	KEGG	Ribosome biogenesis in eukaryotes	10	10.762	<0.0001
		Metabolic pathways	18	2.229	0.0006
	Cellular component	nucleolus	15	19.443	<0.0001
		mitochondrion	10	3.271	0.0031
Biological pathway	rRNA processing	11	22.174	<0.0001	
	ribosome biogenesis	10	25.655	<0.0001	
	nematode larval development	41	2.322	<0.0001	
	reproduction	40	2.048	<0.0001	
	determination of adult lifespan	23	2.660	<0.0001	

Q3/N2 vs. <i>ncl-1</i>	KEGG	hermaphrodite genitalia development	16	2.447	0.0019	
		gonad development	10	3.272	0.0033	
		translation	8	3.473	0.0079	
		RNA binding	10	3.425	0.0023	
		GTP binding	8	3.963	0.0038	
		catalytic activity	10	2.902	0.0068	
	Proteasome	10	22.091	<0.0001		
	Cellular component	proteasome complex	11	56.050	<0.0001	
		nucleus	30	2.915	<0.0001	
		mitochondrion	9	3.894	0.0018	
	Biological function	cytoplasm	17	2.054	0.0052	
		embryo development ending in birth or egg hatching	44	2.364	<0.0001	
		reproduction	33	2.486	<0.0001	
		nematode larval development	30	2.500	<0.0001	
		apoptotic process	12	4.161	0.0001	
		determination of adult lifespan	16	2.723	0.0005	
		hermaphrodite genitalia development	11	2.476	0.0113	
		Molecular function	protein binding	21	2.959	<0.0001
			nucleotide binding	18	2.441	0.0006
nucleic acid binding			10	3.122	0.0040	
hydrolase activity	13		2.252	0.0100		

Acknowledgements

I would like to thank Prof. Dr. Adam Antebi for giving me the opportunity to perform my PhD work in his lab. I still remember the first time you presented the project outline to me and I have never regretted to start working on the nucleolus. Your open mind and your never ending flow of ideas is incredibly inspiring.

I would also like to thank my thesis advisory committee (Prof. Dr. Adam Antebi, Prof. Dr. Thorsten Hoppe, Dr. Peter Tessarz) for continuous, valuable and guiding input on my project.

Importantly, I also want to thank my thesis committee members Prof. Dr. Thorsten Hoppe and Prof. Dr. Jan Riemer for agreeing to evaluate my thesis and to participate in my defense.

Thanks to Torsten Bücher for performing the ribosome profiling experiments and crazy ideas on the connection between the nucleolus and lifespan.

I would like to thank the whole Antebi lab for an incredibly nice working atmosphere. At every time, people are ready to help and I am thankful for our occasional coffee (for me water) break conversations. Thank you for being such a great team (and Raymond for his nice self-made background music in the lab).

Special thanks to Uschi for guiding scientific input and great editorial help while writing my thesis. You pushed it to the next level!

Most importantly, I would like to thank the most important person in my life. Thank you Miriam for supporting me throughout my PhD and at every time. Also thank you for standing my science-induced mood swings and that you managed everything in the background while I was busy writing. I am also grateful for your editorial and mental support. You are the best that ever happened.

Work contributions

I performed all experiments described in this thesis myself, except for:

RNA-Seq analysis was performed at Cologne Center for Genomics, Köln. Bioinformatic analysis on transcriptomic data was in parts performed by Dr. Jorge Boucas, Dr. Rafael Cuadrat and Dr. Franziska Metge at the bioinformatics core facility at the Max-Plank Institute for Biology of ageing.

Proteomics assay and differential expression analysis was performed by Dr. Ilian Atanassov at the proteomic core facility at Max-Plank Institute for Biology of ageing.

My master student Tosten Bücher performed the ribosome profiling experiments under my supervision.

Measurements of overall ubiquitylation via western blot were performed by Dr. Varnesh Tiku.

The Yeast-2-Hybrid assay to identify NCL-1 protein interactors was performed by Hybrigenics Services, France.

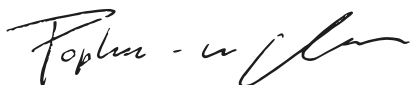
Strains PHX637, PHX702, PHX1044, PHX1037, PHX1035, PHX1094, PHX1065, PHX1056 were generated by Sunybiotech, China.

Erklärung

Hiermit versichere ich an Eides statt, dass ich die vorliegende Dissertation selbstständig und ohne die Benutzung anderer als der angegebenen Hilfsmittel und Literatur angefertigt habe. Alle Stellen, die wörtlich oder sinngemäß aus veröffentlichten und nicht veröffentlichten Werken dem Wortlaut oder dem Sinn nach entnommen wurden, sind als solche kenntlich gemacht. Ich versichere an Eides statt, dass diese Dissertation noch keiner anderen Fakultät oder Universität zur Prüfung vorgelegen hat; dass sie - abgesehen von unten angegebenen Teilpublikationen und eingebundenen Artikeln und Manuskripten - noch nicht veröffentlicht worden ist sowie, dass ich eine Veröffentlichung der Dissertation vor Abschluss der Promotion nicht ohne Genehmigung des Promotionsausschusses vornehmen werde. Die Bestimmungen dieser Ordnung sind mir bekannt. Darüber hinaus erkläre ich hiermit, dass ich die Ordnung zur Sicherung guter wissenschaftlicher Praxis und zum Umgang mit wissenschaftlichem Fehlverhalten der Universität zu Köln gelesen und sie bei der Durchführung der Dissertation zugrundeliegenden Arbeiten und der schriftlich verfassten Dissertation beachtet habe und verpflichte mich hiermit, die dort genannten Vorgaben bei allen wissenschaftlichen Tätigkeiten zu beachten und umzusetzen. Ich versichere, dass die eingereichte elektronische Fassung der eingereichten Druckfassung vollständig entspricht.

Die von mir vorgelegte Dissertation ist von Prof. Dr. Adam Antebi betreut worden.

Köln, 09.07.2020



Till Popkes-van Oepen

Datum, Name und Unterschrift